Universidad de Huelva

Departamento de Física Aplicada

Evaluation of the impact produced by the Huelva phosphogypsum stacks on their estuarine environment

Memoria para optar al grado de doctor
presentada por:

José Luis Guerrero Márquez

Fecha de lectura: 25 de febrero de 2021

Bajo la dirección de los doctores:

Juan Pedro Bolívar Raya

Manuel Olías Álvarez

Huelva, 2021

EVALUATION OF THE IMPACT PRODUCED BY THE HUELVA PHOSPHOGYPSUM STACKS ON THEIR ESTUARINE ENVIRONMENT

José Luis Guerrero Márquez

University of Huelva

Doctoral Thesis 2021

EVALUATION OF THE IMPACT PRODUCED BY THE HUELVA PHOSPHOGYPSUM STACKS ON THEIR ESTUARINE ENVIRONMENT

Conducted by:

JOSÉ LUIS GUERRERO MÁRQUEZ

University of Huelva

Doctoral Thesis 2021

Supervised by:

DR. JUAN PEDRO BOLÍVAR RAYA

DR. MANUEL OLÍAS ÁLVAREZ

This Thesis is presented to fulfil the requirements of the Official PhD programme in Industrial and Environmental Science and Technology of the University of Huelva and to obtain the title of DOCTOR.

JUAN PEDRO BOLÍVAR RAYA, Professor of the Department of Integrated Sciences of the University of Huelva,

MANUEL OLÍAS ÁLVAREZ, Professor of the Department of Earth Sciences of the University of Huelva,

DECLARE: that the Doctoral Thesis called "Evaluation of the impact produced by the Huelva phosphogypsum stacks on their estuarine environment", has been carried out by Mr. JOSÉ LUIS GUERRERO MÁRQUEZ in the Department of Integrated Sciences of the University of Huelva under their supervision, to obtain the title of Doctor of the University of Huelva

Huelva, January 2021

BOLIVAR RAYA JUAN PEDRO - 30451377K

Firmado digitalmente por BOLIVAR RAYA JUAN PEDRO - 30451377K
Fecha: 2021.01.10 21:09:28 +01'00'

Signed: Dr. Juan Pedro Bolívar Raya

OLIAS ALVAREZ MANUEL MARIA - 75420695S

Firmado digitalmente por OLIAS ALVAREZ MANUEL MARIA - 75420695S
Nombre de reconocimiento (DN): c=ES, serialNumber=IDCES-75420695S, givenName=MANUEL MARIA, sn=OLIAS ALVAREZ, cn=OLIAS ALVAREZ MANUEL MARIA - 75420695S
Fecha: 2021.01.11 08:48:07 +01'00'

Signed: Dr. Manuel Olías Álvarez

FUNDING

This work has been partially supported by the Spanish Ministry of Economy and Competitiveness (MINECO), through the project ‘‘Fluxes of radionuclides emitted by the phosphogypsum piles located at Huelva; assessment of the dispersion, radiological risks and remediation proposals” (Ref.: CTM2015-68628-R), by the Spanish Ministry of Science, Innovation and Universities (MICINN) through the project “Supply and installation of an interdisciplinary laboratory of the Huelva Scientific-Technological Center” (Ref.: EQC2018-004306-P) and by the Regional Government of Andalusia through the project “Basic processes regulating the fractionation and enrichment of natural radionuclides under Acid Mine Drainage” (Ref.: FEDER2018-UHU-1255876)

On the other hand, for the development of this Doctoral Thesis has been fundamental the research contract granted to José Luis Guerrero through the Training Programme for Academic Staff (FPU) scholarships (Ref.: FPU15/00646), financed by the Spanish Ministry of Education, Culture and Sport (MECD). Part of the work has been developed in the Silesian Centre for Environmental Radioactivity (SCER) in the Central Mining Institute (GIG), Poland, with the help of the Research and Transfer Policy Strategy (EPIT) grant of the University of Huelva.

A mis padres,
Antonio y Coronada
A mi abuela Josefa

AGRADECIMIENTOS

Como es de bien nacido ser agradecido, y no me cabe duda de que durante el desarrollo de esta Tesis han sido muchas las personas que han aportado su granito de arena, este es el momento de agradecer a todas ellas su contribución. Sabiendo que es imposible, tanto por la extensión de este documento como por la extensión de mi memoria, nombrarlas a todas, me gustaría empezar por agradecer de forma general a todos aquellos que colaboraron de forma directa o indirecta en la elaboración de esta Tesis.

En primer lugar, no cabe duda de que tengo que mencionar a Juan Pedro Bolívar, que durante este tiempo tuvo una ardua tarea, ya que no solo ha ejercido de director de esta Tesis, sino que también lo ha hecho como padre, amigo y mentor. Han pasado muchos momentos buenos durante este periodo, pero también muchos malos, tanto a nivel personal como profesional, y él siempre estuvo ahí, apoyándome, animándome, y confiando en mí hasta cuándo ni yo mismo lo hacía. Siempre conseguiste sacar lo mejor de mí en el trabajo, algo que no es nada fácil. Muchas gracias por todo Juan Pedro.

En segundo lugar, quiero gradecer a mi codirector, Manuel Olías, su inestimable aporte y participación en el desarrollo de esta Tesis, estando siempre disponible cuando he requerido de su tiempo.

Quiero hacer un agradecimiento general a todos los integrantes del área de Física Aplicada del Departamento de Ciencias Integradas, por su buena acogida, su amabilidad y su ayuda siempre que he necesitado algo de cualquiera de ellos.

A Rafael Tenorio, por su consejo, ayuda y supervisión científica de parte de los artículos presentados en esta Tesis. Podría considerarse casi como un segundo codirector, sabiendo además que los resultados presentados en este manuscrito tuvieron su origen en el trabajo conjunto liderado por él y Juan Pedro hace ahora una década.

A nuestro Antonio Padilla (Padi), y digo “nuestro” porque no sé qué sería de este grupo de investigación sin él. Siempre estuviste disponible para todo aquello en lo que he necesitado de tu ayuda, con la amabilidad y predisposición que te caracteriza. Te admiro mucho Padi, tanto por tu forma de ser, como por tu profesionalidad y saber hacer en el laboratorio y fuera de él.

A mi buen amigo Fernando (¡mi primer jefe!) y del que he aprendido mucho tanto dentro como fuera del ámbito académico. Imposible enumerar todas las veces que he

necesitado algo de ti y siempre has estado ahí. Tenemos anécdotas para escribir un libro, y seguro que seguiremos sumando más en el futuro.

A Isidoro, me siento afortunado de tenerte como amigo, y de ver como hemos llevado a buen puerto ambas Tesis de forma casi paralela. Hemos pasado muchos buenos ratos tanto dentro de la facultad como fuera, un placer haber compartido este "viaje" contigo.

Daniela, gracias por los buenos momentos y los ratitos de desahogo mutuos. Sirvan están líneas para expresarte mi apoyo, todos estamos seguros de que muy pronto tú también estarás escribiéndolas y que serás Doctora.

A Silvia, por su colaboración en parte de esta Tesis y por los buenos momentos juntos, en especial por lo bien que lo pasamos en el ENVIRA2019, mi primer congreso internacional, nunca olvidaré esos días en Praga y tú formas parte de ese bonito recuerdo. Gracias también por cedernos desinteresadamente tu casa de campo siempre que se requiere de ella para realizar algún tipo de celebración FRYMA jaja.

A Manuel Gázquez, por tu ayuda, colaboración y apoyo en el desarrollo de esta Tesis. Siempre sacas una sonrisa con tu buen humor y tu gracia. Espero que sigamos trabajando juntos en el futuro.

A Manuel Contreras, por los ratos compartidos en la sala de becarios, y por su ayuda cuando la he requerido.

Angie, aunque ya no estés en Huelva no me olvido de ti, ¡Se te echa de menos!, gracias también por las risas y buenos momentos tanto en la sala como fuera de ella.

A Almudena Hierro, que, aunque ya no estaba en Huelva cuando comencé la Tesis, la considero una compañera más. Desde que coincidimos en persona, siempre te he tenido un gran aprecio, y creo que es mutuo. Gracias por tu aporte en esta Tesis, ya que parte de ella se debe a tu trabajo de muestreo y laboratorio.

A Raúl Moreno, por las charlas y ratitos juntos en la sala, me alegra saber que pronto alcanzarás la meta de ser Doctor, te deseo mucha suerte en la futura defensa.

Agradecer a Lorenzo Lidueña su buen hacer, paciencia y profesionalidad en las innumerables gestiones burocráticas que han sido necesarias en relación con la beca FPU de la que he disfrutado estos años. Los dos sabemos que el Ministerio a veces no ha puesto fácil las cosas, especialmente este último año.

Como no dar las gracias a Manuel Ceada y a Laureano, por su amabilidad y predisposición a colaborar con el trabajo de muestreo llevado a cabo en las balsas de fosfoyeso, el cual ha sido esencial para el desarrollo de esta Tesis. Sin vuestra colaboración este trabajo no hubiera sido imposible.

A todas las personas que me acogieron como si fueran mi familia y me hicieron sentir como uno más en el Śląskie Centrum Radiometrii Środowiskowej durante mi estancia en Polonia: Bogusław Michalik, Malgorzata, Michał, Sandra, Stanislaw, Piotr, Grzegorz, Izabela (Iza), Anna, Krzysztof, Agata, Maria y Robert. Es imposible expresar con palabras lo agradecido que os estoy, y lo mucho que hicisteis por mi cada uno de vosotros, aún me parece increíble todo lo que me ayudasteis en una situación tan complida como la vivida en esos días. Y me he reservado agradecer todo lo que hicieron por mí tanto Urszula (Ula) como su marido Krzysztof, ya que se merecen unas palabras especiales. Gracias a los dos por mostrarme algunos de los parajes naturales más bonitos en los que he estado en mi vida, nunca olvidaré la belleza de las montañas Beskidy. Ula, “my polish mom” ó “my angel”, con esos dos términos que he usado para referirme a ti más de una vez cualquiera puede imaginar lo mucho que me ayudaste durante la estancia. Sé que cuento con tu amistad para toda la vida, y lo mismo digo por mi parte, espero que mantengamos siempre el contacto como hemos hecho hasta ahora. DZIĘKUJĘ BARDZO!

A mis buenos amigos Merchy, David, Jesús, Sara, Bea, Antonio, Javi y Juani (nuestra presi), por todos los buenos momentos que me han hecho pasar durante estos años y que son tan necesarios para desconectar y coger fuerzas. Su amistad llegó más o menos cuando comenzó esta Tesis, y estoy seguro de que durará muchos años más.

A mi compañera de vida, Nuria. Llegaste a mí cuando este proyecto de Tesis llevaba mucho recorrido, pero estaba tan estancado como yo en mi vida personal. Contigo a mi lado todo volvió a cobrar sentido, se hizo más fácil y grato. Gracias por estar ahí, por aguantarme en mis malos ratos, por apoyarme y por animarme cada vez que me vengo abajo. Me complementas y me haces ser mejor.

Por último, me reservo el agradecimiento a mis familiares más cercanos. En especial, quiero mencionar a alguien que ya no está con nosotros, alguien que no cabría en ella de orgullo y felicidad si pudiera verme ahora mismo, mi querida abuela Josefa. Abuelita, no me olvidaré nunca de tus risas, tus bromas y tu buen humor. Gracias por todo lo que

hiciste por mí en vida y después de marcharte. Y finalmente, como no voy a agradecer esta Tesis a mis padres, Antonio y Coronada, ellos me educaron, y me enseñaron que nada en la vida se consigue sin esfuerzo y sacrificio. Aún recuerdo ver a mi padre llegar a casa por la mañana "negro de arriba abajo" después de haber trabajado toda la noche chorreando y decirme, si el día de mañana no te quieres ver como yo, ya sabes lo que tienes que hacer… Nunca olvidaré esas palabras. A mi madre le estaré eternamente agradecido por toda la atención, cuidados, apoyo y amor que me brindó siempre. Ellos me alentaron a que estudiara, a que hiciera lo que me gustara como me solían decir y nunca dudaron de mi capacidad, por ello esta Tesis os la dedico a vosotros. ¡Os quiero!

RESUMEN

La producción de ácido fosfórico a partir del ataque químico de la roca fosfórica con ácido sulfúrico (vía húmeda), genera fosfoyeso (FY) como residuo. El FY está compuesto principalmente de yeso, pero también contiene altos niveles de contaminantes como metales pesados, ácidos, radionúclidos naturales y otros elementos traza. Las cinco plantas de ácido fosfórico incluidas en el complejo químico industrial de Huelva generaron unos 100 Mt de FY desde 1968 hasta finales de 2010 cuando cesó su actividad productiva. Estos residuos se almacenan en grandes pilas sobre las marismas del estuario del Río Tinto cubriendo una superficie de aproximadamente 1000 ha, junto al casco urbano de la ciudad de Huelva (SO de España). Las balsas de FY se dispusieron directamente sobre el sedimento sin ningún tipo de aislamiento, y actualmente se encuentran en gran parte de su extensión sin ningún tipo de capa de cobertura, estando expuestas a los agentes externos. Esta gestión del FY ha generado su meteorización y una emisión significativa de contaminantes a su entorno.

El principal objetivo de esta Tesis ha sido evaluar el impacto producido por las balsas de FY de Huelva en su entorno estuarino, centrándose en el impacto producido en los sedimentos de marisma subyacentes y las aguas de la ría del Tinto.

Se tomaron muestras sedimentarias de diferentes profundidades, seleccionadas de siete testigos recogidos en diversas ubicaciones de las balsas, de las cuales se analizaron los principales elementos contaminantes y radionucleidos naturales. Por otro lado, durante un año se recolectaron de forma mensual muestras de agua de los ríos Odiel y Tinto y sus respectivos estuarios y se determinó la concentración de actividad de isótopos U y Th y ^{210}Po. Además, se estudió mediante experimentos de mezcla el comportamiento de metales pesados y radionucleidos naturales cuando los lixiviados ácidos de las balsas alcanzan el medio marino.

Los resultados de esta Tesis mostraron que los sedimentos de marisma actúan como una “barrera” para los contaminantes procedentes de las balsas de FY y la infiltración de los lixiviados es muy limitada, alcanzando una profundidad máxima de unos 50 cm. La contaminación por ^{230}Th, ^{226}Ra y ^{210}Pb se restringe principalmente a los primeros 20 cm de sedimentos debido a procesos de mezcla, mientras que los isótopos de U alcanzan profundidades algo mayores (hasta unos 50 cm) en relación con procesos de lixiviación debido a su menor reactividad y mayor concentración en los lixiviados. Estos resultados

tienen una enorme relevancia para el diseño del proyecto de restauración de las balsas de FY, y concretamente para el nuevo canal perimetral que se proyecta construir, sugiriendo que este debe alcanzar como mínimo 1 m de profundidad por debajo de la base de las balsas, para asegurar la recolección completa de los lixiviados y evitar su liberación en el estuario del río Tinto.

Las aguas de los ríos Tinto y Odiel presentan concentraciones de isótopos de U y Th y ^{210}Po de uno a tres órdenes de magnitud superiores a las aguas continentales no perturbadas, debido al fuerte impacto producido por el drenaje ácido de minas (DAM). Los radionucleidos estudiados muestran un claro comportamiento estacional en estos ríos, con tres etapas bien diferenciadas durante el año. Se demostró un comportamiento no conservativo de los radionucleidos analizados en los estuarios debido a los procesos de coprecipitación/adsorción producidos por el aumento del pH. Se observó el importante impacto radiactivo que producen las salidas de borde de las balsas de FY al estuario del Tinto, principalmente durante los meses más lluviosos, aumentando la concentración de isótopos de U y ^{210}Po en la fase particulada.

Finalmente, los experimentos de mezcla arrojaron conclusiones relevantes. Los lixiviados ácidos del FY presentan concentraciones de metales pesados y radionucleidos naturales (isótopos de U y ^{210}Po), de dos a tres y de cuatro a cinco órdenes de magnitud superiores, respectivamente, a sistemas acuáticos no perturbados. Los elementos mayoritarios y algunos metales pesados como Mn, Ni, Cd, As, Sb y Co mostraron un comportamiento conservativo durante la neutralización de los lixiviados con agua de mar, permaneciendo en la fase líquida, mientras que otros como Al, Fe, Cr, Zn, Cu y Pb precipitaron y/o se adsorbieron sobre la fase sólida. Los isótopos U y ^{210}Po presentaron un claro comportamiento no conservativo probablemente debido a procesos de coprecipitación/adsorción en los precipitados formados. Estos precipitados mostraron concentraciones de metales pesados y radionucleidos naturales (isótopos de U y ^{210}Po) de uno a tres órdenes de magnitud mayores que suelos no perturbados, evidenciando el importante impacto ambiental producido por las balsas en su entorno.

.

ABSTRACT

The manufacturing of phosphoric acid from the chemical attack of the phosphate rock with sulfuric acid (wet process), generates phosphogypsum (PG) as a waste. PG is mainly composed of gypsum, but also contains high levels of pollutants such as heavy metals, acids, natural radionuclides, and some others trace elements. The five phosphoric acid plants included in the chemical industrial complex of Huelva generated around 100 Mt of PG from 1968 to the end of 2010 when its productive activity stopped. These wastes are stored in large piles on the salt marshes of the Tinto River covering an area about 1000 ha, close to the urban centre of Huelva (SW of Spain). The PG stacks were directly disposed on the salt marsh sediments without any type of insulation, and in large proportion of their extension they are currently without any type of cover layer, being exposed to the external agents. This management of PG has generated its weathering and significant emissions of pollutants into their surroundings.

The main objective of this Thesis has been to evaluate the impact produced by the Huelva PG stacks on their estuarine environment, focusing on the impact produced into the underlaying salt marsh sediments and the waters of the Tinto estuary.

Sediment samples from different depths were taken, which were selected from the seven cores collected at different locations of the stacks, and the pollutant elements and natural radionuclides were analysed. On the other hand, water samples from the Odiel and Tinto rivers and their respective estuaries were collected monthly throughout a year and the activity concentration of U-Th isotopes and ^{210}Po was determined. In addition, the behaviour of heavy metals and natural radionuclides when the acidic leachates from the stacks reach the marine environment was studied by means of mixing experiments.

The results of this Thesis showed that the salt marsh sediments act as a “barrier” for the pollutants coming from the PG stacks and the infiltration of leachates is very limited, reaching a maximum depth of about 50 cm. The pollution by ^{230}Th, ^{226}Ra and ^{210}Pb is mainly restricted to the first 20 cm of sediments due to mixing processes, while U-isotopes reach a bit higher depths (up to around 50 cm) in relation to leaching processes due to their lower reactivity and higher concentration in the polluted leachates. These results are of great relevance in the design of the restoration project of the PG stacks, and specifically for the new perimeter channel that is planned to build, suggesting that it

should reach a depth of at least 1 m below the base of the stacks, to ensure the complete collection of leachates and prevent their release in the Tinto River estuary.

The waters of the Odiel and Tinto rivers showed concentrations of U-Th isotopes and ^{210}Po from one to three orders of magnitude higher than unperturbed continental waters due to the strong impact produced by the acid mine drainage (AMD). The studied radionuclides show a clear seasonal behaviour in these rivers, with three well-differentiated stages during the year. A non-conservative behaviour of the analysed radionuclides in the estuaries was demonstrated due to coprecipitation/adsorption processes produced by the increase of pH. It was also observed the significant radioactive impact produced by the polluted outflows from the PG stacks into the Tinto estuary, mainly during the rainiest months, increasing the concentration of U-isotopes and ^{210}Po in the particulate phase.

Finally, the mixing experiments provided relevant conclusions. The acidic PG leachates show heavy metals and natural radionuclides (U-isotopes and ^{210}Po) concentrations from two to three and from four to five orders of magnitude higher, respectively, than unperturbed aquatic systems. Major elements and some heavy metals as Mn, Ni, Cd, As, Sb and Co showed a conservative behaviour during the neutralisation of the leachates with seawater, remaining in the liquid phase, while other ones as Al, Fe, Cr, Zn, Cu and Pb precipitated and/or were adsorbed onto the solid phase. The U-isotopes and ^{210}Po showed a clear non-conservative behaviour probably due to coprecipitation/adsorption processes onto the formed precipitates. These precipitates exhibit heavy metal and natural radionuclide (U-isotopes and ^{210}Po) concentrations from one to three orders of magnitude higher than unperturbed soils, demonstrating the serious environmental impact produced by the stacks into their surroundings.

CONTENTS

Chapter 1
Introduction

1.1. BACKGROUND

The production of phosphoric acid (PA) from phosphate ore deposits is key part in the human development due to phosphorus is an essential element to all living systems, and particularly for the plants, and hence for the modern agriculture. PA is used as the raw material for the phosphate fertilizers and animal feeds (among others) manufacturing. Phosphorus is a critical element for life, and its bioavailability is usually very low in most agricultural soils, for this reason, it is necessary to fortify the substrate by adding it as soluble phosphate.

The world's phosphate reserves are estimated to be around $1.6 \cdot 10^9$ t. Most of these deposits have a sedimentary origin, with only a 4% being of igneous origin (Notholt et al., 2005). Phosphatic materials are commonly characterized according to their P_2O_5 concentration expressed as a percentage. The concentration of P_2O_5 generally ranges from 4 to 40% in the phosphate ores.

In a simplified form, phosphate ore is converted into commercial products by using the following three main steps:

I. After being mined, phosphate ore is beneficiated to produce a concentrate known as phosphate rock (PR).

II. According to the International Fertilizer Industry Association (IFA, 2006), up to 85% of the produced PR in the above step is converted into intermediate or final products using a process of acid digestion known as the "wet process". A relatively small amount of PR is converted directly into elemental phosphorus by reduction in an electric arc furnace in a process known as the "thermal process", to obtain an extra pure PA. It is estimated that 71% of all the obtained PR is processed into phosphoric acid, with the consequent generation of great amounts of a by-product called "phosphogypsum" (PG). Otherwise, the 24% of manufactured PR is directly processed into fertilizer without the PG generation, whereas the remaining 5% is converted directly into various other products. The worldwide annual production of P_2O_5 in the form of PA is more than 30 Mt.

III. Most of the phosphoric acid produced in step (II) (75-90%) is subjected to further chemical processing to convert it into fertilizers. The fertilizer products so derived from PA thus account for some 55-60% of total phosphate rock production. About half of the

remaining 10-25% produced PA in step (II) is processed into animal feed supplements, while the other half into a variety of other products.

The world PG generation is estimated around 300 Mt every year (Yang et al., 2016). The sedimentary PR used as raw material in the manufacturing of phosphate fertilizers contains metal(oid)s and U-series radionuclides as impurities that are released during its dissolution in the digestion step of the PA industrial production process, remaining these species distributed between both PA and PG fractions. PG is essentially composed of gypsum ($CaSO_4 \cdot 2H_2O$), but also contains high levels of pollutants such as heavy metals, acids, natural radionuclides, and some others trace elements (Pérez-López et al., 2007; Bolívar et al., 2009; Rentería-Villalobos et al., 2010; Madruga et al., 2019). As a result, the market for the reuse of this waste is very limited and only 15% of this amount is recycled. Therefore, the generated PG is mainly disposed, without any prior treatment, usually by dumping in large stacks generally located in coastal areas close to phosphoric acid plants (Sanders et al., 2013; El Samad et al., 2014). This management of PG frequently generates its weathering which can provoke significant emissions into their surroundings (Tayibi et al., 2009).

On the salt marshes of the Tinto River (SW Spain), close the Huelva city, large PG stacks are located. The confluence of the Tinto and Odiel rivers form the Huelva estuary, which is an ecosystem of great interest and special characteristics, due to the acid mine drainage (AMD) provoked mainly by old abandoned sulphide mines located upriver, and the chemical industrial complex located at their mouths. The five phosphoric acid plants included in the chemical industrial complex of Huelva have generated around 100 Mt of PG from 1968 to the end of 2010 when the production of PA stopped, which is stored in large piles on the salt marshes of the Tinto River covering an area about 1000 ha. In these factories, the manufacturing of phosphoric acid (H_3PO_4) was developed by the wet chemical attack of the PR, fluorapatite ($Ca_5(PO_4)_3F$) in this case, with sulfuric acid (H_2SO_4), generating PG as a waste. The process can be summarized in the following general reaction:

$$Ca_5(PO_4)_3F + 5H_2SO_4 + 10H_2O \rightarrow 3H_3PO_4 + 5CaSO_4 \cdot 2H_2O + HF \qquad \text{(Eq. 1.1)}$$

The phosphate rock used in the factories of Huelva came mainly from Morocco (Bolívar et al., 1996a), and contained metal(oid)s in levels similar to typical soils, but with U-series radionuclides concentrations of about 1500 Bq kg^{-1} per nuclide (about fifty

times higher than unperturbed soils), with ^{238}U in radioactive equilibrium with its daughters. About 20% of U, more than 70% of Th, and the majority of Ra, Pb and Po (>95%) contained in the phosphate rock remain in the PG (Bolívar et al., 1996a; Bolívar et al., 2009). In the European Union, PG is currently considered as a Naturally Occurring Radioactive Material (NORM) because of the high concentration of both ^{226}Ra and ^{230}Th radionuclides (IAEA, 2003; EU, 2013). On the other hand, the remaining phosphoric acid trapped between the PG particles explains the high acidity and polluting potential of the aqueous leachates produced by this waste (Pérez-López et al., 2010; Pérez-Moreno et al., 2018).

The Huelva PG stacks and their pathways of contamination into the environment has been previously studied in many works. The potential atmospheric impact of these stacks has been analysed by several studies (Dueñas et al., 2007; Borrego et al., 2007; Abril et al., 2009; Lopez-Coto et al., 2014; Hernandez-Ceballos et al., 2015, Torres-Sánchez et al., 2019, 2020), concluding that the impact as a source of ^{222}Rn it is negligible while the emission of particulate matter and HF can provoke a certain impact in the surroundings.

On the other hand, the pollution of the surface sediments and waters of the Huelva estuary caused by the PG leachates has been intensively studied and especially in recent years. The PG stacks were directly disposed on the salt marsh sediments without any type of insulation, and in a high proportion of their extension they are currently without any type of cover layer, being exposed to weathering conditions. Rainfall favours the generation of leachates due to surface runoff and the infiltration provokes the existence of polluted groundwater fluxes to the borders generating edge outflows in numerous points (Pérez-López et al., 2015, 2016), reaching the estuarine environment. These acidic leachates (pH ≈ 2) show high concentrations of phosphates, sulphates, chlorides, fluorides, heavy metals (Cd, Cu, Ni, Fe, Mn, Al, Zn, Sb and Sr) (Pérez-López et al., 2016, Millán- Becerro et al., 2019), and U-series radionuclides, being these last ones in the order: $^{234,238}U$ (10^2 Bq L^{-1}), ^{210}Po (10 Bq L^{-1}), and ^{226}Ra and ^{230}Th (1 Bq L^{-1}) (Gázquez et al., 2014; Pérez-Moreno et al., 2018).

The analysis of the concentration and behaviour of metals and radionuclides in the waters and surface sediments of the estuarine system demonstrated the impact of the stacks due to the increase of these species in the surrounding environment (Bolívar et al., 2002; Villa et al., 2011; Hierro et al., 2013; Gázquez et al., 2014; Perez-López et al., 2015, 2016; 2018; Cánovas et al., 2018; Papaslioti et al., 2018). Despite the numerous studies,

and the fact that the PG piles were placed on the salt marshes without any impermeable layer to prevent percolation, the impact on the sediments under the stacks has not been previously studied. In this regard, it is very important to know the possible existence of deep leachates into the underlying sediments and their degree of affectation.

Estuaries are complex coastal systems controlled by tidal action and riverine flows, which comprise transition zones between freshwater and seawater, controlling the flux of elements from the land into the oceans. In these transition systems, meaningful modifications of water chemistry take place with strong gradients in physicochemical parameters such as pH, redox potential, and dissolved ions (Benoit et al., 1994; Hierro et al., 2014a). When anthropogenic pollutants reach the marine environment, different geochemical processes occur, as precipitation and/or adsorption onto formed solid phases, and on the opposite, dissolution, desorption and migration, changing the elemental concentrations in dissolved phase and the bottom sediments (Zhou et al., 2003; Hierro et al., 2014a). Therefore, to study the hydrochemical processes taking place during the mixing of PG leachates with seawater is crucial to understand the intake of radionuclides and other pollutants into the open ocean.

The authorities in collaboration with the responsible companies, are currently designing an engineering a project for the environmental remediation of the impact generated by Huelva phosphogypsum stacks. Furthermore, the obtained results in this work will provide helpful information to assess the routes of contamination and develop restoration methodologies to others NORM repositories.

1.2. OBJECTIVES

The main objective of this Thesis was to evaluate the impact produced by the Huelva phosphogypsum stacks on their estuarine physical environment.

To achieve the main objective, the following specific objectives were established:

1. To characterize the salt marsh sediments under the stacks (mineralogy, granulometry, physicochemical parameters and chemical composition).

2. To study the degree of affectation of the salt marsh sediments under the PG due to both pollutant elements and natural radionuclides.

3. To study the processes involved in the migration of pollutants from the PG stacks to the salt marsh sediments.

4. To study the concentrations and behaviour of U-Th isotopes and ^{210}Po in the fluvial and estuarine sections of the Odiel and Tinto rivers in order to evaluate the impact produced by the acid mine drainage and the leachates from the PG stacks.

5. To evaluate the behaviour of heavy metals and natural radionuclides (U-isotopes and ^{210}Po) and the involved hydrochemical processes during the mixing of PG leachates with seawater.

1.3. OUTLINE

This manuscript is organised in four chapters. The first chapter introduces the work developed in this Doctoral Thesis, including the background that contextualise the research carried out, the objectives pursued and the current section showing the structure of the Thesis.

The second chapter develops the materials and methods applied in this work. Firstly, the study area is detailed, describing from the bibliography its geographical location, the main natural characteristics, and the anthropogenic influence (mining and industrial pollution). Then, the different samplings carried out are described as well as the pre-treatments applied to the collected solid and liquid samples. And finally, the techniques used for the measurement and characterization of the samples are detailed.

Chapter three is the core of this Thesis where the results are presented, and it is divided into four sections. Each one of these sections correspond to a complete copy of each one of the four articles included in this Thesis, according to the Regulation of PhD studies from the University of Huelva, article 35, 2nd section, chapter IV. The first one (section 3.1.), evaluates the pollution of the salt marsh sediments under the PG stacks due to deep leachates by means of the characterization (mineralogy, granulometry, physicochemical parameters and chemical composition) of seven cores collected in the disposal area. Depth profiles of the main physicochemical parameters and pollutant elements were obtained, and the processes involved in the migration of these pollutants to the sediments were evaluated. This work was published in Chemosphere (Guerrero et al., 2019).

The section 3.2. is focused on the radioactive pollution of the estuarine sediments under the PG stacks. Some of the previous analysed samples from the cores were selected, and the main natural radionuclides of interest (U-Th-Ra isotopes as well as ^{210}Pb and ^{40}K) were measured. A comparison of the activity concentration of these radionuclides and the main activity ratios in shallow and deeper sediments was developed. This work was published in Environmental Pollution (Guerrero et al., 2020).

The following section 3.3. reports the seasonal evolution of natural radionuclides (U-Th isotopes and ^{210}Po) in the fluvial and estuarine sections of the Odiel and Tinto rivers. Both dissolved and particulate matter were analysed to know the impact produced by the acid mine drainage and the leachates coming from the PG stacks. The behaviour of these

radionuclides in the estuarine mixing zone was also assessed. This work was published in Catena (Guerrero et al., 2021a).

Last section 3.4. deepens in the behaviour of heavy metals and natural radionuclides (U-isotopes and ^{210}Po) and the main hydrochemical processes occurring when the acidic polluted leachates coming from the stacks are neutralised after reaching the marine environment. For that purpose, mixing experiments with PG leachates and seawater were carried out and both the dissolved phases and the obtained precipitates were analysed. This work was published in Environmental Pollution (Guerrero et al., 2021b).

To conclude, in the chapter four the main conclusions of this Thesis are described, as well as future lines of research. A list of all references used in this work is appended at the end of this section.

Chapter 2
Materials and methods

2.1. STUDY AREA

2.1.1. Huelva estuary

The Tinto and Odiel rivers are located in the province of Huelva (SW of Spain). The Tinto River is 101 km long while the Odiel River is 140 km long, and their catchments cover 1600 and 2300 km^2, respectively. They present marine influence in their final reach, converging in the common Ría of Huelva estuary (Fig. 2.1), to flow into the Atlantic Ocean. The Huelva estuary is 25 km long and it is underlying by Neogene sandy-silty sediments. The landward estuarine limits are established at the localities of Gibraleón (Odiel estuary) and Niebla (Tinto estuary), where the tidal effect is negligible (Braungardt et al., 2003).

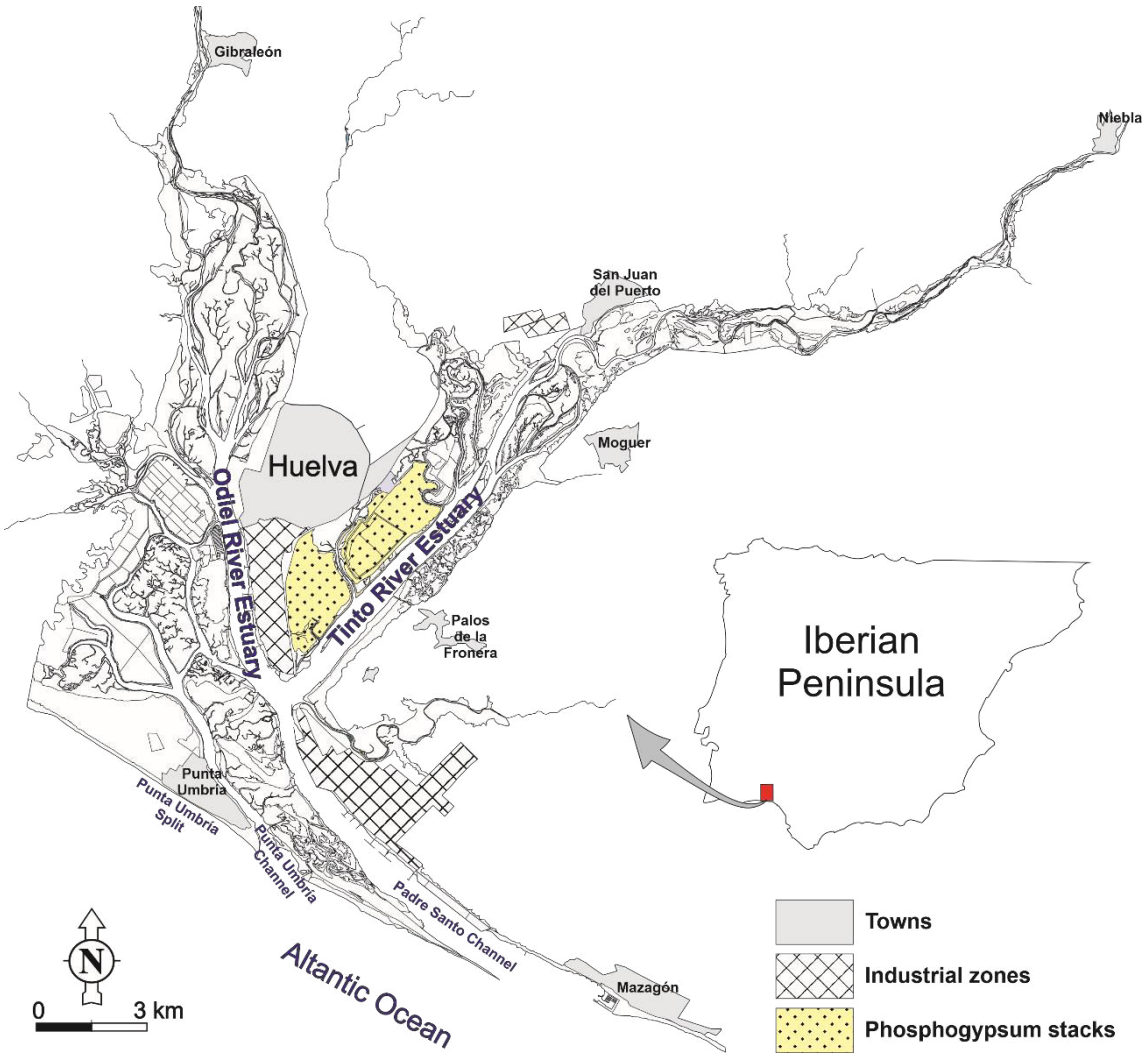

Figure 2.1. Geographical location of the Tinto and Odiel river estuaries.

The estuary of Huelva is an ecosystem of special concern, due to it is one of the most polluted in the world, being strongly affected by both the acid mine drainage (AMD) from abandoned sulphide mines located upstream of both the Tinto and Odiel rivers (pH around

2-3 is measured along these rivers), and secondly due to the chemical industrial complex and PG stacks located at their surroundings (Fig. 2.1). As consequence its waters and sediments are highly polluted by metal/oids and radionuclides coming from both the AMD and the leachates from the PG stacks.

The hydrodynamic processes of the Ría of Huelva estuary are controlled by tidal regime, wave action and fluvial discharges which regulate most of the physical and chemical parameters such as pH, salinity, metal contents, etc. (Fernández-Caliani et al., 1997). The Ría of Huelva is a mesotidal estuary (mean tidal range between 2 and 4 m) and semidiurnal with a low diurnal inequality due to the existence of a small difference in the heights reached during high tides and low tides (Borrego and Pendón, 1989). The estuary is vertically mixed, and tidal influence controls the salt induced mixing processes that are typical of marine estuaries. The Huelva coast could be classified as wave-dominated due to development of numerous coastal spits in this area (Borrego, 1992). The dominant waves direction is from the SW, associated with the Atlantic circulation regime of the winds.

The differences between the physicochemical parameters of marine and fluvial waters produce a strong pH gradient in the estuarine mixing zone due to the neutralisation of the fluvial acidic waters and the precipitation of metals and other pollutants from the dissolved into the particulate phase (Achterberg et al., 2003; Braungardt et al., 2003; Hierro et al., 2013, 2014a). It is important to take into account that this mixing process does not occur at a fixed area. A spatial displacement has been demonstrated, and while during the dry seasons the mixing takes place in the most internal zones of the estuary, during the wet seasons this process takes place in sectors closer to the coast (Carro et al., 2011).

The climate of the region is Mediterranean-type. Rainfall in the province of Huelva is very irregular, with high intra- and interannual variability. This irregularity in the precipitation together with the low permeability of the Tinto and Odiel river basins explains the large variations in the flow of these rivers (Olías et al., 2006). The rainfall is concentrated throughout the wet season, between the months of October and April, preceded by the low flow-season between the months of May and September. The average annual flows of the Odiel and Tinto rivers are 29 and 1.6 $m^3 s^{-1}$ respectively (Olías et al., 2006), but the flows can increase up to two orders of magnitude during floods, mainly in the autumn and winter months.

2.1.2. Mining pollution

The Odiel and Tinto rivers (Fig. 2.2) drain one of the biggest metallogenic regions of massive sulfides in the world, the Iberian Pyrite Belt (IPB). The IPB extends from Seville Province, in the east, across Huelva Province, to Portugal, in the west. It is considered the biggest sulfide deposit in the world with a length of over 200 km, a width of about 40 km and estimated reserves around 1700 Mt of sulfide ore (Sáez et al., 1999). Mining works date from the year 2500 B.C. in this region, although the large-scale exploitation of these deposits took place during the nineteenth and twentieth centuries (Leblanc et al., 2000). The sulfide deposits are predominately composed of pyrite (FeS_2, > 90% of volume), with variable amounts of sphalerite (ZnS), chalcopyrite ($CuFeS_2$) and galena (PbS) (Sáez et al., 1999; Venkateswarlu et al., 2016). The exposure of these sulfides to oxygen and water liberates sulfate ions and metals and leads to acidity (pH = 2.5-3.0), (Cánovas et al, 2007), producing the so-called acid mine drainage (AMD).

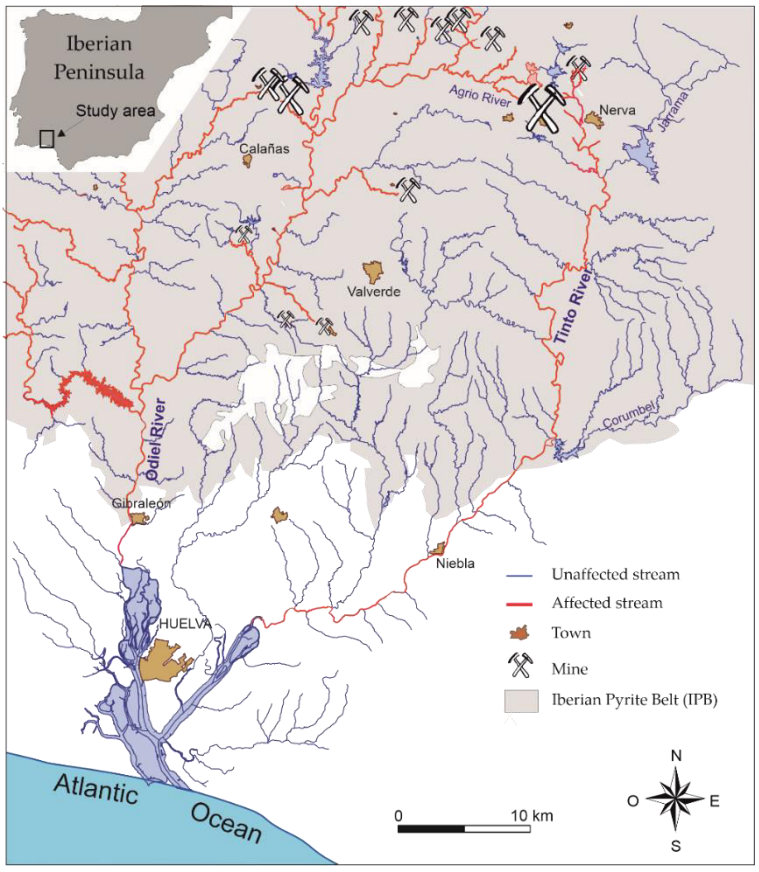

Figure 2.2. Map of the Tinto and Odiel Rivers indicating the streams contaminated by AMD, location of the main mines. The size of the symbol is proportional to the amount of sulphides extracted (modify from Olías et al., 2020).

AMD is one of the most important water pollutant processes in the world. This process originates from the oxidation of sulfide minerals, mainly pyrite (FeS_2), which is

the most abundant sulfide in nature. These minerals are stable and very insoluble in anoxic environments. However, oxidation of sulfides occurs when they are exposed to atmospheric conditions, releasing acidity, SO_4^{2-} and Fe as the following overall reaction states (Nordstrom and Alpers, 1999):

$$FeS_{2(s)} + \frac{7}{2}O_{2(aq)} + H_2O \rightarrow Fe^{2+}{}_{(aq)} + 2SO_4^{2-}{}_{(aq)} + 2H^+{}_{(aq)} \quad \text{(Eq. 2.1)}$$

In the presence of oxygen, ferrous iron suffers the reaction

$$Fe^{2+}{}_{(aq)} + \frac{1}{4}O_{2(aq)} + H^+{}_{(aq)} \rightarrow Fe^{3+}{}_{(aq)} + \frac{1}{2}H_2O \quad \text{(Eq. 2.2)}$$

And subsequently the Fe(III) can also oxidise sulphide minerals,

$$FeS_{2(s)} + 14Fe^{3+}{}_{(aq)} + 8H_2O \rightarrow 15Fe^{2+}{}_{(aq)} + 2SO_4^{2-}{}_{(aq)} + 16H^+{}_{(aq)} \quad \text{(Eq. 2.3)}$$

Or precipitate as Fe secondary (idealised as $Fe(OH)_3$):

$$Fe^{3+}{}_{(aq)} + 3H_2O \rightarrow Fe(OH)_{3(s)} + 3H^+{}_{(aq)} \quad \text{(Eq. 2.4)}$$

These reactions also liberate accessory metals and metalloids abundant in this kind of deposits (As, Cd, Co, Cu, Ni, Pb, Zn etc.). The acidic leachate reacts with the surrounding silicate mineral host rock releasing also numerous ions (Al, Ca, Mg, Mn, Si, etc.). The sulfide abiotic oxidation rates are very slow but are highly accelerated by the presence of oxidizing bacteria (Nordstrom and Alpers, 1999; Gónzalez-Toril et al., 2003; Cánovas et al., 2007). Thus, the oxidation of mining wastes by biologically-catalyzed processes is quite rapid and leads to a decrease in pH, while the mobility of trace elements tends to increase. With decreasing pH, those bacteria can thrive, producing therefore a more intense pyrite oxidation.

Some previous works also shown large concentrations of natural radionuclides with enhanced contents of U-Th isotopes and ^{210}Po in both waters and sediments (Hierro et al., 2012, 2013). Therefore, the AMD confers extreme physicochemical conditions to these rivers, which maintain high concentrations of toxic elements (Cánovas et al., 2007; Nieto et al., 2007; Hierro et al., 2014a) and natural radionuclides in solution, including U-Th isotopes and ^{210}Po (Hierro et al., 2013; Blasco et al., 2016; Manjón et al., 2019a). These pollutants arrive at the Huelva estuary, where they produce a severe environmental impact (Vicente-Martorell et al., 2009; Cánovas et al., 2010; Sánchez-Moyano et al., 2010)

2.1.3. Industrial pollution

Huelva city underwent an extensive industrialization process in the 1960's due to the relatively flat surface, the nearby water availability and the proximity of the sea for material transport. A large chemical and petrochemical industrial complex was installed on the estuary of the Ría of Huelva, pouring their heavy metal-rich wastewaters directly into the estuary. These industrial discharges were totally uncontrolled before the local government elaborated an effluent remediation plan in 1988 to mitigate the environmental impacts (Sáinz et al., 2004).

The Huelva Industrial Complex is divided into three zones surrounding both the city and estuary of the Ría of Huelva (Fig. 2.3): (1) Punta del Sebo, (2) Nuevo Puerto and (3) Tartessos. The major industrial activities which have or have had an important influence on water pollution in the estuary are the following: air gases plants, cellulose paste plants, chemical plants, hydrocarbons storage plants, metallurgical plants, petrochemical plants, pigment plants, power generation plants and fertilizer plants. Among these, the most important were the five acid phosphoric factories which were in operation since 1968 until the end of 2010, generating around 2.5 Mt of PG waste annually (Bolívar et al., 2002). These wastes were placed on the right bank of the Tinto River estuary, forming the so-called Huelva phosphogypsum stacks.

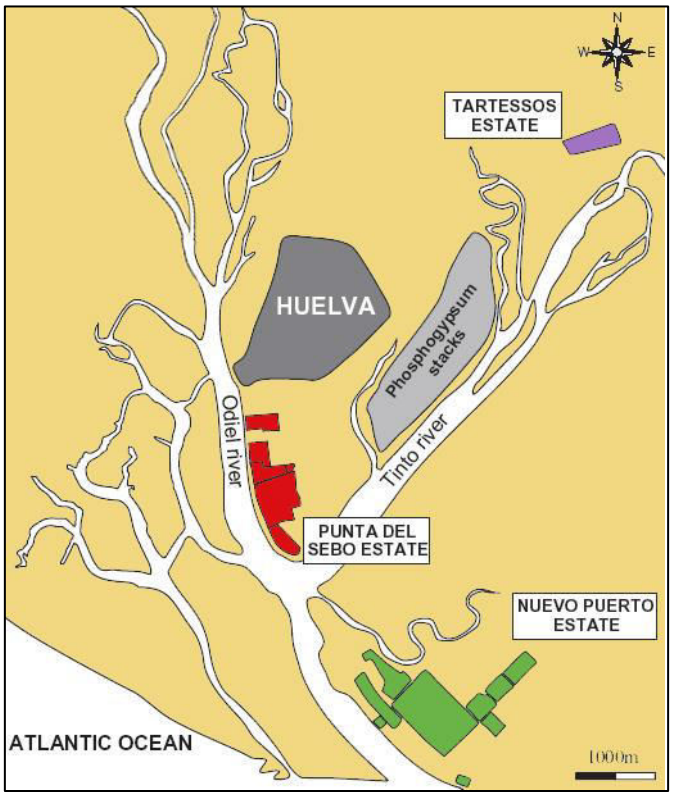

Figure 2.3. Location map of the Huelva Industrial Estate (adapted from Pérez-López et al., 2011).

2.1.4. Huelva phosphogypsum stacks

During the more than 40 years of operation period of the acid phosphoric factories of Huelva about $2 \cdot 10^6$ t of phosphate rock were processed annually and around 100 Mt of PG were generated. These wastes were transported and disposed as an aqueous slurry, without any prior treatment or insulation layer, forming large stacks on the salt marshes of the Tinto River estuary. The total extension of the disposal area is about 1000 ha, and it is located less than 1 km from the Huelva city (Fig. 2.4).

Figure 2.4. Evolution over time of the disposal area of the Huelva phosphogypsum stacks. A: year 1956 (before phosphogypsum deposition); B: year 1999; C: year 2001; D: year 2007. Source: Ministry of Development (IDEE: National Spanish Spatial Data Infrastructure).

Until 1998, about 20% of the generated PG was discharged into the Odiel River channel, while the remaining 80% was pumped in suspension with seawater into the stacks, where PG was decanted, and the polluted acidic (pH ≈ 2) seawater (around 10^7 m^3 $year^{-1}$) was released into the Tinto River channel without any treatment (Bolívar et al., 2000). Due to a change in the environmental policy according to the OSPAR convention (OSPAR, 2002, 2007), from 1998 until the end of the production (31 December 2010), all the PG was pumped with freshwater in a closed circuit and placed into the piles.

In the Figure 2.4, the state of the salt marshes before the start of the PG deposition (Fig 2.4A) and the evolution over time of the phosphogypsum stacks (Fig 2.4B-D) can be observed. It is important to note the large number of tidal channels existing in the salt marshes before deposition, which are related with the current edge-outflows, acting as preferential pathways for the PG leachates.

Currently, four zones can be identified in the phosphogypsum stacks of Huelva (Fig. 2.5). Zones 1 (located to the south) and 4 (located to the north) are considered already restored. Despite the reclamation of these zones, some edge outflows reaching the waters of the Tinto estuary can be observed in both, mainly in Zone 4 (Pérez-López et al., 2016).

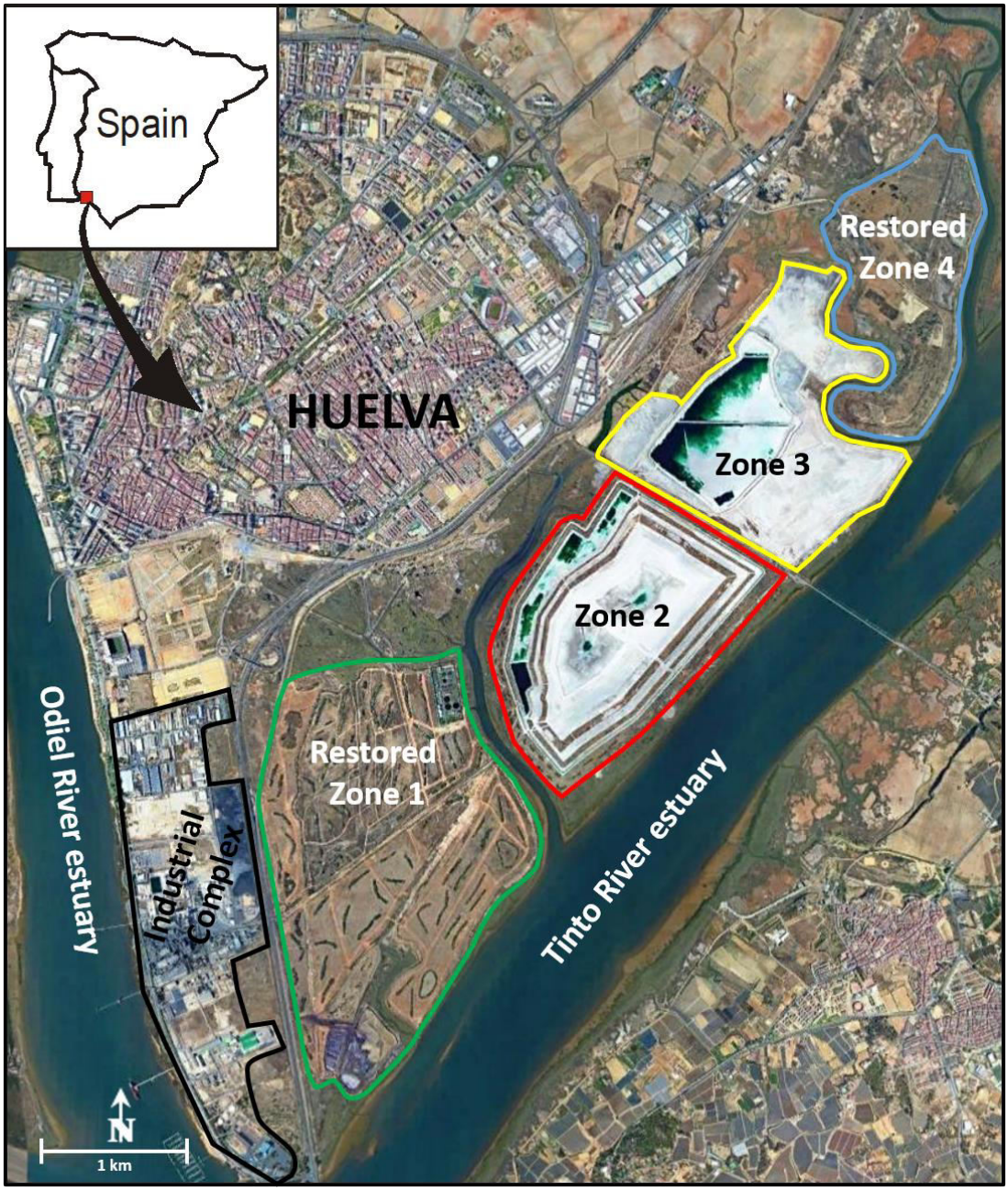

Figure 2.5. Location map of the Huelva phosphogypsum stacks defining the different zones.

Zone 1, located in the "Marismas del Pinar", shows a surface about 400 ha and it was the first area submitted to reclamation measures. It is calculated that about $12 \cdot 10^6$ t of PG, including unknown amounts of urban and mining wastes, were released in this sector. Restoration tasks were performed between the end of the 80s and early 90s by the Regional Government of Andalusia to minimize both the visual and the environmental impact associated with the different wastes that were disposed there. The restoration consisted of a soil cover of about 30 cm average thickness with a vegetal coverage above the naked PG surface.

The Zone 4 is located in the "Marismas de Mendaña" and has a surface of around 150 ha. The restoration was carried out at the beginning of this century and was more complex, comprising the following layers (from bottom to top): a 1 m layer of building wastes, a 2 m layer of inert industrial wastes and more than 50 cm of topsoil (Más et al., 2006a, b).

In Zones 2 and 3, located in the "Marismas del Rincón", the uncovered PG is directly exposed to weathering and show surface ponds of industrial process acidic water (green colours in Fig. 2.5), which are getting shallower and smaller due to the evaporating process that is been developing to proceed to their restoration.

Zone 2 accumulates about 25 Mt of PG and covers over 250 ha. The PG deposition in this area can be divided into two different moments in time. Until 1997, the PG was transported by seawater in open circuit and deposited above the salt marsh generating a 5 m high PG pile. With the change in the management policy, from 1998 to 2010 all the PG produced was stored in this zone over the previous pile by using a close circuit with freshwater, forming a pyramidal pile of up to 30 m high. A network of perimeter channels surrounds this zone in order to collect the leachates from the stack.

Zone 3 (15 Mt, 200 ha and an average of 6 m in height) is a sector where PG was disposed previously to 1997. Since then, this zone has been used to store process water in a central pond that is part of the closed-circuit freshwater system installed after the change of management policy. This zone has been subject to weathering and no preventive measures were adopted until 2012/13, when a perimeter channel was built to collect the leachates. Due to the relatively flat surface and the late preventive measures this is the most damaged sector of the PG stacks.

Furthermore, one sector of the zone 4 stacks was contaminated some years ago by radioactive ashes. In 1998, an industrial ^{137}Cs radioactive source was accidentally melted with iron wastes in a steel factory of the province of Cádiz (Acerinox). These wastes were treated in a plant from the industrial complex of Huelva. Finally, the treated wastes and a certain amount of ashes were disposed in the Zone 4 and mixed with the PG. For that reason, the Spanish National Radioactive Waste Company (ENRESA) sealed the sector and restoration works were developed consisting in a clay cover layer to minimize the migration of radioactive cesium. Finally, different vegetal species were planted in the sector, and a vigilance program was established (Más et al., 2006a).

2.2. SAMPLINGS AND PRE-TREATMENTS

In order to determine the impact of the Huelva phosphogypsum stacks on their estuarine environment, two sampling strategies were carried out. On the one hand, solid samples of different depths from the salt marsh base layer were analysed. These sediment samples were selected from the seven cores collected at different locations of the stacks and the pollutant elements and natural radionuclides were analysed. On the other hand, water samples from the Tinto and Odiel rivers and their respective estuaries were collected during a year to study the impact produced by the mining pollution and the edge outflows from the PG stacks in the concentration and behaviour of natural radionuclides. In addition, laboratory experiments were developed by the mixing of phosphogypsum leachates with seawater to improve the understanding of the behaviour of heavy metals and natural radionuclides when the acidic pollutant flows from the stacks reach the marine environment.

2.2.1. Solid samples

In order to determine the potential pollution of the PG stacks into the underlying salt marshes, 7 cores were drilled in November 2009; 3 from the Zone 2 and 4 from Zone 3 (Fig. 2.6).

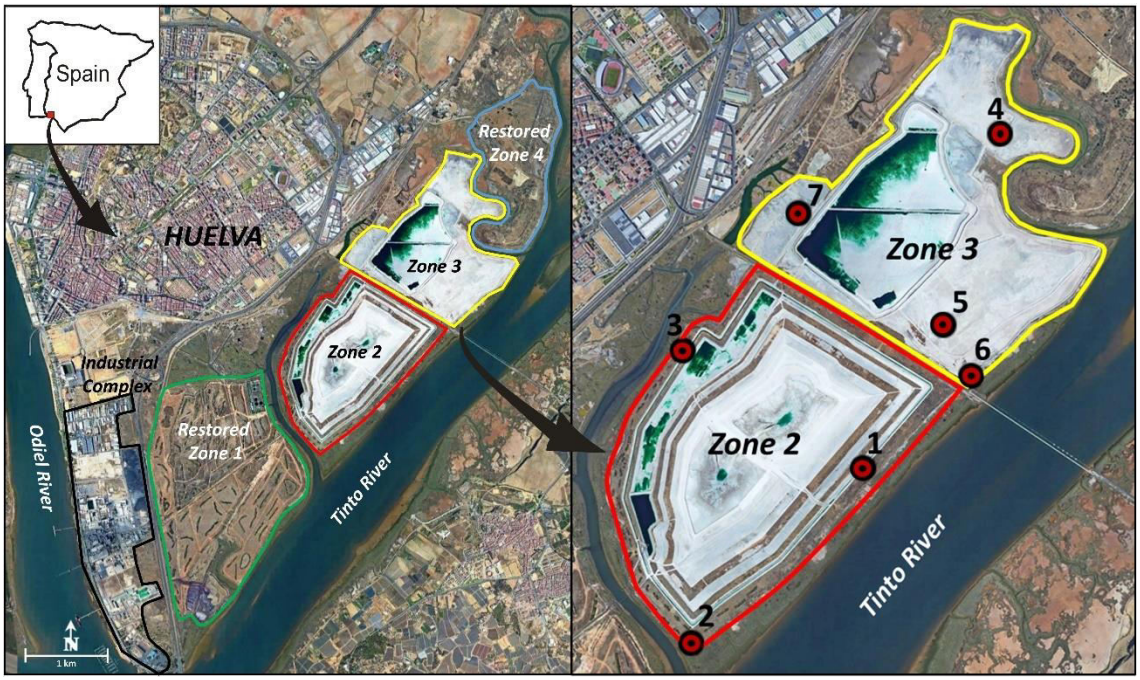

Figure. 2.6. Location map of the seven cores in the Huelva phosphogypsum stacks.

In Table 2.1, the coordinates and depth of the seven cores are indicated. The PG layer thickness varied from 2.4 m up to 8.2 m in the selected locations.

Table 2.1
Location, depth and PG thickness in the collected cores.

Core	Zone	UTM (WGS89)	Depth (m)	PG thickness (m)
1	2	29 S 685500, 4124308	15	5.6
2	2	29 S 684532, 4123293	15	5.1
3	2	29 S 684456, 4124971	16	5.1
4	3	29 S 686257, 4126285	15.8	3.5
5	3	29 S 685947, 4125146	18	8.2
6	3	29 S 686101, 4124858	14	6.5
7	3	29 S 685089, 4125768	13.2	2.4

The cores were collected by rotation drilling with continuous recovery. Core recovery was very high, and the material was only moderately disturbed and fragmented (Fig. 2.7).

Figure 2.7. Picture of the PG – sediment contact zone in the core 5.

From the collected cores, a total of 110 samples with a thickness of 5 cm and a diameter of 9 cm (28 PG samples and 82 sediments samples), were taken for the analysis of major and trace elements (Table 2.2). From these ones, 57 slices (11 PG and 46 sediment samples) were selected for the additional analysis of natural radionuclides. The samples were codified with a "XYZ" code, where "X" is the core number (1-7), "Y" represents the type of material ("P" for phosphogypsum, and "S" for sediment), and "Z" is the order in depth of the samples, listing separately the PG and sediment samples. The samples were selected from different depths, but while the PG samples were taken homogenously along the column, the sediment samples were mainly selected from the first meter under the contact in order to study its degree of affectation due to the leachates from the stacks.

Table 2.2
Samples taken of the cores and depth from the surface. *Samples selected for natural radionuclides measurement.

Sample	from (m)	to (m)	Sample	from (m)	to (m)	Sample	from (m)	to (m)	Sample	from (m)	to (m)
1P1	0.7	0.75	3P1	0.9	0.95	5P1	4	4.05	6S7*	7.1	7.15
1P2	2.9	2.95	3P2*	4.95	5	5P2	4.55	4.6	6S8	9.05	9.1
1P3	4.05	4.1	3P3	5	5.05	5P3	7.55	7.6	6S9	11.32	11.37
1P4*	5.45	5.5	3S1*	5.2	5.25	5P4	8.05	8.1	6S10*	11.37	11.42
1S1*	5.65	5.7	3S2*	5.25	5.3	5P5*	8.1	8.15	6S11	11.7	11.75
1S2*	5.7	5.75	3S3*	5.4	5.45	5S1*	8.25	8.3	6S12*	11.75	11.8
1S3*	5.75	5.8	3S4*	5.45	5.5	5S2*	8.3	8.35	6S13	13.15	13.2
1S4*	5.95	6	3S5*	5.6	5.65	5S3*	8.35	8.4	6S14*	13.25	13.3
1S5*	6.25	6.3	3S6*	5.95	6	5S4*	8.45	8.5	6S15	16.05	16.1
1S6*	9.2	9.25	3S7	6.9	6.95	5S5*	8.7	8.75	7P1	0.65	0.7
1S7	12.3	12.35	3S8*	10.35	10.4	5S6	9.45	9.5	7P2	1.25	1.3
1S8	13.1	13.15	3S9	15.65	15.7	5S7	9.85	9.9	7P3	1.7	1.75
2P1*	4.65	4.7	4P1	0.9	0.95	5S8	11.3	11.35	7P4*	2.2	2.25
2P2*	4.95	5	4P2*	3.1	3.15	5S9	12.25	12.3	7P5	2.25	2.3
2S1*	5.15	5.2	4P3*	3.2	3.25	5S10	13.9	13.95	7P6*	2.35	2.4
2S2	5.2	5.25	4S1*	3.5	3.55	5S11*	16.1	16.15	7S1*	2.5	2.55
2S3*	5.25	5.3	4S2	3.55	3.6	6P1	1.4	1.45	7S2	2.55	2.6
2S4*	5.35	5.4	4S3*	3.6	3.65	6P2	3.05	3.1	7S3*	2.6	2.65
2S5*	5.5	5.55	4S4*	3.75	3.8	6P3	5.75	5.8	7S4*	2.65	2.7
2S6	5.65	5.7	4S5*	3.85	3.9	6P4*	6.1	6.15	7S5*	2.9	2.95
2S7*	5.7	5.75	4S6*	4	4.05	6P5*	6.3	6.35	7S6	3.05	3.1
2S8*	6.25	6.3	4S7	4.95	5	6S1*	6.55	6.6	7S7	3.1	3.15
2S9	8.45	8.5	4S8	5	5.05	6S2*	6.6	6.65	7S8	4.65	4.7
2S10*	9.7	9.75	4S9	5.05	5.1	6S3*	6.75	6.8	7S9	7.55	7.6
2S11	10.35	10.4	4S10	8.8	8.85	6S4*	6.95	7	7S10	9.25	9.3
2S12	13.8	13.85	4S11	12.2	12.25	6S5*	7	7.05	7S11	11.3	11.35
2S13	16.2	16.25	4S12	14.6	14.65	6S6*	7.05	7.1	7S12	13.05	13.1
									7S13	14.47	14.52
									7S14*	14.52	14.57

An aliquot of 20 g per slice was taken for the determination of physicochemical parameters. These portions were air drying, and then the fine fraction (< 2 mm) was separated and preserved in plastic bags. Another 50 g aliquot was preserved for the analysis of the granulometric fractions by laser diffraction spectroscopy. For the mineralogical, chemical, and radioactive analysis, an aliquot of 50 g was dried in the oven at 60 ºC to constant weight within the first 24 h of the collection. The dried samples were grinded by a ring mill and after that mechanically homogenized. The dried and grinded samples were preserved in labelled plastic bags to avoid the alteration until the analysis.

The pH and electrical conductivity (EC) were determined in the preserved fine fraction of the PG and salt marsh sediments by 1:2 (sample:water) mix with a Crison MM40+ portable multimeter, with a 5048 (Ag/AgCl) electrode previously calibrated.

2.2.2. Liquid samples

To study the influence of the mining pollution and PG stacks in the waters of the Tinto and Odiel rivers and their common estuary four sampling points were selected: OR and TR were located in the Odiel and Tinto rivers, while OE and TE were located in the

Odiel and Tinto estuaries, respectively (Fig. 2.8). OR and TR represent fluvial composition without any marine influence. At these four points, water samples were collected monthly throughout a year (from October 2009 to September 2010). In total, 48 water samples of 10 L each one, were collected.

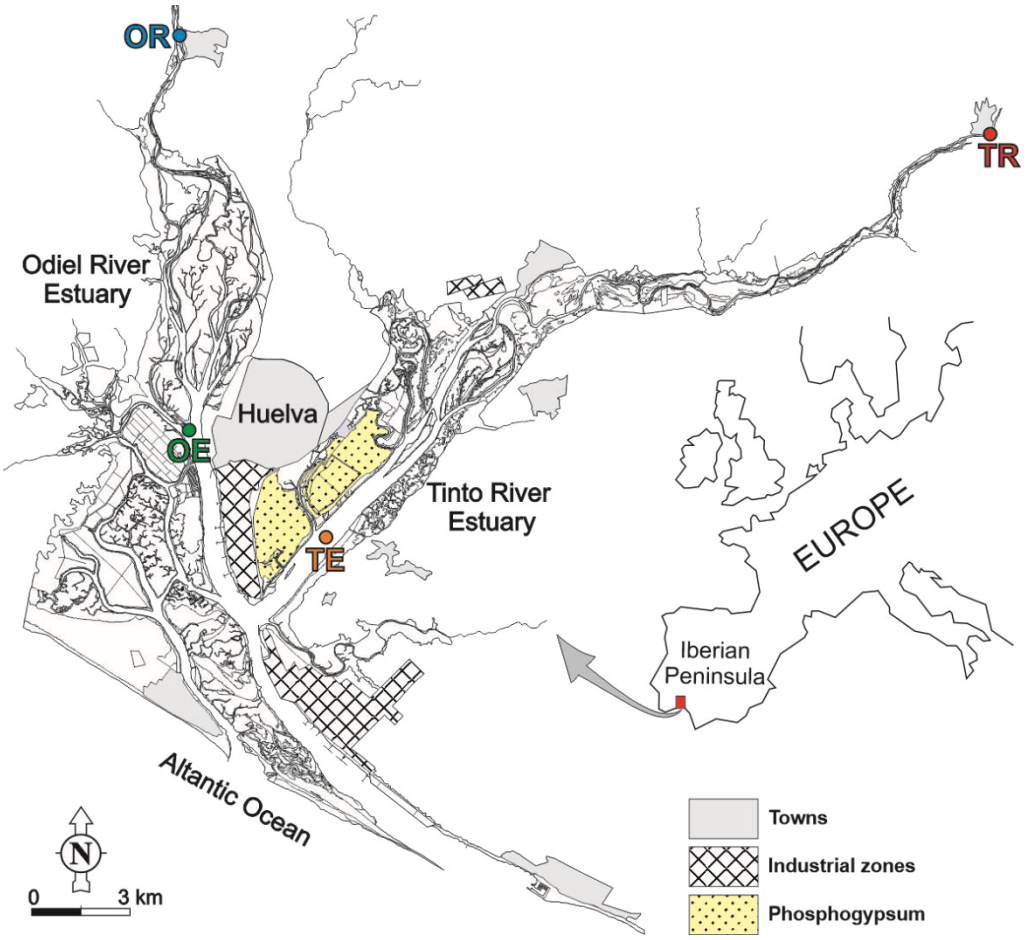

Figure 2.8. Map of the study area showing the sampling points: Odiel River (OR), Odiel Estuary (OE), Tinto River (TR) and Tinto Estuary (TE).

Water samples were filtered in the laboratory by polycarbonate filters 9.0 cm in diameter with a pore size of 0.45 μm. The liquid phase was stored in polyethylene containers, and concentrated HNO_3 was added to achieve pH < 2 in order to prevent the adsorption of radionuclides and metals onto the container walls until the analysis. The filters were dried in a dehumidifier and weighed on an analytical balance (precision 0.001 g), and the particulate matter (PM) content was calculated by subtracting the mass of the blank filter. The filters were cleaned with HNO_3, and the liberated particulate matter was dissolved applying atmospheric acid digestion with aqua regia (3 HCl:1 HNO_3). The dry residue was re-dissolved in HNO_3 (8M) and storage in polyethylene containers until the analysis.

On the other hand, laboratory experiments were carried out to improve the understanding of the behaviour of heavy metals and natural radionuclides during mixing of phosphogypsum leachates with seawater. To develop the mixing experiments three phosphogypsum leachates (PGL) samples and a seawater sample (SW) of about 200 L were collected in March 2019 (Fig. 2.9). The PGL samples, with a volume about 5 L each one, were taken in three different points from the Zone 2, two of them in boreholes (samples B1 and B2) which collect the polluted groundwater in the border of the stack, and the third one in the perimeter channel (sample PCh), which collects the lateral leachates.

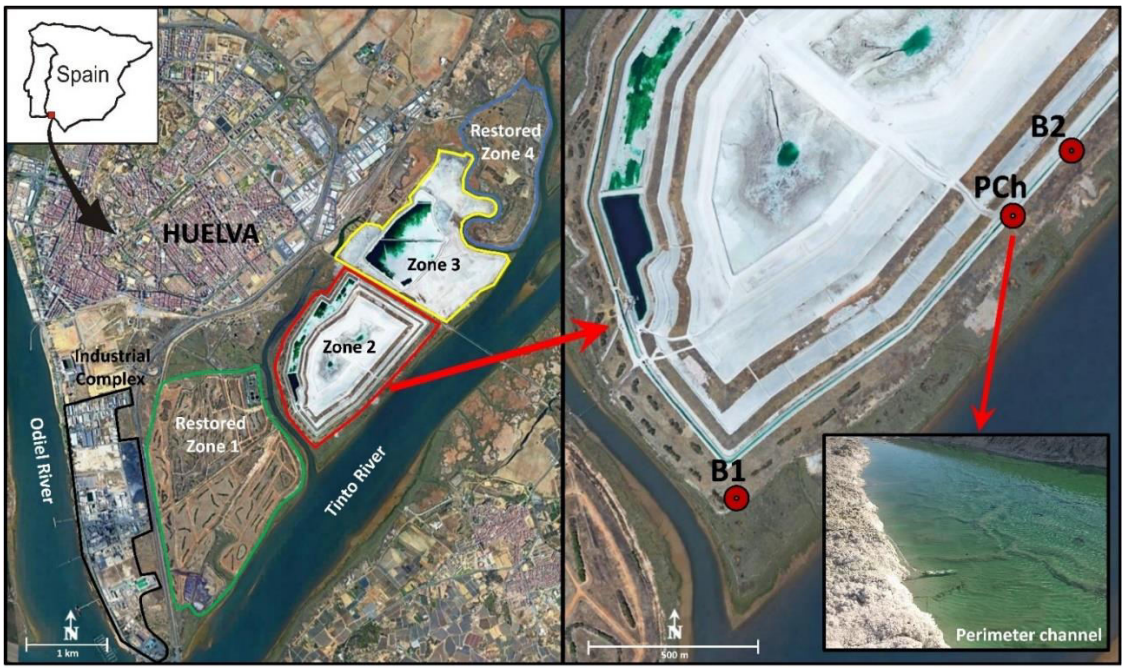

Figure 2.9. Location of the phosphogypsum leachates sampling points: boreholes (B1 and B2) and perimeter channel (PCh) located in the zone 2 of the phosphogypsum stacks of Huelva.

The PGL sampling points were chosen to show similar hydrochemical characteristics than the edge outflows, whose access is complex and a partial mix with the estuarine water is observed. The SW sample was collected in the open ocean close to the Port of Mazagón (Huelva Atlantic coast), to avoid the input of metals and other pollutants provided by the Tinto and Odiel rivers due to the their strong AMD affectation as was previously indicated. Water samples were filtered in the laboratory by using 0.45 μm pore size polycarbonate filters and stored until analysis. Concentrated HNO_3 was added to the seawater sample to achieve pH < 2 to prevent the adsorption of radionuclides and metals onto the container walls.

In all the collected liquid samples the main physicochemical parameters [temperature (T), pH, EC, and oxidation reduction potential (ORP)], were measured *in situ* using a Crison MM40+ portable multimeter, with a 5048 (Ag/AgCl) electrode. The instruments were calibrated before sampling, and the ORP was corrected to obtain the potential relative to the hydrogen electrode (Eh) according to Nordstrom and Wilde (1998).

2.3. MEASURING TECHNIQUES

2.3.1. Alpha spectrometry

Alpha particle spectrometry is a powerful and extremely sensitive analytical method for the determination of several alpha emitting radionuclides in environmental, biological and nuclear technology related samples. This technique is based on the interaction of α-particles emitted in the decay process with matter, in order to detect and count them for analytical purpose, i.e., its aim is to determine the activity concentration of a specific radionuclide in a sample. This technique requires the previous minimisation of the α-particle self-absorption effects at the source since the alpha particles are absorbed in several microns of solid matter. Therefore, a chemical separation procedure is required to isolate and purify the radioelements before being either electrodeposited or self-deposited a uniform thin layer of the sample onto an acceptable backing material in order to detect the emitted alpha particles.

2.3.1.1. Radiochemical method

For isolating the radioelements of interest (U-isotopes, Th-isotopes and ^{210}Po), a well-established sequential radiochemical method was applied to the samples before the measure of the sources by alpha-particle spectrometry with PIPS (Passivated Implanted Planar Silicon) detectors.

Before applying the radiochemical method, the samples must be prepared by the addition of tracers and preconcentration or digestion of the liquid and solid samples respectively:

Selection of the tracers

Due to the losses of radionuclides during the chemical isolation process, a known quantity of an artificial radioactive isotope was added to evaluate the recovery of the method. The tracers used and some information about them are shown in the Table 2.3. To note that three requirements must be met by these tracers: (1) their emission energy must be different than the one of the radionuclide of interest, (2) the tracer should be an isotope of the selected radioelement (same chemical behaviour) and, (3) the tracer must be an artificial radionuclide, to ensure that it is not previously contained in the sample.

Table 2.3
Isotopes of U, Th and Po used as tracers in alpha spectrometry.

Isotope	Activity (mBg/g) and reference date	$T_{1/2}$ (years)	Energy (MeV) and emission probability (%)
^{209}Po	105.6 ± 0.1 (15/03/1994)	125	4.88 (99 %)
^{229}Th	177.6 ± 1.1 (31/12/2007)	7340	4.797 (1.2 %), 4.814 (9.30 %); 4.837 (4.8 %); 4.845 (56.2 %); 4.901 (10.20 %); 4.967 (5.97 %); 4.978 (3.17 %); 5.050 (5.2 %); 5.052 (1.6 %)
^{232}U	72.5 ± 0.3 (25/03/2003)	68.9	5.32 (68 %); 5.27 (32 %)

Preconcentration of the liquid samples by using MnO_2

For dissolved isotopes, a volume from 1 to 5 L, depending on the activity concentration of the sample, previously filtered was used. To each sample HNO_3 was added until pH = 2 is reached. After that, the tracers were added in amounts according to the expected activity concentrations of the samples. After homogenization, 2 mL of $KMnO_4$ (2M) was added as indicator. After the equilibration, NH_4OH was added drop-wise up to pH ≈ 8-9 was reached, and 2 mL of $MnCl_2$ (0.3 M) as a carrier per each liter of sample was added. The mix was homogenized and settled for 4-5 hour. The precipitated was separated from the supernatant by filtration and dissolved with 20-30 mL of HCl (1.2M) - H_2O_2 (1%). The sample was evaporated to dryness, and the residue was redissolved with 5 mL of HNO_3 (65%) and evaporated to dryness again. The solid was finally redissolved with 5 mL of HNO_3 (8M).

Digestion of filters

The filters were cleaned with HNO_3, the tracers were added, and the particulate matter was dissolved applying an acid atmospheric digestion with aqua regia (3 HCl:1 HNO_3) and evaporated to dryness. The dry residue was redissolved with 5 mL of HNO_3 (8M).

Digestion of sediments

The sediment samples were subjected to a digestion in microwave with hard acids up to total dissolution. It was taken from 0.2 to 0.5 g of sample and was transferred into the reaction vessel. The suitable amount of the tracers and the strong agents (9 mL HNO_3, 2 mL HCl, 3 mL HF and 2 mL of H_2O_2) were added to the vessels. Vessels were placed in the microwave and heated to 180 °C. After digestion, the sample was transferred to a

teflon vessel and the reaction vessel was rinsed with 5 mL of HCl. Then, the sample was evaporated to dryness. 6 mL of $HClO_4$ was added and it was evaporated to dryness again. After that, it was added 10 mL of HNO_3, and the mix was transferred to a glass beaker and evaporated to dryness. Another 10 mL of HNO_3 was added and the sample was evaporated to dryness again to finally been redissolved with 5 mL of HNO_3 (8M).

Radioelements sequential isolation based on TBP and ion exchange resins and thin sources preparation

This radiochemical method has been performed by our research group (Bolívar et al., 2000) (Fig. 2.10), and is based on the property of TBP (tributyl phosphate, $C_{12}H_{27}PO_4$) to absorb the actinides.

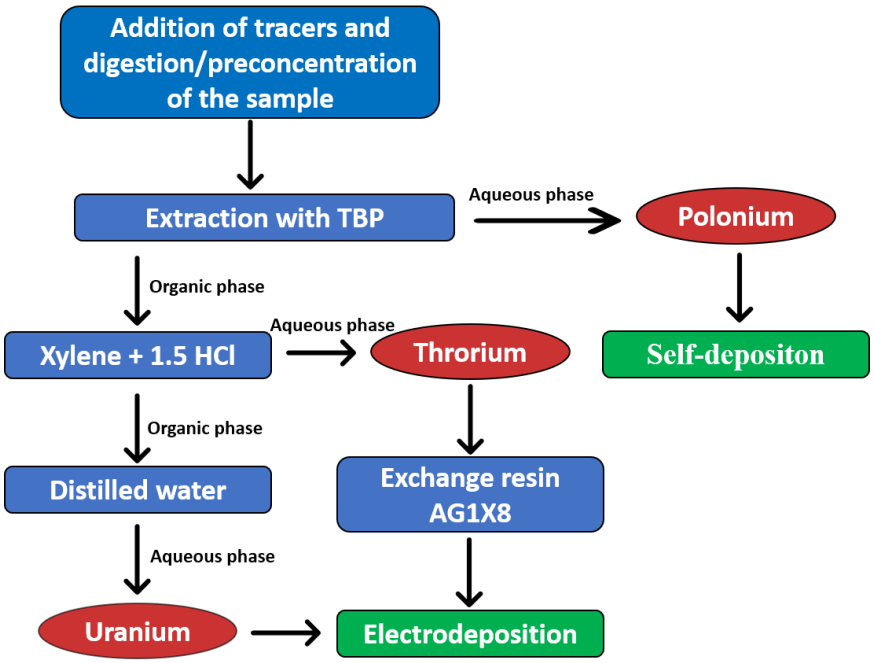

Figure 2.10. Diagram of TBP radiochemistry method.

The sample (dissolved in 5 mL of 8M HNO_3) was transferred to a separatory funnel. The beaker was rinsed with another 5 mL of HNO_3 (8M) and transferred to the funnel. 5 mL of TBP was added and the funnels were agitated for 10 min and settled for another 10 min without cover until separation of phases was reached. The aqueous phase (8M HNO_3), which contains ^{210}Po, was collected in glass beakers and evaporated to dryness.

The residue was dissolved with 5 mL of HCl, and then evaporated to dryness again. 10 mL of HCl (2M) was added to dissolve the previous residue. Then, ascorbic acid for reduce Fe^{3+} to Fe^{2+} was added. The sample was transferred to a bottle which include inside a silver disc where Po was self-deposited under mechanical agitation during 5 h.

The next step was the back-extraction of Th and U from the TBP. 20 mL of xylene ($C_6H_8O_6$) and 15 mL of HCl (1.5 M) were added to the organic phase in the separatory funnel, and shaken for 10 min. The aqueous phase was separated (Th fraction). To separate the remaining U from the organic phase 15 mL of distilled water was added into the funnel, shaken, and saved in a glass beaker (U fraction in aqueous phase). The Th fraction was evaporated to dryness and the residue is dissolved with 5 mL of HNO_3 (65%) and evaporated to dryness again and 10 mL of HNO_3 (8M) was added. Then a column chromatography was used to purify the Th fraction from U. The column was filled with 3 g anion exchange resin AG1X8 (100 - 200 mesh). Th solution was passed through the column, and the eluted solution was discarded. Then, the column was washed with 40 mL HNO_3 (8M) and Th was eluted with 40 mL of HCl (9 M).

Finally, U- and Th-isotopes once isolated and purified were electrodeposited onto stainless steel discs applying a method reported by Hallstadius (1984). Sodium sulfate was used as the electrolyte solution in the electrodeposition cell and the current was 1.2 A during 1 h for U and 2.5 h for Th.

2.3.1.2. Alpha spectrometric system with passivated implanted planar silicon (PIPS) detectors

Silicon-based semiconductor detectors are mainly used for charged particle detectors. A semiconductor detector is a radiation detector which is based on a semiconductor, such as silicon, to measure the effect of incident charged particles or photons. As ionizing radiation enters the semiconductor, it interacts with the semiconductor material. It may excite an electron out of its energy level and consequently leave a hole. This process is known as electron–hole pair generation. The energy necessary to form a single electron-hole is directly proportional to the energy of the stopped particle. The electric field in this region sweeps the electrons to one terminal and the holes to the other one. By collecting electron-hole pairs, the detection signal is formed and recorded. This charge pulse is integrated in a charge sensitive preamplifier to yield the observed voltage pulse and perform the alpha spectrum.

The alpha spectrometry was performed using an EG&G Ortec system with an integrated Octete PC PLUS with eight chambers. Each chamber consists of 450 mm^2 ion-implanted silicon PIPS detector, each one housed inside a vacuum chamber. In addition, each alpha spectrometer chamber includes a vacuum gauge, variable detector bias supply, a preamplifier, a shaping amplifier with adjustable gain, pulse stretcher and bias amplifier,

a test pulser generator with variable amplitude, and leakage current monitor. Following, all chambers are coupled to an analog-to-digital converter (ADC), and a multichannel analyser (MCA) which forms the voltage pulses in a way that they have a well-defined height (no sharp peak) and their pulse height is proportional to the initial amount of charge (Fig. 2.11)

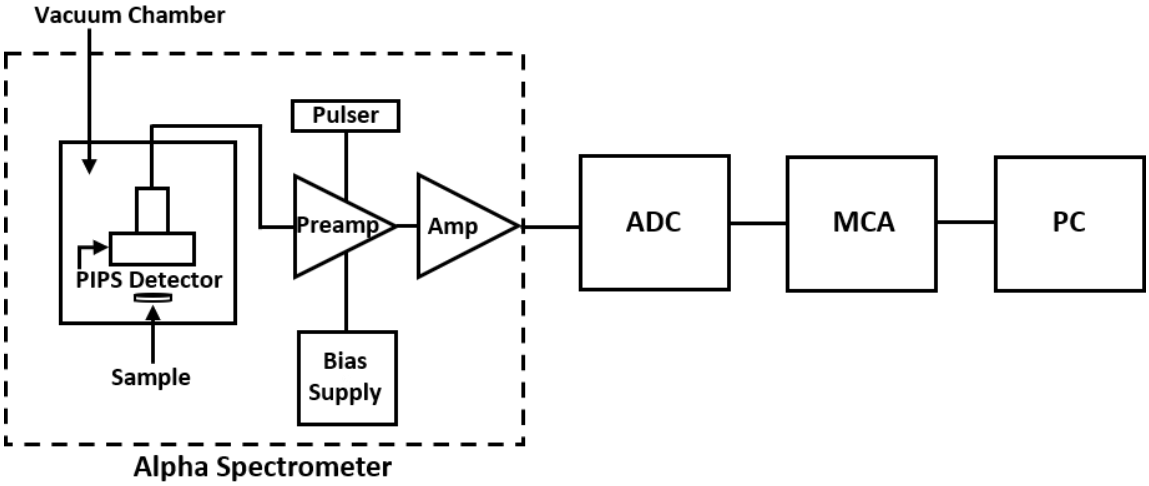

Figure 2.11. Scheme of the alpha spectrometry system.

The detectors have a maximum FWHM (Full Width Half Maximum) of 20 keV by using a mono-energetic emission of ^{241}Am, with detection efficiency close to 25 % for distances less than 10 mm. A background counting rate less than 30 counts per day is expected in the energy range from 3-8 MeV, about (1-2) 10^{-5} cps under a typical alpha peak, energy interval for the most interest natural alpha particle emitters. The detectors operate at a polarisation voltage of 50 V.

2.3.1.3. Counting efficiency

The main factors affecting the absolute counting efficiency are the detector size, the source-detector solid angle, and the intrinsic detention efficiency. It is well known that for PIPS detectors the intrinsic detention efficiency is the unit (Vioque et al., 2002).

The absolute counting efficiency (ε) is defined as the number of detections without background (counts, N) in relation to the number of emissions of the radioactive source (N_0):

$$\varepsilon = \frac{N}{N_0} \qquad \text{(Eq. 2.5)}$$

Therefore, to determine experimentally the counting efficiency, a certified standard source with known activity (A_s) with the same geometry that sample is used, being calculated the counting efficiency by the formula:

$$\varepsilon = \frac{(G-B)}{A_S \cdot P_S \cdot t} \quad \text{(Eq. 2.6)}$$

, where G is the gross count of the peak, B the background, P_s is the emission probability of the standard source, and t the counting time. In the energy range from 4 MeV to 8 MeV and for a given geometry, the counting efficiency can be considered constant (Knoll, 1989). Once established our detector configuration, the counting efficiency for our 8 alpha-detectors was around 25 %.

2.3.1.4. Activity concentration calculation

Once the radioactive thin sources counting is done, activity concentrations and uncertainties of the radionuclides of interest will be calculated from their respective spectra. This requires transforming the net number of counts (response of the system) in activity concentration (measured quantity).

The activity concentration (a) at the moment of the isolation (date, F_0) for a given alpha-emitter radionuclide can be calculated by applying the equation:

$$a = \frac{N \cdot I_0 \cdot m_0 \cdot a_0}{N_0 \cdot I \cdot m} \cdot e^{-\lambda_0 (F_0 - F_r)} \cdot e^{\lambda (F_1 - F_0)} \quad \text{(Eq. 2.7)}$$

, where N, is the net counts at the peak of the radionuclide of interest, N_0 the net counts at the peak of tracer radionuclide, a_0 the tracer activity concentration at the reference date of the certificate, t the live counting time, I the probability of the alpha emission in the peak of interest (often is 1), I_0 the probability of the alpha emission in the peak of interest for the tracer (often is 1), m the mass (or volume) of sample, m_0 the mass (or volume) taken from the certified standard tracer solution, F_0 the isolation date, F_1 the counting date, F_r the reference date for tracer activity concentration of the certificate (a_0), λ the decay constant for the radionuclide of interest and λ_0 the decay constant for the tracer radionuclide.

The previous equation is valid if the contribution of the blank sample is negligible (blank activity = A_b), but in general this one must be considered. Therefore, the real activity concentration of the sample (a_s) will be calculated trough the next expression:

$$a_s = a - \frac{N}{m} \quad \text{(Eq. 2.8)}$$

The yield (Y) of the radiochemical procedure is calculated as:

$$Y = \frac{N_0}{\varepsilon I_0 m_0 a_0 t} \quad \text{(Eq. 2.9)}$$

The average chemical yields obtained to ^{210}Po, Th- and U-radionuclides were 90, 60 and 80 %, respectively.

2.3.1.5. Lower Limit of Detection (LLD) and Minimum Detectable Activity (MDA)

The Lower Limit of Detection (LLD) for any radionuclide is critically dependent on the detector background (B, counts), and procedure blank count rates. However, an attempt has been made to give typical limits assuming low background detectors (see next table). LLD can be calculated by using the next formula derived by Lochamy (1981).

$$LLD\ (counts) = k^2 + 2.8 \cdot k\sqrt{B} \quad \text{(Eq. 2.10)}$$

, where B is the background counts, and k is the one-sided confidence factor (k = 1.65 if is 95% of measurements give a count rate above the Minimum Detectable Activity).

Then, the Minimum Detectable Activity (MDA) at 95% confidence level (k = 1.65), will be given by:

$$MDA\ (Bq) = \frac{LLD\ (counts)}{\varepsilon \cdot Y \cdot t} = \frac{k^2 + 2.8 \cdot k\sqrt{B}}{\varepsilon \cdot Y \cdot t} = \frac{2.7 + 4.6\sqrt{B}}{\varepsilon \cdot Y \cdot t} \quad \text{(Eq. 2.11)}$$

A valid alternative to assess the MDA, is to use n replicate measurements of the blank by using an equation similar to the previous one:

$$MDA\ (Bq) = k\sqrt{1 + \frac{1}{n}}\sigma_b \quad \text{(Eq. 2.12)}$$

Where σ_b denotes the standard deviation of the blank activity, and n is the number of replicate blank measurements. Therefore, a detection decision is made for a real sample by comparing the measured net activity to the critical net activity. This approach should work best if all samples and blanks are analysed under similar conditions, using instruments with similar counting efficiencies and background levels. Each sample and each blank must still be corrected for instrument background. The estimated MDA of Th and U isotopes is 1 mBq, while for ^{210}Po is 2 mBq.

2.3.1.6. Quality Control (QC)

The method used for the radiochemical measures carried out in this Thesis was validated by mean of a quality control system (QC) which consists of the analysis of replicates, blanks, certified standard materials, and the participation in national and international intercomparison exercises.

Table 2.4 shows that the obtained results in our laboratory agreed with the certified values of the analysed reference materials. IAEA-327 is a soil from Moscow containing certified activity concentrations, while H1 and C1 are solutions with known activity. The statistical parameter Z_{Score} was calculated as follow:

$$Z_{Score} = \frac{x_{meas-\mu_{ref}}}{\sqrt{\sigma^2_{meas}+\sigma^2_{ref}}} \quad \text{(Eq. 2.13)}$$

, where x_{meas} is the measured value, μ_{ref} is the reference value, σ_{meas} is the standard deviation of the measured value and σ_{ref} is the reference standard deviation.

All the obtained results showed a $|Z_{Score}| \leq 2$, thus no significant differences between the reference and the values measured with a confidence level of 95 % were observed.

Table 2.4
Activity concentrations (Bq kg^{-1}) certified and measured of some reference materials analysed by alpha spectrometry. Uncertainties as standard combined uncertainty. *$|Z_{Score}| \leq 2$ (no significant differences with a confidence level of 95 %)

Reference material	Radionuclide	Reference value	Measured value	$\|Z_{Score}\|$*
IAEA-327	^{238}U	32.8 ± 1.4	30 ± 3	0.76
	^{234}U	32.4 ± 1.0	30 ± 2	1.11
	^{232}Th	38.7 ± 1.5	38.5 ± 1.5	0.10
	^{230}Th	34.1±1.7	35.5 ± 1.4	0.63
H1	^{238}U	153.88 ± 1.05	157 ± 3	0.98
C1	^{232}Th	97.09 ± 0.72	95.75 ± 1.64	0.42

The Nuclear Safety Council (CSN) organises every year an intercomparison exercise with different matrices (sediment, soil, filters, water, etc.). The results obtained in the exercises of 2016 and 2019 when a calcareous soil and deionised spiked water were analysed respectively are shown in Table 2.5. The obtained concentrations were in accordance with the reference values as can be observed.

Table 2.5
Activity concentrations of a soil (Bq kg^{-1}) and a water (Bq L^{-1}) sample analysed in inter-comparison exercises by alpha spectrometry. Uncertainties as standard combined uncertainty. *$|Z_{Score}| \leq 2$ (no significant differences with a confidence level of 95 %).

Organiser	Year	Sample	Radionuclide	Reference value	Measured value	$\|Z_{Score}\|$*
CSN	2016	Calcareous soil	^{238}U	28.6 ± 5.1	27.3 ± 1.9	0.25
			^{234}U	29.4 ± 5.2	29.8 ± 1.9	0.08
			^{230}Th	30.0 ± 5.4	30.8 ± 1.8	0.15
	2019	Spiked water	^{234}U	0.197 ± 0.037	0.196 ± 0.011	0.0
			^{235}U	0.0100 ± 0.0027	0.0100 ± 0.0020	0.0
			^{238}U	0.193 ± 0.028	0.204 ± 0.011	0.4
			^{230}Th	0.100 ± 0.013	0.100 ± 0.010	0.0
			^{210}Po	0.253 ± 0.048	0.210 ± 0.040	0.9
			^{226}Ra	1.12 ± 0.26	1.19 ± 0.08	0.3

2.3.2. Gamma spectrometry

High-resolution gamma ray spectrometry allows the identification and quantification of γ-emitting radionuclides of environmental matrices with different compositions. The measurement gives a spectrum of lines, whose amplitude is proportional to the radionuclide activity, and the position on the horizontal axis provides its energy. This method has some advantages over alpha spectrometry as it is non-destructive, detects several γ-emitting radionuclides (multi-elemental) in one spectrum, only physical preparation of the samples is required, and detection efficiency only depends on physical parameters. Otherwise, some disadvantages are found regarding alpha spectrometry as larger sample mass are required, background gamma spectrum is higher and more complicated, detection efficiency varies with gamma energy and self-absorption of gamma radiation in the sample must be considered.

The gamma spectrometry system used comprises a Canberra Extended Range coaxial Ge detector (XtRa), model GX3519, with a unique carbon thin-window (0.5 mm thick), 153 cm^3 active volume and 4 mm length from the detector to the window. Its relative efficiency in relation to a 3 x 3“ NaI(Tl) detector is 38 % and have FWHMs (Full Width Half Maximum) of 0.95 keV at 122 keV and 1.9 keV at 1330 keV. The detector is cooled by liquid nitrogen and coupled to a conventional electronic chain, including a PC-based 8K multichannel analyser and an ADC with the Genie 2000 software for data acquisition and analysis.

This detector, which is suited for low-level counting, contains very low concentrations of natural and artificial radionuclides impurities. A background reduction was achieved by a cylindrical 10 cm thick lead outer layer as a shield. The lead shield is

covered internally by a thin copper layer of 2 mm, to attenuate the X-rays generated by the interaction of the outer radiation and the lead layer.

As gamma spectrometry technique is a multi-element and non-destructive technique, the sample preparation was reduced to its drying to constant weight and grinding to homogenise the particle size. An aliquot between 20 - 50 g was placed in a cylindrical polyethylene container with a previously calibrated geometry (see next section). The samples measurements were conducted during around 48 h.

2.3.2.1. Detector system calibration

The detector system was both energy and efficiency calibrated by our research group (Bolivar et al., 1996a; Pérez-Moreno et al., 2002). Cylindrical polyethylene containers were used with 6.50 cm of diameter and a variable, between 0 and 5.0 cm, sample height. Furthermore, the self-absorption effect should be taken into account which depends on the sample characteristics (density and chemical composition), and the sample height.

The efficiency in the real sample (ε_s) was calculated by multiplying the efficiency in the calibrating sample (ε_c) by the correction factor (f), which considers the self-absorption differences between both:

$$\varepsilon_s = f \cdot \varepsilon_c \qquad \text{(Eq. 2.14)}$$

The efficiency calibration method was performed by using a standard mixed radionuclide source (IAEA-RGU-1, IAEA-RGTh-1, IAEA-RGK-1) of a known concentration of ^{238}U and ^{232}Th series radionuclides, and ^{40}K. The full energy peak efficiency ($f\varepsilon p\varepsilon$) for the calibration sample (ε_c) was determined by measuring the reference materials at different energies and heights (from 0 to 5 cm in 0.5 cm intervals).

The full energy peak efficiency was obtained according to:

$$\varepsilon_c = \frac{N}{amP_\gamma t} = \varepsilon_c(E_\gamma, h) = \varepsilon_c(E_\gamma, m_c) \qquad \text{(Eq. 2.15)}$$

,where ε_c is the full energy peak efficiency for the calibration sample, N is the net area under the photo peak of interest, a (Bq kg^{-1}) is the ^{226}Ra activity concentration in reference sample, m (kg) the sample mass for a certain height h, P_γ is the probability of emission for the considered energy ($E\gamma$) taken from tabulated data (Kocher, 1981), t is the

counting time, m_c (g) is the mass of calibration sample ($m_c = \pi r^2 \delta_c h = kh$), δ_c (g cm^{-3}) its apparent density and r (cm) the radius of cylindrical container.

The calibration procedure is detailed in Pérez- Moreno et al. (2002), being given the general relation for $f\varepsilon p\varepsilon$ in calibration sample by the equation:

$$\varepsilon_c = 14.52(E_\gamma)^{-0.95} \cdot e^{(-0.424(E_\gamma{}^{-0.138}h)} \quad \text{(Eq. 2.16)}$$

The calibration sample has an apparent density of 1.60 g cm^{-3}, the radius of the cylindrical container is 3.25 cm, h is the height of sample in cm, and E_γ, in keV, is the energy of the considered gamma emission.

The correction factor (f) due to the different self-sorption between both the problem and the calibration samples was given by:

$$f = \frac{N_1}{N_2} = \frac{1-e^{\mu\rho h}}{\mu\rho} \cdot \frac{\mu_c\rho_c}{1-e^{-\mu_c\rho_c h}} \quad \text{(Eq. 2.17)}$$

, where μ (cm^{-1}) is the self-attenuation coefficient, and ρ is the apparent density of the sample. Therefore, to calculate the μ, it is convenient to know the composition of both sample and calibration matrix.

For high energy ($E\gamma$ > 150 keV) samples containing elements with Z < 26 (Fe), the self-attenuation coefficient could be approximated to the following expression enabling to calculate the $f\varepsilon p\varepsilon$ for any energy and sample type:

$$\eta(E_\gamma) = (0.556 \pm 0.013) - (0.113 \pm 0.004)\, Ln\,(E\gamma) + (0.0059 \pm 0.0003)\,[\mathrm{Ln}(E_\gamma)]^2 \quad \text{(Eq. 2.18)}$$

2.3.2.2. Activity concentration calculations

After detector calibration, the samples were measured, and the respective gamma-spectrum acquired. The activity concentration, a, for a given gamma-emitter radionuclide can be calculated by applying the equation:

$$a = \frac{G-F-B}{mtP_\gamma\varepsilon} \quad \text{(Eq. 2.19)}$$

, where G is the total counts in the photopeak of the radionuclide of interest, determined in the sample with a counting time t; F is the number of counts in the photopeak of the radionuclide of interest observed without any sample for the counting time t; B is the background due to the Compton component, m is the mass of the sample, P_γ is the intensity of the gamma emission and ε is the counting efficiency.

The standard uncertainty of the activity concentration (σ_a), and only considering the counting errors, is given by the next equation:

$$\sigma_a = a\frac{\sqrt{G-F-B}}{G+F+B} \quad \text{(Eq. 2.20)}$$

2.3.2.3. Lower Limit of Detection (LLD) and Minimum Detectable Activity (MDA)

Another important subject in gamma spectrometry measurements is the evaluation of the Lower Limit of Detection limit (LLD). Before to determine this parameter, the background should be measured by using a similar sample to the measuring one, without a measurable amount of the target radionuclide.

The Lower Limit of Detection (LLD) is calculated according to the following equation (Currie,1968):

$$LLD = 2.72 + 3.30\sqrt{F + \sigma_F^2 + B + \sigma_B^2} \quad \text{(Eq. 2.21)}$$

, where F is the background from ambient gamma radiation but may also be affected by the presence of other radionuclides than the target one of the sample, σ_F is the standard deviation of F, B is the continuous background, mainly due to the Compton component, and σ_B is the standard deviation of B.

The continuous background (B) due to the Compton component is obtained by:

$$B = \frac{N}{2n}(B_d + B_i) \quad \text{(Eq. 2.22)}$$

, where N is the number of photons coming out from the real sample at the detector, B_d is the number of counts accumulated in the n channels before the interest peak region and B_i is the total counts in the n channels after of the interest peak region.

The standard deviation of B is calculated as follows:

$$\sigma_B^2 = \left(\frac{N}{2n}\right)^2 (B_d + B_i) \quad \text{(Eq. 2.23)}$$

, where N is the number of photons coming out from the real sample at the detector, and B_d and B_i are the number of counts accumulated in the n channels before and after of the interest peak region.

The Minimum Detectable Activity (MDA) for a particular radionuclide, is given by:

$$MDA = \frac{LLD}{tP_\gamma \varepsilon} \quad \text{(Eq. 2.24)}$$

, where LLD is the Lower Limit of Detection, t is the counting time, P_γ is the intensity of the gamma emission and ε is the counting efficiency.

Furthermore, the minimum detected activity concentration (MDAC), can be calculated by:

$$MDAC = \frac{MDA}{m} \quad \text{(Eq. 2.25)}$$

, where *MDA* (Bq) is the minimum detectable activity and m (kg) is the mass of the sample.

The estimated MDA of some of the most relevant radionuclides are as follows: ^{210}Pb = 10 Bq kg^{-1}, ^{234}Th = 15 Bq kg^{-1}, ^{226}Ra (^{214}Pb) = 2 Bq kg^{-1}, ^{228}Ra (^{228}Ac) = 5 Bq kg^{-1}, ^{228}Th (^{208}Tl) = 3 Bq kg^{-1} and ^{40}K = 20 Bq kg^{-1}.

2.3.2.4. Quality Control (QC)

As in the case of alpha spectrometry, the gamma spectrometry quality control has been performed by the analysis of replicates, blanks, certified standard materials, and the participation in national and international intercomparison exercises. The certified material IAEA-327 was also measured by gamma spectrometry, and the obtained results showed a $|Z_{Score}| \leq 2$, thus no significant differences between the reference and the measured values with a confidence level of 95 % were observed (Table 2.6).

Table 2.6
Activity concentrations (Bq kg^{-1}) certified and measured in the reference material IAEA-327 analysed by gamma spectrometry. Uncertainties as standard combined uncertainty. *$|Z_{Score}| \leq 2$ (no significant differences with a confidence level of 95 %)

IAEA-327 reference material			
Radionuclide	Reference value	Measured value	$\|Z_{Score}\|$*
^{228}Th	38.2 ± 1.0	33.5 ± 2.0	1.21
^{226}Ra	34.1 ±1.4	30.3 ± 1.8	1.36
^{228}Ra	38.7 ± 1.4	33.5 ± 2.0	1.82
^{210}Pb	58.8 ± 4.9	65.2 ± 4.0	1.04
^{137}Cs	24.9 ± 0.6	23.5 ± 1.4	0.92
^{40}K	621 ± 9	710 ± 42	1.89

Regarding to the intercomparisons, in the above CSN intercomparison (2016) several gamma emitters were also measured in the soil sample while in the worldwide open proficiency exercise (2008) organised by the International Atomic Energy Agency

(IAEA), ^{226}Ra and ^{210}Pb were measured in both spiked water and phosphogypsum samples. In both cases, the results are in accordance with the certified values, within 1σ of their nominal values (Table 2.7). The calculated Z_{Score} of each evaluated radionuclide is ≤ 2, therefore our laboratory performance was evaluated as satisfactory.

Table 2.7.
Activity concentrations (Bq kg^{-1}) of some samples analysed in inter-comparison exercises by gamma spectrometry. Uncertainties as standard combined uncertainty. *$|Z_{Score}| \leq 2$ (no significant differences with a confidence level of 95 %).

Organiser	Year	Sample	Radionuclide	Reference value	Measured value	$\|Z_{Score}\|$*
IAEA	2008	Phosphogypsum	^{226}Ra	780 ± 31	862 ± 41	1.60
			^{210}Pb	680 ± 29	633 ± 39	0.97
		Spiked water	^{226}Ra	1.93 ± 0.09	2.02 ± 0.03	0.95
CSN	2016	Calcareous soil	^{234}Th	31.3 ± 5.6	37.9 ± 8.5	1.17
			^{228}Ac	32.2 ± 3.9	34.8 ± 2.7	0.67
			^{208}Tl	10.6 ± 1.3	12.66 ± 0.86	1.62
			^{226}Ra	32.9 ± 5.9	36.1 ± 2.1	0.54
			^{214}Pb	32.5 ±3.9	36.2 ± 2.1	0.91
			^{212}Pb	33.0 ± 4.0	35.7 ± 1.8	0.68
			^{210}Pb	30.7 ± 5.5	40.3 ± 6.5	1.87
			^{40}K	361 ± 43	395 ± 19	0.79

2.3.3. ICP-OES

ICP-OES (Inductively Coupled Plasma-Optical Emission Spectrometry) is a trace-level, elemental analysis technique that uses the emission spectra of a sample to identify and quantify the elements present. Samples are introduced into the plasma in a process that desolvates, ionises, and excites them. The constituent elements can be identified by their characteristic emission lines and quantified by the intensity of the same lines.

ICP-OES is suitable for the trace elements analysis present at high concentrations (100 ppb -1000 ppm) and is used for numerous matrices of environmental samples especially for high effect-matrix samples. The advantages of using ICP-OES over other elemental analysis techniques such as Inductively Coupled Plasma-Mass Spectrometry (ICP-MS) include its wide linear dynamic range, high matrix tolerance, and the enhanced speed of analysis that can be achieved. Therefore, this technique is more robust than ICP-MS for analyzing samples as ground water, wastewater, soil, and solid waste.

Sample introduction into the ICP as liquid form is the most common technique for sample introduction, while the solid sample is converted into liquid by dissolving it into proper solvent. After acidic, aqueous dissolution, the sample is conducted by a peristaltic pump though a nebulizer into a spray chamber. Different steps when the sample is injected

to the ICP are shown in Figure 2.12. The produced aerosol is lead into an argon plasma. The plasma is generated at the end of a quartz torch by a cooled induction coil through which a high frequency alternate current flow. Consequently, an alternate magnetic field is induced which accelerated electrons into a circular trajectory. Due to collision between the argon atom and the electrons ionization occurs, giving rise to a stable plasma. The plasma shows high temperatures about 6000-7000 K, whereas in the induction zone it can even reach 10000 K. In the torch desolvation, atomization and ionizations of the sample take place. Due to the thermic energy taken up by the electrons, they reach a higher "excited" state. When the electrons drop back to ground level energy is liberated as light (photons). Each element has an own characteristic emission spectrum that is measured with a spectrometer. The light intensity on the wavelength is measured and with the calibration calculated into a concentration.

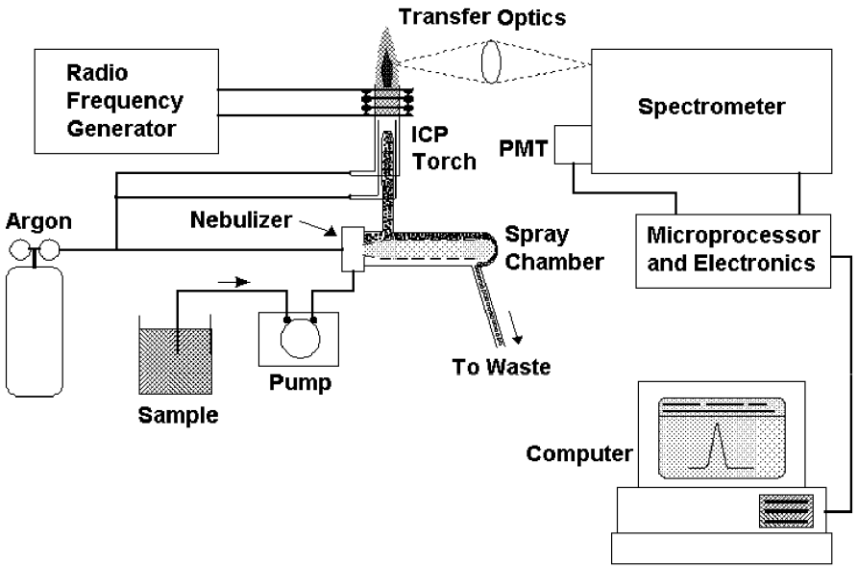

Figure 2.12. Operating principle ICP-OES (Hou and Jones, 2008).

The analysis of major and minor elements of both solid and liquid samples was carried out at the Activation Laboratories Ltd. (Actlabs, Ontario, Canada) using an ICP-OES Jobin Yvon JY ULTIMA 2 spectrometer. The quality control (QC) was developed by the measurement of Certified Reference Materials (CRMs) as well as a duplicate and a blank every ten samples. Actlabs is accredited to international standards as ISO/IEC 17025:2017 and ISO 9001:2015.

2.3.4. ICP-MS

The ICP-MS (Inductively Coupled Plasma-Mass Spectrometry) technique has a multi-element character and a high sample throughput, like ICP-OES, but it allows one

to perform more sensitive measurements, in the range from 1 ppt to 100 ppb, depending of each particular element. While ICP-OES technique measures the radiation emitted by the different atoms through an optical detector, the ICP-MS detects the ions by using the mass spectrometer based on the mass-to-charge ratio (m/z).The advantages of the ICP-MS technique above ICP are the extremely low detection limits, a large linear range and the possibility to detect isotope composition of elements. On the contrary, the disadvantages of the ICP-MS detection are the occurrence of spectral and non-spectral interferences and the high costs, and the fact that this technique is not able to measure some non-metallic elements as S, P, Ti, Sc etc., which can be determined by ICP-OES.

The operating principle of ICP-MS is shown in Figure 2.13. Like for the ICP-OES, the sample solution is introduced into the device by means of a peristaltic pump. There it becomes nebulized in a spray chamber. The resulting aerosol is injected into an argon-plasma that has a temperature of 6000-8000 K. Inside the plasma torch, solution is removed from the sample and also atomization and ionization occur. Then, these ions are sorted on account of their mass.

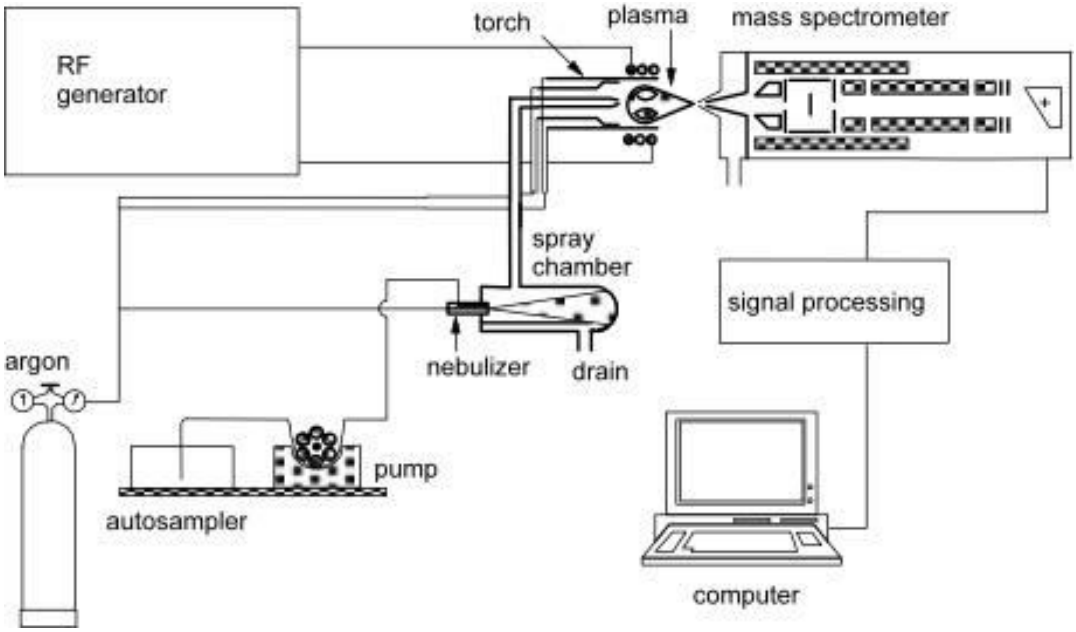

Figure 2.13. Operating principle ICP-OES (Hou and Jones, 2008).

Trace elements were determined by ICP-MS at Actlabs, using an HP branded computer model HP4500, which meet the ISO/IEC 17025 Quality System standard. The quality control (QC) included the measurement of Certified Reference Materials (CRMs) and replicates and the use of reagent blanks.

2.3.5. Laser diffraction

The particle size distribution of solid samples was determined by laser diffraction. Laser diffraction analysis, also known as Laser Diffraction Spectrometry (LDS), is a technology that utilizes diffraction patterns of a laser beam passed through any object ranging from nanometres to millimetres in size to quickly measure geometrical dimensions of a particle.

Laser diffraction analysis is based on the Mie theory and Fraunhofer approximation, stating that the intensity of light scattered by a particle is directly proportional to the particle size. The angle of the laser beam and particle size have an inversely proportional relationship, where the laser beam angle increases as particle size decreases and vice versa. Therefore, this technique measures particle size distributions by determining the angular variation in intensity of light scattered when a laser beam passes through the suspended sample in water or another liquid where the sample is not soluble. The angular scattering intensity data is then analysed to calculate the size of the particles responsible for creating the scattering pattern. The particle size is reported as a volume equivalent sphere diameter. The main components of a laser diffraction particle size analyser are shown in Figure 2.14.

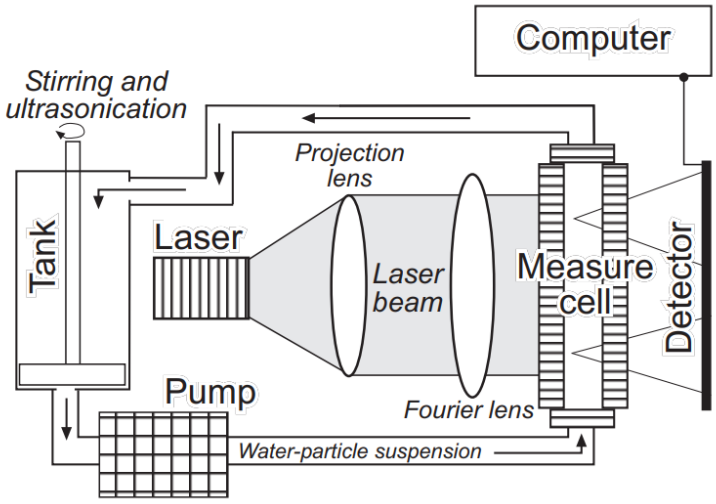

Figure 2.14. Main components of a laser diffraction particle size analyser (Storti and Balsamo, 2010).

The particle size analysis was performed in both wet and dry dispersion using a BecKman Coulter LS 13 320 with a screen between 0.01 and 10000 mm in the University of Murcia (Spain), according to the recommended procedure of the Beckman User Manual. A duplicate every set of ten samples was analysed.

2.3.6. SEM-EDS

In scanning electron microscopy (SEM), a highly energetic and focused electron beam scans the sample and normally provides an extremely enlarged image of its morphology. The beam generates a variety of signals at the surface of the solid sample. The signals that derive from electron-sample interactions reveal information about the external morphology (texture), chemical composition, and crystalline structure and orientation of materials making up the sample. In most applications, data are collected over a selected area of the surface of the sample, and a 2-dimensional image is generated that displays spatial variations in these properties. Areas ranging from approximately 1 cm to 5 μm in width can be imaged in a scanning mode using conventional SEM techniques. If an X-ray detector is incorporated, the SEM is also capable of performing analyses of the sample by using Energy-Dispersive X-Ray Spectroscopy (EDS), to obtain a qualitative and/or semi-quantitative elemental analysis at micrometer spatial resolution. A schematic representation of an energy-dispersive spectrometer can be observed in Figure 2.15.

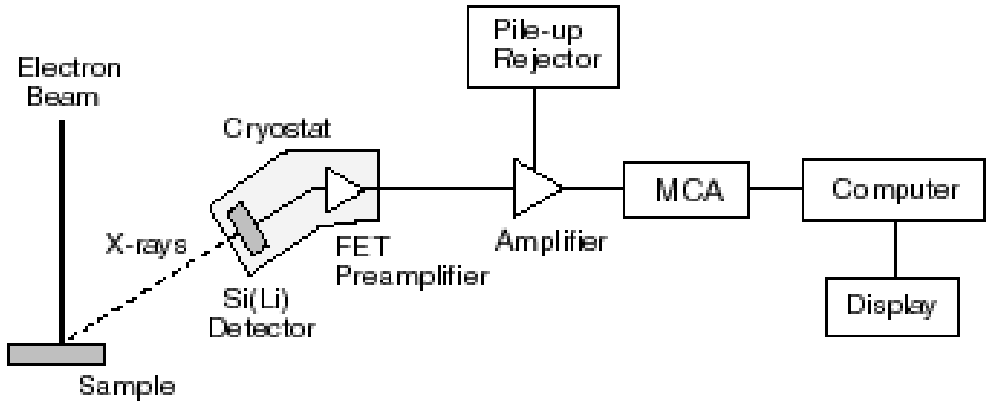

Figure 2.15. Schematic representation of an energy-dispersive spectrometer (Goldstein et al. 1981).

Accelerated electrons in an SEM carry significant amounts of kinetic energy, and this energy is dissipated as a variety of signals produced by electron-sample interactions when the incident electrons are decelerated in the solid sample. These signals include secondary electrons (that produce SEM images), backscattered electrons (BSE), diffracted backscattered electrons (EBSD), photons (characteristic and continuous X-rays) visible light (cathodoluminescence), and heat. Secondary electrons and backscattered electrons are commonly used for imaging samples: secondary electrons are most valuable for showing morphology and topography on samples and backscattered electrons are most valuable for illustrating contrasts in composition in multiphase samples. X-ray generation

is produced by inelastic collisions of the incident electrons with electrons in discrete orbitals (shells) of atoms in the sample. As the excited electrons return to lower energy states, they yield X-rays that are of a fixed wavelength (that is related to the difference in energy levels of electrons in different shells for a given element). Thus, characteristic X-rays are produced for each element in a mineral that is "excited" by the electron beam. SEM analysis is considered a "non-destructive" method due to x-rays generated by electron interactions do not lead to volume loss of the sample, so it is possible to analyze the same materials repeatedly.

The analysis of the samples was performed by using a scanning electron microscopy (SEM) JEOL (model JSM-5410) equipped with an Energy Dispersive Spectrometer (EDS) in the University of Huelva (Spain).

2.3.7. XRD

X-ray diffraction (XRD) is powerful nondestructive analytical technique primarily used for characterizing crystalline materials. The analyzed material is finely ground, homogenized, and average bulk composition is determined. It provides information on structures, phases, preferred crystal orientations (texture), and other structural parameters, such as average grain size, crystallinity, strain, and crystal defects.

This technique works by irradiating a material with incident X-rays and then measuring the intensities and scattering angles of the X-rays that leave the material. These incident X-rays are generated by a cathode ray tube, filtered to produce monochromatic radiation, collimated to concentrate, and directed toward the sample. The interaction of the incident rays with the sample produces constructive interference (and a diffracted ray) when conditions satisfy Bragg's Law (Eq. 2.27):

$$n\lambda = 2d \sin \theta \qquad \text{(Eq. 2.26)}$$

, where λ is the wavelength of the rays, θ is the angle between the incident rays and the surface of the crystal, d is the spacing between layers of atoms and n is the order of diffraction integer (integer number). The key component of all diffraction is the angle between the incident and diffracted rays.

This law relates the wavelength of electromagnetic radiation to the diffraction angle and the lattice spacing in a crystalline sample. These diffracted X-rays are then detected, processed and counted. By scanning the sample through a range of 2θ angles, all possible

diffraction directions of the lattice should be attained due to the random orientation of the powdered material. Conversion of the diffraction peaks to d-spacings allows identification of the mineral because each mineral has a set of unique d-spacings. Typically, this is achieved by comparison of d-spacings with standard reference patterns.

X-ray diffractometers consist in an X-ray tube where electrons are produced and accelerated onto the target (Fig. 2.16). When electrons have sufficient energy to dislodge electrons of the target material, characteristic X-ray spectra are produced. The specific wavelengths are filtered by a crystal monochromator to produce monochromatic X-rays. These X-rays are collimated and directed onto the sample, placed in a sample holder. The refracted X-rays are detected by the counter. In addition, the X-ray tube and X-ray detector are installed in a rotation system around the sample holder.

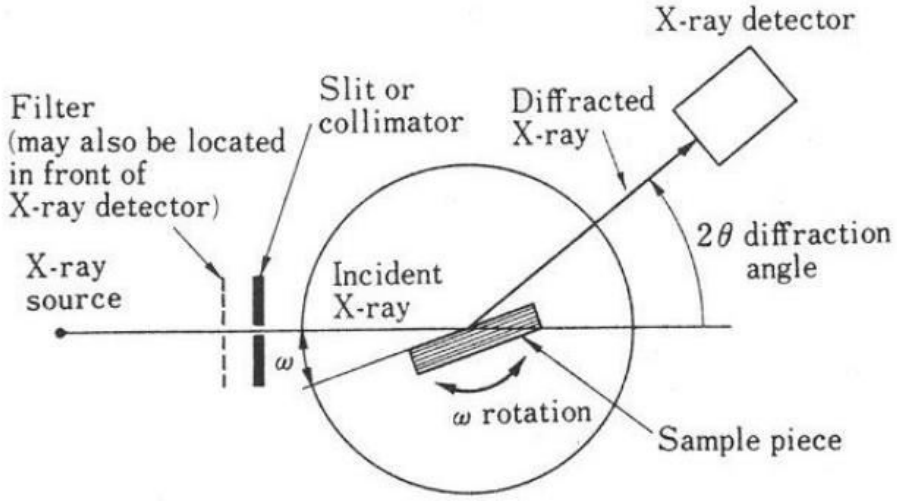

Figure 2.16. Schematic representation of an X-ray diffractometer (Kikuchi, 1990).

The characteristic x-ray diffraction pattern generated in a typical XRD analysis provides a unique “fingerprint” of the crystals present in the sample. When properly interpreted, by comparison with standard reference patterns and measurements, this fingerprint allows identification of the crystalline form.

This technique was performed in the University of Murcia by using a Philips X'Pert spectrometer with Cu target, equipped with a PDP 11/23 processor with 10 Mb Winchester and two 400 Kb minifloppys, VT220B terminal and Philips X'Pert graphic printer and software developed by Philips Electronics NV 1996-1999 (version 1.2d).

Diffractometer settings were 45 kV, 40 mA, a scan range of 3.02 - 69.98° (2θ) with a step size of 0.02º and a counting time of 1 s per step. Under these measurement

conditions, the detection limit was around 5%. The analyses were performed in triplicate to ensure reproducibility of the results.

The sample was grinded in a ball mill to a fine powder, less than 50 μm, and deposited into the aluminum sample holder. Then, the sample was compacted with a solid piston to make it homogeneous and firm, being subsequently introduced into the sample carriage available in the diffractometer.

The interpretation of the diagrams was carried out using the Philips X´Pert Grafics and Identify program, belonging to the RX Philips PW3040 software, comparing the peaks of the diagram with those of the mineral of interest in the program's database.

2.4. DATA TREATMENT

2.4.1. XLSTAT

XLSTAT is a suite of statistical add-ins for Microsoft Excel to enhance its analytical capabilities. The XLSTAT software relies on Microsoft Excel for the input of data and the display of results. Computations are done using autonomous software components that are optimized for speed and efficiency. The XLSTAT results are benchmarked against other statistical packages to have reliable findings. This statistical add-in offers a wide range of statistical and data analysis functions, ranging from descriptive statistics to multivariate data analysis. This software was used in this Thesis to perform box and whiskers plots and Principal Component Analysis (PCA).

Chapter 3
Results and discussion

3.1. POLLUTION EVALUATION ON THE SALT MARSHES UNDER THE PHOSPHOGYPSUM STACKS OF HUELVA DUE TO DEEP LEACHATES

J. L. Guerrero, I. Gutiérrez-Álvarez, F. Mosqueda, M. Olías, R. García-Tenorio and J. P. Bolívar

Chemosphere 230 (2019) 219-229, IF: 5.778 (2019), Category: environmental sciences, Quartile: Q1, Position: 29/265.

Graphical abstract

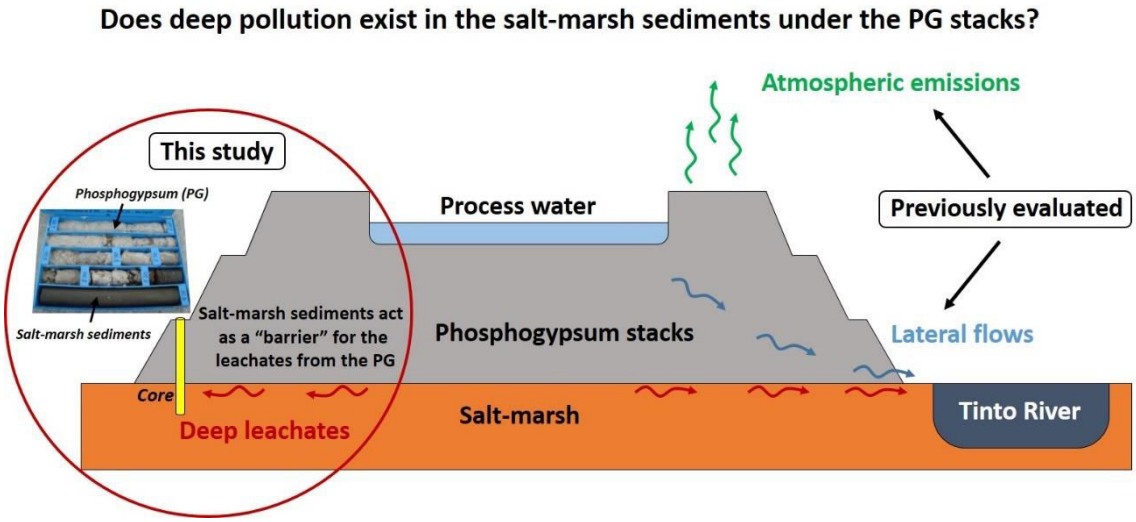

Abstract

In the salt marshes of the Tinto River (Huelva estuary, SW Spain), are stored in stacks around 100 Mt of PG, covering a surface of 1000 ha without any type of isolation, which produce an important impact in the surrounding environment. On the other hand, this ecosystem it is affected by acid mine drainage (AMD) from sulphide mines located upstream the Tinto River.

The aim of this study is to evaluate the deep pollution of the underlying salt marsh sediments due to leachates from the PG stacks. For that purpose, 7 cores were collected from zones 2 and 3 of the stacks, and PG and salt marsh sediments samples from different depths were analyzed. The physicochemical parameters, mineralogy, granulometry and the concentration of the main elements of interest were determined in the samples.

Most analysed salt marsh sediments are not affected by PG stacks pollution, because sediments act as a "barrier" for the leachates from the PG, concentrating the contaminants in the first decimetres (0.5 m) under PG-sediments contact, and the deep infiltration is very limited. The obtained results suggest that the perimeter channel which is projected to build in the restauration project, should has a depth of 1m below the level of the PG

stacks for assuring the complete collection of leachates from the stacks, and avoid their liberation into the Tinto River estuary.

Keywords: phosphogypsum; pollution; salt marsh; Tinto River estuary.

3.1.1. Introduction

The Huelva estuary, formed by the Tinto and Odiel rivers common mouths, is a 25 km long incised valley on the southwestern coast of Spain, underlying by Neogene sandy-silty sediments. It is an ecosystem of special concern because of it is strongly affected by both an acid mine drainage (AMD) from sulphide mines located upstream of both the Tinto and Odiel rivers (pH around 2-3 is measured along these rivers), and secondly due to a chemical industrial complex and phosphogypsum (PG) waste stacks located at their surroundings. As consequence its waters and sediments are highly polluted by heavy metals and radionuclides coming from both the AMD and the leachates inputs from the PG stacks.

Several works have been published for evaluating the pollution of the Odiel-Tinto estuary by heavy metals (HM), natural radionuclides (NRN), and other chemical species due to AMD (Martín et al., 2002; Cánovas et al., 2007; Nieto et al., 2007; de la Torre et al., 2011). In the estuary, the acidic river waters increase the pH to neutral values due to mixture with seawater producing precipitation of high amounts of metals in solution and accumulation in the estuarine sediments (Santos-Bermejo et al., 2003, Hierro et al., 2014a,b).

On the other hand, on the right salt marshes of the Tinto River estuary a big phosphogypsum (PG) waste repository is located, covering about 1000 ha. The worldwide PG generation is estimated up to 280 Mt per year (Yang et al., 2009), and it is mainly disposed without any treatment usually by dumping in big stacks generally located in coastal areas near the production plants. PG is mainly composed by gypsum ($CaSO_4 \cdot 2H_2O$), being generated in the production of phosphoric acid (H_3PO_4) based on the wet chemical attack of phosphate rock ore (in the case of Huelva fluorapatite ($Ca_5(PO_4)_3F$) was used, with sulfuric acid (H_2SO_4).

The process can be summarized in the following general reaction (Eq. 3.1):

$$Ca_5(PO_4)_3F + 5H_2SO_4 + 10H_2O \rightarrow 3H_3PO_4 + 5CaSO_4 \cdot 2H_2O + HF \qquad \text{(Eq. 3.1)}$$

From 1968 to 2010 the five acid phosphoric factories located in Huelva processed annually about $2 \cdot 10^6$ t of phosphate rock, which mainly came from Morocco (Bolívar et al., 1996a), and produced approximately $2.5 \cdot 10^6$ t of PG (Bolívar et al., 2002). The PG was transported and disposed as an aqueous slurry in huge, aboveground stockpiles, without any prior treatment, forming stacks on the salt marshes of the right bank of the Tinto River without any type of isolation, less than 1 km from the Huelva city, accumulating about 100 million tones. Until 1997, when the management policy changed following the OSPAR convention (OSPAR, 2002, 2007), the PG was pumped by using seawater in an open circuit and around 20% of PG was directly released into the Odiel River estuary. Since 1998 to the end of 2010 the PG was pumped with freshwaters in a closed circuit, and all the PG wastes should be stored in stacks with no discharges into the marine environment.

Phosphate rock contain metal(oid)s and U-series radionuclides as impurities that are released during the dissolution of the phosphorite in the digestion step of the phosphoric acid (PA) industrial production process, remaining these species distributed between both PA and PG fractions. The majority of Ra, Pb and Po remains in PG (>95%), while less than 20% of U and around 70% of Th are bound to PG (Guimond and Harding, 1989; Bolívar et al., 1996a, 2009). These wastes are currently considered a NORM (Naturally Occurring Radioactive Material) material due to the high natural radionuclide concentrations of the ^{238}U series of the raw material (IAEA, 2003, 2013/59/Euratom). In addition, the residual phosphoric acid trapped in the interstices of PG particles explains the acidic nature and the high contaminant potential under leaching conditions of this waste (Pérez-López et al., 2010; Pérez-Moreno et al., 2018). Consequently, the market for the reuse of this waste is very limited and, hence, its production leads to stacking in large disposal areas close to phosphoric acid plants, where PG is often exposed to weathering conditions and may cause serious environmental impacts (Tayibi et al., 2009).

The PG stacks of Huelva and its pathways of contamination into the environment (atmospheric and lateral flows), has been previously studied in many works. The potential atmospheric impact of these stacks has been analysed by several studies (Dueñas et al., 2007; Borrego et al., 2007; Abril et al., 2009; Lopez-Coto et al., 2014; Hernandez-Ceballos et al., 2015), concluding that both the impact as a source of ^{222}Rn and radioactive particulate matter it is negligible. On the other hand, the lateral contamination mainly caused by the leachates emerging as edge outflows had been intensively studied and

especially in recent years. The analysis of the concentration and behaviour of metals and radionuclides in the waters and surface sediments of the estuarine system showed the impact of the stacks due to the increase of this species in the surrounding environment (Bolívar et al., 2002; Villa et al., 2011; Hierro et al., 2013; Gázquez et al., 2014; Perez-López et al., 2015, 2016; 2018; Cánovas et al., 2018; Papaslioti et al., 2018). Related to this last problem, the authorities, in collaboration with the responsible companies, are currently under design and approval of a project for the environmental remediation of them.

Despite the large number of studies developed in this area, none of them has analysed the impact in the salt marshes directly under the PG stacks. It may highlight that the stacks were disposed directly on the salt marshes without any impermeable barrier to prevent infiltration, in this way it is very important to know the possible existence of deep leachates into the sediments under the stacks and, if so, the degree of affection. Furthermore, the phosphogypsum stacks of Huelva are the most studied worldwide and the results obtained provided useful information to evaluate the pollution pathways and developed restoration methodology to others NORM repositories.

Taking into account the previous facts, the main objective of this work is to characterize the salt marshes under the PG stacks in order to determine the possible deep migration of contaminants from the PG stacks.

3.1.2. Study area

Currently, four zones are clearly recognized within the study area (Fig. 3.1). Zones 1 (located to the south) and 4 (located to the north) are considered to be already restored. Zone 1 show a surface about 400 ha and was restored covering it with a 30 cm layer of natural soil and vegetation (Más et al., 2001). In Zone 4, which show a surface of around 150 ha, the restoration was more complex and comprises the following layers (in ascending order): a 1m layer of building wastes, a 2 m layer of theoretically inert industrial wastes and more than 50 cm of topsoil (Más et al., 2006a, b). By that reasons these zones were not included in this work.

In Zones 2 and 3, the uncovered PG is directly exposed to the environmental weathering and show surface ponds of industrial process acidic water (green colours in Fig. 3.1), which are actually under drying process towards the restoration project. In Zone 2 accumulates about 25 Mt of PG and covers over 250 ha. The PG deposition in this area

can be divided into two different moments in time. Until 1997, a 5m in height PG pile was formed above the salt marsh, transporting by seawater in open circuit. With the change in the management policy, since 1998 to 2010 all the PG produced was stored in this zone over the previous pile using a close circuit with freshwater, forming a pyramidal pile of up to 30 m high. A network of perimeter channels surrounds this zone in order to collect leachates from the stack. Zone 3 (15 Mt; 200 ha and an average of 6m in height) is a sector where PG was disposed previously to 1997. Since then, this zone has been used to store process water in a central pond that is part of the closed-circuit freshwater system installed after the change of management policy. This zone has been subject to weathering and no preventive measures have been adopted, being the most affected sector.

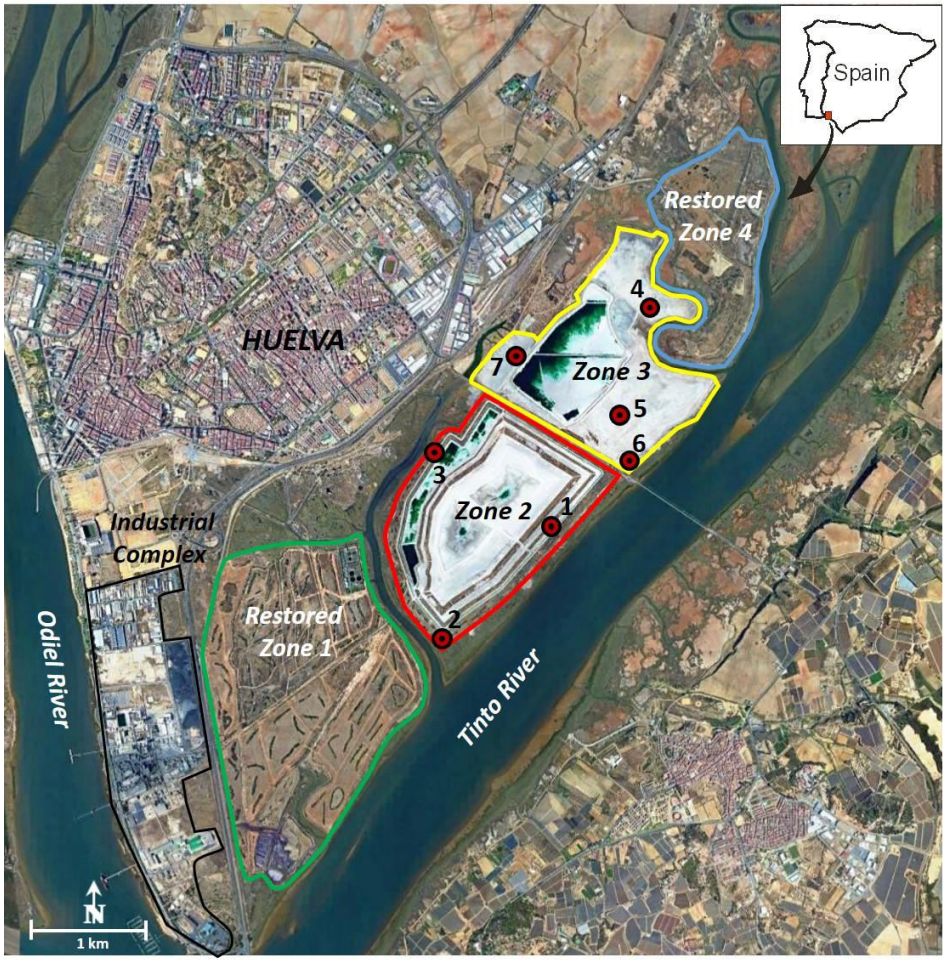

Figure 3.1. Study area of the Huelva phosphogypsum stack on the salt marshes of the Tinto River, defining the different zones and locating the 7 collected cores.

3.1.3. Material and methods

In order to determine the potential pollution of the PG stacks into the underlying salt marshes, 7 cores were collected in November 2009; 3 from the Zone 2 and 4 from Zone 3 (Fig. 3.1). In Table 3.1, a summary of the number and type of samples is shown.

Table 3.1
Location, depth and number of samples taken from the cores.

Core	Zone	UTM (WGS89)	Total depth (m)	Sediment samples	PG samples
1	2	29 S 685500.10, 4124308.75	15	8	4
2	2	29 S 684532.11, 4123293.78	15	13	2
3	2	29 S 684456.12, 4124971.76	16	9	3
4	3	29 S 686257.11, 4126285.73	15.8	12	3
5	3	29 S 685947.11, 4125146.74	18	11	5
6	3	29 S 686101.10, 4124858.74	14	15	5
7	3	29 S 685089.12, 4125768.75	13.2	14	6

Core recovery was very high, and the core material was only moderately disturbed and fragmented; consequently, there is no uncertainty in depth control (Fig. 3.2). A total of 110 samples, 28 PG samples and 82 sediments samples, were taken. The samples were codified with a "XYZ" code, where "X" is the core number (1-7), "Y" represents the type of material ("P" for phosphogypsum, and "S" for sediment), and "Z" is related with the order in depth of the samples, listing separately the PG and sediment samples in order to know the relative distance to the contact. The samples, 5 cm length and 9 cm diameter, were selected from different depths, but while PG samples were taken homogenously covering the full PG column, the sediment samples were selected in general covering the first meter under the contact in order to study the degree of affectation of the salt marsh sediments due to possible deep leachates from the stacks.

Figure 3.2. PG-sediment contact zone in the core 5.

The samples were analysed for the determination of the physicochemical parameters (pH and EC), mineralogy, granulometry and the concentration of the main elements of interest. A portion about 50 g of sample was selected for the pH and EC determination. These portions were previously air drying, and then the fine fraction (<2 mm) was

separated. In this fine fraction the pH and EC were measured by 1:2 (sample:water) mix. Another 50 g portion of the samples was preserved for the analysis of the granulometric fractions which were determined by mean of a laser diffraction particle size analyzer BecKman Coulter LS 13 320 with a screen between 0.01 and 10000 mm, according with the recommended procedure of the Beckman User Manual. Three duplicates were analysed in total.

For the mineralogical and chemical analysis, a portion of about 30 g were dried in the oven at 60 ºC to a constant weight within the first 24 h of the collection. The dried samples were grinded by a ring mill and after that mechanically homogenized. The dried and grinded samples were preserved in labelled plastic bags to avoid the alteration until the analysis. Mineralogical composition of the samples was determined by X-ray diffraction by mean of a Philips X'Pert spectrometer and the associated software. Chemical analysis for major and trace elements were performed on the bulk samples by ICP Mass in the Activation Laboratories (Actlabs) from Canada. The quality control (QC) was conducted by the analysis at the beginning and end of each batch of samples of certified standard reference materials (USGS GXR-1, GXR-4 6, OREAS 45d SdAR-M2). Internal control standards are analysed and a duplicate is run for every 10 samples.

3.1.4. Results and discussion

3.1.4.1. Mineralogy

A statistical summary of the mineral composition of the samples is listed in Table 3.2. The mineralogical composition of 20 PG samples and 46 selected sediment samples was determined. As expected, the PG samples are composed almost completely by gypsum (mean value = 95%), ranging from 93% to 97%. With respect to sediment samples, silicate minerals group are dominant, with a mean percentage above 80% in most of the samples. The main silicates are quartz (12-91%), illite (3-57%), plagioclase (10-32%) and chlorite (5-16%). The iron oxides are represented by hematite and goethite. The first one, was found in 27 of the samples ranging from 1.0 to 15%, while the second one only appears in 5 samples with a range from 5 to 16%. The existence of these iron oxides in the sediments could be related with the AMD affecting the Tinto River. Calcite was found in 10 of the samples, ranging from 1 to 25% (mean value = 10%), in some samples it was found as carbonates nodules. In the sample 7S2, located between 15 and 20 cm under the PG-sediment contact, vivianite was found with a concentration of 15%.

This iron phosphate seems to indicate the formation of a new mineral in the interphase PG-sediments.

Table 3.2
Mineralogical composition of the samples. Concentration in %. *Other minerals in low proportions. Gp: gypsum; Chl: chlorite; Ill: Illite; Qtz: quartz; Pl: plagioclase; Hem: hematite; Cal: calcite; Hbl: hornblende; Gt: goethite; Viv: vivianite.

	PG		Sediments										
	Gp	Others*	Gp	Chl	Ill	Qtz	Pl	Hem	Cal	Hbl	Gt	Viv	Others*
N	20	20	11	42	46	46	40	27	10	5	5	1	46
Mean	95	4.6	20	9.2	17	36	20	4.9	9.9	9.0	12	15	8.8
Min.	93	3.0	6.0	5.0	3.0	12	10	1.0	1.0	6.0	5.0	15	3.0
Median	96	4.0	14	9.0	15	34	22	4.0	8.5	8.0	15	15	7.0
Max.	97	7.0	42	16	57	91	32	15	25	14	16	15	48
SD	1.1	1.1	12.6	2.5	11.3	14.4	5.7	3.0	7.1	3.0	4.7	-	6.8

Finally, gypsum appears in 11 of the sediment samples, with a minimum of 6% and a maximum up to 41%. Most of these samples are located up to 50 cm under the PG-sediment contact, and the concentration of this mineral is probably due to mechanical mixing process with the PG from the stacks, producing contamination of these sediments. In some deeper samples (>4 m under the contact), high concentrations of gypsum can be found, which was formed by natural processes.

3.1.4.2. Granulometry

The particle size of 10 PG and 23 sediment samples were determined (Fig. 3.3). The PG samples show in general the same grain size distribution with one high peak between 10 and 100 mm, being composed by silts and fine sand particles. The ISO 14688-1:2017 was used to classify the grain size fractions: Gravel (>2 mm), coarse sand (630-2000 μm), medium-sand (200-630 μm), fine sand (63-200 μm), silt (2-63 μm) and clay (<2 μm). Sediment samples show a wider size particle range compared to the PG. In general, two peaks are observed at particle size intervals of 0.05-0.2 μm (clay fraction) and 2-20 μm (silt). On the other hand, there are sediments samples with coarser particles, showing higher proportions of sands from fine to coarse, some of them located in the first decimetres under the contact zone (1S1, 1S2, 3S1, 3S2, 5S1, 7S1 and 7S2). This is significant because, while fine sediments (silts and clays) show a very low permeability values, these coarser sediments would have higher permeability values (Shepherd, 1989), and due to the location near the contact zone, could allow the migration of contaminants from the PG to the underlying sediments.

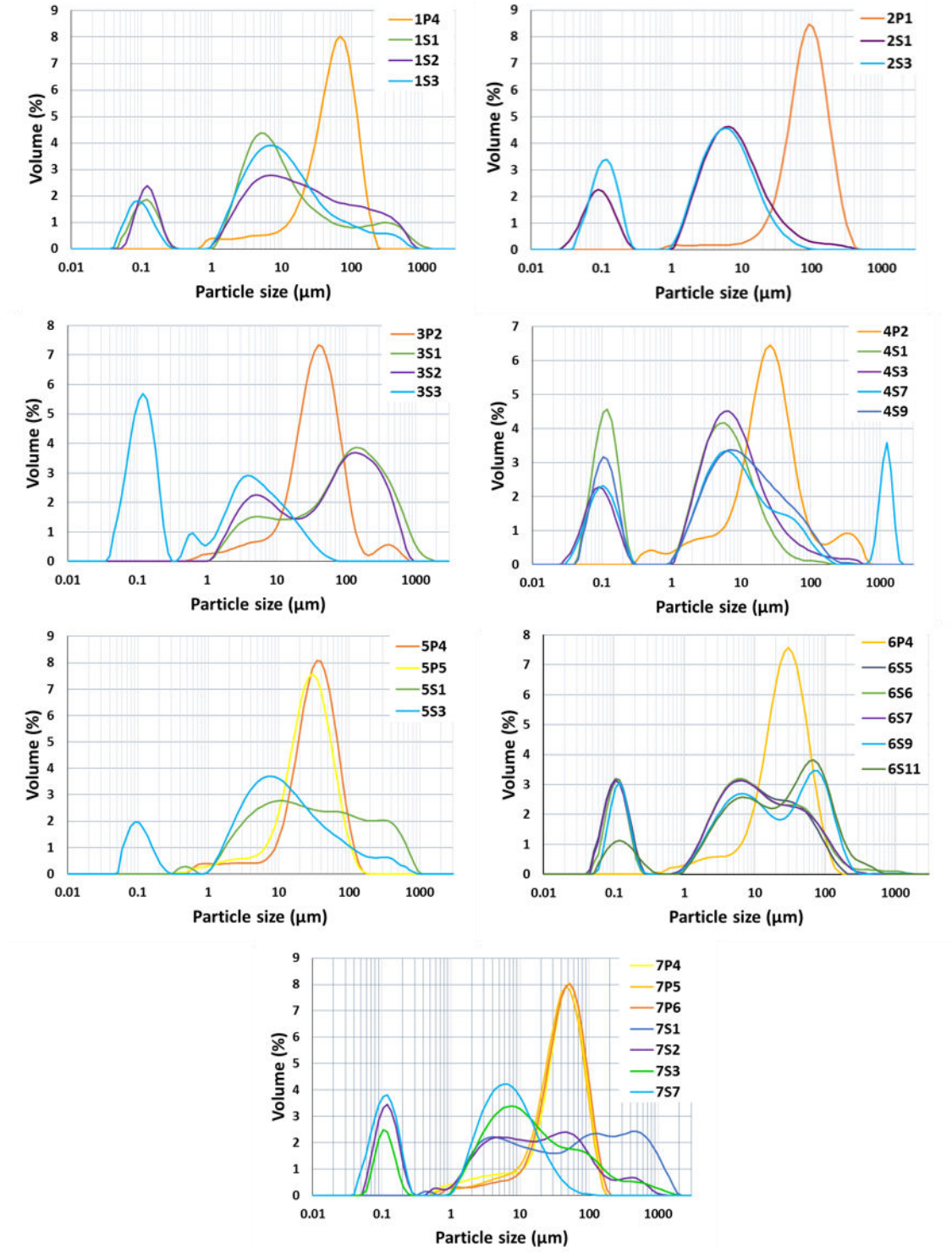

Figure 3.3. Particle size of sediments and PG samples.

3.1.4.3 Physicochemical parameters

A statistical summary of the physicochemical parameters results for the PG and sediments samples are listed in Table 3.3. The pH was determined in 20 PG samples and shows in general similar values regardless of the core location and depth, with a mean value of 2.9 ± 0.2. The uncertainty is given as the standard deviation of the mean,

SD/N1/2, with N being the number of data and SD the standard deviation of the samples set. These values demonstrate the acidity presented by the PG, due to the residual acids (mainly phosphoric acids), which remain between the PG particles after the industrial process.

Table 3.3
Statistical summary of the pH and EC values in the PG and sediments in the different cores.

Core	Material	pH				EC ($mS \cdot cm^{-1}$)			
		N	Mean	Range	SD	N	Mean	Range	SD
1	PG	4	3.1	2.4-4.3	0.9	4	12.3	4.5-17.6	6.3
	sediments	5	7.2	5.9-8.0	0.8	5	16.7	13.8-21.9	3.3
2	PG	1	2.9	-	-	1	13.7	-	-
	sediments	8	7.0	5.0-7.9	0.6	8	16.5	12.6-22.4	3.2
3	PG	2	3.3	2.5-4.1	1.1	2	9.7	4.1-15.3	7.9
	sediments	7	6.3	4.0-7.9	1.5	7	23.6	18.0-31.9	6.5
4	PG	2	4.2	3.8-4.7	0.7	2	8.2	1.1-15.3	10
	sediments	5	7.4	6.1-8.3	0.8	5	25.3	10.0-33.4	10
5	PG	4	2.6	2.5-2.7	0.12	4	12.3	6.1-15.9	4.3
	sediments	8	6.8	5.2-8.0	1.1	8	19.1	15.2-23.1	2.4
6	PG	3	2.6	2.3-3.0	0.4	3	5.3	1.9-9.8	4.1
	sediments	6	8.0	7.4-8.2	0.3	6	17.7	12.4-24.1	4.4
7	PG	4	2.3	2.3-2.3	0.10	4	11.0	10.4-12.6	1.1
	sediments	8	7.3	5.5-8.3	0.9	8	16.0	6.5-24.4	7.6
Total	PG	20	2.9	2.3-4.7	0.7	20	10.4	1.1-17.6	5.2
	sediments	47	7.1	4.0-8.3	1.1	47	19.0	6.5-33.4	6.3

On the other hand, the 47 sediment samples showed in general neutral pH, with a mean of 7.1 ± 0.8. The minimum value was 4.0 (sample 3S2, affected by the leaching from PG) while the maximum rise to 8.3. These higher acidity values of some sediment samples are clearly related to the influence of the PG on the sediments closer to the contact, as discussed below.

In Figure 3.4, the depth profiles of pH and EC for the 7 cores are shown. The PG-sediment contact is located at different depths according to the PG thickness of the stack but for representing the depth profiles we considered the contact as “0 m depth”, being positive the values for PG samples and negative for sediments samples. In this way, the comparison between the cores is clearer. As Figure 3.4A shows, the pH increases from around 3 (PG samples) to approximately 7 (sediments), finding intermediate acid values in the first 50 cm of sedimentary column due to the influence of the PG.

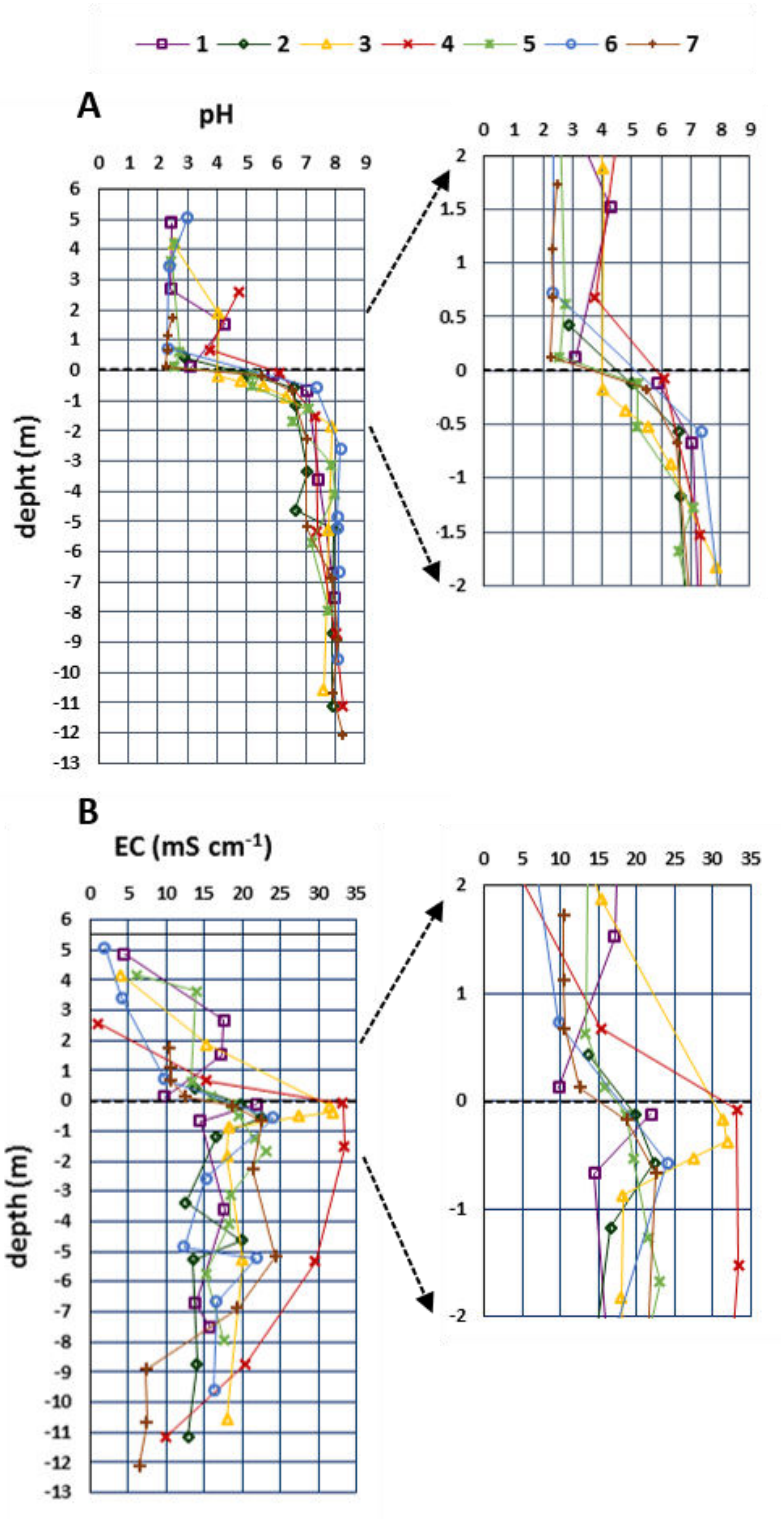

Figure 3.4. Depth profiles of pH and EC for the seven cores. Zero depth represents the contact between PG and sediments.

The PG shows an EC mean value of 10.4 ± 1.2 mS cm^{-1}, ranging from 1.1 (core 4) to 17.6 mS cm^{-1} (core 1), while for the sediments the mean value was 19.0 ± 1.0 mS cm^{-1}, with a minimum of 6.5 mS cm^{-1} (core 7), and a maximum of 33.4 mS cm^{-1} (core 4). By considering the standard uncertainties, it can be affirmed that mean EC of the sediments

is higher than the PG ones. The EC shows a certain degree of dispersion both among the different cores and between the cores in depth (Fig. 3.4B). In the case of PG, an increase in the EC values is observed with depth probably related with the weathering and washing of the more superficial PG. In addition, other factors involved in the differences between the EC of PG samples are the year of PG production, variations in the industrial process, original characteristic of the raw material etc., while in the sediments samples the heterogeneity is related to the complexity and heterogeneity of the estuarine system and the different conditions of sedimentation.

3.1.4.4. Chemical composition

Phosphogypsum

The concentration of the major (%) and trace elements (ppm) in PG samples, as well as a comparison of those same elements in PG from the same sedimentary origin is shown in Table 3.4.

The major elements with higher mean concentration in the PG samples, as expected, are Ca (24.3 ± 0.6%), followed by S (19.5 ± 0.5%). The concentration of P also shows a high value (mean = 0.35 ± 0.05%) which is due to the concentration of this element in the raw material (phosphorite). Other major elements with significant concentrations are Na (0.41 ± 0.06%), and Fe (0.15 ± 0.10%). In these PG samples, most of the major elements show similar concentrations to those reported by authors in PG obtained from sedimentary phosphate rocks from other locations, however, contents of Fe and Na are higher while Ti shows lower values in our samples (Table 3.4).

Table 3.4
Mean value and range of element concentrations in PG samples of this study as well as mean values of other PG of sedimentary origin from other locations. The sites are the origin of the phosphate rock used as raw material. [a]El Zrelli et al. (2018), [b]Rutherford et al. (1994).

Elements	This study (Morocco)		Tunisia[a]	Florida[b]	Idaho[b]
Al (%)	0.07 ± 0.01	0.03 - 0.16	0.032 ± 0.005	0.095	0.12
Ca (%)	24.3 ± 0.6	21.2 - 27.1	26.4 ± 2.6	-	-
Fe (%)	0.15 ± 0.10	0.01 - 1.2	0.091 ± 0.001	0.084	-
K (%)	0.019 ± 0.004	0.005- 0.05	0.025 ± 0001	0.025	0.066
Mg (%)	0.04 ± 0.01	0.02 - 0.08	0.042 ± 0.006	0.03	-
Na (%)	0.41 ± 0.06	0.11 - 0.70	0.037 ± 0.001	0.022	0.022
P (%)	0.35 ± 0.05	0.22 - 0.73	0.49 ± 0.05	0.37	0.59
S (%)	19.5 ± 0.5	17.0 - 21.7	15.0 ± 1.5	-	-
Ti (%)	0.010 ± 0.001	0.004 - 0.017	-	0.062	0.044
As (ppm)	16 ± 7	0.5 - 83	1.0 ± 0.1	0.4	0.6
Ba (ppm)	56 ± 8	21 - 111	10.0 ± 0.7	43	47
Cd (ppm)	1.8 ± 0.4	0.8 - 4.4	17.7 ± 1.8	< 0.2	10.7
Cr (ppm)	16 ± 3	8 - 36	13.0 ± 1.3	5	48
Cu (ppm)	32 ± 11	1.3 - 113	9.6 ± 1.4	3.4	11.4

Elements	This study (Morocco)		Tunisia[a]	Florida[b]	Idaho[b]
Li (ppm)	0.25 ± 0.03	0.05 - 0.4	0.30 ± 0.03	<1	-
Ni (ppm)	1.6 ± 0.6	0.05 - 6.1	4.10 ± 0.41	5	5
Pb (ppm)	36 ± 31	0.6 - 344	0.90 ± 0.09	10	13
Sb (ppm)	2.8 ± 2.3	0.1 - 23.9	0.09 ± 0.01	10	13
Mn (ppm)	15 ± 2	4 - 20	< 5	-	-
Sr (ppm)	420 ± 102	193 - 1320	390 ± 43	750	660
Th (ppm)	0.9 ± 0.2	0.2 - 2.1	0.74 ± 0.07	1.5	-
U (ppm)	12 ± 2	2.8 - 28	1.6 ± 0.16	4.5	7.3
V (ppm)	6.3 ± 2.4	2 - 28	3 ± 0.3	6	20
Zn (ppm)	22 ± 8	2 - 98	137 ± 13.7	6.4	30.7
Y (ppm)	50 ± 4	30 - 78	53.2 ± 8.0	71	125

In relation with trace elements, the high concentration of Ba (mean = 56 ± 8 ppm) and Sr (mean = 420 ± 102 ppm) is due to the fact that Ca may be substituted in gypsum by this elements due its similar chemical behaviour. Y, commonly considered as an REE due to its similar properties to those of the lanthanide series, also shows a high mean concentration in PG (50 ± 4 ppm) but significantly lower than previous studies which showed a mean concentration around 150 ppm (Martín et al., 1999; Rentería-Villalobos et al., 2010).

In these PG samples, most trace elements show similar concentrations to those reported in PG obtained from sedimentary phosphate rock. However, contents of As (mean value = 16 ± 7 ppm), Cu (32 ± 11 ppm) and U (12 ± 2 ppm) are higher in our PG (Table 3.4). On the other hand, Cd shows a mean value (1.8 ± 0.4 ppm) lower than the one observed in PG from Tunisia and Idaho. The high mean value of Pb (36 ± 31 ppm), is due to high concentration of this element in the sample 1P4 (344 ppm), which is located near the contact with the salt marsh. The rest of the samples showed in general values below 10 ppm.

Rentería-Villalobos et al. (2010), analysed 10 surface PG samples from the same factories of Huelva, and the concentrations found were similar to this study in most cases by considering the standard uncertainties of the average values.

Sediments

In Figure 3.5 the concentration depth profile in salt marsh sediments of some selected elements measured in the first meter below the contact is shown. To point out that the concentration of these elements in deeper samples (>1 m) show similar values than non-polluted sediments of the first meter, and by that reason are not shown in Figure 3.5. Ca shows an intense decrease in the concentration below the contact (Fig. 3.5A), from values

above 20% in PG to values below 5% in the sediments for depths higher than 10-15 cm, indicating that mechanical mixing between PG and sediments is only produced in the first centimetres, showing this fact the low mobility of this element in the sediments.

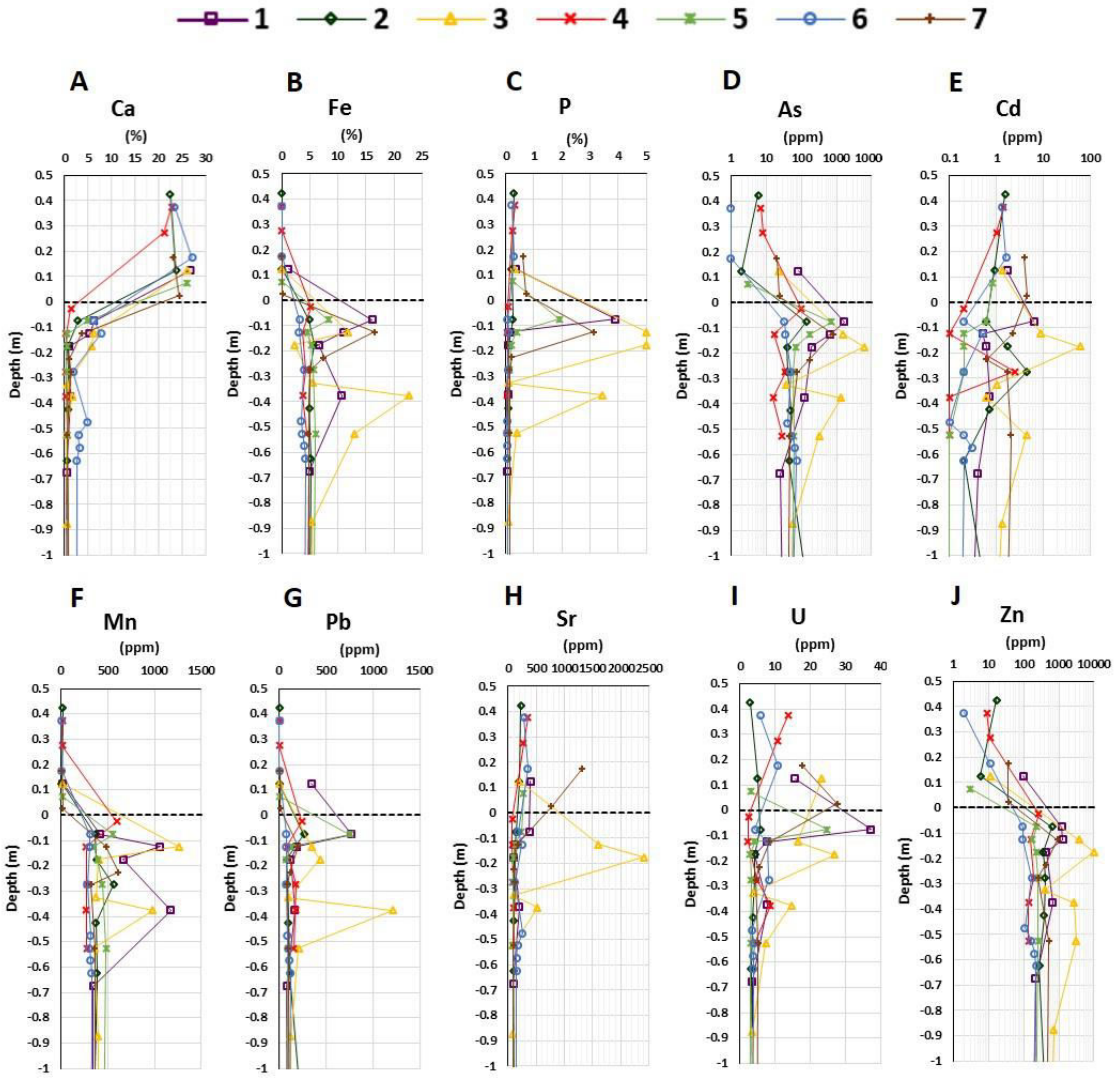

Figure 3.5. Depth profiles of some elements, only the zone close to the PG-sediment contact is shown.

On the contrary, the phosphorus (P), is the most mobile element contained in the PG pile since the P is dissolved in the porewater of the PG as phosphoric acid. Perez-López et al. (2015), reported a mean concentration of this element of 1950 ± 170mg L^{-1} in edge outflows from zone 3, being this value 6 orders of magnitude higher than unperturbed freshwater (≈ 10^6 times) (Wetzel, 2001). On the other hand, the concentration of this element in the salt marsh is similar to unperturbed sediments, since the AMD does not increase its concentration, and therefore, the P is a very good tracer for evaluating the potential impact of the PG piles on the underlying sediments. In Figure 3.5C it is observed that enhanced P concentrations are measured up to 20 cm, reaching 50 cm only in the

core 3, showing this fact the low affection on the sediments by in depth leachates from the stacks. This result leads us to consider the hypothesis that in general the flow below the PG-sediment interface is almost horizontal and restricted to a depth of less than 50 cm. This results is very relevant for the design of the restauration project, and suggest that the perimeter channel which is projected to build should has a deep of 1m below the level of the PG stacks for assuring the complete collection of leachates from the stacks.

The previous conclusion is ratified by observing the common behaviour for most of the metals (Fe, As, Cd, Mn, Pb, U, Sr and Zn, and other ones not plotted in Fig. 3.5), given enhanced concentrations in the first centimetres under the contact (mainly in cores 1 and 3), and always at depths smaller than 50 cm under the PG-sediment contact. The idea that affection of the stacks is limited to the first 50 cm is also ratified by the pH, observing in Figure 3.4A that for z > 50 cm under the contact, neutral sediment pH is found. It is very well stablished that metals mobility in soils is strongly regulated by its acidity (pH), increasing the mobility of the metallic elements according to decreases the sediment/soil pH (Reddy et al., 1995; Tack et al., 1996; Cerquería et al., 2011). In this regard, the first centimetres under the contact showed lower pH values, as was observed in Figure 3.4A, due to PG influence, rapidly increasing up to neutral pH values found in deeper sediments.

Although the concentrations of heavy metals in the PG are similar, and even lower, than typical undisturbed soils, Perez-López et al. (2015), analysed PG pore waters and lateral flows in the zones 2 and 3 of the stacks, and very high mean values of metal concentrations were reported: Fe (54 ±7 mg L^{-1}), As (18.7 ± 1.6mg L^{-1}), Cd (1.7 ± 0.2 mg L^{-1}), Cr (2.7 ± 0.3 mg L^{-1}) Cu (3.3 ± 0.4 mg L^{-1}), Ni (1.5 ± 0.2 mg L^{-1}), Pb (0.17 ± 0.04 mg L^{-1}), Sb (0.23 ± 0.02 mg L^{-1}), U (1.7 ± 0.5 mg L^{-1}) and Zn (14.6 ± 1.3 mg L^{-1}). These authors explained this result by the very high acidity of these PG waters (pH = 1.5-3), deducing that these outflows from the stacks could generate a significant affection by heavy metals and natural radionuclides in the shallow sediments, since they will precipitate during the mixing with estuarine waters and the consequent pH increase.

As it has been demonstrated, the affection of the leachates from PG stacks is limited to the first 50 cm under the interphase, which suggests that the sediment act as a “barrier” for the leachates from the PG, concentrating the contaminants in the first centimetres. This process is less intense mainly in cores 1 and 3, which have diameter particles near the sediment contact (Fig. 3.3), favouring the pollutant migration. Due to the low particle

size of the salt marsh sediments, mainly formed by clay and silt (Fig. 3.3), consequently they will have a very low permeability, and therefore the infiltration toward deeper zones is very much reduced, assuring that outflows under the stacks is horizontal and limited to the first 50 cm under them.

In order to better understand the influence of the PG leachates into the sediments, the mean value of the elements in samples located in the first 50 cm under the contact and in the deeper samples (z > 50 cm) was showed in Figure 3.6. In the supplementary material, the individual elemental concentrations of the samples have been indicated.

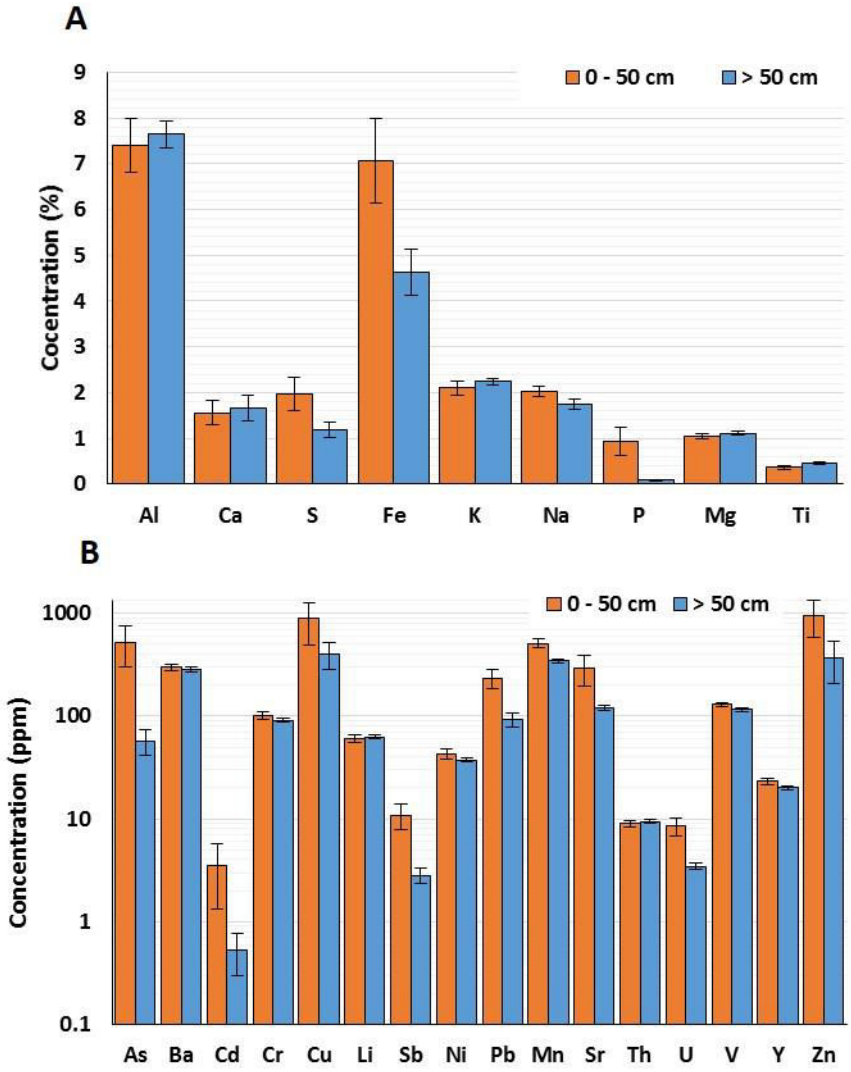

Figure 3.6. Comparison between mean value of the major (A) and trace elements (B) in the sediments located in the 50 first cm under the contact with the PG and in the deeper ones.

As it has been previously commented, the P is the most mobile element related to the pore water of the PG stacks, being its concentrations one order of magnitude higher in the upper sediments (0-50 cm), than in the deeper ones (>50 cm) (Fig. 3.6A). It is clear that

AMD does not increase P concentrations into the sediments, this fact together with its high mobility in acidic aqueous environments, lead us to affirm that P is an ideal tracer of the impact generated by the leaching coming from PG stacks. In addition, could be expected a significant increase of S coming from the PG dissolution, but this fact is not found if the standard uncertainty is considered (2 sigma or 95% of significant level). A great number of metals (Al, Ca, K, Mg, Na, Ti, Ba, Cr, Cu, Li, Ni, Th, V, Zn and Y) show similar mean values in the upper and deeper sediments (Fig. 3.6A and B), which indicate no contribution into the salt marsh from the PG stacks.

Otherwise, some metal and metalloids (Fe, As, Cd, Pb, Sb, Mn, Sr, U), exhibit higher concentrations in the sediments nearest to the contact (0-50 cm) than in deeper layers (>50 cm) (Fig. 3.6A and B), which are also typically found in high concentration in sediments affected by AMD processes, therefore can be affirmed that the increased of these elements are produced by both AMD and outflows leaching coming from PG stacks. As it was mentioned in the introduction, the AMD affecting the Tinto River provokes high heavy metal concentrations in recent estuary sediments formed during the last 150 years, with highly polluted levels due to the peak of mining activities between 1875 and 1930 (Ruiz et al., 1998; Davis et al., 2000). For that reasons, the baseline of these metals in these salt marsh sediments is very high in relation to other similar unperturbed estuarine sediments as, for example, the Piedras River ones (Borrego et al., 2013). By considering that average below 50 cm is the baseline introduced by the AMD, and that this contribution is the same in the upper 50 cm, the difference upper-below can be considered as the concentration enhancement generated by leaching from PG stacks. This way the calculated increase of concentration in the upper sediments due to leachates the PG stacks is the following: Fe (2.4 ± 1.1%), As (470 ± 230 ppm), Cd (3 ± 2 ppm), Pb (140 ± 50 ppm), Sb (8 ± 3 ppm), Mn (170 ± 60 ppm), Sr (170 ± 100 ppm), U (5 ± 2 ppm).

3.1.4.5. Principal component analysis

In order to understand the pollution processes affecting the sediments near the contact a Principal Components Analyses (PCA) was carried out. A PCA is a method for reduce a large number of variables, finding new variables (principal components), which make the data easier to understand. The PCA is used to study the relationship between variables and identify how groups of variables change with respect to each other. Graphs of the PCA results are shown in Figure 3.7, including both variable loadings (Fig. 3.7A) and

observation scores (Fig. 3.7B). The PCA shows that 74.9% of the data set total variance is accounted by the two first components (F1: 53.6%, and F2: 21.3%).

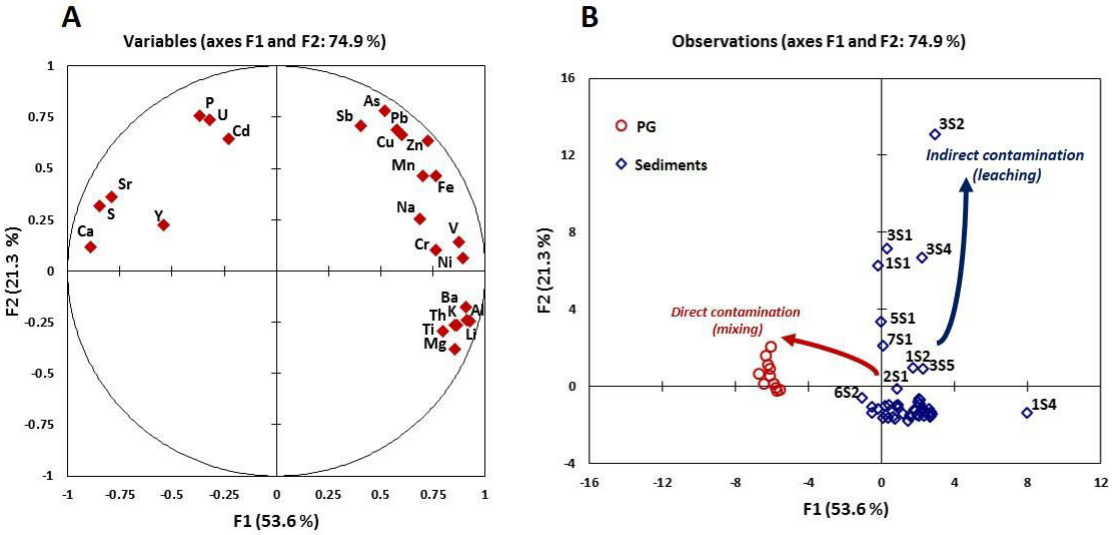

Figure 3.7. PCA results. A: Loading plot of variables and B: score plot of observations.

The F1 component is highly positively contributed by most of the elements: Li, Ni, Al, V, Ba, K, Fe, Mg, Cr, Mn, Ti, Th and Zn (elements related to AMD in most cases), and negatively by Ca, S, Sr, Y, P and U (elements related to PG, Table 3.4). In the observations scores (Fig. 3.7B), all PG samples are located in a small zone of the negative F1 axis, ratifying the fact that negative F1 is controlled by PG pollution. On another hand, almost all sediment samples are located in the positive part of this component, but with a very low loading, with the exception of sample 1S4, which show the highest positive score for this component. Sample 1S4 is very different to the other sediments (see supplementary material), containing the highest concentrations for Mg, Th, Ti, Li, K, Ba and Al. This component discriminates the PG and sediments samples due to the different element concentrations. There are only some sediment samples, such as 6S2, 5S1, 1S1 in the negative part, all of them located near the contact with PG, but with a low contribution to this component. This suggests that contamination of samples by mechanic mixing (direct contamination), have a very low contribution to the total contamination of the sediments.

Regarding the F2 principal component, the variables with higher influence are P, U, Cd, As, Cu, Sb, Pb, and Zn, which are in very high levels in the leaching waters coming from the PG stacks (Perez- López, 2015; Papaslioti et al., 2018), but in the case of heavy metals also in sediments affected by AMD as was discussed in the previous subsection. The samples 3S4, 1S1, 3S1, and specially 3S2, show very high positive component with

F2. It should be remembered that cores 1 and 3 showed the coarser sediments (Fig. 3.3) and high pollution peaks near the contact (Fig. 3.5), and in the case of core 3 the lowest pH values (Fig. 3.4). All these facts suggest that this component is due to indirect contamination of sediments produced by leaching waters from the PG stacks base that percolate into the first decimetres of the salt marsh. The distribution of samples along the positive part of the axis F2 demonstrate that the contamination from leachates is the main route of contamination of the sediments by the PG stacks.

As final remark, as can be seen in Fig. 3.7B, most salt marsh sediments are located together in a small portion, with very low loading of the F1 and F2 components, which indicate that majority of the samples are not affected by pollution from the stacks, either direct mixing and/or leaching from the stacks.

3.1.5. Conclusions

The salt marsh sediments under the phosphogypsum stacks of Huelva has been characterize, in order to know the degree of deep contamination due to leachates from the PG stacks. The conclusions are:

1. The mineralogical analysis showed that gypsum appears in some sediments located very near the PG-sediment contact, indicating mechanical mixing process with the PG from the stacks.

2. The location of coarser sediments in some locations near the contact could allow the migration of contaminants in-depth from the PG due to its higher permeability.

3. The analysis of physicochemical parameters showed the influence of PG acidity affecting sediments in the first 0.5 m under the contact, with intermediate pH values between PG (pH ≈ 3) and salt marsh sediments (pH ≈ 7).

4. Due to the high mobility of P, dissolved in the pore water of the PG as phosphoric acid, and the fact that AMD does not increase its concentration in the salt marsh sediments, this element can be considered as a good tracer for evaluating the potential impact of the PG piles on the underlying sediments.

5. The PCA demonstrate that most salt marsh sediments are not affected by PG stacks pollution, and only the samples located near the contact show peaks of concentrations due to the indirect contamination by leachates from the stacks as the

main source of pollution, while the direct contamination of the sediments by mechanical mixing shows a minimal impact.

6. The salt marsh sediment act as a "barrier" for the leachates from the PG, concentrating the contaminants in the first decimetres (0.5 m) under PG-sediments contact. This is especially relevant, and due to most of these sediments show a low particle size and consequently a very low permeability, the infiltration in depth is very limited.

7. The results of this research work are very relevant for the design of the restauration project, and suggest that the perimeter channel which is projected to build should has a deep of 1 m below the level of the PG stacks for assuring the complete collection of leachates from the stacks, and avoid their liberation into the Tinto estuary.

3.2. EVALUATION OF THE RADIOACTIVE POLLUTION IN THE SALT MARSHES UNDER A PHOSPHOGYPSUM STACK SYSTEM

J. L. Guerrero, I. Gutiérrez-Álvarez, F. Mosqueda, M.J. Gázquez, R. García-Tenorio, M. Olías and J. P. Bolívar

Environmental Pollution 258 (2020) 113729, IF: 6.793 (2019), Category: environmental sciences, Quartile: Q1, Position: 21/265.

Abstract

Next to the city of Huelva (SW of Spain), around 100 Mt of phosphogypsum (PG) are stored in stacks on the salt marshes of the Tinto River estuary covering a surface of about 1000 ha. Due to the high content of ^{238}U series natural radionuclides of the PG, its acidic nature (pH about 3), and the fact that PG stacks were disposed without any kind of isolation from the substrate, they could produce a potential radioactive impact into the underlying sediments.

The aim of this work is to assess the pollution of the underlying sediments by natural radionuclides coming from the PG stacks. To this end, seven cores were taken, and PG and sediments samples collected at different depths were analysed. The activity concentrations of the main long half-live natural radionuclides of interest were determined by applying both gamma-ray and alpha-particle spectrometry radiometric techniques.

The results of this study showed that the first decimeters of salt marsh sediment act as a “barrier” for the radionuclides coming from the PG stacks decreasing rapidly its activity concentration in depth, affecting mainly sediments located in the first 20 cm below the contact due to mixing processes. While ^{230}Th, ^{226}Ra and ^{210}Pb pollution is mainly restricted to the first 20 cm of sediments, U-isotopes can reach higher depths (up to around 50 cm) by leaching processes due to their lower reactivity and higher concentration in the polluted leachates. The obtained results have high relevance for the design of the perimeter channel which is projected to build in the restoration project, suggesting that should has around 1 m deep under the base of the PG stacks, to ensure the full collection of polluting leachates, and to prevent their release into the estuary of the Tinto River.

Graphical abstract

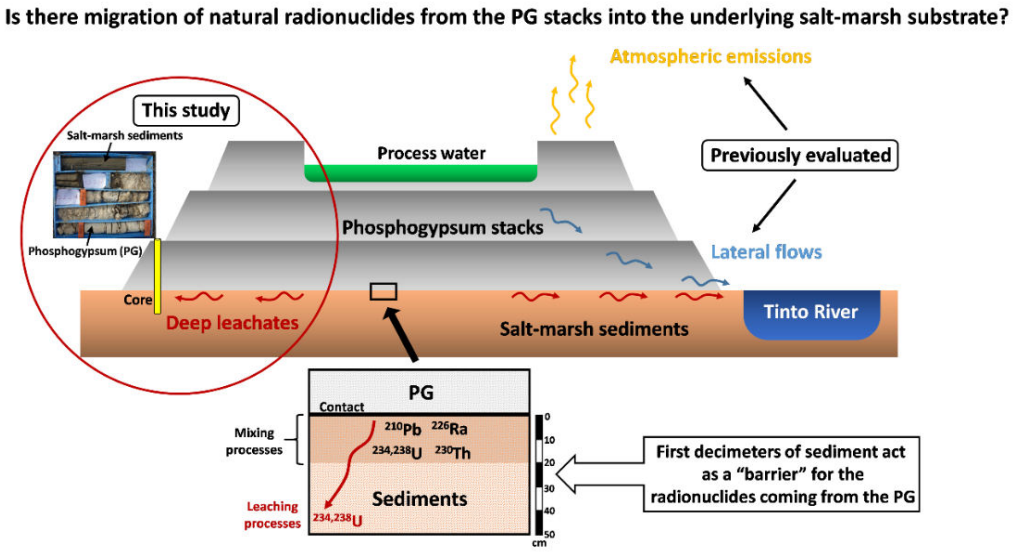

Keywords: phosphogypsum; natural radionuclides; radioactive pollution; radionuclide mobility; salt marsh.

3.2.1. Introduction

On the salt marshes of the Tinto River (SW Spain), close the Huelva city, large phosphogypsum (PG) stacks are located (Fig. 3.8). The confluence of the Tinto and Odiel Rivers form the Huelva estuary, which is an ecosystem of great interest and special characteristics, due to the acid mine drainage (AMD) provoked mainly by old abandoned sulphide mines located upriver, and the chemical industrial complex located at their mouths.

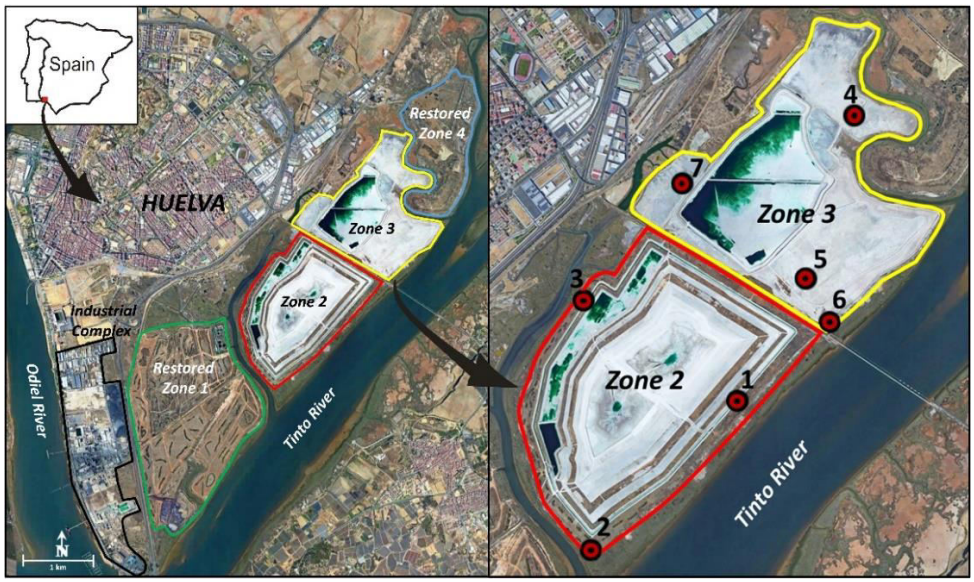

Figure 3.8. Location map of the Huelva phosphogypsum stacks, determining the four zones and indicating the points were the seven cores were taken.

About 300 Mt of PG are produced worldwide every year (Yang et al., 2016). Only 15% of world PG production is recycled, and hence it is mainly disposed by dumping in large stacks, usually placed in coastal zones close to the factories, where PG is frequently exposed to weathering agents and may provoke severe environmental damages (Tayibi et al., 2009). The manufacturing of phosphoric acid (H_3PO_4) from the wet chemical attack of the phosphate rock with sulfuric acid (H_2SO_4) generate PG as a waste, which is more than 95% constituted by gypsum ($CaSO_4 \cdot 2H_2O$).

Since 1968 the five acid phosphoric factories included in the industrial complex of Huelva (Spain), have produced annually around $2.5 \cdot 10^6$ t of PG (Bolívar et al., 2002) until the end of 2010, when the production of phosphoric acid stopped. The phosphate rock used in the factories of Huelva came mainly from Morocco (Bolívar et al., 1996a), and contained metal (oid)s in levels similar to typical soils, but with U-series radionuclides concentrations of about 1500 Bq kg^{-1} per nuclide (about 50 times higher than unperturbed soils), with ^{238}U in radioactive equilibrium with its daughters. About 20% of U, more than 70% of Th, and the majority of Ra, Pb and Po (>95%) contained in the phosphate rock remains in the PG (Bolívar et al., 1996a; Bolívar et al., 2009). In the European Union, PG is currently considered a Naturally Occurring Radioactive Material (NORM) because of the high concentration of both ^{226}Ra and ^{230}Th radionuclides (IAEA, 2003; EU, 2013). On the other hand, the remaining phosphoric acid trapped between the PG particles explains the high acidity and polluting potential of the aqueous leachates produced by this waste (Pérez-López et al., 2010; Pérez-Moreno et al., 2018).

The potential contamination pathways from the PG stacks of Huelva into the environment, atmospheric by ^{222}Rn and radioactive particulate matter and surface sediments and waters of the Huelva estuary by the leachates emerging as edge outflows, have been previously studied in numerous works (Bolívar et al., 2002; Borrego et al., 2007; Hierro et al., 2013; Gázquez et al., 2014; Lopez-Coto et al., 2014; Hernández-Ceballos et al., 2015; Pérez-López et al., 2015, 2016; Papaslioti et al., 2018; Gutiérrez-Álvarez et al., 2019). The results of these works showed an increase in the concentration of metals and radionuclides in the surrounding environment. In this regard, the authorities in cooperation with the responsible companies, are designing an engineering a project for their remediation at this time.

Despite the numerous studies, and that the PG piles were placed on the marshes without any impermeable layer to prevent percolation, the impact on the sediments under

the stacks only have allowed to characterize the salt marsh sediments under the stacks (mineralogy, granulometry, and geochemistry), but ^{238}U series radionuclides, which are key part of the potential impact of the PG stacks were not analysed. The results obtained in this work will provide helpful information to assess the routes of contamination and develop restoration methodologies to others NORM repositories.

Considering the previous facts, the objective of this work is to determine the degree of affection of the salt marsh sediments under the PG stacks of Huelva due to natural radionuclides coming from the stacks.

3.2.2. Study area

In the industrial process of Huelva, PG was transported as an aqueous slurry and disposed, without any type of isolating, forming large stacks on the salt marshes of the Tinto River, accumulating about 100 Mt and covering an area of about 1000 ha, at a distance less than 1 km from the Huelva city.

The area where the generated PG during the production time was disposed is currently divided into 4 zones (Fig. 3.8). Zones 1 (around 400 ha) and 4 (around 150 ha) located to the south and north respectively were previously restored. On this basis, this study was not extended to these zones.

In zones 2 and 3 PG is directly exposed to weathering conditions, without any type of cover layer, and acidic waters (pH < 2) from the industrial process are stored in surface ponds (Fig. 3.8).These acidic waters are evaporating for the restoration project.

The Zone 2, with an extension of 250 ha, store around 25 Mt of PG. Until 1997, the PG was transported by seawater in open circuit and deposited above the salt marsh generating a 5 m high PG pile. From 1998 until the end of 2010, due to a change in the environmental policy according to the OSPAR (OSPAR, 2002, 2007) convention, all the PG generated was placed in this zone by a close circuit pumped with fresh water, generating a pyramid-shaped stack of up to 20 m in height. In addition, a net of perimeter channels to collect lateral fluxes surrounds this zone.

The zone 3 covers a surface of 200 ha, and stores about 15 Mt of PG with an average height of 6 m over the marsh. In this sector, the PG was store before 1997, and a perimeter channel was constructed in 2015. Since the PG deposition stopped in this zone, its main

role has been to store industrial process water in a central pond, which was part of the closed-circuit freshwater system fitted after the environmental policy change.

3.2.3. Material and methods

In November 2009, 7 cores were collected from the Zones 2 and 3 of the stacks (Fig. 3.8, Table S3.5). From the cores, 57 slices (11 PG and 46 sediment samples) with thickness of 5 cm and a diameter of 9 cm for the analysis of physicochemical parameters, chemical composition and the main long half-live natural radionuclides of interest were selected. Samples from different depths were taken, but most of them around the PG-sediment contact (Fig. S3.1), in order to focus on the migration of natural radionuclides from the stacks to these upper sediment layers.

An aliquot of 20 g per slice was taken for the pH and electrical conductivity (EC) measurement. These portions were previously air drying, and the physicochemical parameters were determine by 1:2 (sample:water) mix. For chemical and radioactive analysis an aliquot of 30 g per slice were dried in an oven at 60 ºC to constant weight. The analysis of major and trace elements was conducted by ICP Mass in the Actlabs from Canada. The quality control (QC) was performed by the analysis at the beginning and end of each set of samples of Certified Standard Reference Materials. In addition, a duplicate for every 10 samples is run and internal control standards are analysed.

The radioactive characterization of all the samples was performed by applying two independent techniques: gamma-ray and alpha-particle spectrometry. ^{226}Ra, ^{228}Ra and ^{40}K were determined by gamma-ray spectrometry with the same equipment and the methodology described in Pérez-Moreno et al. (2002). U-, Th-isotopes, and ^{210}Po were determined by alpha particle spectrometry (Martin and Hancock, 1992; Pérez-Moreno et al., 2018). Because of ^{210}Po come from the decay of ^{210}Pb and secular equilibrium is assumed between these radionuclides (more than 2 years elapsed between the sampling and the measurement), the activity concentration of ^{210}Po (half-life = 138 d) was interpreted as ^{210}Pb (half-life = 22.2 y). The QC for the alpha-particle spectrometry was made taking part in annual international proficiency tests (International Atomic Energy Agency [IAEA] and the Spanish Nuclear Safety Council [CSN]), and by analysing both blank and Certified Standard Reference Materials, IAEA-326 (soil) and IAEA-434 (phosphogypsum), every batch of 10 samples.

3.2.4. Results and discussion

3.2.4.1. Physicochemical parameters

The depth profiles of pH and EC for the different cores are displayed in Figure 3.9. In order to make clearer the comparison between cores the PG-sediment contact is considered as "0 m depth", applying positive depth values for PG and negative for sediments. The pH of PG is homogeneous regardless the location of the cores, with a global mean value of 2.9 ± 0.2, and ranging from 2.1 (6P5) to 4.1 (3P2) (Table S3.6). The low pH values of PG are related with the remaining acids (mainly phosphoric), trapped between the particles of PG after the industrial process. The acidity of this waste favoured the liberation and mobility of metals, radionuclides, and other chemical species present into the PG. Table S3.7 shows the individual values of the physicochemical parameters for all the analysed samples.

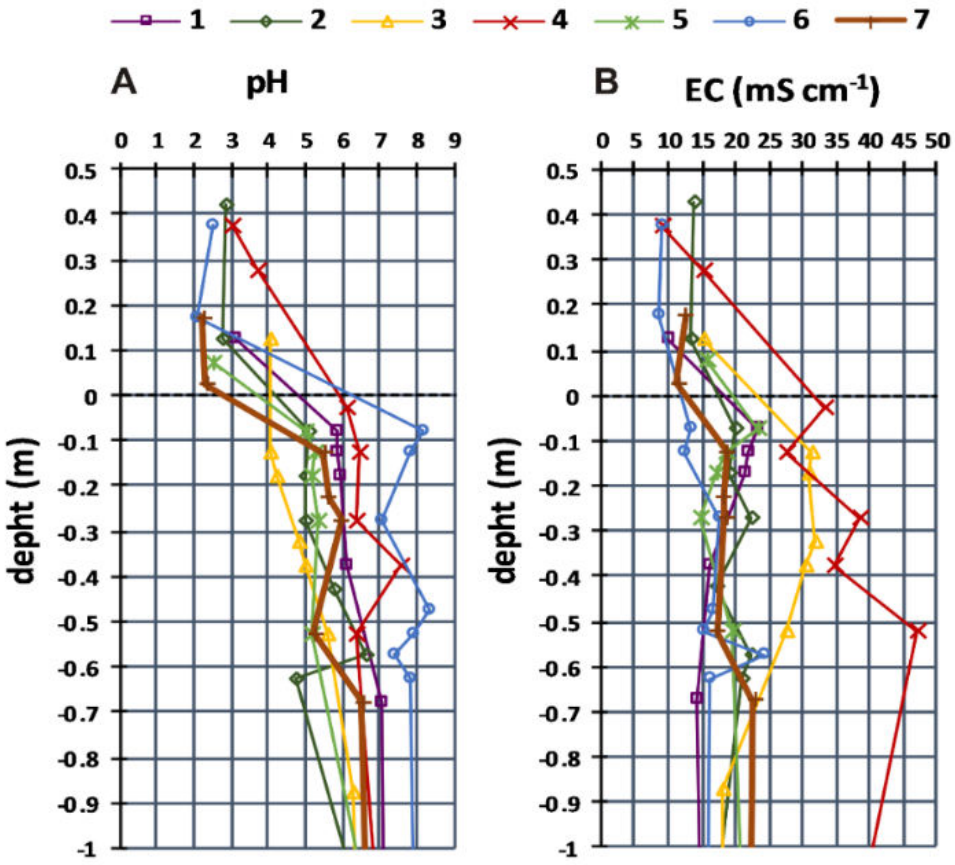

Figure 3.9. Depth profiles of pH (A) and EC (B).

On the other hand, sediments samples taken in the first 50 cm below the contact showed a mean pH value of 5.9 ± 0.2, while the deeper ones showed a neutral mean value of 7.0 ± 0.3 (Table S3.6). The minimum pH was 4.0 in the sample 3 S, which is located 10 cm under the contact. The acidic pH values of the shallower sediments are obviously

due to the impact of the PG stack. Differences in the pH values are observed between cores. In this sense, cores 2, 5 and mainly 3, show lower pH values in the first 20-30 cm below the contact (Fig. 3.9A), probably due a higher influence of the PG acidity into the salt marsh at these locations.

Regarding the EC, the PG shows a mean value of 12.2 ± 0.8 mS cm^{-1}, while for the sediments located in the first 50 cm below the contact the mean value was 22.6 ± 1.4 mS cm^{-1}, similar to mean value obtained for the deeper ones 19.5 ± 1.8 mS cm^{-1} (Table S3.6). Salt marsh sediments show in general higher EC values than PG ones. This fact is due to salinity of the sediments in the studied estuarine environment. It is necessary to highlight the higher EC of sediment samples located in the cores3 and 4, which show values above 30 mS cm^{-1} in the first 50 cm below the contact (Fig. 3.9B). Taking into account that Pérez-López et al. (2015) determined a mean EC value of edge outflows from the PG of 40.3 ± 9.9 mS cm^{-1}, and the acidic of sediments in the core 3, the high EC values of this location could be related with the existence of leachates from the stacks. In the case of core 4, these higher EC values are probably related with natural processes.

3.2.4.2. Natural radionuclides

The variation in the activity concentrations of the most significant ^{238}U-series natural radionuclides (^{238}U, ^{230}Th, ^{226}Ra and ^{210}Pb), ^{232}Th and ^{40}K with depth in the first meter after the contact is shown in Figure S3.2. The activity concentration for all the samples is included in Table S3.8. The activity concentration of ^{238}U-series radionuclides is higher in the PG and decrease rapidly with depth from the contact zone. This behaviour is very clear in the cores 1, 2, 4, 5, and 7, where the increase of natural radionuclide concentrations is only observed in the first 20 cm under the contact, being the thickness of sediment affected even lower in some cores. This decrease in the activity concentration with depth is not as clear and not as homogeneous in the cores 3 and 6, which show a deeper affection, but only until around 50 cm under the contact zone (Fig. S3.2C). In this sense and in order to clarify the impact of the PG stacks into de sediments, the activity concentration of the natural radionuclides in the PG samples, the shallow sediments (0-20 cm under the contact) and deeper sediments (z > 20 cm under the contact) is displayed as modified box and whisker plots in Figure 3.10 (the modified box and whisker plots consider the existence of outliers).

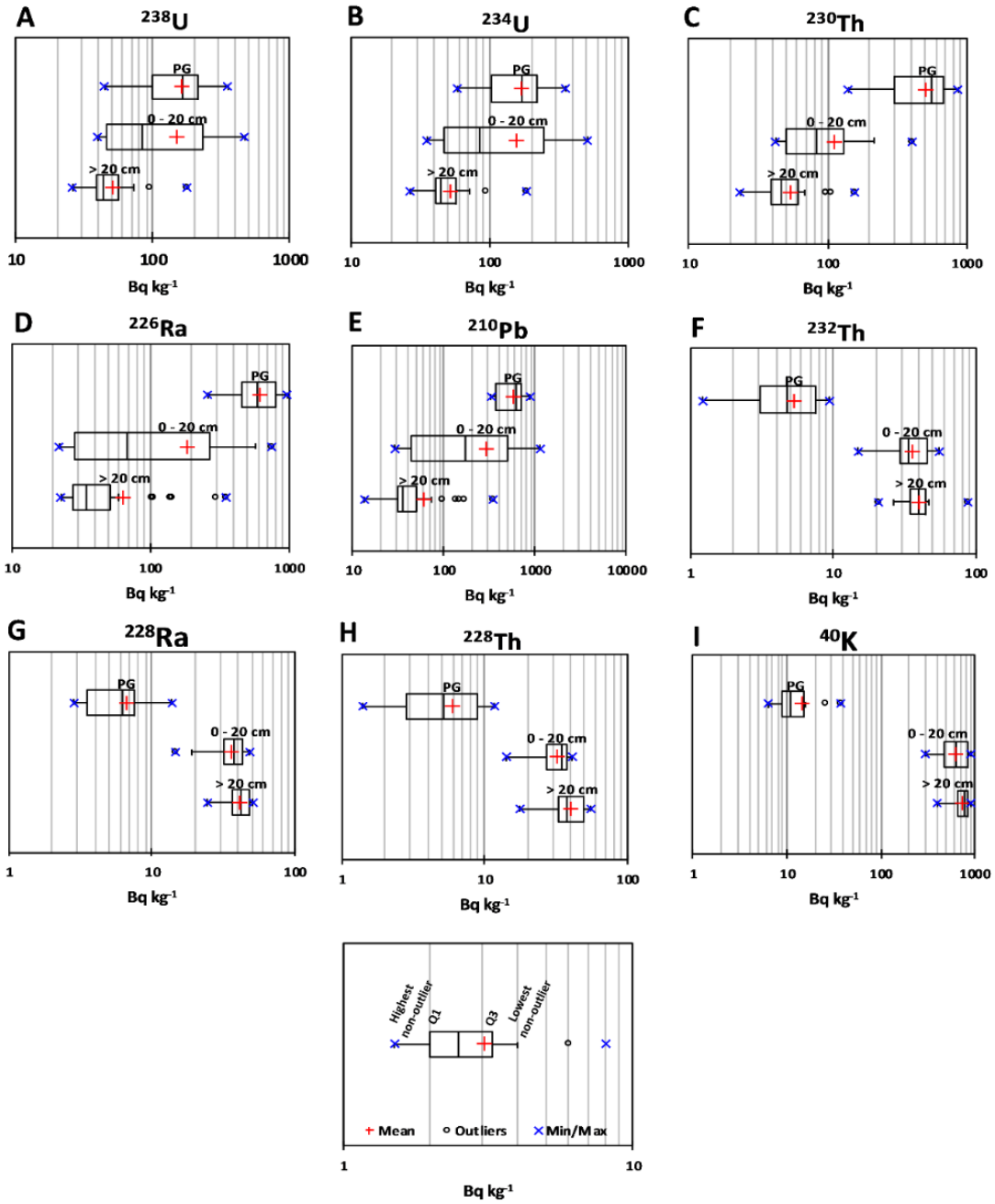

Figure. 3.10. Modified box and whisker plots of the analysed natural radionuclides in the PG samples, shallow sediments (0e20 cm under the contact) and deeper sediments (>20 cm under the contact). Ordered by radioactive series and mass number.

The main potential radionuclide pollution pathway from the PG stacks into the underlying sediments is the migration of natural radionuclides due to the deep percolation of leachates. In this regard, two properties should be taken into account for each radionuclide, the "mobility" and the "reactivity" of the radionuclides. The mobility can be defined as the capacity of a radionuclide to be released from the solid phase (PG) into the aqueous media. This property was analysed by Pérez-Moreno et al. (2018), demonstrating that U is the most mobile radionuclide contained in the PG, while Th has

a very low mobility, and both Po and Ra present an intermediate mobility. Due to this fact, the radionuclide concentrations in the acid waters from the perimeter channel which collect the leachates from PG stacks are as follow: $^{238}U \approx 300$ Bq L^{-1}, $^{210}Pb \approx 10$ Bq L^{-1}, and ^{226}Ra and $^{230}Th < 1$ Bq L^{-1} (Gázquez et al., 2014; Pérez-Moreno et al., 2018). On the other hand, the reactivity, or capacity to be adsorbed onto the surface of the salt marsh sediments of Th, Pb, and Po is very high, as a consequence, they are considered particle-reactive radionuclides (Wei et al., 2011). The underlying salt marsh is mainly composed by fine particle size sediments (mainly clays) (Guerrero et al., 2019) which have a very low permeability and high specific surface area, hence, a low percolation rate and high pollutant adsorption. Therefore, it is expected that these reactive radioelements (Th, Pb, Po) remain adsorbed in few centimeters below the PG. Accordingly, the in depth migration of these natural radionuclides must be mainly conducted by molecular diffusion, while other pollutant transport processes, as dispersion and advection, only are significant in some points where some coarser particle size strata are located. PG samples present a ^{238}U mean activity concentration of 163 ± 27 Bq kg^{-1}, ranging from 45 ± 2 (5P5) to 354 ± 10 Bq kg^{-1} (3P2) (Fig. 3.10A).

^{234}U is in secular equilibrium with ^{238}U in the PG samples, as found by many researchers in other locations in the world (Mazzilli et al., 2000; Boryło et al., 2009; El Afifi et al., 2009). Samples located in the first 20 cm below the contact show a mean ^{238}U activity concentration of 151 ± 39 Bq kg^{-1}, which is slightly smaller than the measured one in the PG, and obviously due to the influence of the PG stacks. In deeper samples ($z > 20$ cm under the contact), the activity concentration of ^{238}U decrease quickly until background values, with a mean value of 51 ± 5 Bq kg^{-1} and a median of 44 Bq kg^{-1}. These values of deeper sediments are in agreement with the ^{238}U worldwide median concentration in unperturbed soils which is 35 Bq kg^{-1}, ranging from 16 to 110 Bq kg^{-1} (UNSCEAR, 2000). ^{234}U show secular equilibrium in the salt marsh sediments with the parent nuclide of the decay chain, displaying therefore the same behaviour that ^{238}U (Fig. 3.10A and B).

Regarding ^{230}Th, shows a mean activity concentration of 519 ± 73 Bq kg^{-1} in the PG, and decrease until a mean value of 113 ± 25 Bq kg^{-1} in the first 20 cm under the contact, while deeper salt marsh samples show a mean concentration of 55 ± 5 Bq kg^{-1} (Fig. 3.10C). Whereas in the case of U isotopes, the mean activity concentration is similar

in the PG and shallow sediments, ^{230}Th mean activity concentration is five times lower in the sediments located near the contact than in the PG.

This fact is due to both, the very low mobility of this radionuclide as was previously discussed, and their higher reactivity (capacity to be adsorbed) onto the salt marsh sediments, producing a quicker decrease of its activity concentration with depth.

^{226}Ra and ^{210}Pb showed a mean activity concentration in PG samples of 618 ± 74 and 566 ± 59 Bq kg^{-1} respectively (Fig. 3.10D and E), similar than the values obtained in previous studies for the whole stacks (Bolívar et al., 1998; Más et al., 2006a). Samples located in the first 20 cm under the contact show a mean ^{226}Ra activity concentration of 185 ± 58 Bq kg^{-1}, and a mean ^{210}Pb activity concentration of 281 ± 84 Bq kg^{-1}. In the case of deeper salt marsh sediments showed a mean activity concentration for ^{226}Ra and ^{210}Pb of 64 ± 14 and 59 ± 12 Bq kg^{-1} respectively, values even higher than the third quartile (Fig. 3.10D and E) due to the existence of some samples with high extreme values (outliers). It is remarkable that median values of ^{226}Ra and ^{210}Pb in shallow sediments was 68 and 170 Bq kg^{-1}, while in the deeper ones was 34 and 35 Bq kg^{-1}, respectively. The median ^{226}Ra value for deeper sediments (z > 20 cm below the contact) is similar than that the worldwide concentration in natural soils 35 Bq kg^{-1} (range: 17-60 Bq kg^{-1}) (UNSCEAR, 2000), demonstrating the low affection in depth of the salt marsh due to PG-stacks influence.

It is interesting to comment the abnormally high activity concentrations (outliers) of natural radionuclides from the ^{238}U series observed in the box and whisker plots in some samples located more than 20 cm below the contact (Fig. 3.10A-E). These polluted samples were found in the cores 3 and 6 (Figs. S3.1C and F), reaching a maximum depth until around 50 cm under the contact zone. The $^{234\text{-}238}$U outliers were located in the core 3, while ^{230}Th, ^{226}Ra and ^{210}Pb outliers were located mainly in the core 6.

It seems clear that salt marsh sediments act as a “barrier” for the radioactive pollution, and the influence of the PG stacks in the underlying sediments due to natural radionuclides is restricted to the first decimetres (around 50 cm). It should take into account that the cores were taken after more than 40 years from the start of PG storage, when the production of this waste stopped. Obviously, the system will continue to evolve, but due to the characteristics of the salt marsh sediments (low permeability and high specific surface area) the penetration velocity of the pollutants into deeper sediments is

very low, even probably already reaching a steady-state in some cases. In addition, the PG acidic waters are under evaporation process during the restoration project, which also include the covering of the stacks with an impermeable geotextile, a 60 cm clay layer, and a final layer of 40 cm of soil. All these actions will avoid the main source of deep pollution, which is the generation of new polluted acid leachates. Therefore, the in-depth migration of these radionuclides into the salt marsh sediments is not an important concern. On the other hand, these findings are also highly relevant due to suggest that the new perimeter channel planned to build in the restoration should has at least 1 m deep under the base of the PG piles to ensure the full collection of polluting leachates, and to prevent their release into the Tinto estuary.

Regarding the natural radionuclides from the ^{232}Th series, and ^{40}K, show very low activity concentrations in the PG samples, with values below the detection limit in some samples. Thus, the activity concentration of ^{228}Th, ^{232}Th and ^{228}Ra, show in general values below 10 Bq kg^{-1} while ^{40}K show activity concentration values below 20 Bq kg^{-1}, similar values than those observed in previous studies (Bolívar et al., 1998; Más et al., 2006). The mean activity concentration of ^{232}Th, ^{228}Ra, ^{228}Th and ^{40}K in the samples located in the first 20 cm under the contact were 36 ± 3 Bq kg^{-1}, 36 ± 2 Bq kg^{-1}, 36 ± 3 Bq kg^{-1}, and 640 ± 54 Bq kg^{-1} respectively, while in the deeper sediments samples the mean values were 41 ± 1 Bq kg^{-1}, 40 ± 2 Bq kg^{-1}, 40 ± 2 Bq kg^{-1}, and 737 ± 25 Bq kg^{-1} respectively (Fig. 3.10F-I). The slightly decrease of concentration of these radionuclides in the shallower samples, seem to confirm the existence of mixing processes between PG and salt marsh sediments, producing a decrease in the activity concentration of these radionuclides in the sediment directly in contact with the PG stacks. To understand the existence of this mixing processes we must look back to the initial conditions of PG storage, which was spilled as an aqueous slurry, as was indicated in the material and methods section, over the wet and low cohesive marsh sediments. Thus, a mixing between the PG and sediment particles during this first storing stage took place, polluting the sediments in direct contact with the base of the stacks. The activity concentration of ^{232}Th series radionuclides in salt marsh sediments are pretty similar than the worldwide median concentration in soils which is 30 Bq kg^{-1} (range: 11-64 Bq kg^{-1}) (UNSCEAR, 2000), while the ^{40}K worldwide median concentration in common types of soils is 400 Bq kg^{-1} (range: 140-850 Bq kg^{-1}) (UNSCEAR, 2000), data notably lower than the values obtained for the salt marsh sediments analysed in this study.

3.2.4.3. Activity ratios

In Figure 3.11 are displayed as modified box and whisker plots the most representative activity ratios (AR), following the same scheme than in Figure 3.10. Table S3.9 shows the values of these activity ratios for all the analysed samples.

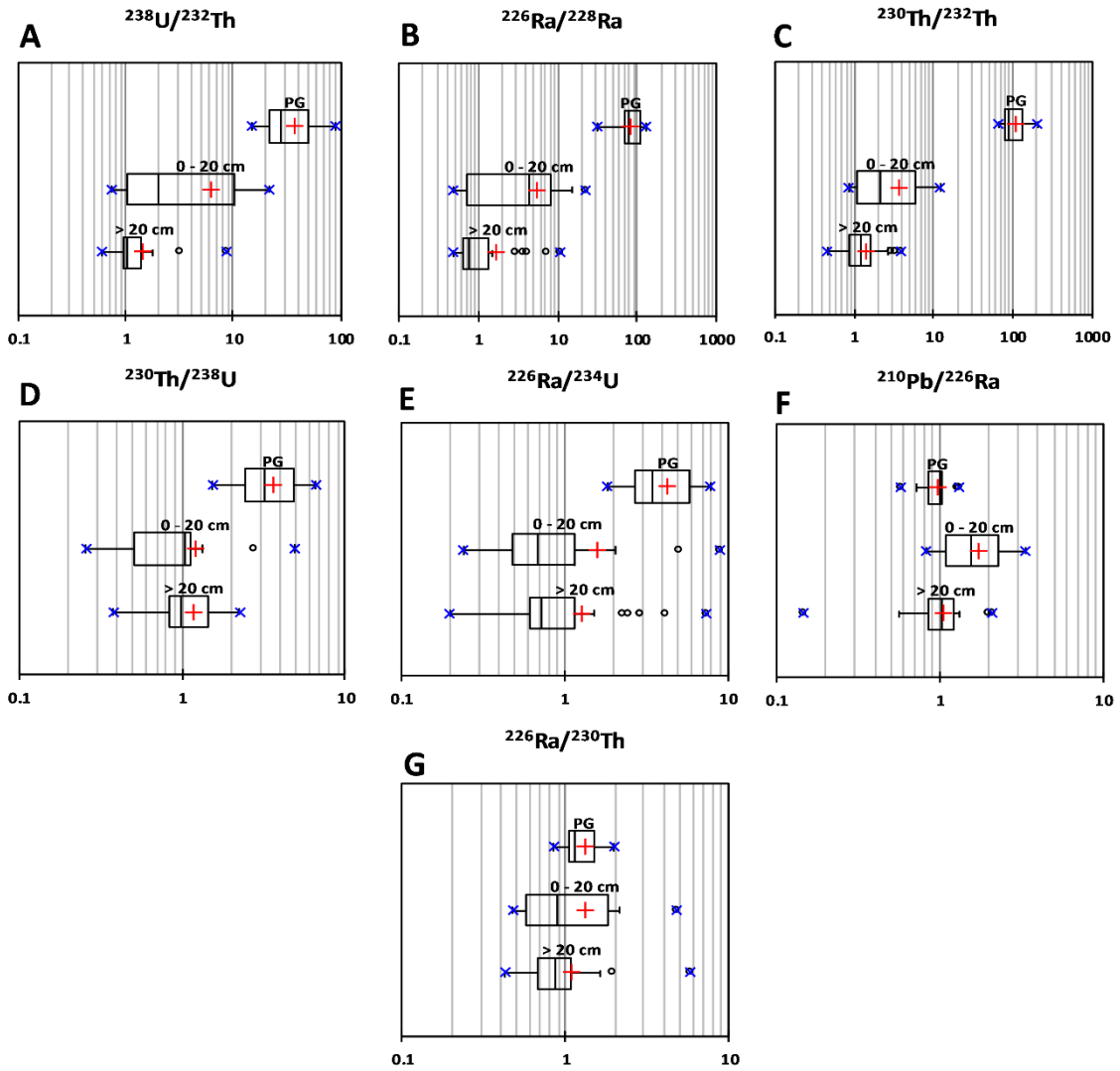

Figure 3.11. Modified box and whisker plots of the most representative activity ratios in the PG samples, shallow sediments (0-20 cm under the contact) and deeper sediments (z > 20 cm under the contact).

The analysis of the activity ratios ratifies some of the previously commented findings. In this way, the activity ratios between natural radionuclides from the ^{238}U series and ^{232}Th series show high values in the PG samples with mean activity ratios for ^{238}U/^{232}Th, ^{226}Ra/^{228}Ra, ^{230}Th/^{232}Th of 37 ± 7, 83 ± 9 and 110 ± 14 respectively (Fig. 3.11A-C). These ratios are in agreement with the found ones in the raw material (phosphate rock) (Bolívar et al., 2009), and in the PG stacks (Más et al., 2006a). In the sediment samples located near the contact with the PG stacks, the mean value was around 6 for ^{238}U/^{232}Th and ^{226}Ra/^{228}Ra, and around 4 for ^{230}Th/^{232}Th. While in the deeper sediment samples

(z > 20 cm under the contact) the mean value decreases up to around 1.4 for $^{238}U/^{232}Th$ and $^{230}Th/^{232}Th$, and around 1.7 for $^{226}Ra/^{228}Ra$, while median values are significantly lower, mainly for $^{226}Ra/^{228}Ra$ activity ratio, which is 0.7. These values are similar to the found ones in unpolluted salt marshes of this geographical area in previous works (Bolívar et al., 1996b; Aguado et al., 1998; Bolívar et al., 2002). It should be noted the existence of some outliers for these activity ratios in the deeper samples, with maximum values of 8.7 ± 0.7 and 10.8 ± 1.2 for $^{238}U/^{232}Th$ and $^{226}Ra/^{228}Ra$ respectively, determined in the core 3, and a maximum value of 3.9 ± 0.3 for $^{230}Th/^{232}Th$ activity ratio measure in the core 6. These abnormally high values for deeper samples were located in all cases in the first 50 cm under the contact. The decrease of these activity ratios with depth confirm the fact that the salt marsh sediments act as a "barrier" for the leachates from the PG stacks, and the impact is only observed in the first sediment decimetres.

The activity ratios between the ^{238}U-series radionuclides in the sediments provide information about their relative impact into the salt marsh. PG samples show a mean $^{230}Th/^{238}U$ and $^{226}Ra/^{234}U$ activity ratio of 3.6 ± 0.5 and 4.3 ± 0.6, respectively, while in the shallow sediments these activity ratios show mean values close to the unity, with values of 1.2 ± 0.3 and 1.6 ± 0.6, respectively (Fig. 3.11D and E). The decrease of these activity ratios in the upper sediments is related with the lower reactivity, around 3 times lower, and the higher activity concentration in the leachates of U-isotopes, which provokes a deeper impact by these radionuclides. The concentration of ^{226}Ra in the leachates is two orders of magnitude lower than the ^{238}U one. Therefore, the increase of ^{226}Ra in the sediments due to percolation is not detectable and can be considered as negligible in relation to the increase of the U-isotopes activity concentrations. The samples located more than 20 cm below the contact present mean values around secular equilibrium (AR ≈ 1), taking into account the uncertainties, for these activity ratios.

With regard to $^{210}Pb/^{226}Ra$ activity ratio (Fig. 3.11F), to point out that mean values around secular equilibrium were determined for PG and deeper sediment samples, while in the first 20 cm below the contact the mean value was higher than 1 (1.7 ± 0.2), probably due to the unsupported ^{210}Pb by the atmospheric deposition existing before the PG stacks. Finally, the $^{226}Ra/^{230}Th$ activity ratio (Fig. 3.11G), with a mean value of 1.3 for both PG and sediments located near the contact, and a mean value around secular equilibrium for the deeper sediments, confirm that these two radionuclides are affected by the same processes, polluting the upper sediments mainly by mixing.

3.2.4.4. Principal component analysis

In order to deepen in the understanding of the processes involved in the migration of natural radionuclides from the PG stacks into the underlying salt marsh, a Principal Components Analysis (PCA) was performed (Fig. 3.12). PCA is a method for reduce a large number of variables, finding new variables (principal components), which are ordered so that the first few retain most of the variation present in all of the original variables, making the data easier to understand (Jolliffe, 2002). The PCA is used to study the relationship between variables and identify how groups of variables change with respect to each other. In this analysis, element concentrations were included to know its relationship with the natural radionuclides and improve the understanding of pollution processes that affects the salt marsh sediments. The first two factors (F1 and F2) explain the 73.3% of the data set total variance.

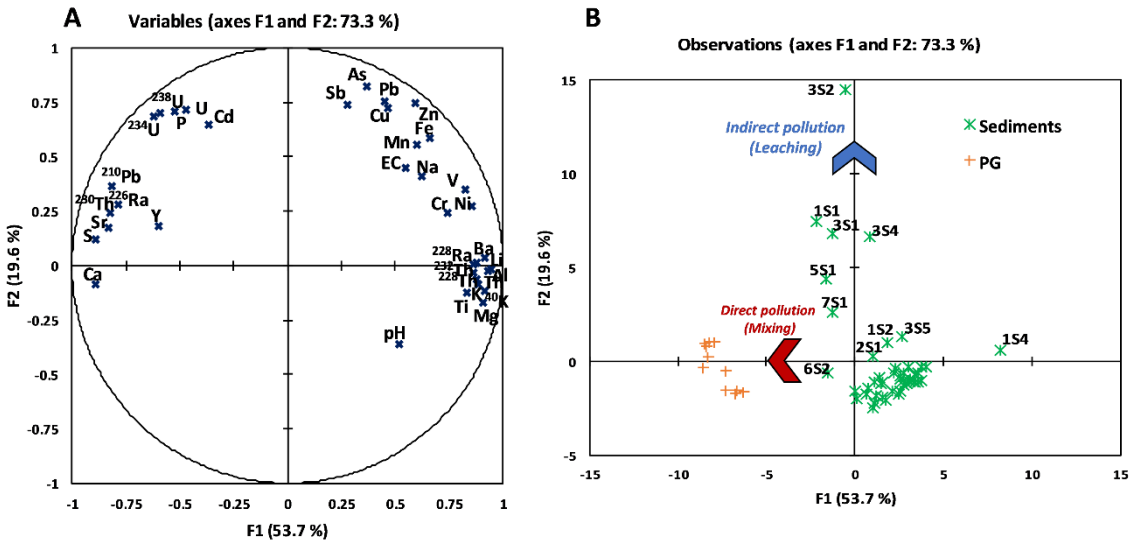

Figure 3.12. PCA results. A: Loading plot of variables and B: score plot of observations.

The F1 factor (53.7% of the variance) show high positive scores for Al, K, Mg, Ti, Ba, Cr, Li, Ni, Th, V, and from ^{232}Th-series radionuclides (^{232}Th, ^{228}Th and ^{228}Ra), and ^{40}K (Fig. 3.12A). These elements and radionuclides are clearly related to unpolluted sediments, that is to say, with the geological background of this geographical area. On the other hand, the F1 factor is highly negatively contributed by Ca, S, Sr, Y, and natural radionuclides from the ^{238}U series (^{238}U, ^{234}U, ^{230}Th, ^{226}Ra and ^{210}Pb), which are clearly related to the PG.

In the PCA for observations (Fig. 3.12B), most sediment samples are grouped in the positive part of this factor, but with very low scores, while all PG samples are situated in

a reduced area of the negative F1 axis. It should be noted the location of some upper sediment samples (1S1, 3S1, 3S2, 5S1, 6S2, and 7S1) in the negative part of F1 axis, which are clearly affected by mixing processes with PG (negative F1 represents direct contamination by PG-sediment mixing). These shallow sediment samples show a low contribution to F1 component, which confirms the low affection of the salt marsh sediments by mixing processes with PG. This way, F1 component discriminates the PG samples and unpolluted salt marsh sediments, and it is controlled in the negative part by direct PG pollution, due to mixing.

Regarding the F2 factor (19.6% of the variance), there is a group of variables very related to PG, which show high positive scores on F2 axis (P, Cd, U, ^{238}U, ^{234}U). High concentrations of these elements and radionuclides in the PG leachates have been measured (Pérez-López et al., 2015; Pérez-Moreno et al., 2018), which clearly demonstrate that the origin of these ones is the PG. The samples 1S1, 3S1, 3S3, and mainly 3S2, present very high positive scores along F2. Moreover, the core 3 show a deeper affection by natural radionuclides, mainly ^{238}U (Fig. S3.2C), and the lowest pH values (Fig. 3.9A), probably due to the higher grain size of the sediments located near the contact in this point (Guerrero et al., 2019).

It is very interesting the presence of P with high positive contribution in this factor. It was demonstrated that due to the high mobility of this element it is a good tracer to assess the impact of the PG stacks into the underlying salt marsh substrate due to deep leachates (Guerrero et al., 2019), since this element is not increased by the AMD of the Tinto River. On the other hand, in the positive part of this component are located the natural U-isotopes which are the most mobile and low reactive analysed radionuclides of this study as was previously observed. All of this indicate that F2 factor is closely related to the indirect polluting pathway of sediments, which is produced by leachates from the PG piles that infiltrate into upper decimetres of sediment.

To summarize, the PG-sediment mixing processes explain the radioactive pollution by ^{230}Th, ^{226}Ra, ^{210}Pb of the upper salt marsh layers, while for $^{234\text{-}238}$U produce a deeper affection of the salt marsh (up to around 50 cm) by leaching processes due to their higher mobility and lower reactivity. And finally, it is remarkable that most sediment samples are plotted in a small zone, with very low scores for the F1 and F2 factors (Fig. 3.12B), demonstrating than most of the salt marsh sediments are not polluted by natural radionuclides from the PG piles.

3.2.5. Conclusions

The obtained conclusions in this work are:

1. The salt marsh sediment produces a "barrier effect" for the ^{238}U series natural radionuclides coming from the PG stacks decreasing rapidly their activity concentration with depth, hence, most of the analysed sediments are not polluted by natural radionuclides from the PG stacks.

2. The sediments with a higher degree of affection are mainly located in the first 20 cm under the contact and are affected by mixing processes, while pollution of deeper sediments due to leaching processes only take place in some of the studied locations, affecting samples located maximum up to around 50 cm under the contact.

3. While ^{230}Th, ^{226}Ra and ^{210}Pb pollution is mainly restricted to the first 20 cm of sediments, U isotopes can reach higher depths (up to around 50 cm) by leaching processes due to their higher mobility and lower reactivity.

4. The obtained results in this research work have high relevance for the design of the projected perimeter channel in the restoration project, suggesting that should has at least 1 m deep under the base of the PG piles, to ensure the full collection of polluting leachates, and to avoid their release into the estuary of the Tinto River.

3.3. SEASONAL EVOLUTION OF NATURAL RADIONUCLIDES IN TWO RIVERS AFFECTED BY ACID MINE DRAINAGE AND PHOSPHOGYPSUM POLLUTION

J. L. Guerrero, I. Gutiérrez-Álvarez, A. Hierro, S.M. Pérez-Moreno, M. Olías and J. P. Bolívar

Catena 197 (2021) 104978, IF: 4.333, Category: geosciences, Quartile: Q1, Position: 21/200; Category: water resources, Quartile: Q1, Position: 8/94; Category: soil sciences, Quartile: Q1, Position: 5/38.

Abstract

The Odiel and Tinto rivers show singular characteristics due to the significant acid mine drainage (AMD) generated in the first section of their basins and the phosphogypsum (PG) stacks located on their common estuary. AMD leads to low pH and high redox potential, which keep high amounts of toxic elements and radionuclides in dissolution. The objective of this work was to analyse the seasonal evolution of U-Th isotopes and ^{210}Po in these rivers and the estuarine mixing zone. Four sampling points were selected (a fluvial point and an estuarine one for each river) and water samples were collected monthly throughout a year. The concentrations of natural radionuclides in the dissolved and particulate phases were determined by alpha spectrometry. The Odiel and Tinto rivers show concentrations of U-Th isotopes and ^{210}Po from one to three orders of magnitude higher than background continental waters due to the strong effect of AMD, and ^{234}U/^{238}U activity ratios up to 2.

The studied radionuclides show a clear seasonal behaviour in these rivers, with three different stages during the year: (1) concentration peaks observed during November and December due to the "washing effect" produced by the first rainfalls of the hydrological year, (2) a "dilution effect" by runoff in the rainy winter, and (3) a progressive "concentration effect" during the spring and summer. A non-conservative behaviour of the analysed radionuclides in the estuaries was demonstrated due to precipitation processes produced by the increase of pH. The polluted outflows from the PG stacks located in the Tinto estuary produce a significant radioactive impact, mainly during the rainiest months, increasing the concentration of U-isotopes and ^{210}Po in the particulate phase.

Keywords: natural radionuclides; acid mine drainage; phosphogypsum, non-conservative; water mixing.

3.3.1. Introduction

The Tinto and Odiel rivers are located in southwest Spain in the province of Huelva. They present marine influence in their final reach, converging in the common Huelva estuary (Fig. 3.13). The Tinto River is 101 km long while the Odiel River is 140 km long, and their catchments cover 1600 and 2300 km^2, respectively. These rivers and their estuary have a great hydrochemical and environmental interest due to two factors. The first is the extensive acid mine drainage (AMD) affecting both rivers because of the existence of several old abandoned sulfide mines in their basins and second is the large chemical industrial complex and phosphogypsum (PG) stacks located by the Huelva estuary.

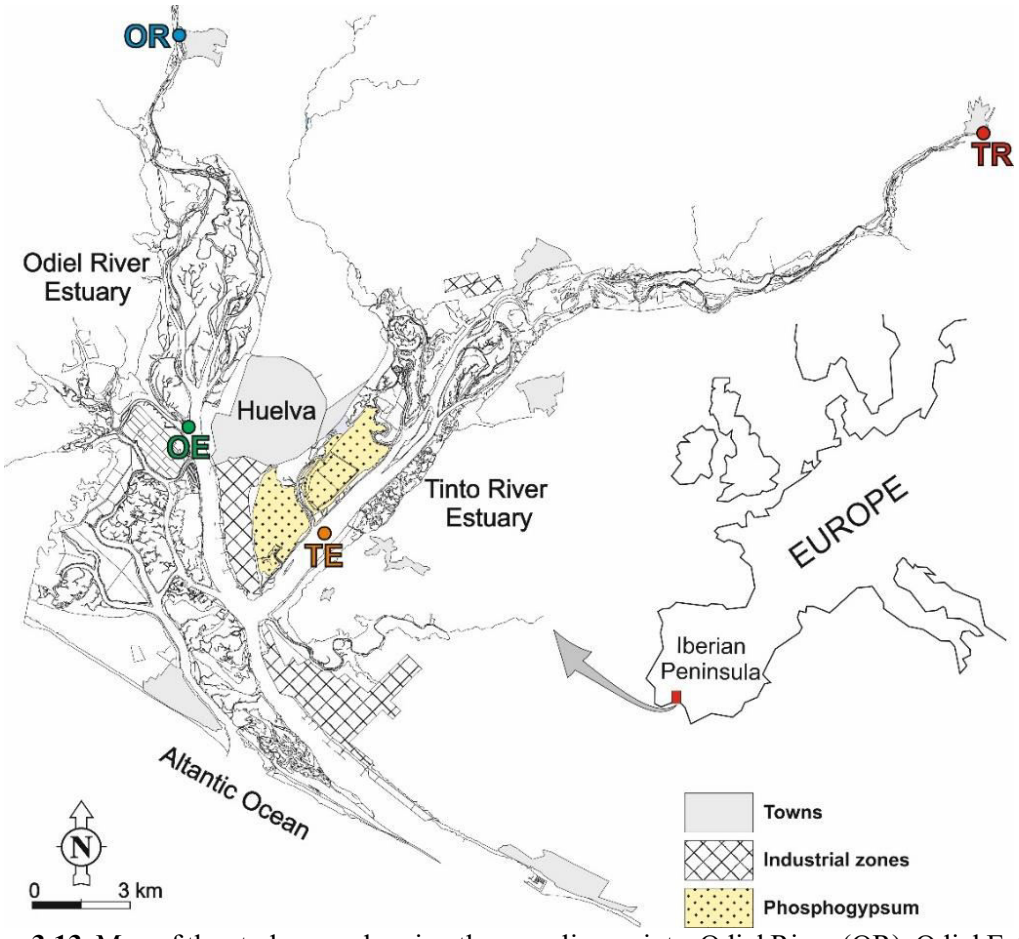

Figure 3.13. Map of the study area showing the sampling points: Odiel River (OR), Odiel Estuary (OE), Tinto River (TR), and Tinto Estuary (TE).

Regarding the AMD, these rivers drain one of the biggest metallogenic regions of massive sulfides in the world: the Iberian Pyrite Belt (IPB). Mining works date from the year 2500BCE in this region, although the large-scale exploitation of these deposits took place during the nineteenth and twentieth centuries (Leblanc et al., 2000). The sulfide deposits are predominately composed of pyrite (FeS_2, > 90% of volume), with variable

amounts of sphalerite (ZnS), chalcopyrite ($CuFeS_2$) and galena (PbS) (Sáez et al., 1999; Venkateswarlu et al., 2016). The exposure of these sulfides to oxygen and water liberates sulfate ions and metals and leads to acidity (pH = 2.5-3.0), polluting the waters (Cánovas et al., 2007). There are few works worldwide about concentrations and behaviour of natural radionuclides in locations affected by AMD, but high activity concentrations in these polluted environments have been found mainly for U-isotopes (Fernandes et al., 1998; Yamamoto et al., 2010; Durand, 2012; Madzivire, et al., 2014). In the study area some previous works also shown large concentrations of natural radionuclides with enhanced contents of U-Th isotopes and ^{210}Po in both waters and sediments (Blasco et al., 2016; Hierro et al., 2012, 2013; Manjón et al., 2019).

The AMD confers extreme physicochemical conditions on these rivers, which maintain high concentrations of toxic elements in solution (Cánovas et al., 2007; Nieto et al., 2007; Hierro et al., 2014) and radionuclides (Hierro et al., 2013). When these pollutants arrive at the Huelva estuary, they produce a severe environmental impact (VicenteMartorell et al., 2009; Cánovas et al., 2010; Sánchez-Moyano et al., 2010). The differences between the physicochemical parameters of the marine and fluvial waters produce a strong pH gradient in the estuarine mixing zone due to the neutralisation of these acidic waters and the precipitation of heavy metals and other pollutants from the dissolved into the particulate phase (Achterberg et al., 2003; Braungardt et al., 2003; Hierro et al., 2013, 2014). It is important to take into account that this mixing process does not occur at a steady point. A spatial displacement has been demonstrated, and while during the dry seasons the mixing takes place in the most internal zones of the estuary, during the wet seasons this process takes place in sectors closer to the coast (Carro et al., 2011).

The five phosphoric acid plants included in the chemical industrial complex located on the Huelva estuary generated around 100 Mt of a waste called phosphogypsum (PG) between 1968 and 2010, which is stored in large piles on the salt marshes of the Tinto River covering an area about 1000 ha (Fig. 3.13). PG is generated during the production of phosphoric acid, and it is essentially composed of gypsum ($CaSO_4 \cdot 2H_2O$) but contains high concentrations of ^{238}U series natural radionuclides and other impurities such as P_2O_5 (pH ≈ 1.5), F, and toxic metals (Pérez-López et al., 2007; Bolívar et al., 2009). The high concentration of natural radionuclides of PG comes from the raw material used in the industrial process, which in the case of Huelva was sedimentary phosphate rock from

Morocco (Bolívar et al., 1996). This phosphate rock contains U-series radionuclide concentrations of around 1500 Bq kg^{-1} (≈50 times higher than unperturbed soils), with 238U in radioactive equilibrium with its daughters. About 20% of the U, > 70% of the Th, and the majority of the Ra, Pb and Po (> 95%) contained in the phosphate rock remain in the PG after the industrial process (Bolívar et al., 1996; Bolívar et al., 2009). Therefore, PG is currently considered a Naturally Occurring Radioactive Material (NORM) (IAEA, 2003; Directive 2013/59/Euratom). On the other hand, the remaining phosphoric acid trapped between the PG particles explains the high acidity and polluting potential of the aqueous leachates produced by this waste (Pérez-López et al., 2010; Pérez-Moreno et al., 2018).

Until 1998, about 20% of the generated PG was discharged into the Odiel River channel, while the remaining 80% was pumped in suspension with seawater into the stacks, where PG was decanted, and the polluted acidic (pH ≈ 2) seawater (around 10^7 m^3 $year^{-1}$) was released into the Tinto River channel without any treatment (Bolívar, 2000). From 1998 until the end of the production (31 December 2010), due to a change in the environmental policy according to the OSPAR convention (OSPAR, 2002, 2007), all the PG was pumped with fresh water in a closed circuit and placed into the piles, which reached around 30 m in height in some sectors. The northern and southern areas of the stacks (around 550 ha) have been partially restored (Más et al., 2006). Nevertheless, there are several points were the acidic polluted waters from the PG piles (restored and unrestored) are reaching the waters of the Tinto estuary (Pérez-López et al., 2015, 2016; Papaslioti et al., 2018).

Considering these facts, the aim of this work is to study the concentrations and behaviour of U-Th isotopes and ^{210}Po during a year in the acidic mining waters of these rivers and their polluted estuaries.

3.3.2. Material and methods

For this study, four sampling points were selected: OR and TR are located in the Odiel and Tinto rivers, while OE and TE are located in the Odiel and Tinto estuaries, respectively (Fig. 3.13). OR and TR represent fluvial composition without any marine influence. At these four points, water samples were collected monthly throughout a year (from October 2009 to September 2010). In total, 48 water samples of 10 L each were collected. Temperature, pH, electrical conductivity (EC) and redox potential (Eh) were

measured *in situ* using a Crison MM40+ portable multimeter, with a 5048 (Ag/AgCl) electrode. The instruments were calibrated before sampling, and the redox potential was corrected to obtain the potential relative to the hydrogen electrode (Eh) according to Nordstrom and Wilde (1998).

Water samples were filtered in the laboratory by using polycarbonate filters 9.0 cm in diameter with a pore size of 0.45 μm. Concentrated HNO_3 was added to achieve pH < 2 in order to prevent the adsorption of radionuclides onto the container walls. The filters were dried and weighed, and the particulate matter (PM) content was calculated by subtracting the filter mass. The filters were cleaned with HNO_3, and the liberated particulate matter was dissolved by applying atmospheric acid digestion with aqua regia (3 HCl:1 HNO_3). The dry residue was re-dissolved in 8 M HNO_3. Major and minor elements were determined in the dissolved matter by Inductively Coupled Plasma Optical Emission Spectroscopy (ICP-OES) and Inductively Coupled Plasma Mass Spectroscopy (ICP-MS) at Actlabs (Canada). The quality control (QC) was developed by the measurement of Certified Reference Materials (CRMs) and a duplicate every ten samples.

Radionuclides in dissolved and particulate matter were determined by a sequential extraction technique based on the use of tributyl phosphate (TBP) (Bolívar, 2000), subsequent electrodeposition onto a stainless-steel disc (U-Th isotopes) and selfdeposition onto a silver disc (^{210}Po), and measurement of the activities by α-spectrometry using ion-implanted silicon detectors (Bolívar et al., 2000) with 25% absolute efficiency. The QC for alpha-particle measurements was conducted by participating in annual international proficiency tests (International Atomic Energy Agency [IAEA] and the Spanish Nuclear Safety Council [CSN]), and by measuring both a blank and CRMs for every set of six samples (IAEA-434).

3.3.3. Results and discussion

3.3.3.1. Fluvial discharges

Rainfall in the province of Huelva is very irregular, with high intra-and interannual variability. This irregularity in the precipitation together with the low permeability of the Tinto and Odiel river basins explains the large variations in the flow of these rivers (Olías et al., 2006). The rainfall is concentrated throughout the wet season, between the months of October and April, preceded by the low flow-season between the months of May and September. The average annual flows of the Odiel and Tinto rivers are 29 and 1.6 $m^3 s^{-1}$

respectively (Olías et al., 2006), but the flows can increase by up to two orders of magnitude during floods, mainly in the autumn and winter months.

The average rainfall recorded during the study period at meteorological stations located close to the fluvial sampling points (OR and TR) was very high (960 mm) compared to the average rainfall in the area (550 mm). The highest precipitations were registered in the winter months, with occasional rain during the spring and very low rainfall during the summer and autumn months (Fig. S3.3 of the supplementary material). Figure 3.14 shows the Odiel River flow data recorded in the stream gauging station close to the OR sampling point (unfortunately, there are no data for the Tinto River flow). It should be noted that during the autumn there was no flow in the Odiel River, which is unusual since November is normally one of the rainiest months. The highest flows, like the precipitations, were recorded during the winter months with a maximum in February (1755 $m^3 s^{-1}$).

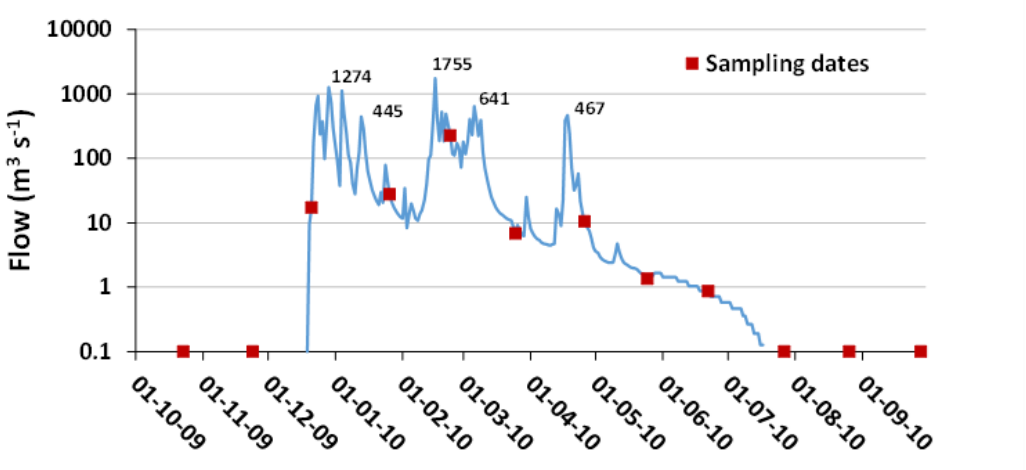

Figure 3.14. Daily flow of the Odiel River during the study period indicating the sampling dates.

3.3.3.2. Hydrochemistry

The measured physicochemical characteristics are in Table S3.10 of the supplementary material. The pH of the Odiel and Tinto rivers shows the acidity of their waters during the year, with median pH values of 3.2 and 2.7, respectively. The lower pH in the Tinto River is due to the greater impact produced by the AMD on its course (Olıas et al., 2004). In both estuaries, the pH values are very similar and notably higher than the fluvial ones, with almost neutral mean values (OE = 7.0, TE = 6.9) due to the influence of the seawater (pH ≈ 8). Regarding the temporal evolution (Fig. 3.15A), the behaviour of the pH at the estuarine points (OE and TE) is opposite to that in the rivers (OR and TR). This is explained by the fact that the intense rain decreases the acidity of the rivers during the winter and spring months due to the dilution effect by runoff. On the other

hand, the large discharge of fluvial water during these months (mainly January and February) displaces the seawater out of the estuaries, making the marine influence less important and increasing the acidity of their waters (Fig. 3.15A).

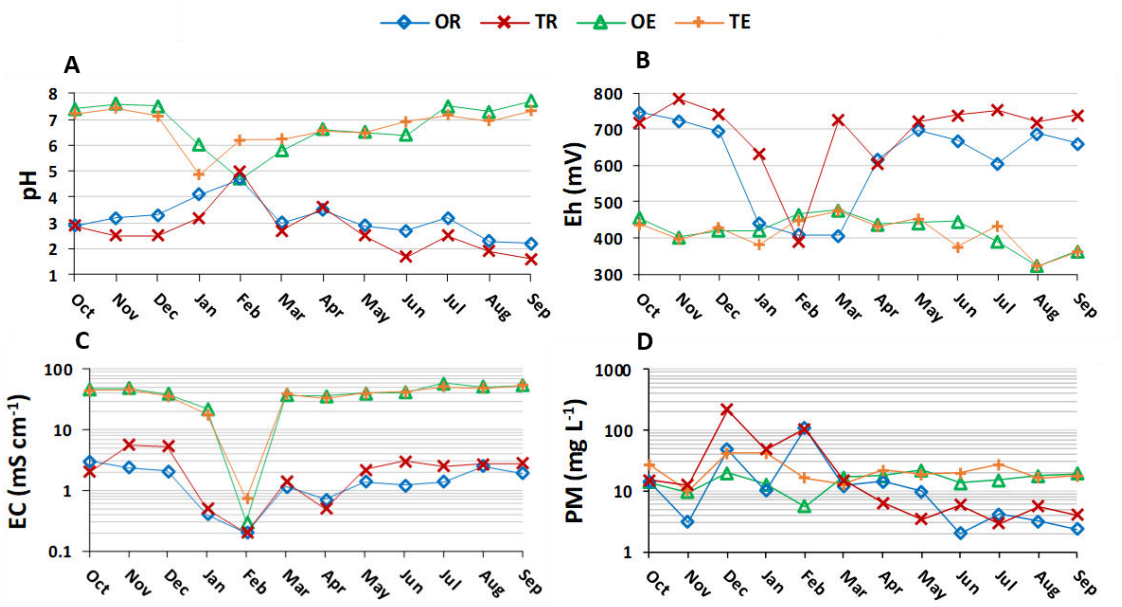

Figure 3.15. Evolution of pH (A), redox potential (B), electrical conductivity (C) and particulate matter (D) during the year in the riverine and estuarine sampling points.

The Eh showed the same mean value (≈ 420 mV) in both estuaries, similar to the value of seawater (400-435 mV) (Kennish, 2017), while in the rivers it is significantly higher (OR = 613 and TR = 689 mV) (Fig. 3.15 B). Under these oxidising conditions, U is found primarily as U (VI) in the form of the highly soluble uranyl ion UO_2^{2+}, which forms complexes mainly with carbonate and phosphate under neutral conditions or with sulfate and fluorides at acidic pH values (Porcelli and Swarzenski, 2003), while under reducing conditions, uranium is predominantly present as U(IV) and tends to precipitate as insoluble minerals. In the rivers, the Eh decreased significantly during the winter months due to the dilution effect caused by rainfall, while in the estuaries it remained approximately constant during the year.

The mean values of EC in the fluvial waters were 1.5 and 2.4 mS cm^{-1} at the sampling points OE and TE, respectively, showing the large amount of dissolved ions transported by these rivers. The higher EC of the Tinto River is consistent with its higher acidity. In the estuaries the mean EC was around 40 mS cm^{-1}, slightly lower than the typical one of seawater (50 mS cm^{-1}), as expected due to the mixing. The temporal evolution of the EC (Fig. 3.15C) shows a similar pattern to the pH, with a large decrease during the rainy

season (around two orders of magnitude) due to the great intake of fluvial water, mainly in February.

The particulate matter (PM) showed similar concentrations at both estuarine points with a mean of 15 and 23 mg L^{-1} in the Odiel and Tinto estuaries, respectively. At fluvial sampling points the median concentration was around 10 mg L^{-1}, with significant higher values (> 100 mg L^{-1}) during the winter months in relation to flood events, which produce an increase in the water turbidity (Fig. 3.15D).

The concentrations of major and trace elements in the dissolved phase are listed in Tables S3.11-S3.14 of the supplementary material, showing the values at the sampling points. The high concentrations of sulfate and metals in these rivers are due to the effects of AMD. The mean sulfate concentrations in the Odiel and Tinto rivers were 970 and 1550 mg L^{-1}, respectively. The metals and metalloids with the highest concentrations at the fluvial sampling points were the following (mean concentration in brackets): Al (OR = 58 and TR = 86 mg L^{-1}), Zn (OR = 15 and TR = 21 mg L^{-1}), Mn (OR = 11.9 and TR = 8.6 mg L^{-1}), Cu (OR = 5.3 and TR = 18.9 mg L^{-1}) and Fe (OR = 7.5 and

TR = 144 mg L^{-1}). All these elements decrease their concentrations in the rivers by around one order of magnitude during the flood events (January, February, and April in this study) due to the dilution effect and increase their concentrations during the dry season (Tables S3.11 and S3.12). At the estuarine points, the compositions of the waters are clearly influenced by seawater and are very similar to one another. The measured species with higher concentrations and their mean values (in brackets, mg L^{-1}) are as follows: Na (OE = 7800 and TE = 7400), SO_4^{2-} (OE = 2200 and TE = 2100), Ca (OE = 300 and TE = 330), K (OE and TE = 330), and Sr (OE and TE = 5.4). Several metals (Al, Fe, Cr, Pb, Sn) showed concentrations below the DL during the year. Almost all metals increase their concentrations in the estuaries by around one order of magnitude during the rainiest months due to the higher fluvial flow, while the elements with higher concentrations in seawater notably decrease their concentrations during these periods (Tables S3.13 and S3.14). These concentrations and behaviour agree with previous studies (Olías et al., 2006; Cánovas et al., 2007; Hierro et al., 2014).

In order to know the influence of the rivers on their estuaries during the year, the percentages of fluvial water in this mixing zone were determined based on the

conservative behaviour of Na (Loder and Reichard, 1981; Gordeev and Lisitzin, 2014), according to:

$$\% \text{ fluvial water} = \frac{[X_{Na}(E)] - X_{Na}(SW)}{[X_{Na}(R)] - X_{Na}(SW)} \cdot 100 \qquad \text{(Eq. 3.2)}$$

where $X_{Na}(E)$ and $X_{Na}(R)$ are the concentrations of Na at the estuarine and fluvial sampling points, respectively, and $X_{Na}(SW)$ is the approximate concentration of Na in seawater (10^4 mg L^{-1}). These percentages are displayed in Figure 3.16. The high percentage of fluvial water at the estuarine points during the rainy season is noteworthy, mainly after the flood events of January (49 and 62% in the Odiel and Tinto estuaries, respectively), February (≈ 99% in both estuaries) and April (37 and 44% in the Odiel and Tinto estuaries, respectively). These values demonstrate the similarity between these two systems and the fact that the mixing zone is not spatially steady during the year; on the contrary, during the wet season, the mixing process takes place at more outward sectors.

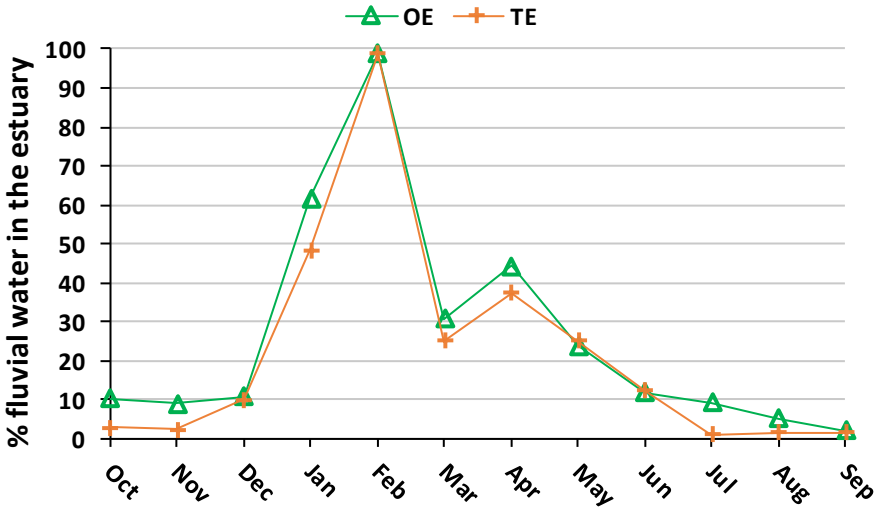

Figure 3.16. Percentage of river water in the estuarine sampling points.

3.3.3.3. Natural radionuclides

U-isotopes

The ^{238}U activity concentrations for the dissolved and particulate matter are displayed as box and whiskers plots in the Figure 3.17A, and the temporary evolution is shown in Figure 3.17B and C. Data are shown in Table S3.15 of the supplementary material. The mean concentrations in the dissolved phase were 49 and 57 mBq L^{-1} in the Odiel and Tinto rivers, respectively, approximately 10 times higher than the background values of continental surface waters in Europe (around 4 mBq L^{-1}) and worldwide (6 mBq L^{-1}) (De

Vos and Tarvainen, 2006). In the estuaries, the dissolved ^{238}U activity concentrations were similar, with means of 33 and 36 mBq L^{-1} for the Odiel and Tinto estuaries, respectively (Fig. 3.17A), slightly lower than the mean for marine water (40 mBq L^{-1}; Ku et al., 1977). Nevertheless, concentrations higher than 50 mBq L^{-1} were reached, mainly in the Tinto estuary.

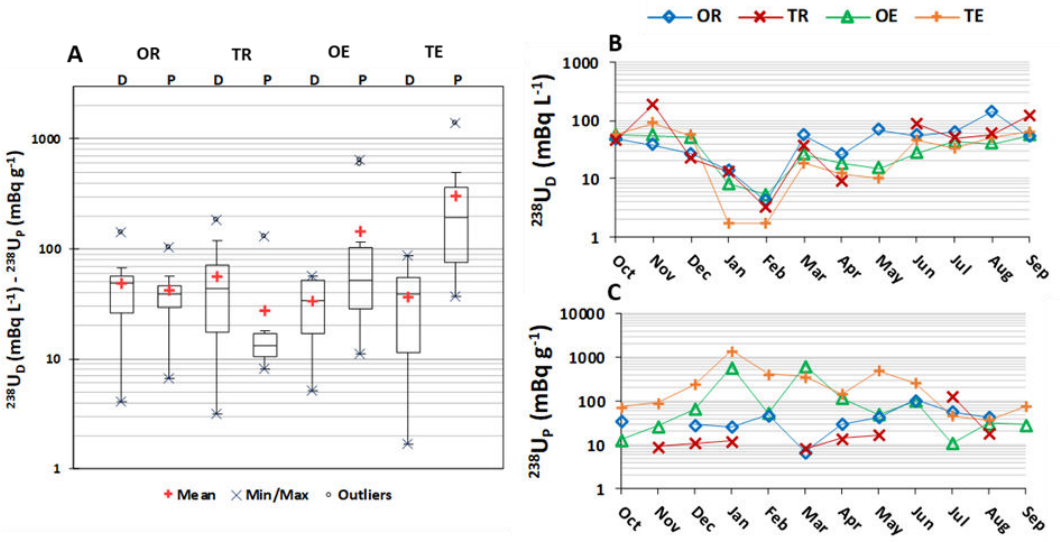

Figure 3.17. Box whisker plots of ^{238}U concentration in the dissolved and particulate phases (A), and temporal evolution for the dissolved (B) and particulate phases (C). Central line: median; box limits: first and third quartiles; whiskers: minimum and maximum non-outliers.

According to Figure 3.17B and taking into account the obtained uncertainties, which were lower than 10% (Table S3.15 of the supplementary material), the dissolved ^{238}U shows a clear seasonal pattern in both rivers and estuaries with an important decrease during the winter months because of the dilution effect during the rainy season. During the rainiest months, an additional U input in the Tinto estuary should be considered: the lateral polluted outflows from the PG stacks, which show a mean concentration of ^{238}U of $4.5 \cdot 10^4$ mBq L^{-1} (Pérez-Moreno et al., 2018), because of the surface runoff and groundwater. The dissolved activity concentrations increase progressively during the dry season at all the sampling points due to the decrease in the river flows (Fig. 3.14). While the maximum concentration for the Odiel River was measured in the month of August (140 ± 4 mBq L^{-1}), the Tinto River reached its maximum in November (182 ± 13 mBq L^{-1}). This peak of dissolved ^{238}U in the Tinto River is related to the dissolution of the efflorescences precipitated during the dry season by the first rainfalls of the hydrological year, similarly as was previously observed for metal/oids (Cánovas et al., 2007).

In the particulate matter, the mean ^{238}U concentrations at the fluvial points were 42 and 27 mBq g^{-1} in the Odiel and Tinto rivers, respectively, while in the estuaries they

were significantly higher, at 143 and 300 mBq g^{-1} in the Odiel and Tinto estuaries, respectively (Fig. 3.17C). The ^{238}U concentration in the particulate matter of the estuaries is one order of magnitude higher than the worldwide median concentration in unperturbed sediments, which is 35 mBq g^{-1} with a range from 16 to 110 mBq g^{-1} (UNSCEAR, 2000). The high concentration of this radionuclide in the Tinto estuary is probably related with the releases from the PG stacks. The particulate ^{238}U activity concentration does not show a seasonal pattern as clearly as the dissolved one. The highest activity concentrations in the particulate matter of the estuaries were observed during the rainy season, with ≈600 mBq g^{-1} in January and March in the Odiel estuary and ≈1400 mBq g^{-1} in February in the Tinto estuary, probably due to the decrease of pH in the estuaries and consequent coprecipitation/sorption of dissolved U, as discussed below. This behaviour is not observed at the fluvial points, which show more or less constant concentrations during the year, with the highest values (> 100 mBq g^{-1}) during the summer months.

The percentage of ^{238}U associated with the particulate matter at the sampling points was determined (Table S3.16 of the supplementary material). In general, the particulate ^{238}U shows low percentages in both rivers, below 2% in most cases, with a median value of around 1%, which indicates that it is mainly transported in the dissolved phase. During the winter months, a notable increase of this percentage is observed, with a maximum of 55% in the Odiel River in February, probably due to the high rainfall in this month, and therefore an increase in pH to around 5 (Fig. 3.15A), producing the U precipitation. Unfortunately, the particulate matter in the Tinto River in this month was not determined. In the estuaries, the percentage of ^{238}U associated with the particulate matter is notably higher than the fluvial one, with means of 9 and 25% in the Odiel and Tinto estuaries, respectively. The maximum values for both estuaries were reached in January and were 49% in the Odiel River estuary and up to 97% in the Tinto River estuary.

The relationship between the pH and the dissolved ^{238}U activity concentration and the distribution coefficients (K_d) is shown in Figure 3.18, where it can be observed that the concentration of ^{238}U decreases as pH increases in the rivers. The lowest ^{238}U activity concentrations in the dissolved phase (< 30 mBq L^{-1}) were observed in the pH range from 4 to 6, which are reached during the rainy season in both rivers and estuaries as previously mentioned. For pH values higher than 6, which are observed in the estuarine points mainly during the dry season, the dissolved ^{238}U again increases its concentration, reaching values above the concentration in seawater (40 mBq L^{-1}) at pH values above 7 (Fig.

3.18A). The precipitation and/or adsorption of U by the particulate matter was low at pH values lower than 4 and higher than around 6 ($K_d \approx 10^2 - 10^4$ L kg^{-1}), while for pH values from 4 to 6, the K_d values were one to two orders of magnitude higher (Fig. 3.18B). The abnormal maximum values of K_d (> 10^5 L kg^{-1}) observed in the Tinto estuary in January and February are probably due to the increase of U in the particulate matter due to the input of this radionuclide from the PG stacks. This behaviour has been observed in previous studies (Hsi and Langmuir, 1985; Serkiz and Johnson, 1994) and is probably due to the coprecipitation of U with Fe-Mn hydroxides (McKee et al., 1987) in the pH range from 4 to 6. On the other hand, the abnormal increase of dissolved U for pH values > 7 is explained by the existence of redissolution processes and the formation of carbonated complexes (Hierro et al., 2013). Therefore, in the Odiel and Tinto estuaries, U shows a nonconservative behaviour.

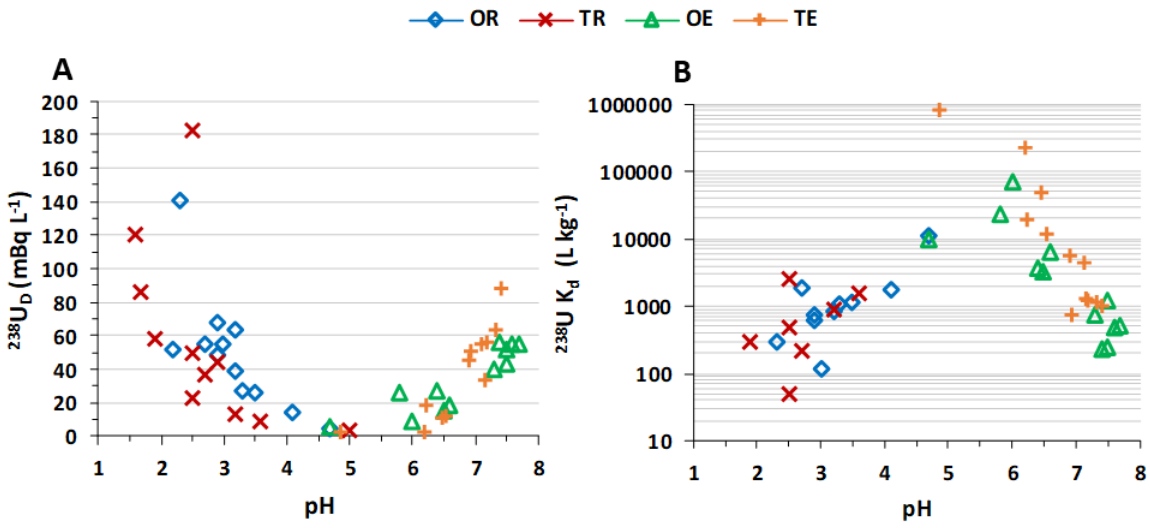

Figure 3.18. Dissolved ^{238}U activity concentration (A) and ^{238}U distribution coefficients (B) vs pH.

The ^{234}U/^{238}U activity ratio (AR_U) in the dissolved and particulate phases was also studied (Fig. 3.19 and Table S3.17 of the supplementary material). The AR_U in surface waters is generally higher than secular equilibrium (AR = 1) due to nuclide recoil during alpha-decay of ^{238}U and preferential dissolution of ^{234}U (Henderson et al., 2006). The dissolved AR_U presented values above 1 for most of the samples, with higher disequilibrium in the rivers than the estuaries. Mean values of 1.61 and 1.93 were obtained for the Odiel and Tinto rivers respectively (Fig. 3.19A), with some values higher than 2 in the Tinto River (Fig. 3.19B) due to more acidic conditions (Barbero et al., 2014; Manjón et al., 2019). In the Odiel and Tinto estuaries, the mean values in the dissolved phase were 1.21 and 1.11 respectively (Fig. 3.19A), very near to the value for seawater (AR_U = 1.14) (Boryło and Skwarzec, 2014). AR_U has a similar and constant value in both

estuaries during the year, except for January and February (Fig. 3.19B). During these two months, the percentage of fluvial water at the estuarine points is higher than that in seawater, as was previously described, and therefore an increase of the AR_U is expected, as was observed in the Odiel estuary. On the contrary, the Tinto estuary showed values around secular equilibrium, probably due to the great release of polluted leachates from the PG stacks favoured by the rains, which show AR_U around 1 (Gázquez et al., 2014; Pérez-Moreno et al., 2018).

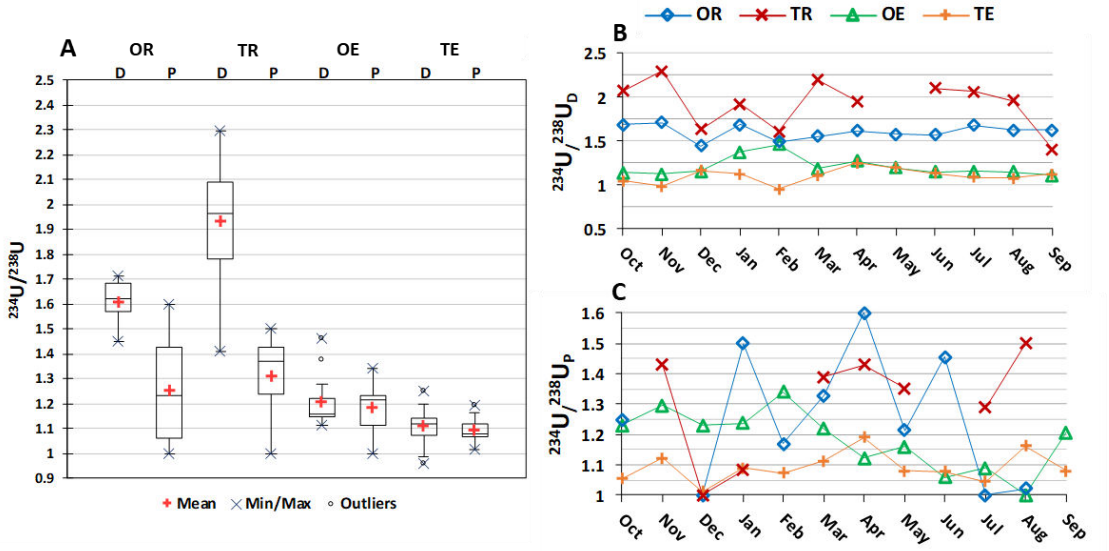

Figure 3.19. Box and whisker plots of the $^{234}U/^{238}U$ activity ratio in the dissolved and particulate phases (A), and temporal evolution for the dissolved (B) and particulate phases (C). Central line: median; box limits: first and third quartiles; whiskers: minimum and maximum non-outliers.

Regarding the particulate matter, lower AR_U values than in the dissolved phase were observed at the fluvial points. The mean values for the Odiel and Tinto rivers were 1.25 and 1.31 respectively (Fig. 3.19A), ranging from values around the secular equilibrium up to higher than 1.5 (Fig. 3.19C). At the estuarine points, the mean values in the particulate phase were 1.18 and 1.09 for the Odiel and Tinto estuaries, respectively (Fig. 3.19A). The lower observed values of this ratio in the Tinto estuary, mainly during the first half of the studied year (Fig. 3.19C), are probably once again related to the influence of the PG stacks.

^{210}Po

The activity concentrations of ^{210}Po in the dissolved and particulate phases are shown in Figure 3.20 and in Table S3.18 of the supplementary material. Both rivers and estuaries showed similar dissolved concentrations, with means of around 5 and 0.6 mBq L^{-1} at the fluvial and estuarine points, respectively (Fig. 3.20A). It highlights the observed

dissolved concentration peaks in December in both rivers, with concentrations higher than 20 and 30 mBq L^{-1} in the Tinto and Odiel rivers, respectively (Fig. 3.20B), one order of magnitude higher than background data observed in surface waters (1-5 mBq L^{-1}; IAEA, 2017). These peaks are probably related to the dissolution of efflorescences precipitated during the dry months (Romero et al., 2006; Sánchez España, 2008; Gázquez et al., 2014) by the first rainfalls of the hydrological year (Fig. S3.3A, B). In both rivers, the concentrations of dissolved ^{210}Po decrease below 1 mBq L^{-1} during the rainy and increase again to concentrations from 3 to 8 mBq L^{-1} during the summer. In the estuaries, the concentrations of dissolved ^{210}Po are approximately constant during the year around the mean value (Fig. 3.20B) and are similar to the estimated concentration of this radionuclide in seawater (0.4 to 0.6 mBq L^{-1}) (Skwarzec and Bojanowski, 1988; Uddin et al., 2015) but slightly lower than the concentration on the coast of Huelva (≈ 1 mBq L^{-1}) (Bolívar et al., 2000).

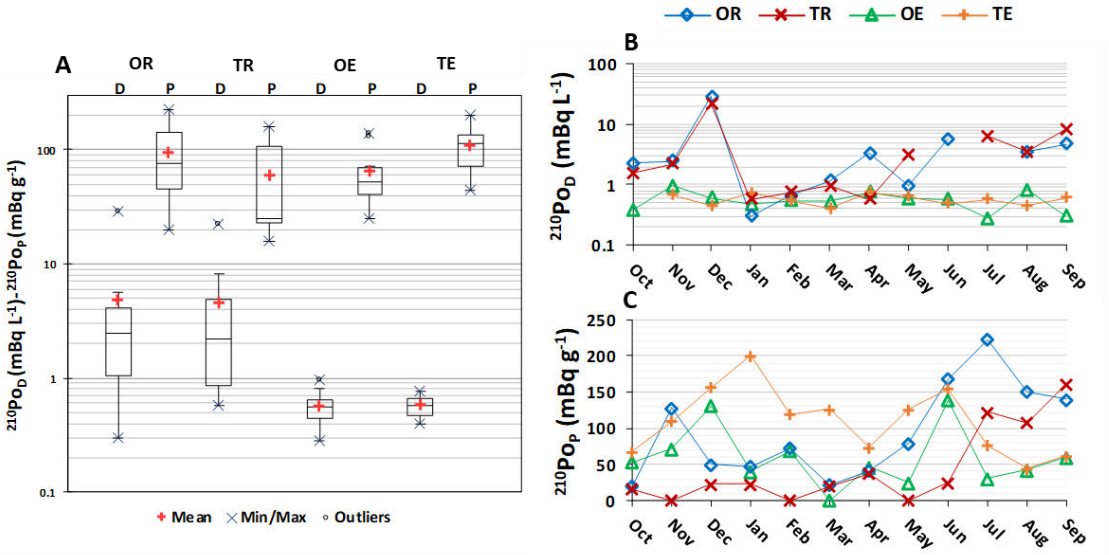

Figure 3.20. Box and whisker plots of the ^{210}Po activity concentration in the dissolved and particulate phases (A), and temporal evolution for the dissolved (B) and particulate phases (C). Central line: median; box limits: first and third quartiles; whiskers: minimum and maximum non-outliers.

In the particulate phase, the concentrations showed mean values of 95 and 59 mBq g^{-1} for the Odiel and Tinto rivers, respectively, and 64 and 110 mBq g^{-1} for the Odiel and Tinto estuaries, respectively (Fig. 3.20A). These concentrations are two to three times higher than the worldwide median value for natural soils (35 mBq g^{-1}) (UNSCEAR, 2000). A great dispersion in the concentrations was observed in both rivers and estuaries during the year (Fig. 8C). While the concentrations are higher in the Odiel River than in the Tinto River, in the estuaries the opposite is observed, with higher concentrations in the Tinto estuary, especially during the rainy season. This fact is probably related to the

input from the PG stacks due to the high concentration of this radionuclide in the edge outflows from the piles (mean ≈ $2 \cdot 10^4$ mBq L^{-1}) (Pérez-Moreno et al., 2018). The ^{210}Po shows greater association with the particulate matter than ^{238}U (Table S3.19 of the supplementary material). The mean values were 25 and 23% in the Odiel and Tinto rivers, respectively, with the highest values during the winter months, as in the case of ^{238}U. A percentage above 60% was obtained in both rivers in January, while during the month of February a percentage above 90% was obtained for the Odiel River. The mean values increased up to 59 and 77% in the Odiel and Tinto estuaries, respectively. These higher percentages of ^{210}Po are indicative of the lower solubility of this radionuclide under estuarine conditions.

The activity concentration of ^{210}Po in the dissolved phase tends to decrease with an increase in the pH in the studied rivers, similarly to ^{238}U. The dissolved ^{210}Po shows values < 1 mBq L^{-1} in both rivers and estuaries at pH values > 4, and unlike U, does not show an increase in the concentrations at pH values above 6 (Fig. 3.21A). In this sense, Figure 3.21B shows values of K_d one order of magnitude lower (10^4 –10^5 L kg^{-1}) at pH below 4 than at higher pH > 4 (> 10^5 L kg^{-1}). These facts demonstrate that ^{210}Po tends to (co)precipitate or to be adsorbed by the particulate matter for pH values higher than 4, showing a non-conservative behaviour. The K_d values are one to two orders of magnitude higher than those of the ^{238}U for the same pH values, which confirms its lower solubility.

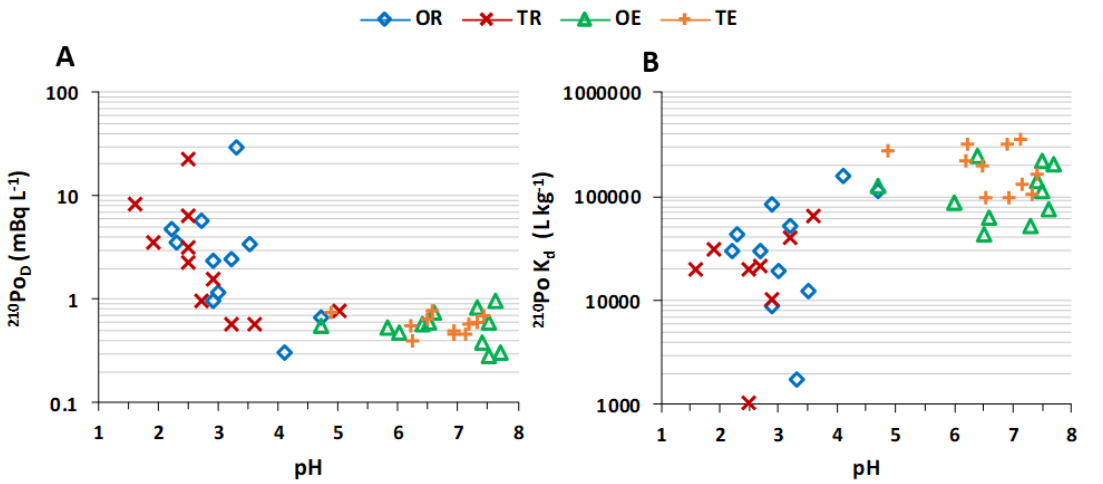

Figure 3.21. Dissolved ^{210}Po activity concentration (A) and ^{210}Po distribution coefficients (B) vs pH.

Th-isotopes

The results obtained for ^{232,230}Th activity concentration in the rivers are shown in Figure 3.22. In many cases concentrations below the DL were obtained (Tables S3.20 and S3.21 of the supplementary material). Th has a low solubility under neutral conditions,

but in waters affected by AMD, due to the high acidity and sulfate concentrations, tends to form soluble sulfate complexes such as $Th(SO_4)^{2+}$ and $Th(SO_4)_{2(aq)}$ (Kim and OsseoAsare, 2012). Considering only the detected samples, the dissolved phase showed mean concentrations of ^{230}Th and ^{232}Th of 27 and 16 mBq L^{-1} and 53 and 29 mBq L^{-1} in the Odiel and Tinto rivers, respectively (Fig. 3.22A). The Tinto River generally showed higher dissolved concentrations than the Odiel River, with a maximum of 50 mBq L^{-1} of ^{232}Th and 100 mBq L^{-1} of ^{230}Th, three to four orders of magnitude higher than in surface continental waters (Zhang et al., 2004; Amrane and Oufni 2017; Manjón et al., 2019b). In the estuaries, the dissolved concentrations of these radionuclides were below the DL (≈0.5–1 mBq L^{-1}) (Tables S3.20 and S3.21), which indicates that Th tends to precipitate due to its high particle reactivity (Wei et al., 2011), showing a non-conservative behaviour in the estuary.

The dissolved concentrations of Th-isotopes also showed a clear seasonal pattern in these rivers, with maxima during the end of autumn and early winter (before the first intense rains) and during the summer and were below the DL during the rainy season (Fig. 3.22B). As in the cases of U and Po, this pattern could be explained by three different stages during the year: (1) concentration peaks observed during November and December, probably related to the "washing effect" of salts and efflorescences produced by the first rainfalls after the summer, (2) a "dilution effect" by runoff in the rainy winter, and (3) a progressive "concentration effect" during the spring and summer.

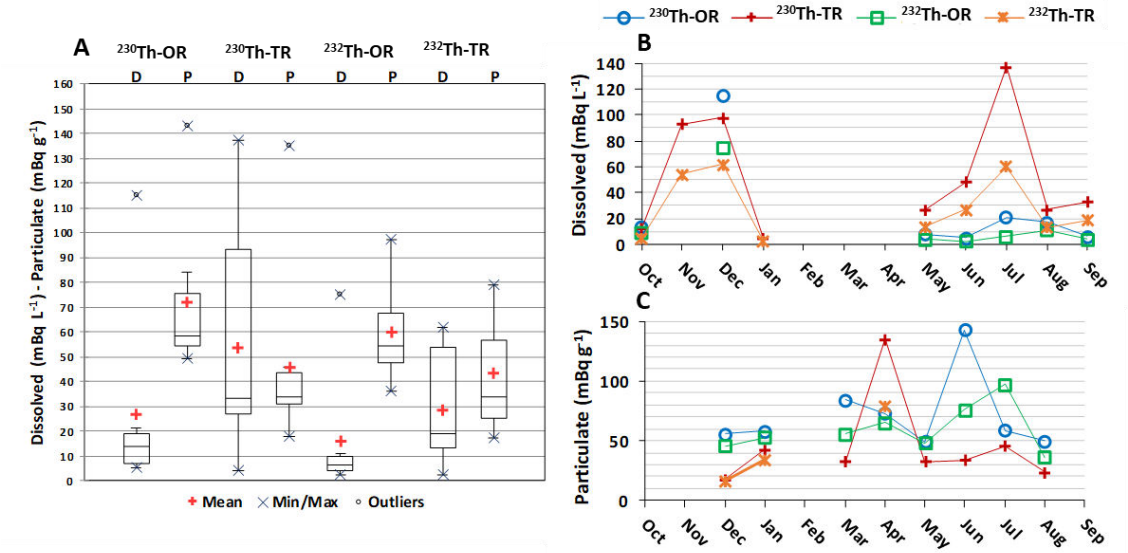

Figure 3.22. Box and whisker plots of the $^{230,232}Th$ activity concentration in the dissolved (D) and particulate (P) phases (A), and temporal evolution of the dissolved (B) and particulate phases (C). Central line: median; box limits: first and third quartiles; whiskers: minimum and maximum non-outliers.

The particulate matter of the rivers showed mean concentrations of ^{230}Th and ^{232}Th of 70 and 60 mBq g^{-1} and 46 and 43 mBq g^{-1} in the Odiel and Tinto rivers, respectively. At the estuarine points, similar concentrations were observed, with means of ^{230}Th and ^{232}Th of 43 and 17 mBq g^{-1} and 35 and 18 mBq g^{-1} in the Odiel and Tinto estuaries, respectively (Fig. 3.22A). Despite the abnormally high concentrations of Th-isotopes in the dissolved phase of the rivers, the activity concentrations of ^{232}Th in the particulate phase of the estuarine points are in agreement with the worldwide median concentration in unpolluted soils which is 30 mBq g^{-1} (range: 11-64 mBq g^{-1}) (UNSCEAR, 2000). This could indicate that the coprecipitation/sorption of Th occurs at a point previous to the sampling ones. In the rivers, the highest concentrations in the particulate phase were observed during the spring and summer (> 130 mBq g^{-1} of ^{230}Th), with higher values in the Odiel River (Fig. 3.22C). The estuarine points show a low variability during the year, with slightly higher concentrations during the winter months. For Th-isotopes, the influence of the PG stacks on the Tinto estuary is not observed, probably due to the low concentrations of these radionuclides in the edge outflows (< 100 mBq L^{-1}) (Pérez-Moreno et al., 2018).

3.3.4. Conclusions

The evolution and behaviour of U-Th isotopes and ^{210}Po in two rivers affected by AMD and their common polluted estuary during a year were studied. The conclusions obtained were as follows:

1. The Odiel and Tinto rivers show concentrations of U-Th isotopes and^{210}Po from one to three orders of magnitude higher than background continental waters due to the impact produced by the AMD. ^{238}U showed a mean concentration of around 50 mBq L^{-1} in these rivers, with maxima above 100 mBq L^{-1}. ^{210}Po showed a mean concentration around 5 mBq L^{-1} with maxima above 20 mBq L^{-1}. ^{230}Th and ^{232}Th showed maxima above 100 and 50 mBq L^{-1}, respectively.

2. The dissolved AR_U presented high disequilibrium in these AMD polluted rivers, with mean values of 1.6 and 1.9 in the Odiel and Tinto rivers, respectively, and maxima above 2, while in both estuaries a similar mean value to seawater was obtained (AR_U ≈1.1).

3. The studied radionuclides show a clear seasonal behaviour in these rivers, with three different stages during the year: (1) concentration peaks observed during November

and December due to the "washing effect" produced by the first rainfalls of the hydrological year, which dissolve the salts and efflorescences precipitated during the dry season, (2) a "dilution effect" by runoff in the rainy winter, and (3) a progressive "concentration effect" during the spring and summer.

4. A non-conservative behaviour of the analysed radionuclides in the estuarine mixing zone was demonstrated due to precipitation processes as a result of the increase of pH. The particulate phase of the estuaries is mainly enriched in U-isotopes and ^{210}Po, with values around one order of magnitude higher than in unpolluted sediments. Maxima of ^{238}U and ^{210}Po above 10^3 and 10^2 mBq g^{-1}, respectively, were observed.

5. The polluted outflows from the PG stacks produce a significant radioactive impact on the Tinto estuary, mainly during the rainiest months, increasing the concentration of U-isotopes and ^{210}Po in the particulate matter due to the high concentrations of these radionuclides in the releases and consequent precipitation after the mixing.

3.4. BEHAVIOUR OF HEAVY METALS AND NATURAL RADIONUCLIDES IN THE MIXING OF PHOSPHOGYPSUM LEACHATES WITH SEAWATER

J.L. Guerrero, S.M. Pérez-Moreno, I. Gutiérrez-Álvarez, A, M.J. Gázquez and J. P. Bolívar

Environmental Pollution 268 (2021) 115843, IF: 6.793 (2019), Category: Environmental sciences, Quartile: Q1, Position: 21/265.

Abstract

Phosphogypsum (PG) is disposed worldwide in large stacks usually placed in coastal zones, as in the case of Huelva (SW of Spain), where around 100 Mt of PG are stored on the salt marshes of the Tinto River estuary covering a surface of about 1000 ha. This management generates the weathering of PG, and due to its high acidity (pH ≈ 2) and pollutant load can provoke significant emissions into their surroundings. In this work were evaluated by laboratory experiments the effects of pH increase in the behaviour of heavy metals and natural radionuclides during the mixing of phosphogypsum leachates with seawater.

The acidic phosphogypsum leachates showed concentrations of heavy metals from two to three orders of magnitude higher than natural continental waters, and natural radionuclides (U-isotopes and ^{210}Po) from four to five orders of magnitude higher than unperturbed aquatic systems. Major elements and some heavy metals as Mn, Ni, Cd, As, Sb and Co showed a conservative behaviour during the neutralisation of the leachates with seawater, remaining in the liquid phase, while other ones as Al, Fe, Cr, Zn, Cu, Pb precipitated and/or were adsorbed onto the solid phase. The U-isotopes and ^{210}Po showed a clear nonconservative behaviour probably due to coprecipitation/adsorption processes onto the formed precipitates, but while ^{210}Po reached a total removal at pH ≈ 7, U-isotopes after a total removal at pH ≈ 5 returned into the liquid phase due to redissolution/desorption processes at near neutral pH.

The formed precipitates, mainly composed by iron phosphates particles, showed heavy metal and natural radionuclide concentrations from one to three orders of magnitude higher than unperturbed soils. All these facts demonstrate the serious environmental impact produced by the PG stacks into their surroundings and the urgency of effective restoration measures.

Graphical abstract

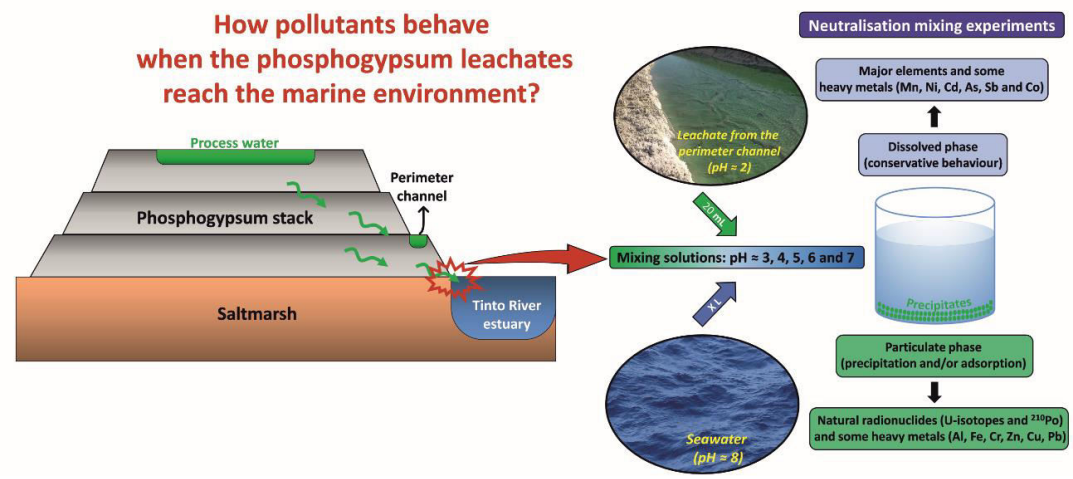

Keywords: heavy metals; natural radionuclides; phosphogypsum; water mixing; precipitation; acidity.

3.4.1. Introduction

Phosphogypsum (PG) is a by-product from the manufacturing fertilizer industry generated during the production of phosphoric acid (H_3PO_4), mainly composed by gypsum ($CaSO_4 \cdot 2H_2O$), but also contains high levels of pollutants such as heavy metals, acids, natural radionuclides, and some others trace elements (Rentería- Villalobos et al., 2010; Madruga et al., 2019) which may be leached. Globally, about 300 Mt of PG are produced every year (Yang et al., 2016) but only 15% of this amount is recycled, being mainly disposed by dumping in large stacks, usually placed in coastal zones close to the factories (Sanders et al., 2013; El Samad et al., 2014). This management of PG frequently generates its weathering which can provoke significant emissions into their surroundings (Tayibi et al., 2009).

Close to the Huelva city (SW of Spain), around 100 Mt of PG are stored in piles on the salt marshes of the Tinto River estuary covering a surface of about 1000 ha. This PG was generated in five acid phosphoric plants located in the industrial complex of Huelva at a rate of around $2.5 \cdot 10^6$ t $year^{-1}$ (Bolívar et al., 2002) since 1968 until the end of 2010, when the production of phosphoric acid stopped. The industrial process is based on the wet chemical attack of phosphate rock ore, in the case of Huelva fluorapatite ($Ca_5(PO_4)_3F$) was used, with sulphuric acid (H_2SO_4). The process can be summarized in the following general reaction (Eq. 3.3):

$$Ca_5(PO_4)_3F + 5H_2SO_4 + 10H_2O \rightarrow 3H_3PO_4 + 5CaSO_4 \cdot 2H_2O + HF \qquad \text{(Eq. 3.3)}$$

The PG stacks were directly disposed on the salt marsh sediments without any type of insulation, and in large proportion of their extension they are currently without any type of cover layer, being exposed to weathering conditions. Rainfall favours the generation of leachates due to surface runoff and the infiltration provokes the existence of polluted groundwater fluxes. These acidic leachates (pH ≈ 2) show high concentrations of phosphates, sulphates, chlorides, fluorides, heavy metals (Cd, Cu, Ni, Fe, Mn, Al, Zn, Sb and Sr) (Pérez-López et al., 2016; Millán-Becerro et al., 2019), and U-series radionuclides, being these last ones in the order: $^{238,234}U$ (10^2 Bq L^{-1}), ^{210}Po (10 Bq L^{-1}), and ^{226}Ra and ^{230}Th (1 Bq L^{-1}) (Gázquez et al., 2014; Pérez-Moreno et al., 2018). Previous works (Guerrero et al., 2019, 2020) have demonstrated that the small grain size salt marsh sediments act as an impermeable barrier for in-depth leachates coming from the PG stacks, and the increase in the concentrations of natural radionuclides and other pollutants only reach the first decimetres of sediments below the contact zone. Therefore, the polluted groundwater travel across the piles to the borders generating small edge outflows in numerous points (Pérez-López et al., 2015, 2016), which reach the estuarine environment. In this regard, the authorities in cooperation with the responsible companies are currently designing an engineering a project for their remediation.

Estuaries are complex coastal systems regulated by tidal action and riverine flows, which comprise transition zones between freshwater and seawater, controlling the flux of elements from the land into the oceans. In these transition systems, meaningful modifications of water chemistry take place with strong gradients in physico-chemical parameters such as pH, redox potential, and dissolved ions (Benoit et al., 1994; Hierro et al., 2014). On the other hand, when anthropogenic polluted releases reach the marine environment, different geochemical processes occur, as precipitation and/or adsorption onto formed solid phases, and on the opposite, dissolution, desorption and migration, changing the elemental concentrations in the dissolved phase and the bottom sediments (Zhou et al., 2003; Hierro et al., 2014). Therefore, to study the hydrochemical processes taking place during the mixing of PG leachates with seawater is crucial to understand the intake of radionuclides and other pollutants into the open ocean. One of the main parameters involved in the mixing process is the pH, which directly controls the chemical composition of the mix, and thereby, the precipitation and mineralogy of the particulate phase.

Taking a similar approach to this work, Papaslioti et al. (2018) studied the effects of pH increase on trace elements mobility in the mix of PG leachates with seawater. In regard with the problematic of the leachates, Millán-Becerro et al. (2019) evaluated the alkaline treatment of this wastewater to provoke the precipitation and immobilization of the dissolved pollutants, achieving the almost totally removal of fluorides, phosphates and most metals with the exception of As and Sb.

According to these facts, the main aim of this work is to evaluate the behaviour of heavy metals and natural radionuclides (U-isotopes and ^{210}Po) and the involved hydrochemical processes during the mixing of phosphogypsum leachates with seawater, simulating the mix produced when the wastewaters from the PG stacks reach the coast environment.

3.4.2. Material and methods

3.4.2.1. Study area

The PG stacks of Huelva are on the salt marshes of the right bank of the Tinto River (Fig. 3.23). The Tinto River joins in its mouth with the Odiel river to flow into the Atlantic Ocean forming the Huelva Estuary.

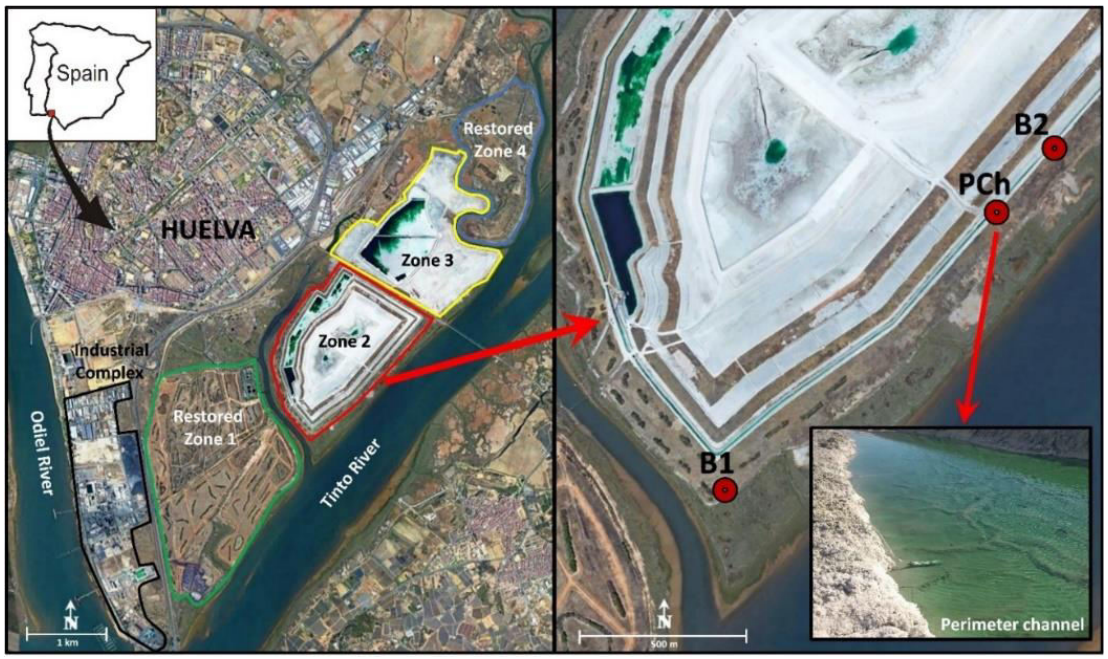

Figure 3.23. Location map of the Huelva phosphogypsum stacks and location of the phosphogypsum leachates sampling points: Boreholes (B1 and B2) and perimeter channel (PCh) located in the Zone 2 of the stacks.

This estuary is severely polluted (Vicente-Martorell et al., 2009; Cánovas et al., 2010; Sánchez-Moyano et al., 2010) due to both the acid mine drainage (AMD) affecting these

two mining rivers which go through the Iberian Pyrite Belt (IPB) transporting in solution high concentrations of metals and metalloids (Sáinz et al., 2004; Nieto et al., 2013), and the intense activity of the Huelva industrial complex, generating a huge volume of polluted effluents into the estuary.

In their current state, four zones can be identified in the PG stacks of Huelva (Fig. 1). Zones 1 and 4 (around 550 ha in total), located to the north and south respectively, are considered already restored. Despite the regeneration of these zones, some edge outflows points can be observed in both, mainly in Zone 4 (Pérez-López et al., 2016). In the Zones 2 and 3, the PG is exposed to the external agents without any kind of cover layer, and show surface ponds of industrial process acidic water (green colors in Fig. 1), which are getting shallower and smaller by the evaporation process developed to proceed with the restoration of this areas. In the Zone 2 about 25 Mt of PG are stored in a surface of about 250 ha forming a pyramidal pile of up to 30 m in height. A network of perimeter channels surrounds this zone to collect the leachates from the PG stack. The Zone 3, with about 15 Mt of PG piled, shows a surface about 200 ha and an average of 6 m in height, and also include it a perimeter channel which was built in recent years.

3.4.2.2. Sampling and pretreatment

To develop the mixing experiments, three PG leachates (PGL) samples and a seawater sample (SW) of about 200 L were collected in March 2019. The PGL samples, with a volume of about 5 L each one, were taken in three different points from the Zone 2, two of them in boreholes (samples B1 and B2) which collect the polluted groundwater in the border of the stack, and the third one in the perimeter channel (sample PCh), which collects the existing lateral leachates. The PGL sampling points were chosen to show similar hydrochemical characteristics than the edge outflows, whose access is complex and a partial mix with the estuarine water is observed. The SW sample was collected in the open ocean, in the surrounding of the Port of Mazagón (Huelva Atlantic coast), to avoid the input of pollutants transported by the Tinto and Odiel rivers due to their strong affectation by AMD as was previously indicated.

The pH, electrical conductivity (EC) and oxidation reduction potential (ORP) of the samples were measured in situ with a Crison MM40+ portable multimeter, with a 5048 (Ag/AgCl) electrode. The instruments were calibrated before sampling, and the ORP was corrected to obtain the potential relative to the hydrogen electrode (Eh) according to

Nordstrom and Wilde (1998). Water samples were filtered in the laboratory by using 0.45 mm pore size polycarbonate filters.

3.4.2.3. Titration curves

A titration curve is a plot showing the change of the pH of a solution during a titration, i.e. the addition of a reagent (acid or base). In our case, the objective was to increase the pH of the PGL by the addition of a basic solution. Firstly, a strong base (1.5 M NaOH) was added to the acidic PGL to study its alkaline neutralisation improving the knowledge about the origin of this acidity. A volume of 100 mL of PGL from the perimeter channel (PCh) was selected, and the reagent was added dropwise with a graduated burette under continuous stirring. The titration curves with SW were carried out to estimate the amount of seawater required to neutralize the leachates (pH ≈ 7-8). Approximately 300 mL of SW were taken, and each one of the three PGL collected were added individually dropwise with a graduated burette under stirring. For these experiments the pH values were determined with a Crison MM40+ multimeter.

3.4.2.4. Precipitation method

The precipitation experiments were developed by using the PGL collected in the perimeter channel (PCh sample), which was selected as the most representative of the leachates arriving to the estuary. For every experiment, 20 mL of PCh were taken, and the suitable amount of SW (up to around 15 L) to obtain the target pH (3, 4, 5, 6 and 7), according to the obtained ratios in the titration curve. A duplicate of every experiment was carried out, and therefore, ten experiments were developed in total. The mix of SW and PGL was stirred during a few minutes to reach equilibrium (constant pH), and then, it was filtrated through 0.45 mm pore size polycarbonate filters to obtain the precipitates. The physicochemical parameters (pH, Eh and EC, and T) of the resulting solution were measured with a Crison MM40+ multimeter. The filtrated solutions (dissolved phase) from each mixing experiment were store and the filters with the formed solid phase were preserved in a dryer until the chemical and radiological analysis were carried out.

3.4.2.5. Analytical methodology

Chemical composition of the samples (starting samples and obtained ones after the experiments) was determined by Inductively Coupled Plasma Optical Emission Spectroscopy (ICP-OES) and Inductively Coupled Plasma Mass Spectrometry (ICP-MS)

techniques at Actlabs (Canada). The quality control (QC) was developed by the measurement of Certified Reference Materials (CRMs) and one duplicate every ten samples.

Natural radionuclide concentrations in dissolved and particulate matter were determined by a sequential extraction technique based on the use of tributyl phosphate (TBP) (Bolívar et al., 2000), subsequent electrodeposition onto stainless-steel disc (U-Th-Ra isotopes), and self-deposition onto silver discs for the case of ^{210}Po. The radioactive sources were counted by α-particle spectrometry using ion-implanted silicon detectors, with a 25% absolute efficiency. The QC for alpha-particle measurements was conducted by participating in annual international proficiency tests (International Atomic Energy Agency [IAEA] and the Spanish Nuclear Safety Council [CSN]), and by measuring both a blank and CRMs (IAEA- 434) every set of six samples.

Two of the obtained precipitates (pH ≈ 5 and 7) were also analyzed by Scanning Electron Microscopy (SEM), via a JEOL (JSM 5410) scanning electron microscope, coupled with an Energy Dispersive X-ray Spectrometer (EDS) in the central research services of the University of Huelva.

3.4.3. Results and discussion

3.4.3.1. Physicochemical parameters of the starting samples

The physicochemical parameters of the starting samples are shown in Table 3.5. The SW sample showed typical values of marine waters, with an alkaline pH (≈ 7.8), an electrical conductivity (EC) of 61.5 mS cm^{-1} due to its high salinity, and a redox potential (Eh) of 465 mV, similar to the observed values for seawaters from Huelva coast and other places worldwide (Papaslioti et al., 2018; Abdel-Halim and Aly-Eldeen, 2016; Akmal Idrus et al., 2017).

Table 3.5
Values of the physicochemical parameters of the starting samples. SW (seawater), PCh (perimeter channel), B1 and 2 (borehole 1 and 2).

Code	pH	EC (mS cm^{-1})	Eh (mV)
SW	7.78	61.5	465
PCh	1.68	40.8	623
B1	1.75	29.4	532
B2	1.62	39.1	414

Regarding the PGL samples, all of them show an extreme acidity (pH ≈ 1.7) as expected, and EC values around 40 mS cm^{-1} for the PCh and B2 samples, while the sample B1 showed a slightly lower value around 30 mS cm^{-1}. The lower EC of the sample B1 is probably related to a higher influence of the rainwater due to sealing problems of the borehole. The Eh of these leachates showed oxidising values in all cases, significantly higher in the sample PCh (Eh ≈ 620 mV) probably due to it is a surface sample, while the samples B1 and B2 are groundwaters from boreholes. As a conclusion, the physicochemical parameters of these leachates are in agreement with the observed ones in previous works (Gázquez et al., 2014; Pérez-Moreno et al., 2018).

3.4.3.2. Titration curves

Figure 3.24A displays the titration curve of the sample PCh with a strong base (1.5M NaOH). The obtained curve shows a similar pattern than the theoretical titration curve with a strong base for the phosphoric acid. Phosphoric acid is a triprotic acid with the following pK_a: $pK_{a1} = 2.12$, $pK_{a2} = 7.21$, and $pK_{a3} = 12.32$ (Haynes, 2016), in concordance with the obtained ones in our experimental data. The first two equivalence points, corresponding to base reaction with the first and second protons of this weak acid are also in agreement with the theoretical titration curve. These points were calculated for our experimental data by means of the first and second derivates, being located at pH values 5 and 9, respectively. These facts confirm that the acidity of the leachates mainly comes from the phosphoric acid dissolved in the PGL, and not due to other potential acids as fluorhydric acid or not completely consumed sulphuric acid during the industrial chemical process (Eq. 3.3).

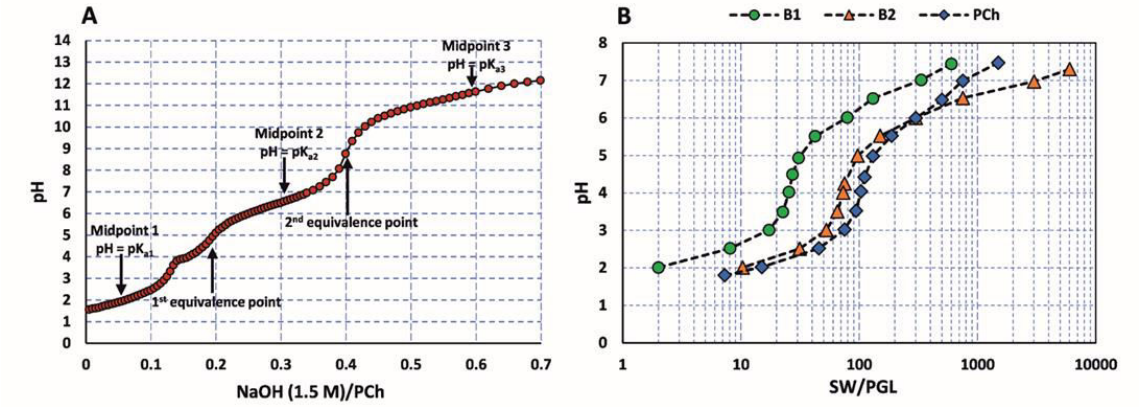

Figure 3.24. A: Titration curve of the phosphogypsum leachate (PGL) with NaOH (1.5M). B: Titration curves of the phosphogypsum leachates with seawater.

Regarding the curves obtained during the titration of the three collected PGL (B1, B2 and PCh) with SW (Fig. 3.24B), a similar pattern between them can be observed. Only the equivalence point, and the first two midpoints (pK_a values), are observed. This is because the maximum pH reached by using SW was around 7.5 since the neutralising power of seawater comes from the presence of carbonates and bicarbonates ions. It is interesting to note the large amount of SW required for the neutralisation of the PGL, in the order of 10^3 parts of SW per one part of PGL for reaching a pH = 7. The curve for the sample B1 is slightly displaced to the left indicating that a smaller amount of SW is required to achieve the alkaline neutralisation of this leachate, as expected, due to the pH of this sample was also slightly higher (Table 1). The curve of sample PCh showed an increase in the slope since SW/PGL = 10^2 in relation to the curve of sample B2, which indicates that lower SW amounts are required to increase the pH at this interval. This fact is probably related, despite the similar chemical composition of these two samples as will be discussed in section 3.4, with differences in the concentrations of the dissolved species.

After analyzing these results, it was decided to take the sample collected in the perimeter channel (PCh) to carry out the mixing experiments as was considered the most representative of the leachates that reach the estuary, and because is the one with the easiest access and the greatest availability in order to carry out future experiments.

3.4.3.3. Mixing experiments

The mixing experiments were performed in duplicate (Exp. A and Exp. B), to ensure the repeatability of the results. The amount of PGL and SW, the measured physicochemical parameters (pH, EC, Eh and T) and the obtained mass of precipitate for the target pH values are shown in Table S3.22 of the supplementary material. The variation of some of these physicochemical parameters during the mixing experiments are displayed in Figure 3.25. As can be observed, with equivalent amounts of the starting samples (Fig. 3.25A) the physicochemical parameters reached very similar values during the neutralisation. To confirm this fact, the relative standard deviation (RSD) of the main physicochemical parameters (pH, EC and Eh) was calculated. RSD values < 2% were

obtained with a mean of 0.7%, verifying the repeatability of the experiments.

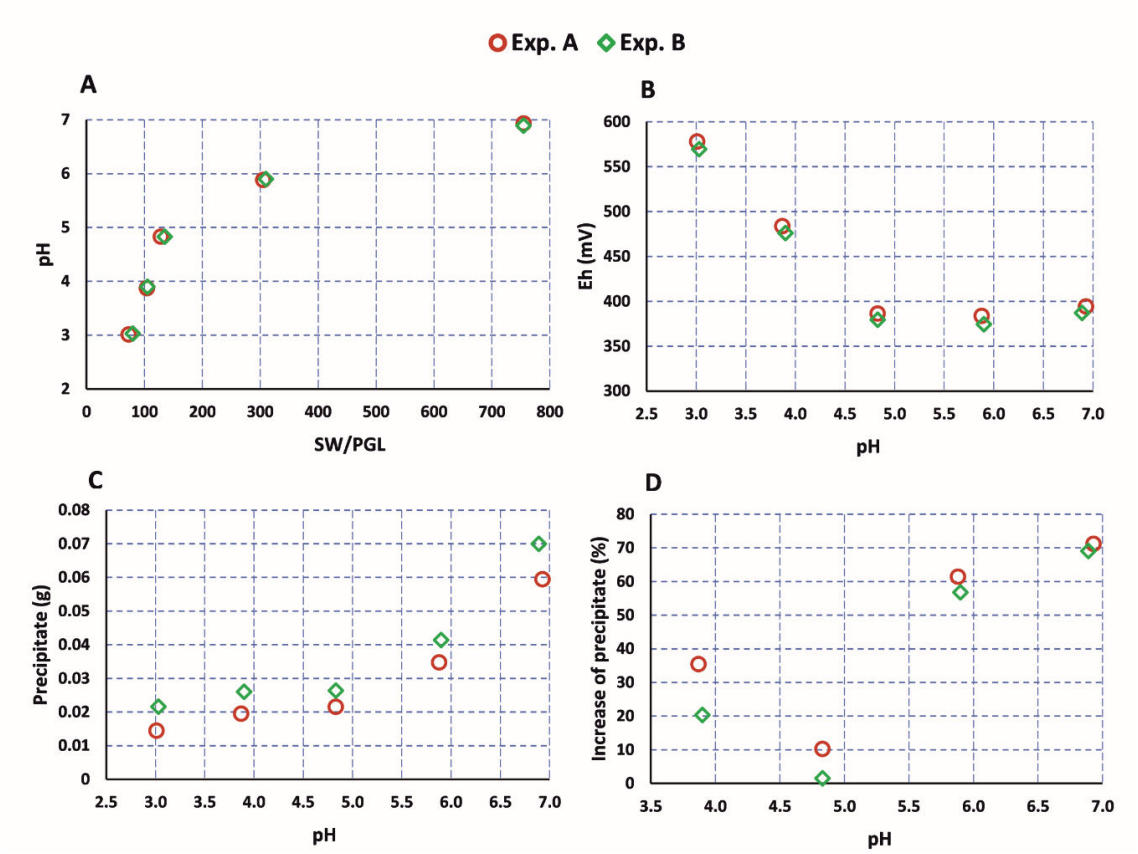

Figure 3.25. Variation of the pH (A), Eh (B), mass of precipitate (C) and increase of the precipitate (D) during the neutralisation carried out in the mixing experiments

The EC was constant for all the pH range (≈ 64 mS cm^{-1}), showing a similar value than the SW due to the large amounts added in comparison to the PGL ones (see Table S3.22), which also indicates the scarce precipitation occurred during the neutralisation. The Eh decreases during the neutralisation from a value close to 600 mV at pH ≈ 3 to around 400 mV at pH ≈ 5, remaining this value constant until pH ≈ 7 (Fig. 3.25B). This fact seems to be related with the lower influence of the PGL (Eh = 620 mV, Table 1), due to the increase of SW amount at higher pH values, which showed a lower Eh value. During the mixing experiments, a solid precipitate was generated for each target pH. The obtained masses were very similar in both experiments, being slightly higher for the experiment B (Fig. 3.25C). It highlights the increase of the mass of precipitates for the pH values 6 and 7 regarding the more acidic pH values.

In Figure 3.25D the increase in the mass of the precipitate (%) with respect to the previous pH was also represented to analyse the precipitate formed per unit of pH increase. It is observed that, from pH ≈ 3 to pH ≈ 4, the mean variation was around 25%, while the variation was even lower from pH ≈ 4 to pH ≈ 5 with a mean increase of around

5%. This fact indicates that from pH ≈ 4 to pH ≈ 5 the new mass of solid generated was practically negligible. On the contrary, from pH ≈ 5 to 6, and from pH ≈ 6 to 7 a notable increase in the amount of formed solid was observed, with an average about 65% in both cases. This fact shows the notable increase in the amount of precipitate generated per unit of pH increase for pH > 5, which indicates that the precipitation of chemical species increases significantly from this pH value.

3.4.3.4. Stable elements

The concentrations of the elements in the starting samples (PGL collected in the PCh and SW), the mixing solutions, and the obtained precipitates for each target pH value in the experiment A are shown in Table 3.6. The concentrations of the dissolved elements in the others collected PGL (B1 and B2) are shown in Table S3.23 of the supplementary material. Samples PCh and B2 showed in general similar concentrations, while slightly lower concentrations were obtained in B1 in agreement with the lower EC of this sample (Table 3.5). The concentrations observed in the mixing solutions of the Experiment B were very similar to the ones of the Experiment A as can be consulted in Table S3.24 of the supplementary material, and the calculated RSD showed a mean and median values of 6.5 and 2.7%, respectively. According to the high repeatability observed in this section and section 3.4.3.3, the analysis in this work will be performed with the samples of the experiment A.

Table 3.6
Concentration (mg L^{-1}) of the most significant elements in the starting samples and the mixing solutions, and in the solid precipitates (mg g^{-1}) of the experiment A.

	Starting samples		Mixing solutions					Precipitates				
	PGL	SW	pH ≈ 3	pH ≈ 4	pH ≈ 5	pH ≈ 6	pH ≈ 7	pH ≈ 3	pH ≈ 4	pH ≈ 5	pH ≈ 6	pH ≈ 7
Al	6.4	0.13	0.205	0.180	0.170	0.130	0.118	1.0	1.0	1.0	3.5	5.1
Ca	1640	441	457	459	450	443	454	9.3	9.6	14.2	19.3	19.4
Fe	139	0.0081	1.017	0.404	0.271	0.148	0.036	92	97.4	95.4	54.9	39.9
K	268	440	422	432	425	428	438	9.2	9.5	9.2	8.8	9.8
Mg	860	1440	1400	1470	1450	1450	1460	17.1	17.8	18.8	25.5	28.5
Mn	14.3	<0.002	0.190	0.142	0.113	0.036	0.016	0.018	0.027	0.026	0.041	0.050
Co	0.982	<0.002	0.013	0.009	0.007	0.003	<0.002	0.0013	0.0014	0.0012	0.0016	0.0019
Ni	6.82	<0.002	0.081	0.060	0.049	0.021	0.008	0.016	0.014	0.012	0.015	0.016
Na	4620	11700	11540	11900	11800	11900	12050	158	153	137	170	202
P	11281	0.278	139	99	80	34	14	99.7	98.1	99.7	64.8	45.2
S	1523	1040	1031	1070	1050	1053	1060	13.4	11.8	10.3	14.3	18.5
Zn	70	0.050	0.818	0.589	0.483	0.225	0.118	0.16	0.16	0.76	1.97	1.81
Cr	20	<0.002	0.165	0.049	0.006	<0.002	<0.002	17.1	20.2	16.3	13.7	5.3
Si	519	<2	7.5	5.3	4.4	<2	<2	0.60	0.41	0.43	0.26	0.15
Cu	9.84	0.0035	0.121	0.092	0.068	0.022	0.006	0.16	0.08	0.31	0.99	1.02

	Starting samples		Mixing solutions					Precipitates				
	PGL	SW	pH ≈ 3	pH ≈ 4	pH ≈ 5	pH ≈ 6	pH ≈ 7	pH ≈ 3	pH ≈ 4	pH ≈ 5	pH ≈ 6	pH ≈ 7
As	21.6	<0.002	0.387	0.287	0.229	0.099	0.040	0.127	0.161	0.172	0.108	0.083
Sr	34.3	8.2	8.5	8.5	8.4	8.2	8.3	0.24	0.45	0.83	1.02	0.85
Cd	9.5	<0.002	0.115	0.082	0.067	0.028	0.010	0.0033	0.0022	0.0036	0.0047	0.0029
Ba	0.042	0.008	0.008	0.008	0.007	0.007	0.007	0.034	0.034	0.067	0.071	0.064
Sb	0.567	0.011	0.036	0.030	0.022	0.017	0.016	0.0066	0.0185	0.0144	0.0113	0.0065
Pb	0.55	0.003	0.010	0.006	0.004	0.003	0.003	0.068	0.21	0.42	0.37	0.24
U	19.1	0.0032	0.30	0.11	0.008	0.013	0.024	2.1	12.4	18.4	10.0	2.0

Regarding the starting samples, the SW contains high concentrations of major elements, such as Na ($11.7 \cdot 10^3$ mg L^{-1}), Mg ($1.44 \cdot 10^3$ mg L^{-1}), S ($1.04 \cdot 10^3$ mg L^{-1}), K and Ca ($4.4 \cdot 10^2$ mg L^{-1}), similar to the found ones in seawater from the Huelva coast in previous studies (Papaslioti et al., 2018; Hierro et al., 2014). The PGL showed high concentrations for major elements, mainly P ($1.1 \cdot 10^4$ mg L^{-1}) being this value six orders of magnitude higher than unperturbed freshwater (Wetzel, 2001), but also for most heavy metals, such as Mn, Fe, Zn, As, Cr, Co, Cu, Cd, Ni, Al, Sb and Pb, from two to three orders of magnitude higher than natural continental waters (Zhou et al., 2020), and U ($1.7 \cdot 10^1$ mg L^{-1}), as expected from the acidic pH value and high EC, and in agreement with previous studies (Pérez-López et al., 2016; Papaslioti et al., 2018). All these pollutants show very low concentrations in the SW, below the detection limit (DL) in most cases, hence its contribution to the mixing solutions is negligible. In the mixing solutions, the major elements tend to show a constant concentration during the neutralisation, similar to the value of SW, indicating a conservative behaviour, i.e., these elements mainly remain in the aqueous phase. On the other hand, the pollutant elements decrease their concentrations in the mixing solutions as larger amounts of SW are added, clearly due to the dilution effect, but also precipitation processes can be occurred due to the increase of pH showing a nonconservative behaviour.

The obtained precipitates are mainly composed by Na, P and Fe (Table 3.6). High concentrations of most heavy metals and U were observed in these precipitates with values about one to three orders of magnitude higher than the background of this region (Lario et al., 2016; Guerrero et al., 2019), which demonstrate the high polluting potential of the leachates and the urgency of restoration measures. The concentrations of these pollutants in the solid phase during the neutralisation process showed different trends, increasing, decreasing, or not showing a clear behaviour. To clarify these results and to

analyze the non-conservative character of these elements, the transfer factor (TF) to solid was calculated according to the following formula (Eq. 3.4):

$$\frac{C_p \cdot M_p}{C_{PGL} \cdot V_{PGL} + C_{SW} \cdot V_{SW}} \cdot 100 \qquad \text{(Eq. 3.4)}$$

Where:

C_p = Concentration of the element in the precipitate

M_p = Mass of the precipitate

C_{PGL} = Concentration of the element in the PGL

V_{PGL} = Volume of PGL

C_{SW} = Concentration of the element in the SW

V_{SW} = Volume of SW

The TF to aqueous phase was also calculated and the data are in agreement with the obtained ones to solid but were presented these last ones due to the authors consider it more accuracy as a direct measurement. For the elements with concentrations below the DL in the SW, the DL value was applied for the calculations. TF values < 0.1% of Ca, K, Mg, Na, S, Si, Sr and Cd and <1% of Mn, Co, Ni, As, Sb and P were obtained, showing a conservative behaviour of the major elements and some heavy metals during the neutralisation. To note that, the TF only indicates the % of an element that is transferred into the solid phase, hence should be taken into account the total amount of this element added to the mixing solutions, which explain the fact that P and Na are some of the main components of the precipitate due their very high concentrations in the starting samples.

The other elements, including several heavy metals, showed higher TF to solid (Fig. 3.26), and therefore a non-conservative behaviour during the neutralisation, precipitating and/or been adsorbed to a greater or lesser extent onto the solid phase.

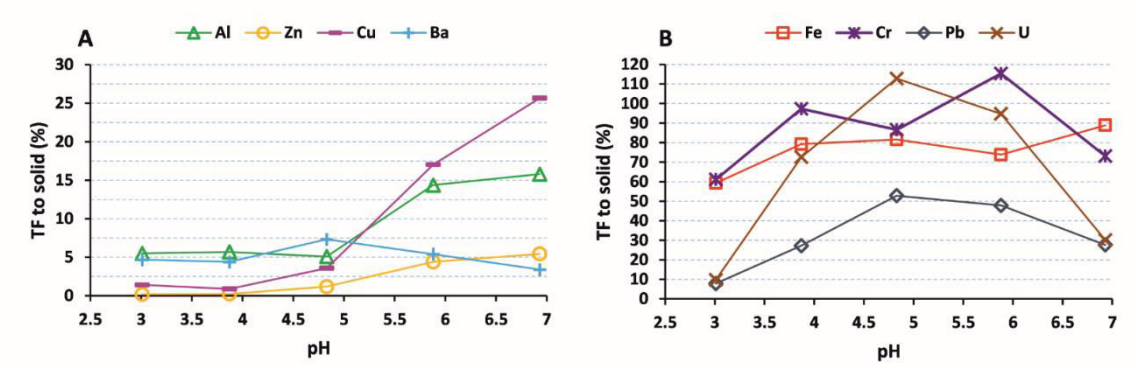

Figure 3.26. Transfer factor (TF) to solid (%) of non-conservative elements.

Zn and Cu showed a conservative behaviour until pH ≈ 5, increasing theirs TF up to 5 and 25% at pH ≈ 7, respectively (Fig. 3.26A). Ba showed TF around 5% during the neutralisation while Al increase its TF since pH ≈ 6-7 reaching values about 15% (Fig. 3.26A). On the other hand, Fe, Pb, Cr and U showed a notably higher TF to solid (Fig. 3.26B). Regarding Pb, the maximum TF (≈ 50%) was observed at pH values around 5-6, while the TF to solid of Fe ranged from around 60% at pH ≈ 3 to 90% at pH ≈ 7. A mean TF around 90% of Cr was observed during the neutralisation. According to Papaslioti et al. (2018), Fe tends to precipitate in the form of phosphates as strengite ($FePO_4 \cdot 2H_2O$) at pH > 3, as goethite (α-FeOOH) at pH > 4, as lepidocrocite (γ-FeOOH) at pH > 5 and as ferrihydrite [Fe(OH)3] at pH > 6, which usually act as sinks for trace elements as Pb and Cr being retained by sorption processes. Lastly, the TF of U increased from a minimum about 10% at pH ≈ 3 to reach a total precipitation at pH ≈ 5 and decreased again up to 30% at pH ≈ 7. This behaviour will be discussed in detail in the next section.

3.4.3.5. Natural radionuclides

The activity concentration of ^{238}U and ^{210}Po, and the $^{234}U/^{238}U$ activity ratio (AR_U) in the starting samples, the mixing solutions, and the obtained precipitates for each target pH in the experiment A are shown in Table 3.7. Ra and Th-isotopes showed low activity concentrations in the PGL with values below 2 Bq L^{-1}, being in the mixing solutions below the DL (0.001 Bq L^{-1}) in most cases, hence were not included in this work. The PGL showed, due to their high acidity, very high activity concentrations for the studied natural radionuclides, with about 300 Bq L^{-1} of ^{238}U and 22 Bq L^{-1} of ^{210}Po. These values are from four to five orders of magnitude higher than the observed ones in unperturbed surface freshwater and seawater (De Vos and Tarvainen, 2006; IAEA, 2017), which demonstrates the extreme polluting potential of these acidic leachates. Although U concentrations in seawater depends on the salinity (Owens et al., 2011), its concentration

is significantly uniform in the world oceans, being generally accepted that the U "oceanic average" concentration is 3.3 ± 0.2 mg L^{-1}, i.e. 0.041 Bq L^{-1} of ^{238}U (Ku et al., 1977), in agreement with our experimental data.

Table 3.7
Activity concentration of the studied radionuclides in the starting samples and the mixing solutions (Bq L^{-1}), and in the solid precipitates (Bq g^{-1}).

		^{238}U	$^{234}U/^{238}U$	^{210}Po
Starting samples	PGL	302 ± 9	1.00 ± 0.01	21.8 ± 1.0
	SW	0.042 ± 0.002	1.08 ± 0.04	0.0036 ± 0.0004
Mixing solutions	pH ≈ 3	3.56 ± 0.17	0.99 ± 0.01	0.19 ± 0.02
	pH ≈ 4	1.473 ± 0.029	1.00 ± 0.02	0.075 ± 0.010
	pH ≈ 5	0.177 ± 0.009	1.02 ± 0.03	0.021 ± 0.005
	pH ≈ 6	0.219 ± 0.018	1.03 ± 0.03	0.006 ± 0.001
	pH ≈ 7	0.325 ± 0.017	1.02 ± 0.02	0.0037 ± 0.0010
Precipitates	pH ≈ 3	22.4 ± 0.6	0.99 ± 0.01	7.6 ± 0.2
	pH ≈ 4	124 ± 2	1.00 ± 0.02	10.6 ± 0.2
	pH ≈ 5	232 ± 12	1.006 ± 0.006	17.0 ± 0.3
	pH ≈ 6	115 ± 5	1.005 ± 0.006	11.8 ± 0.4
	pH ≈ 7	20.7 ± 0.9	1.01 ± 0.01	7.7 ± 0.3

The AR_U showed secular equilibrium in the PGL (AR_U = 1), same ratio than the measured in both PG and phosphate rock used in Huelva and other places worldwide (Boryło et al., 2009; El Afifi et al., 2009; Guerrero et al., 2020) due to the uniform bulk dissolution of the original ore in the phosphoric acid production process (Hussain and Krishnaswami, 1980; Andersen et al., 2009). In the SW sample the ARU was a bit higher (1.08 ± 0.04), in agreement with mean value of marine water (AR_U ≈ 1.14) (Boryło and Skwarzec, 2014). In surface waters this ratio is usually higher than 1 due to nuclide recoil during alpha-decay of ^{238}U and preferential dissolution of ^{234}U (Henderson et al., 2006).

The activity concentrations of natural radionuclides in the mixing solutions showed a clear decrease during the neutralisation, due to the dilution effect by the large amount of SW added, similarly as was previously observed for the stable elements. To note that the activity concentration of ^{210}Po in the solutions continuous decreasing with the increase of pH, while the ^{238}U reach the minimum concentration at pH ≈ 5 and tends to increase again at higher pH values. It highlights that ^{210}Po showed a similar value than SW at pH ≈ 7, while ^{238}U showed activity concentrations from one to two orders of magnitude higher than the SW concentration in the mixing solutions. Concerning the solid precipitates, ^{238}U and ^{210}Po showed a similar trend, being enriched the precipitate until

pH ≈ 5 and decreasing again their concentrations as the pH value increase. The measured concentrations of these natural radionuclides in the precipitates are from two to three orders of magnitude higher than the worldwide median value for natural soils (0.035 Bq g^{-1}) (UNSCEAR, 2000), showing once again the potential environmental impact of these leachates. The AR_U showed values around secular equilibrium in both mixing solutions and precipitates, demonstrating that is strongly influenced by the PGL.

To clarify the behaviour of U-isotopes and ^{210}Po during the alkaline neutralisation of the acidic leachates, the TF to solid and the distribution coefficients (K_d) were calculated (Fig. 3.27). The K_d are used to quantify the affinity of a chemical specie for particles and were calculated according to the following formula (Eq. 3.5):

$$K_d = \frac{C_p}{C_d} \quad \text{(Eq. 3.5)}$$

Where:

C_p = activity concentration of the radionuclide in the precipitate

C_d = activity concentration of the radionuclide in the dissolution

The TF to solid of ^{238}U increased gradually their value from about 10% at pH ≈ 3, up to about 90% at pH ≈ 5, when most of the ^{238}U is found in the precipitate (Fig. 3.27A). The TF slightly decreased at pH ≈ 6 to about a 70%, but reached a 20% at pH ≈ 7, which indicates that at this pH about 80% of ^{238}U is again in solution. This fact is confirmed in Figure 3.27B where the K_d at pH ≈ 5-6 are around 1- 2 orders of magnitude higher than for lower or higher pH values. This behaviour has been observed in previous studies (Hsi and Langmuir, 1985; Serkiz and Johnson, 1994) and was justify due to coprecipitation of U with Fe-Mn hydroxides (McKee et al., 1987) in the pH range from 4 to 6 and the existence of redissolution processes due to the formation of carbonated complexes (Hierro et al., 2013; Guerrero et al., 2021a) at higher pH values. Therefore, the U-isotopes show a non-conservative behaviour and tend to precipitate or to be adsorbed almost totally at pH values around 5, to return into the liquid phase due to redissolution/desorption processes at near neutral pH values.

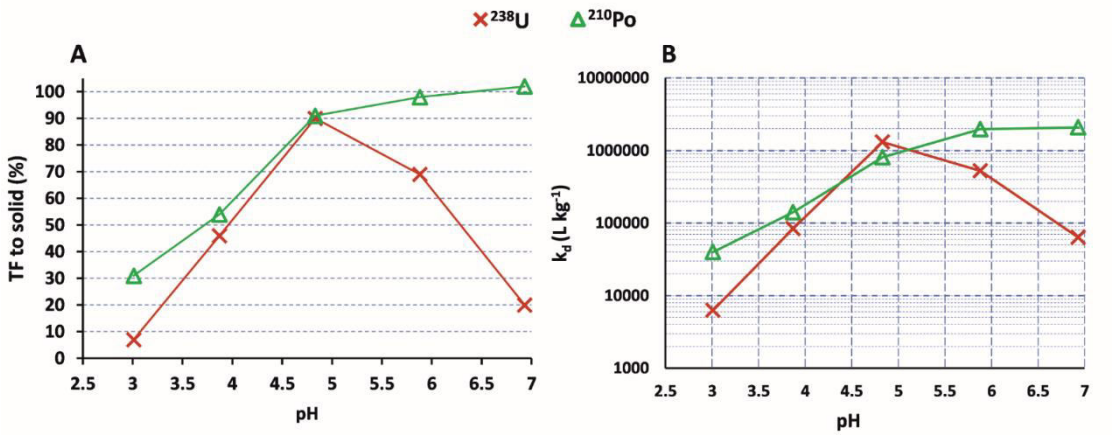

Figure 3.27. Transfer factor (TF) to solid (%) (A) and evolution of the distribution coefficients (K_d) during the increase of pH (B) of the studied radionuclides

The ^{210}Po increased continuously its TF during the alkaline neutralisation of the PGL, reaching values around 90% at pH values ≈ 5, and a total removal (TF ≈ 100%) at pH value ≈ 7 (Fig. 3.27B). In this sense, the K_d values of ^{210}Po increased during the increase of pH, showing values around one order of magnitude higher for pH values above 4, than for lower pH values. The observed K_d are in agreement with the obtained ones in other works where both natural (unperturbed) and polluted systems were studied (Blasco et al., 2016; Manjón et al., 2019; Bam et al., 2020; Guerrero et al., 2021a). These facts demonstrate that ^{210}Po tends to precipitate and/or to be adsorbed by the particulate matter during the neutralisation, showing a non-conservative behaviour.

3.4.3.6. Micro-structural characterization of the obtained precipitates

According to the previous findings, several heavy metals and the studied natural radionuclides showed a non-conservative behaviour during the increase of pH, been removed from the dissolve into the solid phase. Thus, the characterization of the obtained precipitates is of great significance to improve the understanding of the geochemical processes controlling its mobility during the neutralisation of the PGL with SW. The precipitates generated from two target pH were analysed by SEM-EDS, and the images and spectra are shown in Figure 3.28A (pH ≈ 5) and B (pH ≈ 7). The results of this analysis showed that the formed precipitates consist of a cryptocrystalline matrix mainly composed of P and Fe, as expected according to results presented in section 3.4, suggesting precipitation of iron phosphates, as strengite ($FePO_4 \cdot 2H_2O$). A fine layer of salts mainly composed by Cl and Na, probably in the form of halite (NaCl), covering most of the matrix particles was observed (Fig. 3.28A). These salts were probably originated by the evaporation of the remaining solution (mostly SW) in the filter.

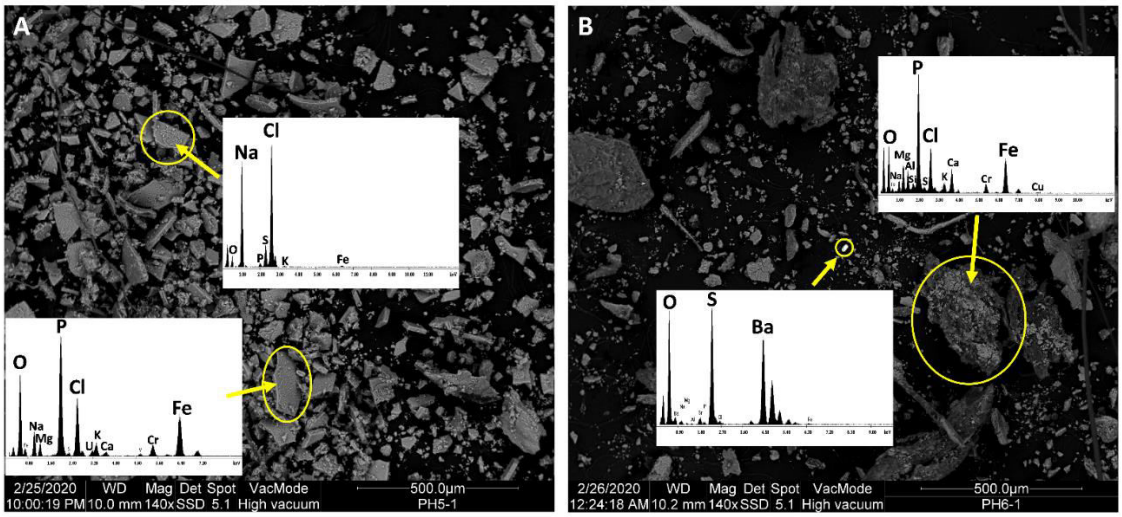

Figure 3.28. SEM images and EDS spectra of the obtained precipitates during the neutralisation at pH ≈ 5 (A) and 7 (B).

It is very interesting the detection of U in the matrix at pH ≈ 5 (Fig. 3.28A), which is in agreement with the previous findings and seems to confirm that U is removed from the dissolved phase due to coprecipitation/adsorption processes onto strengite crystals. Other metals, such as Al, Cr and Cu were detected together with the matrix at pH ≈ 7 (Fig. 3.28B), which is consistent with the observed data in section 3.4.3.4, and probably due to coprecipitation and/or adsorption processes. The higher concentrations of Ca detected at pH ≈ 7 in the matrix and the high concentration of P could be indicative of the precipitation of hydroxyapatite [$Ca_5(PO_4)_3(OH)$]. Finally, it should be noted the small particle mainly composed by S and Ba, probably as barium sulphate in the form of barite ($BaSO_4$), observed at pH ≈ 7. Barite shows a very low solubility and tend to precipitate when the concentration of sulphate increases in solution, in this case due to the input from the PGL.

3.4.4. Conclusions

The PG stacks of Huelva release polluted acidic leachates into the surrounding estuarine environment which produce a serious environmental impact. Seawater mixing experiments were carried out to improve the understanding of the hydrochemical processes occurring when these leachates reach the marine environment increasing their pH, focusing on the behaviour of heavy metals and the natural radionuclides with higher concentrations in the leachates (U-isotopes and ^{210}Po).

The obtained conclusions in this work are:

1. The titration curve of the phosphogypsum leachate with a strong base (NaOH) confirmed that the acidity of the leachates is mainly due to the existence of remaining phosphoric acid, and not due to other potential acids as fluorhydric acid coming from the ore, or sulphuric acid not completely consumed during the industrial chemical process.

2. The acidic phosphogypsum leachates show a high pollutant load, with large amounts of heavy metals, from two to three orders of magnitude higher than natural continental waters, and natural radionuclides, mainly U-isotopes and ^{210}Po, from four to five orders of magnitude higher than unperturbed surface freshwater and seawater. This fact demonstrates the extreme polluting potential of these acidic leachates.

3. The analysis of the transfer factor (TF) to solid showed a conservative behaviour during the alkaline neutralisation of major elements and some heavy metals as Ni, Cd, As, Sb and Co, which remain in the aqueous phase. Several heavy metals as Al, Fe, Cr, Zn, Cu, Ba, and Pb showed higher TF to solid, and therefore a non-conservative behaviour during the neutralisation, precipitating and/or been adsorbed to a greater or lesser extent onto the solid phase.

4. The U-isotopes and ^{210}Po showed a clear non-conservative behaviour according to the TF and distribution coefficient (K_d) values. U-isotopes presented an almost total removal from the dissolved phase at pH values around five, probably due to coprecipitation/adsorption processes onto the formed precipitates, to return into the liquid phase due to redissolution/desorption processes at near neutral pH values. ^{210}Po strongly increases its removal from the dissolved phase during the neutralisation, reaching a total removal at pH $\approx$ 7 due to precipitation and or coprecipitation/adsorption onto the solid precipitates.

5. The formed precipitates during the neutralisation showed heavy metal and natural radionuclide (U-isotopes and ^{210}Po) concentrations from one to three orders of magnitude higher than unperturbed soils, demonstrating the serious environmental impact produced by the stacks into their surroundings in their current state.

6. The SEM-EDS images showed that the generated precipitates consist of a cryptocrystalline matrix mainly composed of P and Fe, due to the precipitation of iron phosphates (strengite), which act as a sink for heavy metals and natural radionuclides by coprecipitation/adsorption processes.

Chapter 4
General conclusions

4.1. CONCLUSIONS

In this Doctoral Thesis the impact produced by the Huelva phosphogypsum stacks on their estuarine environment was evaluated. On the one hand, due to the phosphogypsum stacks were disposed on the salt marshes without any type of insulation layer, the underlying estuarine sediments were characterized to study their degree of affectation due to the migration of pollutants and the possible existence of deep leachates. On the other hand, the seasonal evolution of natural radionuclides in the fluvial and estuarine sections of the Odiel and Tinto rivers was analysed to know the impact produced by the acid mine drainage and the leachates coming from the phosphogypsum stacks. In this regard, mixing experiments with phosphogypsum leachates and seawater were carried out to study the behaviour of heavy metals and natural radionuclides when the acidic polluted leachates reach the marine environment.

The evaluation of the obtained results in the articles included in this Thesis allowed us to obtain the following main conclusions:

Salt marsh sediments under the phosphogypsum stacks

1. Due to the small particle size and consequently its very low permeability, the clayey and silty salt marsh sediments produce a "barrier effect" for the leachates coming from the PG stacks. The pollutants, including both stable elements and natural radionuclides, only reach the first decimetres of the estuarine underlying sediments layer. The sediments with a higher degree of affectation are mainly located in the first 20 cm below the contact and are affected by phosphogypsum-sediment mixing processes.

2. The pollution by ^{230}Th, ^{226}Ra and ^{210}Pb is mainly restricted to the first 20 cm of sediments, while the U-isotopes can reach higher depths (up to around 50 cm) by leaching processes due to their higher mobility.

3. The obtained results in this research work have high relevance for the design of the new perimeter channel that will include the future restoration project, suggesting that should has at least 1 m deep under the base of the phosphogypsum piles, to ensure the full collection of polluting leachates, and to avoid their release into the estuary of the Tinto River.

Odiel and Tinto rivers estuarine waters

1. The Odiel and Tinto rivers show concentrations of U and Th isotopes and ^{210}Po from one to three orders of magnitude higher than background continental waters and high ^{234}U/^{238}U activity ratios with maxima above 2 due to the impact produced by the acid mine drainage.

2. The radionuclides show a clear seasonal behaviour in these rivers, with three different stages during the year: (1) concentration peaks observed during November and December due to the "washing effect" produced by the first significant rainfalls of the hydrological year, which dissolve the salts and efflorescences precipitated during the dry season, (2) a "dilution effect" by runoff due to winter rains, and (3) a progressive "concentration effect" during the spring and summer due to the decrease of the rivers' flow.

3. A non-conservative behaviour of U and Th isotopes and ^{210}Po in the estuarine mixing zone was demonstrated due to precipitation processes related to the increase of pH. The particulate phase of the estuaries is mainly enriched in U-isotopes and ^{210}Po, with values around one order of magnitude higher than unpolluted sediments.

4. The polluted outflows from the phosphogypsum stacks produce a significant radioactive impact on the Tinto estuary, mainly during the rainiest months, increasing the concentration of U-isotopes and ^{210}Po in the particulate matter.

Behaviour of heavy metals and natural radionuclides in the mixing of PG leachates with seawater

1. The acidic phosphogypsum leachates show a high pollutant load, with large amounts of heavy metals, from two to three orders of magnitude higher than natural continental waters, and natural radionuclides, mainly U-isotopes and ^{210}Po, from four to five orders of magnitude higher than unperturbed surface freshwater and seawater. This fact demonstrates the extreme polluting potential of these acidic leachates.

2. Major elements and some heavy metals as Ni, Cd, As, Sb and Co show a conservative behaviour during the alkaline neutralisation of phosphogypsum leachates with seawater, remaining almost totally in the aqueous phase. Several heavy metals as Al, Fe, Cr, Zn, Cu, Ba, and Pb show a non-conservative behaviour during the

neutralisation, precipitating and/or been adsorbed to a greater or lesser extent onto the solid phase.

3. The U-isotopes and ^{210}Po show a clear non-conservative behaviour. The U-isotopes presented an almost total removal from the dissolved phase at pH values around 5, probably due to coprecipitation/adsorption processes onto the formed precipitates, to return into the dissolved phase due to redissolution/desorption processes at near neutral pH values. ^{210}Po strongly increases its removal from the dissolved phase during the neutralisation, reaching a total removal at pH ≈ 7 due to precipitation and or coprecipitation/adsorption onto the solid precipitates.

4. The formed precipitates during the neutralisation presented heavy metal and natural radionuclide (U-isotopes and ^{210}Po) concentrations from one to three orders of magnitude higher than unperturbed soils, demonstrating the serious environmental impact produced by the stacks on their surroundings in the current state.

Future lines of research

The findings of this Thesis point out to future lines of research, such as:

- To model the transport of natural radionuclides (U-Th isotopes and ^{210}Po) and metals through the phosphogypsum stacks, in order to evaluate and quantify the total amount of these pollutants released to the estuary.

- The metals and radionuclides are subjected to different processes when they reach the Tinto estuary as was observed in this Thesis. To develop a dispersion model of these pollutants throughout the Huelva estuary it is a very interesting point in order to evaluate the reach and magnitude of the releases.

- To study the release of metals and natural radionuclides from sediments polluted by the PG stacks releases by means of sequential extraction methods such as the Community Bureau of Reference (BCR) method and/or leaching tests as the Toxicity Characteristic Leaching Procedure (TCLP).

- Regarding to the restoration project and the new perimeter channel which is projected to build for collecting the phosphogypsum leachates, it should be interesting to develop a methodology to manage these leachates in order to decrease or totally remove the metal and natural radionuclide concentrations.

- Related to the above research line, to evaluate the radiological risks under different restoration technologies to find the most suitable option

4.2. CONCLUSIONES

En esta Tesis Doctoral se evaluó el impacto que producen las balsas de fosfoyeso de Huelva en su entorno estuarino. Por un lado, debido a que las balsas de fosfoyeso se dispusieron sobre la marisma sin ningún tipo de capa aislante, se caracterizaron los sedimentos estuarinos subyacentes para estudiar su grado de afectación debido a la migración de contaminantes y la posible existencia de lixiviados profundos. Por otro lado, se analizó la evolución estacional de radionucleidos naturales en los tramos fluviales y estuarinos de los ríos Odiel y Tinto para conocer el impacto producido por el drenaje ácido de mina y los lixiviados procedentes de las balsas de fosfoyeso. En este sentido, se llevaron a cabo experimentos de mezcla con lixiviados de fosfoyeso y agua de mar para estudiar el comportamiento de los metales pesados y radionucleidos naturales cuando los lixiviados ácidos contaminados llegan al medio marino.

La evaluación de los resultados obtenidos en los artículos incluidos en esta Tesis nos permitió obtener las siguientes conclusiones principales:

Sedimentos de marisma bajo las balsas de fosfoyeso

1. Debido al pequeño tamaño de partícula y, en consecuencia, a su muy baja permeabilidad, los sedimentos arcillosos y limosos de marisma producen un "efecto barrera" para los lixiviados procedentes de las balsas de fosfoyeso. Los contaminantes, incluyendo tanto elementos estables como radionucleidos naturales, solo alcanzan los primeros decímetros de la capa estuarina sedimentaria subyacente. Los sedimentos con mayor grado de afectación se localizan principalmente en los primeros 20 cm bajo el contacto y se ven afectados por procesos de mezcla fosfoyeso-sedimento.

2. La contaminación por ^{230}Th, ^{226}Ra y ^{210}Pb se restringe principalmente a los primeros 20 cm de sedimento, mientras que los isótopos de U pueden alcanzar mayores profundidades (hasta alrededor de 50 cm) mediante procesos de lixiviación debido a su mayor movilidad.

3. Los resultados obtenidos en este trabajo de investigación tienen alta relevancia para el diseño del nuevo canal perimetral que incluirá el futuro proyecto de restauración, sugiriendo que debe tener al menos 1 m de profundidad bajo la base del apilamiento de fosfoyeso, para asegurar la recolección completa de lixiviados contaminantes, y evitar su liberación en el estuario del río Tinto.

Aguas estuarinas de los ríos Odiel y Tinto

1. Los ríos Odiel y Tinto presentan concentraciones de isótopos de U y Th y de ^{210}Po de uno a tres órdenes de magnitud superiores a los valores de fondo de aguas continentales y altos cocientes de actividad ^{234}U/^{238}U con máximos superiores a 2 debido al impacto producido por el drenaje ácido de mina.

2. Los radionucleidos presentan un claro comportamiento estacional en estos ríos, con tres etapas diferenciadas durante el año: (1) picos de concentración observados durante noviembre y diciembre por el "efecto lavado" producido por las primeras precipitaciones significativas del año hidrológico, que disuelven las sales y eflorescencias precipitadas durante la estación seca, (2) un "efecto de dilución" por la escorrentía de las lluvias invernales, y (3) un "efecto de concentración" progresivo durante la primavera y el verano debido a la disminución del caudal de los ríos.

3. Se demostró un comportamiento no conservativo de los isótopos U y Th y ^{210}Po en la zona de mezcla del estuario debido a procesos de precipitación relacionadas con el aumento de pH. La fase particulada de los estuarios está principalmente enriquecida en isótopos U y ^{210}Po, con valores alrededor de un orden de magnitud más altos que sedimentos no contaminados.

4. Las salidas contaminadas de las balsas de fosfoyeso producen un impacto radiactivo significativo en el estuario del Tinto, principalmente durante los meses más lluviosos, aumentando la concentración de isótopos U y ^{210}Po en el material particulado.

Comportamiento de metales pesados y radionucleidos naturales en la mezcla de lixiviados de PG con agua de mar

1. Los lixiviados ácidos de fosfoyeso presentan una alta carga contaminante, con grandes cantidades de metales pesados, de dos a tres órdenes de magnitud más altos que las aguas continentales naturales, y radionucleidos naturales, principalmente isótopos U y ^{210}Po, de cuatro a cinco órdenes de magnitud superiores a aguas dulces superficiales y aguas marinas no perturbadas. Este hecho demuestra el extremo potencial contaminante de estos lixiviados ácidos.

2. Los elementos mayoritarios y algunos metales pesados como Ni, Cd, As, Sb y Co muestran un comportamiento conservativo durante la neutralización alcalina de los lixiviados de fosfoyeso con agua de mar, permaneciendo casi totalmente en la fase

acuosa. Varios metales pesados como Al, Fe, Cr, Zn, Cu, Ba y Pb muestran un comportamiento no conservativo durante la neutralización, precipitando y/o siendo adsorbidos en mayor o menor medida sobre la fase sólida.

3. Los isótopos U y ^{210}Po muestran un claro comportamiento no conservativo. Los isótopos de U presentaron una eliminación casi total de la fase disuelta a valores de pH alrededor de 5, probablemente debido a procesos de coprecipitación/adsorción sobre los precipitados formados, para volver a la fase disuelta debido a procesos de redisolución/desorción a valores de pH casi neutros. El ^{210}Po incrementa fuertemente su eliminación de la fase disuelta durante la neutralización, alcanzando una eliminación total a pH ≈ 7 debido a la precipitación y/o coprecipitación/adsorción sobre los precipitados sólidos.

4. Los precipitados formados durante la neutralización presentaron concentraciones de metales pesados y radionúclidos naturales (isótopos de U y ^{210}Po) de uno a tres órdenes de magnitud superiores a los suelos no perturbados, lo que demuestra el grave impacto ambiental que producen las balsas sobre su entorno en el estado actual.

Futuras líneas de investigación

Los hallazgos de esta Tesis apuntan a futuras líneas de investigación, tales como:

- Modelar el transporte de radionucleidos naturales y metales a través de las balsas de fosfoyeso, con el fin de evaluar y cuantificar la cantidad total de estos contaminantes liberados al estuario.

- Los metales y radionucleidos son sometidos a diferentes procesos cuando llegan al estuario del Tinto como se observó en esta Tesis. Desarrollar un modelo de dispersión de estos contaminantes por la ría de Huelva es un punto muy interesante para evaluar el alcance y la magnitud de las emisiones.

- Estudiar la liberación de metales y radionúclidos naturales de sedimentos contaminados por las descargas de las balsas de fosfoyeso mediante métodos de extracción secuencial como el método del "Community Bureau of Reference (BCR)" y/ o ensayos de lixiviación como el "Toxicity Characteristic Leaching Procedure (TCLP)".

- Respecto al proyecto de restauración y al nuevo canal perimetral que se proyecta construir para la recolección de los lixiviados de fosfoyeso, sería interesante desarrollar

una metodología para el manejo de estos lixiviados con el fin de disminuir o eliminar totalmente las concentraciones de metales y radionucleidos naturales.

• Relacionado con la línea de investigación anterior, evaluar los riesgos radiológicos bajo diferentes tecnologías de restauración para encontrar la opción más adecuada.

REFERENCES

Abdel-Halim, A. M., and Aly-Eldeen, M. A., 2016. Characteristics of Mediterranean Sea water in vicinity of Sidikerir Region, west of Alexandria, Egypt. Egypt. J. Aquat. Res., 42(2), 133–140.

Abril, J.M., García-Tenorio, R., Manjón, G., 2009. Extensive radioactive characterization of a phosphogypsum stack in SW Spain: ^{226}Ra, ^{238}U, 210Po concentration and ^{222}Rn exhalation rate. J. Hazard. Mater., 164, 790-797.

Achterberg, E. P., Herzl, V. M., Braungardt, C. B., and Millward, G. E., 2003. Metal behaviour in an estuary polluted by acid mine drainage: the role of particulate matter. Environ. Poll., 121(2), 283–292.

Aguado, J.L., Bolívar, J.P., García-Tenorio, R., García-León, M., 1998. Behaviour and levels of natural radioactivity in sediments from the odiel river. Int. Ver. Theor. Angew. Limnol., 26, 893-895.

Akmal Idrus, F., Dennis Chong, M., Syazwani Abd Rahim, N., Mohd basri, M., Musel, J., 2017. Physicochemical Parameters of Surface Seawater in Malaysia Exclusive Economic Zones Off the Coast of Sarawak. Borneo Journal of Resource Science and Technology 7(1):1-10.

Amrane, M., Oufni, L., 2017. Determination for levels of uranium and thorium in water along Oum Er-Rabia River using alpha track detectors. J. Radiat. Res. Appl. SC., 10(3), 246-251.

Andersen, M.B., Erel, Y., Bourdon, B., 2009. Experimental evidence for ^{234}U-^{238}U fractionation during granite weathering with implications for 234U/238U in natural waters. Geochim. Cosmochim. Acta 73, 4124-4141.

Bam, W., Maiti, K., Baskaran, M., Krupp, K., Lam, P.J., & Xiang, Y., 2020. Variability in ^{210}Pb and ^{210}Po partition coefficients (Kd) along the US GEOTRACES Arctic transect. Mar. Chem., 103749.

Barbero, L., Gázquez, M. J., Bolívar, J.P., Casas-Ruiz, M., Hierro, A., Baskaran, M., Ketterer, M. E., 2014. Mobility of Po and U-isotopes under acid mine drainage conditions: an experimental approach with samples from Río Tinto area (SW Spain). J. Environ. Radioact., 138, 384–389.

Benoit, G., Oktay-Marshall, S.D., Cantu, A., Hood, E.M., Coleman, C.H., Corapcioglu, M.O, Santschi, P.H., 1994. Partitioning of Cu, Pb, Ag, Zn, Fe, Al, and Mn between filter-retained particles, colloids, and solution in six Texas estuaries. Mar. Chem. 45, 307–36.

Blasco, M., Gázquez, M. J., Pérez-Moreno, S.M., Grande, J. A., Valente, T., Santisteban, M., de la Torre, M.L., Bolívar, J. P., 2016. Polonium behaviour in reservoirs potentially affected by acid mine drainage (AMD) in the Iberian Pyrite Belt (SW of Spain). J. Environ. Radioact, 152, 60–69.

Bolívar, J.P., García-Tenorio, R., García-León, M., 1996a. On the fractionation of natural radioactivity in the production of phosphoric acid by the wet acid method. J. Radioanal. Nucl. Chem. Letters, 214 (2), 77-78.

Bolívar, J.P., García-Tenorio, R., García-León, M., 1996b. Radioactive impact of some phosphogypsum piles in soils and salt marshes evaluated by g-ray spectrometry. Appl. Radiat. Isot., 47 (9-10), 1069-1075.

Bolívar, J.P., García-Tenorio, R., Más, J., 1998. Radioactivity of phosphogypsum in south-west of Spain. Radiat. Prot. Dosim., 76 (3), 185-189.

Bolívar, J., García-Tenorio, R., Vaca, F., 2000. Radioecological study of an estuarine system located in the south of Spain. Water Res., 34(11), 2941-2950.

Bolívar, J.P., García-Tenorio, R., Más, J.L., Vaca, F., 2002. Radioactive impact in sediments from an estuarine system affected by industrial waste releases. Environ. Int., 27, 639-645.

Bolívar, J.P., Martín, J.E., García-Tenorio, R., Pérez-Moreno, J.P., Más, J.L., 2009. Behaviour and fluxes of natural radionuclides in the production process of a phosphoric acid plant. Appl. Radiat. Isot., 67, 345-356.

Boryło, A., Nowicki, W., Skwarzec, B., 2009. Isotopes of polonium (^{210}Po) and uranium (^{234}U and ^{238}U) in the industrialised area of Wiślinka (North Poland). Int. J. Environ. Anal. Chem., 89 (8-12), 677-685.

Boryło, A., and Skwarzec, B., 2014. Activity disequilibrium between ^{234}U and ^{238}U isotopes in natural environment. J. Radioanal. Nucl. Ch., 300(2), 719–727.

Borrego, J., Pendón, J.G., 1989. Influencia de la actividad humana sobre la evolución sedimentaria de un sector de la Ría de Huelva (España). Geolis. 3, 125-131.

Borrego, J., 1992. Sedimentología del estuario del río Odiel (Huelva, S.O. España). PhD Thesis. University of Sevilla. 296 pp.

Borrego, E., Mas, J.L., Martín, J.E., Bolívar, J.P., Vaca, F., Aguado, J.L., 2007. Radioactivity levels in aerosol particles surrounding a large TENORM waste repository after application of preliminary restoration work. Sci. Total Environ., 377, 27-35.

Borrego, J., Carro, B., Grande, J.A., de la Torre, M.L., Valente, T., Santisteban, K., 2013. Control factors on the composition of superficial sediments in estuaries of the coast of Huelva (SW Spain): a statistical approach. J. Iber. Geol., 39 (2), 223-232.

Braungardt, C.B., Achterberg, E.P., Elbaz-Poulichet, F., Morley, N.H., 2003. Metal geochemistry in a mine-polluted estuarine system in Spain. Appl. Geochem., 18(11), 1757–1771.

Cánovas, C.R., Olías, M., Nieto, J.M., Sarmiento, A.M., Cerón, J.C., 2007. Hydrogeochemical characteristics of the Tinto and Odiel Rivers (SW Spain). Factors controlling metal contents. Sci. Total Environ. 373(1), 363-382.

Cánovas, C.R., Olías, M., Nieto, J. M., and Galván, L., 2010. Wash-out processes of evaporitic sulfate salts in the Tinto River: Hydrogeochemical evolution and environmental impact. Appl. Geochem., 25(2), 288–301.

Cánovas, C.R., Macías, F., Pérez-López, R., Nieto, J.M., 2018. Mobility of rare earth elements, yttrium and scandium from a phosphogypsum stack: environmental and economic implications. Sci. Total Environ., 618, 847-857.

Carro, B., Borrego, J., López-González, N., Grande, J.A., Gómez, T., de la Torre, M.L., Valente, T., 2011. Impact of acid mine drainage on the hydrogeochemical characteristics of the Tinto–Odiel Estuary (SW Spain). J. Iber. Geol., 37(1), 87–96.

Cerqueria, B., Covelo, E.F., Andrade, M.L., Vega, F.A., 2011. Retention and mobility of copper and lead in soils as influenced by soil horizon properties. Pedosphere, 21 (5), 603-614.

Davis, R.A., Welty, A.T., Borrego, J., Morales, J.A., Pendon, J.G., Ryan, J.G., 2000. Rio Tinto estuary (Spain): 5000 years of pollution. Environ. Geol. 39 (10), 1107-1116.

de la Torre, M.L., Grande, J.A., Graiño, J., Gómez, T., Cerón, J.C., 2011. Characterization of AMD pollution in the River Tinto (SW Spain). Geochemical comparison between generating source and receiving environment. Water Air Soil Pollut., 216, 3-19.

De Vos, W., Tarvainen, T., 2006. The Geochemical Atlas of Europe Part 2. Interpretation of Geochemical Maps, Additional Tables, Figures, Maps, and Related Publications. 690 pp.

Dueñas, C., Liger, E., Cañete, S., Pérez, M., Bolívar, J.P., 2007. Exhalation of ^{222}Rn from phosphogypsum piles located at the Southwest of Spain. J. Environ. Radioact., 95, 63-74.

Durand, J. F., 2012. The impact of gold mining on the Witwatersrand on the rivers and karst system of Gauteng and North West Province, South Africa. J. Afr. Earth Sci., 68, 24-43.

El Zrelli, R., Rabaoui, L., Daghbouj, N., Abda, H., Castet, S., Josse, C., van Beek, P., Souhaut, M., Michel, M., Bejaoui, N., Courjault-Radé, P., 2018. Characterization of phosphate rock and phosphogypsum from Gabes phosphate fertilizer factories (SE Tunisia): high mining potential and implications for environmental protection. Environ. Sci. Pollut. R., 25(15), 14690-14702.

EU, 2013. Council Directive 2013/59/Euratom of 5 December 2013 Laying Down Basic Safety Standards for Protection against the Dangers Arising from Exposure to Ionising Radiation, and Repealing Directives 89/618/Euratom, 90/641/Euratom, 96/29/Euratom, 97/43/Euratom and 2003/122/Euratom.

El Afifi, E.M., Hilal, M.A., Attallah, M.F., EL-Reefy, S.A., 2009. Characterization of phosphogypsum wastes associated with phosphoric acid and fertilizers production. J. Environ. Radioact., 100 (5), 407-412.

El Samad, O., Aoun, M., Nsouli, B., Khalaf, G., Hamze M., 2014. Investigation of the radiological impact on the coastal environment surrounding a fertilizer plant. J. Environ. Radioact., 133, pp. 69-74.

Fernandes, H. M., Franklin, M. R., Veiga, L. H., 1998. Acid rock drainage and radiological environmental impacts. A study case of the Uranium mining and milling facilities at Poços de Caldas. Waste Manag., 18(3), 169–181.

Fernández-Caliani, J.C., Ruiz Muñoz, F., Galán, E., 1997. Clay mineral and heavy metal distributions in the lower estuary of Huelva and adjacent Atlantic shelf, SW Spain. Sci. Total Environ. 198, 181-200.

Gázquez, M.J., Mantero, J., Mosqueda, F., Bolívar, J.P., García-Tenorio, R., 2014. Radioactive characterization of leachates and efflorescences in the neighbouring areas of a phosphogypsum disposal site as a preliminary step before its restoration. J. Environ. Radioact., 137, 79-87.

Goldstein J.I., Newbury D.E., Echlin P., Joy D.C., Fiori C., Lifshin E. (1981) Electron-Beam-Specimen Interactions. In: Scanning Electron Microscopy and X-Ray Microanalysis. Springer, Boston, MA.

Gordeev, V.V., Lisitzin, A. P., 2014. Geochemical interaction between the freshwater and marine hydrospheres. Russ. Geol. Geophys, 55(5-6), 562–581.

Guerrero, J.L., Gutiérrez-Álvarez, I., Mosqueda, F., Olías, M., García-Tenorio, R., Bolívar, J.P., 2019. Pollution evaluation on the salt marshes under the phosphogypsum stacks of Huelva due to deep leachates. Chemosphere, 230, 219-229.

Guerrero, J.L., Gutiérrez-Álvarez, I., Mosqueda, F., Gázquez, M.J., García-Tenorio, R., Olías, M., Bolívar, J.P., 2020. Evaluation of the radioactive pollution in the salt marshes under a phosphogypsum stack system. Environ. Pollut., 258, 113729.

Guerrero, J.L., Gutiérrez-Álvarez, I., Hierro, A., Pérez-Moreno, S.M., Olías, M., Bolívar, J. P., 2021a. Seasonal evolution of natural radionuclides in two rivers affected by acid mine drainage and phosphogypsum pollution. Catena, 197, 104978.

Guerrero, J.L., Pérez-Moreno, S.M., Gutiérrez-Álvarez, I., Gázquez, M.J., Bolívar, J.P., 2021b. Behaviour of heavy metals and natural radionuclides in the mixing of phosphogypsum leachates with seawater. Environ. Pollut., 268, 115843.

Guimond, R.J., Hardin, J.M., 1989. Radioactivity released from phosphate containing fertilizers and from gypsum. Radiat. Phys. Chem., 34, 309-315.

Gutiérrez-Álvarez, I., Guerrero, J.L., Martín, J.E., Adame, J.A., Vargas, A., Bolívar, J.P., 2019. Radon behavior investigation based on cluster analysis and atmospheric modelling. Atmos. Environ., 201, 50-61.

Hallstadius, L., 1984. A method for the electrodeposition of actinides. Nucl. Instrum. Meth. A 223, 266-267.

Henderson, G. M., Hall, B. L., Smith, A., Robinson, L. F., 2006. Control on ($^{234}U/^{238}U$) in lake water: A study in the Dry Valleys of Antarctica. Chem. Geol., 226(3-4), 298–308.

Hernandez-Ceballos, M.A., Vargas, A., Arnold, D., Bolívar, J.P., 2015. The role of mesoscale meteorology in modulating the ^{222}Rn concentrations in Huelva (Spain) - impact of phosphogypsum piles. J. Environ. Radioact., 145, 1-9.

Hierro, A., Bolivar, J.P., Vaca, F., Borrego, J., 2012. Behavior of natural radionuclides in surficial sediments from an estuary impacted by acid mine discharge and industrial effluents in Southwest Spain. J. Environ. Radioact., 110, 13–23.

Hierro, A., Martín, J.E., Olías, M., Vaca, F., Bolívar, J.P., 2013. Uranium behaviour in an estuary polluted by mining and industrial effluents: the Ría of Huelva (SW of Spain). Water Res., 47, 6269-6279.

Hierro, A., Olías, M., Ketterer, M.E., Vaca, F., Borrego, J., Cánovas, C.R., Bolívar, J.P., 2014a. Geochemical behavior of metals and metalloids in an estuary affected by acid mine drainage (AMD). Environ. Sci. Pollut. Res., 21, 2611-2627.

Hierro, A., Olías, M., Cánovas, C.R., Martín, J.E., Bolívar, J.P., 2014b. Trace metal partitioning over a tidal cycle in an estuary affected by acid mine drainage (Tinto estuary, SW Spain). Sci. Total Environ., 497-498, 18-28.

Hou, X., Jones, B.T., 2008. Encyclopedia of Analytical Chemistry, John Wiley & Sons.

Hsi, D., Langmuir, D., 1985. Adsorption of uranyl onto ferric oxyhydroxides: Application of the surface complexation site-binding model. Geochim. Cosmochim. AC., 49(9), 1931–1941.

Hussain, N., Krishnaswami, S., 1980. U-238 series radioactive disequilibrium in groundwaters: implications to the origin of excess U-234 and fate of reactive pollutants. Geochim. Cosmochim. Acta 44 (9), 1287-1291.

IAEA, 2003. Extent of Environmental Contamination by Naturally Occurring Radioactive Material (NORM) and Technological Options for Mitigation. Technical Reports Ser. No 419. IAEA.

IAEA, 2017. The Environmental behaviour of Polonium. Technical Reports Ser. Nº 484.

IFA, 2006. Phosphate production in the new economics. Presentation to Joint IAEA-FIPR Phosphate Workshop. Bartow, Florida.

Jolliffe, I.T., 2002. Principal Component Analysis, second ed. Springer-Verlag New York, Inc, New York.

Kikuchi, T., 1990. Single crystal orientation measurement by x-ray methods. The Rigaku Journal, 7 (1), 27-35.

Kim, E., Osseo-Asare, K., 2012. Aqueous stability of thorium and rare earth metals in monazite hydrometallurgy: Eh–pH diagrams for the systems Th–, Ce–, La–, Nd–(PO_4)–(SO_4)–H_2O at 25°C. Hydrometallurgy, 113-114, 67–78.

Kennish, M.J., 2017. Ecology of Estuaries: Volume 1: Physical and Chemical Aspects. CRC Press. 264 pp.

Knoll, G.F., 1989. Radiation detection and measurement. (Wiley J. & sons, Eds.), New York.

Kocher, D.C., 1981. Radioactive Decay Data Tables. A handbook of decay data for application to radiation dosimetry and radiological assessments. Health and Safety Research Division Oak Ridge National Laboratory. (Smith J.S., Ed.) Technical Information Center U.S. Department of Energy.

Ku, T.L., Knauss, K.G., Mathieu, G.G., 1977. Uranium in open ocean: concentration and isotopic composition. Deep-Sea Res., 24(11), 1005-1017.

Lario, J., Alonso-Azcárate, J., Spencer, C., Zazo, C., Goy, J.L., Cabero, A., Dabrio, C.J., Borja, F., Borja, C., Civis, J., García-Ródriguez, M., 2016. Evolution of the pollution in the Piedras River Natural Site (Gulf of Cadiz, southern Spain) during the Holocene. Environ. Earth Sci., 75, 481.

Leblanc, M., Morales, J.A., Borrego, J., Elbaz-Poulichet, E., 2000. 4500-year-old mining pollution in southwestern Spain: long-term implications for modern mining pollution. Econ. Geol., 95, 655-662.

Lochamy J.C., 1981. The Minimum Detectable Activity concept. Systems and applications Studies. PSD No. 17, EG&G Ortec, Oak Ridge, U.S.A.

Loder, T.C., Reichard, R. P., 1981. The Dynamics of Conservative Mixing in Estuaries. Estuaries, 4(1), 64.

López-Coto, I., Mas, J.L., Vargas, A., Bolívar, J.P., 2014. Studying radon exhalation rates variability from phosphogypsum piles in the SW of Spain. J. Hazard Mater., 280, 464-471.

Madruga, M.J., Prudencio, M.I., Gil Corisco J.A. Mihalik, J., Marques, R., Santos, M., Reis, M., Paiva, I., Dias, M.I., 2019. Distribution of Natural Radionuclides, Rare Earth Elements, Metals and Metalloids in a Phosphogypsum Stockpile. Int. J. Waste Resour., 9:1.

Madzivire, G., Maleka, P.P., Vadapalli, V.R.K., Gitari, W.M., Lindsay, R., Petrik, L.F., 2014. Fate of the naturally occurring radioactive materials during treatment of acid mine drainage with coal fly ash and aluminium hydroxide. J. Environ. Manage., 133, 12–17.

Manjón, G., Mantero, J., Vioque, I., Galván, J., Díaz-Francés, I., García-Tenorio, R., 2019a. Some naturally occurring radionuclides (NORM) in a River affected by acid mining drainages. Chemosphere, 223, 536-543.

Manjón, G., Mantero, J., Vioque, I., Díaz-Francés, I., Galván, J.A., Chakiri, S., Choukric, A., and García-Tenorio, R., 2019b. Natural radionuclides (NORM) in a Moroccan river affected by former conventional metal mining activities. J. Sustain. Min., 18(1), 45–51.

Martín, J.E., García-Tenorio, R., Respaldiza, M.A., Ontalba, M.A., Bolívar, J.P., da Silva, M.F., 1999. TTPIXE analysis of phosphate rocks and phosphogypsum. Appl. Radiat. Isot., 50, 445-449.

Martín, J.E., García-Tenorio, R., San Miguel, E.G., Respaldiza, M.A., Bolívar, J.P., Alves, L.C., da Silva, M.F., 2002. Historical impact in an estuary of some mining

and industrial activities evaluated through the analysis by TTPIXE of a dated sediment core. Nucl. Instrum. Methods Phys. Res., Sect. B, 189, 153-157.

Martin, P., Hancock, G., 1992. Routine Analysis of Naturally Occurring Radionuclides in Environmental Samples by Alpha-Particle Spectrometry. Research Report, vol. 7. Australian Government Publishing Service, Canberra.

Más, J.L., Bolívar, J.P., García-Tenorio, R., Aguado, J.L., San Miguel, E.G., González-Labajo, J., 2001. A dosimetric model for determining the effectiveness of soil covers for phosphogypsum waste piles. Health Phys., 80 (1), 34-40.

Más, J.L., San Miguel, E.G., Bolívar, J.P., Vaca, F., Pérez-Moreno, J.P., 2006a. An assay on the effect of preliminary restoration tasks applied to a large TENORM wastes disposal in the south-west of Spain. Sci. Total Environ., 364, 55-66.

Más, J.L., García-León, M., García-Tenorio, R., Bolívar, J.P., 2006b. Radionuclide concentrations in water. In: Nollet, E. (Ed.), Radionuclide Concentrations in Food and the Environment, 59-113.

Mazzilli, B., Palmiro, V., Saueia, C., Nisti, M., 2000. Radiochemical characterization of Brazilian phosphogypsum. J. Environ. Radioact., 49 (1), 113-122.

McKee, B. A., DeMaster, D. J., Nittrouer, C. A., 1987. Uranium geochemistry on the Amazon shelf: Evidence for uranium release from bottom sediments. Geochim. Cosmochim. AC., 51(10), 2779-2786.

Millán-Becerro, R., Pérez-López, R., Macías, F., Cánovas, C., Papaslioti, EM., Basallote, MD., 2019. Assessment of metals mobility during the alkaline treatment of highly acid phosphogypsum leachates. Sci. Total. Environ. 660, 395-405.

Nieto, J.M., Sarmiento, A.M., Olías, M., Cánovas, C.R., Riba, I., Kalman, J., Delvalls, T.A., 2007. Acid mine drainage pollution in the Tinto and Odiel rivers (Iberian Pyrite Belt, SW Spain) and bioavailability of the transported metals to the Huelva estuary. Environ. Int., 33, 445-455.

Nieto, J.M., Sarmiento, A.M., Cánovas, C.R., Olías, M., Ayora, C., 2013. Acid mine drainage in the Iberian Pyrite Belt: 1. Hydrochemical characteristics and pollutant load of the Tinto and Odiel rivers. Environ. Sci. Pollut. Res. Int. 20 (11), 7509-7519.

Notholt, A.J.G., Sheldon, .RP., Davidson, D.F., 2005. Phosphate Deposits of the World. Vol. 2: Phosphate rock resources. Cambridge, UK: Cambridge University Press, 600 pp.

Nordstrom, D.K., Wilde, F.D., 1998. Reduction-oxidation potential (electrode method). In: National Field Manual for the Collection of Water Quality Data. US Geological Survey Techniques of Water-resources Investigations. Book 9, Chap. 6.5.

Olías, M., Nieto, J.M., Sarmiento, A.M., Cerón, J.C., Cánovas, C.R., 2004. Seasonal water quality variations in a River affected by acid mine drainage: the Odiel River (South West Spain). Sci. Total Environ., 333(1-3), 267-281.

Olías, M., Cánovas, C.R., Nieto, J.M., Sarmiento, A.M., 2006. Evaluation of the dissolved contaminant load transported by the Tinto and Odiel rivers (South West Spain). Appl. Geochem., 21(10), 1733–1749.

Olías, M., Cánovas, C.R., Macías, F., Basallote, M.D., Nieto, J.M., 2020. The Evolution of Pollutant Concentrations in a River Severely Affected by Acid Mine Drainage: Río Tinto (SW Spain). Minerals, 10, 598.

OSPAR, 2002. Discharges of Radioactive Substances into the Maritime Area by Nonnuclear Industry. Radioactive Substances Series. Publication No. 161. OSPAR Commission, London, 60 pp.

OSPAR, 2007. PARCOM Recommendation 91/4 on Radioactive Discharges: Spanish Implementation Report. Radioactive Substances Series. Publication No. 342. OSPAR Commission, London, 49 pp.

Owens, S.A., Buesseler, K.O., Sims, K.W.W., 2011. Re-evaluating the ^{238}U-salinity relationship in seawater: Implications for the ^{238}U-^{234}Th disequilibrium method. Mar. Chem., 127, 31-39.

Papaslioti, E.M., Pérez-López, R., Parviainen, A., Sarmiento, A.M., Nieto, J.M., Marchesi, C., Delgado-Huertas, A., Garrido, C., 2018. Effects of seawater mixing on the mobility of trace elements in acid phosphogypsum leachates. Mar. Pollut. Bull., 127, 695-703.

Pérez-López, R., Álvarez-Valero, A.M., Nieto, J.M., 2007. Changes in mobility of toxic elements during the production of phosphoric acid in the fertilizer industry of Huelva

(SW Spain) and environmental impact of phosphogypsum wastes. J. Hazard. Mater., 148(3), 745–750.

Pérez-López, R., Nieto, J.M., López-Coto, I., Aguado, J.L., Bolívar, J.P., Santiesteban, M., 2010. Dynamics of contaminants in phosphogypsum of the fertilizer industry of Huelva (SW Spain): from phosphate rock ore to the environment. Appl. Geochem., 25, 705-715.

Pérez-López, R., Nieto, J.M., de la Rosa, J.D., Bolívar, J.P., 2015. Environmental tracers for elucidating the weathering process in a phosphogypsum disposal site: implications for restoration. J. Hydrol., 529, 1313-1323.

Pérez-López, R., Macías, F., Cánovas, C.R., Sarmiento, A.M., Pérez-Moreno, S.M., 2016. Pollutant flows from a phosphogypsum disposal area to an estuarine environment: an insight from geochemical signatures. Sci. Total Environ., 553, 42-51.

Pérez-López, R., Carrero, S., Cruz-Hernández, P., Astad, M.P., Macías, F., Cánovas, C.R., Guglierie, C., Nieto, J.M., 2018. Sulfate reduction processes in salt marshes affected by phosphogypsum: geochemical influences on contaminant mobility. J. Hazard Mater., 350, 154-161.

Pérez-Moreno, J.P., San Miguel, E.G., Bolívar, J.P., Aguado, J.L., 2002. A comprehensive calibration method of Ge detector for low level spectrometry measurement. Nucl. Instrum. Methods., 491 (1-2), 152-162.

Pérez-Moreno, S.M., Gázquez, M.J., Pérez-López, R., Vioque, J., Bolívar, J.P., 2018. Assessment of natural radionuclides mobility in a phosphogypsum disposal area. Chemosphere, 211, 775-783.

Porcelli, D., Swarzenski, P.W., 2003. The Behavior of U- and Th-series nuclides in groundwater. Rev. Mineral. Geochem., 52(1), 317-61.

Reddy, K.J., Wang, L., Gloss, S.P., 1995. Solubility and mobility of copper, zinc and lead in acidic environments. Plant. Soil, 171, 53-58.

Rentería-Villalobos, M., Vioque, I., Mantero, J., Manjón, G., 2010. Radiological, chemical and morphological characterizations of phosphate rock and

phosphogypsum from phosphoric acid factories in SW Spain. J. Hazard Mater., 181, 193-203.

Romero, A., González Díez, I., Galán, E., 2006. The role of Sulphates Efflorescences in the Storage of Trace Elements in stream waters polluted by acid mine drainage. the case of Peña del Hierro (SW Spain). Canad. Mineral., 44(6), 1465-1480.

Ruiz, F., González-Regalado, M.L., Borrego, J., Morales J.A., J.A., Pendon, J.G., Muñoz, J.M., 1998. Stratigraphic sequence, elemental concentrations and heavy metal pollution in Holocene sediments from the Tinto-Odiel estuary. Southwestern Spain. Environ. Geol., 34, 270-278.

Rutherford, P.M., Dudas, M.J., Samek, R.A., 1994. Environmental impacts of phosphogypsum. Sci. Total Environ., 149, 1-38.

Sáez, R., Pascual, E., Toscano, M., Almodóvar, G.R., 1999. The Iberian type of volcano–sedimentary massive sulphide deposits. Miner. Deposita, 34, 549–570.

Sáinz, A., Grande, J.A, de la Torre, M.L., 2004. Characterisation of heavy metal discharge into the Ria of Huelva. Environ. Int., 30, 557-66.

Sánchez España, J., 2008. "Acid mine drainage in the Iberian Pyrite Belt: an overview with special Emphasis on Generation Mechanisms, Aqueous Composition and Associated Mineral Phases," Rev. la Soc. Esp. Min., 10, 34-43.

Sánchez-Moyano, J.E., García-Asencio, I., and García-Gómez, J.C., 2010. Spatial and temporal variation of the benthic macrofauna in a grossly polluted estuary from southwestern Spain. Helgol. Mar. Res., 64(3), 155-168.

Sanders, L.M., Luiz-Silva, W., Machado, W., Sanders, C.J., Marotta, H., Enrich-Prast, A., Bosco-Santos, A., Boden, A., Silva, E.V., Santos, I.R., Patchineelam S.R., 2013. Rare earth element and radionuclide distribution in surface sediments along an estuarine system affected by fertilizer industry contamination. Water Air Soil Pollut., 224, 1742.

Sánchez-Moyano, J.E., García-Asencio, I., and García-Gómez, J.C., 2010. Spatial and temporal variation of the benthic macrofauna in a grossly polluted estuary from southwestern Spain. Helgol. Mar. Res., 64(3), 155-168.

Santos-Bermejo, J.C., Beltrán, R., Gómez-Ariza, J.L., 2003. Spatial variations of heavy metal contamination in sediments from Odiel river (Southwest Spain). Environ. Int., 29, 69-77.

Serkiz, S.M., Johnson, W.H., 1994. Uranium Geochemistry in Soil and Groundwater at the F and H Seepage Basins (U). EPD-SGS-94-307. Westinghouse Savannah River Company, Savannah River Site, Aiken, South Carolina.

Shepherd, R.G., 1989. Correlations of permeability and grain size. Gr. Water, 27, 633-638.

Skwarzec, B., Bojanowski, R., 1988. ^{210}Po content in sea water and its accumulation in southern Baltic plankton. Mar. Biol., 97(2), 301-307.

Storti, F., Balsamo, F., 2010. Particle size distributions by laser diffraction: sensitivity of granular matter strength to analytical operating procedures. Solid Earth, 1, 25-48.

Tack, F.M.G., Callewaert, O.W.J.J., Verloo, M.G., 1996. Metal solubility as a function ofpH in a contaminated dredged sediment affected by oxidation. Environ. Pollut., 91, 199-208.

Tayibi, H., Choura, M., López, F.A., Alguacil, F.J., López-Delgado, A., 2009. Environmental impact and management of phosphogypsum. J. Environ. Manag., 90 (8), 2377-2386.

Torres-Sánchez, R., Sánchez-Rodas, D., de la Campa, A.M.S., Kandler, K., Schneiders, K., de la Rosa, J. D. (2019). Geochemistry and source contribution of fugitive phosphogypsum particles in Huelva, (SW Spain). Atmos. Res., 104650.

Torres-Sánchez, R., Sánchez-Rodas, D., Sánchez de la Campa, A.M., de la Rosa, J.D., 2020. Hydrogen fluoride concentrations in ambient air of an urban area based on the emissions of a major phosphogypsum deposit (SW, Europe). Sci. Total Environ., 136891.

Uddin, S., Aba, A., Fowler, S.W., Behbehani, M., Ismaeel, A., Al-Shammari, H., Alboloushia, A., Mietelskic, J.W., Al-Ghadbana, A., Al-Ghunaima, A., Khabbaza, A., Alboloushia, A., and Alboloushi, O., 2015. Radioactivity in the Kuwait marine environment — Baseline measurements and review. Mar. Pollut. Bull., 100(2), 651-661.

UNSCEAR, 2000. Sources and Effects of Ionizing Radiation. Volume I: Sources: Report to the General Assembly of the United Nations Scientific Committee on the Effects of Atomic Radiation. United Nations, New York.

Venkateswarlu, K., Nirola, R., Kuppusamy, S., Thavamani, P., Naidu, R., and Megharaj, M., 2016. Abandoned metalliferous mines: ecological impacts and potential approaches for reclamation. Rev. Environ. Sci. Bio., 15(2), 327-354.

Vicente-Martorell, J.J., Galindo-Riaño, M.D., García-Vargas, M., and Granado-Castro, M.D., 2009. Bioavailability of heavy metals monitoring water, sediments and fish species from a polluted estuary. J. Hazard. Mater., 162(2-3), 823-836.

Villa, M., Manjón, G., Hurtado, S., García-Tenorio, R., 2011. Uranium pollution in an estuary affected by pyrite acid mine drainage and releases of naturally occurring radioactive materials. Mar. Pollut. Bull., 62, 1521-1529.

Vioque, I., Manjón, G., García-Tenorio, R., El-Daoushy, F., 2002. Determination of alpha-emitting Pu isotopes in environmental samples. Analist., 127, 530-535.

Wei, C.-L., Lin, S.-Y., Sheu, D.D.-D., Chou, W.-C., Yi, M.-C., Santschi, P.H., Wen, L.-S., 2011. Particle-reactive radionuclides (^{234}Th, ^{210}Pb, ^{210}Po) as tracers for the estimation of export production in the South China Sea. Biogeosciences, 8 (12), 3793-3808.

Wetzel, R.G., 2001. Limnology. Academic Press, New York, 1006 pp.

Yamamoto, M., Sakaguchi, A., and Kofuji, H., 2010. Uranium in acidic mine drainage at the former Ogoya Mine in Ishikawa Prefecture of Japan. J. Radioanal. Nucl. Chem., 283(3), 699–705.

Yang, J., Liu, W., Zhang, L., Xiao, B., 2009. Preparation of load-bearing building materials from autoclaved phosphogypsum. Constr. Build. Mater., 23, 687-693.

Yang, L., Zhang, Y., Yan, Y., 2016. Utilization of original phosphogypsum as raw material for the preparation of self-leveling mortar. J. Clean. Prod., 127, 204-213.

Zhang, L., Chen, M., Yang, W., Xing, N., Li, Y., Qiu, Y., Huang, Y., 2004. Size-fractionated thorium isotopes (^{228}Th, ^{230}Th, ^{232}Th) in surface waters in the Jiulong River estuary, China. J. Environ. Radioact., 78(2), 199-216.

Zhou, J., Liu, Y., Abrahams, P., 2003. Trace metal behaviour in the Conwy estuary, North Wales. Chemosphere, 51 (5), 429–440.

Zhou, Q., Yang, N., Li, Y., Ren, B., Ding, X., Bian, H., & Yao, X., 2020. Total concentrations and sources of heavy metal pollution in global river and lake water bodies from 1972 to 2017. Glob. Ecol. Conser., e00925.

Annex I

Supplementary material

Figure S3.1. PG– sediment contact zone in the core 2, where the salt marsh sediment, the contact zone, and the PG are observed.

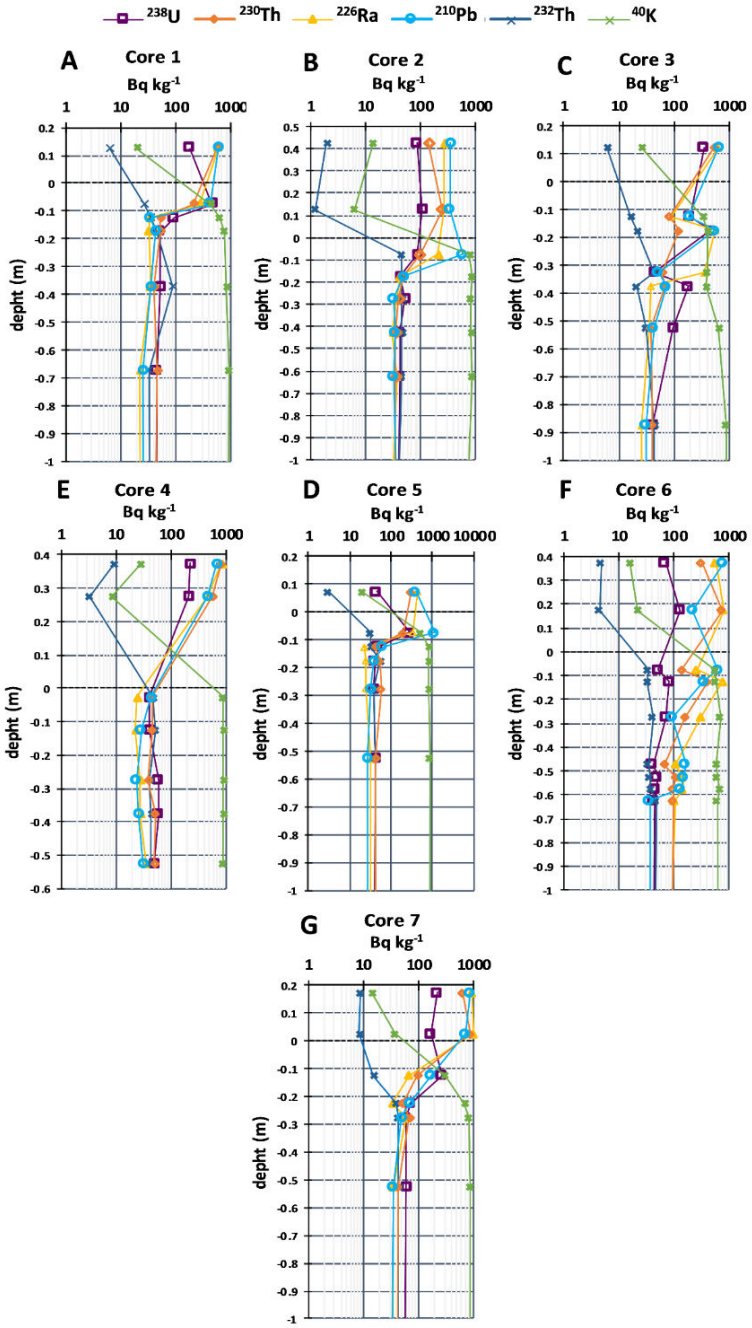

Figure S3.2 Depth profiles of natural radionuclides, only the zone close to the PG-sediment contact (zero depth) is shown.

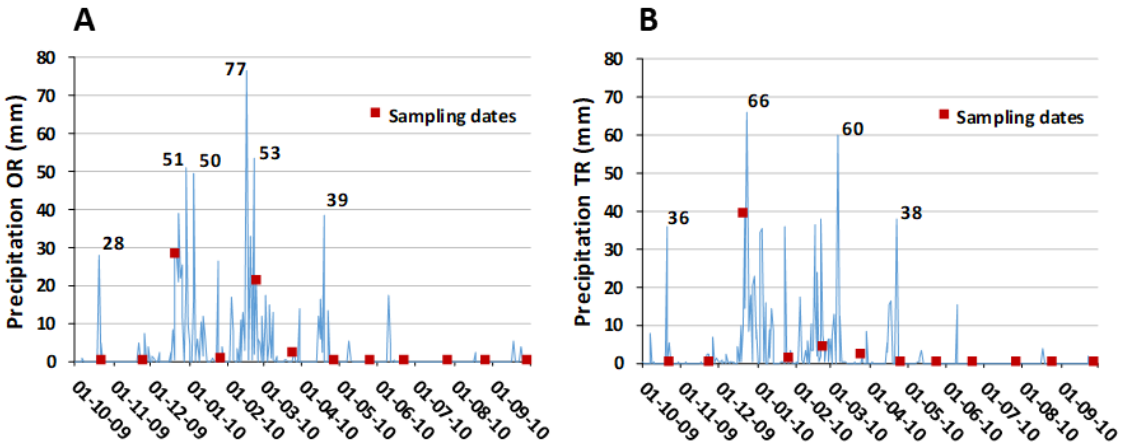

Figure S3.3. Precipitation registered near the fluvial sampling points. A: Odiel River (OR). B: Tinto River (TR)

Table S3.1
Samples.

Code	from (m)	to (m)	Contact	Code	from (m)	to (m)	Contact	Code	from (m)	to (m)	Contact	Code	from (m)	to (m)	Contact
1P1	0.70	0.75		3P1	0.9	0.95		5P1	4.00	4.05		6S7	7.10	7.15	
1P2	2.90	2.95		3P2	4.95	5.00		5P2	4.55	4.60		6S8	9.05	9.15	
1P3	4.05	4.10		3P3	5.00	5.05		5P3	7.55	7.60		6S9	11.32	11.37	
1P4	5.45	5.50		3S1	5.2	5.25		5P4	8.05	8.10		6S10	11.37	11.42	
1S1	5.65	5.70		3S2	5.25	5.30		5P5	8.10	8.15		6S11	11.7	11.75	6.5
1S2	5.70	5.75	5.6	3S3	5.4	5.45	5.1	5S1	8.25	8.30		6S12	11.75	11.8	
1S3	5.75	5.80		3S4	5.45	5.50		5S2	8.30	8.35		6S13	13.15	13.2	
1S4	5.95	6.00		3S5	5.6	5.65		5S3	8.35	8.40	8.2	6S14	13.25	13.3	
1S5	6.25	6.30		3S6	5.95	6.00		5S4	8.45	8.50		6S15	16.05	16.1	
1S6	9.20	9.25		3S7	6.9	6.95		5S5	8.70	8.75		7P1	0.65	0.70	
1S7	12.3	12.35		3S8	10.35	10.4		5S6	9.45	9.50		7P2	1.25	1.30	
1S8	13.1	13.15		3S9	15.65	15.7		5S7	9.85	9.90		7P3	1.70	1.75	
2P1	4.65	4.7		4P1	0.9	0.95		5S8	11.30	11.35		7P4	2.20	2.25	
2P2	4.95	5.00		4P2	3.1	3.15		5S9	12.25	12.30		7P5	2.25	2.30	
2S1	5.15	5.20		4P3	3.2	3.25		5S10	13.90	13.95		7P6	2.35	2.40	
2S2	5.20	5.25		4S1	3.5	3.55		5S11	16.10	16.15		7S1	2.50	2.55	
2S3	5.25	5.30		4S2	3.55	3.6		6P1	1.40	1.45		7S2	2.55	2.60	
2S4	5.35	5.40		4S3	3.6	3.65		6P2	3.05	3.10		7S3	2.6	2.65	
2S5	5.50	5.55		4S4	3.75	3.8		6P3	5.75	5.80		7S4	2.65	2.70	2.4
2S6	5.65	5.70	5.1	4S5	3.85	3.9	3.5	6P4	6.10	6.15		7S5	2.9	2.95	
2S7	5.70	5.75		4S6	4.00	4.05		6P5	6.30	6.35		7S6	3.05	3.10	
2S8	6.25	6.30		4S7	4.95	5.00		6S1	6.55	6.60	6.5	7S7	3.1	3.15	
2S9	8.45	8.50		4S8	5.00	5.05		6S2	6.6	6.65		7S8	4.65	4.70	
2S10	9.70	9.75		4S9	5.05	5.10		6S3	6.75	6.80		7S9	7.55	7.60	
2S11	10.35	10.4		4S10	8.8	8.85		6S4	6.95	7.00		7S10	9.25	9.30	
2S12	13.8	13.85		4S11	12.2	12.25		6S5	7.00	7.05		7S11	11.3	11.35	
2S13	16.2	16.25		4S12	14.6	14.65		6S6	7.05	7.10		7S12	13.05	13.10	
												7S13	14.47	14.52	
												7S14	14.52	14.57	

Table S3.2
Physicochemical parameters.

Code	pH	EC (mS/cm)	Code	pH	EC (mS/cm)	Code	pH	EC (mS/cm)	Code	pH	EC (mS/cm)
1P1	2.46	4.5	3P1	2.53	4.1	5P3	2.74	13.3	6S15	8.08	16.3
1P2	2.44	17.6	3P3	4.05	15.3	5P4	2.55	15.9	7P1	2.49	10.4
1P3	4.27	17.2	3S2	4.02	31.4	5S2	5.22	18.6	7P2	2.31	10.5
1P4	3.11	9.8	3S4	4.79	31.9	5S5	5.18	19.6	7P3	2.33	10.6
1S2	5.89	21.9	3S5	5.58	27.5	5S6	7.07	21.6	7P5	2.25	12.6
1S5	7.04	14.5	3S6	6.32	18.2	5S7	6.57	23.1	7S2	5.51	18.7
1S6	7.44	17.7	3S7	7.86	18	5S8	7.86	18.4	7S6	6.53	22.6
1S7	7.89	13.8	3S8	7.77	20	5S9	7.98	18.3	7S8	7.01	21.4
1S8	7.96	15.7	3S9	7.6	18	5S10	7.18	15.2	7S9	7.01	24.4
2P1	2.86	13.7	4P1	4.73	1.1	5S11	7.77	17.6	7S10	7.86	19.4
2S2	5	19.8	4P3	3.75	15.3	6P1	3	1.9	7S11	8.1	7.4
2S6	6.62	22.4	4S2	6.1	33.2	6P2	2.38	4.2	7S12	7.89	7.5
2S8	6.63	16.6	4S8	7.32	33.4	6P3	2.33	9.8	7S13	8.26	6.5
2S9	7.05	12.6	4S10	7.38	29.6	6S6	7.36	24.1			
2S10	6.63	19.9	4S11	8	20.4	6S8	8.18	15.2			
2S11	7.94	13.5	4S12	8.25	10	6S9	8.07	12.4			
2S12	7.91	14.1	5P1	2.56	6.10	6S11	8.09	21.8			
2S13	7.9	12.9	5P2	2.45	13.9	6S13	8.12	16.6			

Table S3.3
Major elements.

Code	Al %	Ca %	S %	Fe %	K %	Na %	P %	Mg %	Ti %
1P4	0.12	11.7	21.36	1.16	0.02	0.41	0.34	0.04	0.01
1S1	3.2	2.21	4.968	16.1	1.22	1.84	3.89	0.49	0.05
1S2	6.44	1.35	4.28	11.1	1.83	1.55	0.17	0.82	0.39
1S3	8.61	0.94	0.752	6.55	2.3	1.56	0.08	1.08	0.50
1S4	20	1.27	1.016	10.8	5.02	2.84	0.12	2.25	0.70
1S5	8.69	0.41	1.0	4.87	2.57	1.45	0.06	1.1	0.29
1S6	8.01	1.04	2.0	4.11	2.45	1.46	0.05	1.2	0.49
2P1	0.03	5.41	17.928	0.03	0.02	0.42	0.29	0.02	0.02
2P2	0.04	5.71	18.968	0.02	< 0.01	0.11	0.22	0.02	0.01
2S1	6.13	0.89	2.312	4.85	1.14	1.70	0.25	0.92	0.24
2S3	8.03	0.71	0.568	5.73	1.66	1.80	0.10	1.09	0.45
2S4	9.05	0.95	0.76	4.99	2.63	1.87	0.08	1.23	0.56
2S5	8.65	0.66	0.528	4.92	2.65	1.72	0.08	1.2	0.52
2S7	8.81	0.61	0.488	5.13	2.25	1.82	0.07	1.27	0.55
2S8	8.22	0.76	2.0	5.04	2.53	1.55	0.06	1.07	0.54
2S10	4.62	2.79	1.0	2.35	1.79	1.31	0.05	0.67	0.40
3P2	0.07	7.95	20.76	0.02	0.03	0.64	0.31	0.08	0.01
3S1	4.08	3.17	4.936	11.8	1.02	2.42	> 5	0.59	0.06
3S2	6.49	3.84	4.672	2.34	1.26	3.70	> 5	0.57	0.05
3S3	9.26	0.41	0.328	5.48	2.69	1.74	0.08	1.27	0.34
3S4	4.39	1.54	1.232	22.6	1.21	2.40	3.44	0.7	0.06
3S5	6.83	0.47	0.376	13	1.87	1.89	0.39	0.93	0.39
3S6	8.94	0.52	0.416	5.36	2.42	1.74	0.09	1.2	0.41
3S8	7.78	1.13	0.904	4.07	2.59	1.56	0.06	1.2	0.55
4P2	0.06	8.8	18.24	0.03	0.02	0.50	0.32	0.06	0.01
4P3	0.04	7.24	16.992	0.01	< 0.01	0.17	0.23	0.03	0.00
4S1	7.01	0.35	1.08	5.2	2.54	2.35	0.08	1.13	0.39
4S3	7.25	0.34	0.272	3.74	1.57	2.64	0.05	1.23	0.44
4S4	8.62	0.35	0.28	4.33	2.26	3.13	0.07	1.42	0.52
4S5	8.5	0.38	0.304	3.71	2.27	2.86	0.05	1.32	0.48

Code	Al	Ca	S	Fe	K	Na	P	Mg	Ti
	%	%	%	%	%	%	%	%	%
4S6	8.74	0.57	0.456	4.43	2.73	3.45	0.07	1.46	0.51
5P5	0.06	7.14	20.912	0.08	0.02	0.70	0.26	0.05	0.01
5S1	4.85	2.72	3.776	8.32	1.84	1.85	1.91	0.58	0.05
5S2	7.5	0.5	0.4	4.49	2.41	1.49	0.38	0.95	0.17
5S3	8.38	0.46	0.368	5.3	2.75	1.59	0.19	1.15	0.48
5S4	8.71	0.42	0.336	5.66	2.96	1.74	0.14	1.24	0.58
5S5	10.1	0.52	0.416	6.03	2.88	1.72	0.08	1.15	0.55
5S11	6.55	1.69	1.0	3.32	1.97	1.51	0.05	1.05	0.46
6P4	0.09	11.3	18.64	0.02	< 0.01	0.19	0.22	0.02	0.01
6P5	0.16	12.1	21.68	0.03	0.02	0.56	0.29	0.05	0.01
6S1	5.88	3.28	5.024	3.21	1.82	1.66	0.07	0.98	0.42
6S2	5.52	4.75	6.2	3.11	1.64	1.55	0.09	0.95	0.42
6S3	7	1.8	2.0	3.89	2.23	2.01	0.09	1.1	0.52
6S4	5.77	4.94	2.0	3.42	1.89	1.58	0.05	0.97	0.43
6S5	7.09	2.99	2.392	3.66	1.97	1.85	0.07	1.03	0.46
6S6	7.1	3.16	2.528	4.05	2.19	1.89	0.07	1.01	0.48
6S7	7.41	2.59	2.072	4.26	2.17	1.93	0.07	1.13	0.49
6S10	6.54	2.19	1.0	3.22	2	1.60	0.05	1.02	0.44
6S12	6.24	2.83	1.0	3.15	1.71	1.80	0.05	1.09	0.47
6S14	7.23	2.6	2.08	3.71	2.27	1.80	0.06	1.21	0.48
7P4	0.06	7.16	18.528	0.06	0.05	0.36	0.61	0.05	0.01
7P6	0.09	9.4	19.52	0.15	0.02	0.45	0.73	0.05	0.02
7S1	4.17	1.58	2.864	16.5	1.19	1.48	3.12	0.82	0.07
7S3	7.84	1	0.8	7.46	2.31	1.75	0.21	1.04	0.54
7S4	8.5	1.36	1.088	5.04	2.39	1.57	0.14	1.08	0.53
7S5	8.91	0.53	0.424	4.82	2.35	1.76	0.14	1.24	0.45
7S14	7.34	4.22	1.0	3.5	1.9	0.91	0.06	1.13	0.30

Table S3.4
Trace elements.

Code	As	Ba	Cd	Cr	Cu	Li	Sb	Ni	Pb	Mn	Sr	Th	U	V	Y	Zn
	ppm	ppm	ppm	ppm	ppm	ppm	ppm	ppm	ppm	ppm	ppm	ppm	ppm	ppm	ppm	ppm
1P4	83	71	1.7	15	96.1	0.1	25.9	1.2	344	20	398	0.8	15.6	< 4	65.9	98
1S1	1680	152	6.2	86	457	16.6	44.1	14.9	772	422	378	4.9	37.2	169	30.2	1210
1S2	669	285	0.5	85	745	54	11.4	36.2	190	1060	117	8.8	7.6	119	23.7	1290
1S3	197	357	0.6	92	392	69.2	3.4	41.2	121	664	103	10.4	4.1	139	25.2	439
1S4	126	705	0.7	184	485	143	2.8	87.4	174	1180	205	21.4	7.9	205	44.8	687
1S5	25	378	0.4	92	253	75.9	0.4	45.2	84.2	346	92	11	3.5	111	22	217
1S6	55	236	<0.1	82	339	59.8	3.7	36.6	114	335	108	9.4	3.2	118	19	148
2P1	6	27	1.5	14	21.5	0.3	0.2	1	1.5	20	224	0.2	2.8	5	31.8	17
2P2	2	21	0.9	8	23.8	0.3	0.2	0.4	1.3	13	199	0.3	4.9	< 4	29.5	6
2S1	139	324	0.6	107	281	65	8.2	41.2	267	370	139	5.3	5.7	141	21.2	644
2S3	39	359	1.7	88	236	79.1	1.9	45.6	81.7	382	96	10.6	4.2	145	22.7	351
2S4	41	366	4.4	76	186	83.3	2.5	47.2	88.6	563	108	11.4	4.1	154	22	414
2S5	50	372	0.7	195	263	83.9	2.3	47.9	100	377	92	11.3	3.6	146	22	377
2S7	45	381	0.2	91	421	83.9	2.2	45.2	117	388	91	11	3.2	147	21.6	280
2S8	168	300	0.6	87	1960	71.7	3.8	40.7	245	356	97	10.2	3.5	136	20.4	413
2S10	12	254	< 0.1	124	63.6	30.5	0.9	18.8	16.8	278	185	6.5	2.3	68	13.5	51
3P2	23	37	1.3	11	113	0.3	1.4	0.6	3.4	17	193	0.4	23.2	4	45.1	11
3S1	1560	171	8.8	91	5300	12.4	34.1	41.2	344	1260	1600	4.5	16.4	81	15.9	3660
3S2	5950	156	59	247	>10000	13	29.4	146	435	403	2410	4.9	26.8	153	27.7	>10000
3S3	36	368	1	83	272	82.8	0.9	46.4	96	377	90	11.1	3.6	126	21.8	400
3S4	1330	293	0.6	68	692	22.1	65.4	23.3	1210	978	521	5.1	14.5	91	9.9	2730
3S5	315	294	4.3	113	1470	61.2	8.2	44.1	206	358	80	7.7	7.2	132	21.4	3160

Code	As ppm	Ba ppm	Cd ppm	Cr ppm	Cu ppm	Li ppm	Sb ppm	Ni ppm	Pb ppm	Mn ppm	Sr ppm	Th ppm	U ppm	V ppm	Y ppm	Zn ppm
3S6	58	374	1.3	105	590	82.9	3.4	50.6	125	399	84	10.7	3.4	116	22.2	709
3S8	26	330	0.1	80	38.1	66.1	2.2	37.7	52.7	330	108	10	3.1	124	18.6	111
4P2	7	71	1.4	17	19.2	0.2	0.5	1.9	3.9	18	350	1.2	13.6	< 4	59.8	9
4P3	8	67	1	16	9.9	0.4	0.2	0.1	3.1	15	273	0.8	10.6	< 4	43.5	11
4S1	100	307	0.2	94	851	68.2	6	40.5	243	596	75	8.7	2.4	124	16.3	269
4S3	17	283	0.1	115	104	76.4	0.8	40.6	80.2	271	76	8.6	2.2	124	17.2	161
4S4	35	351	2.4	104	127	79.4	6.5	46.1	177	280	85	10	4.6	155	19.1	197
4S5	16	361	0.1	90	109	83.6	6.3	46.2	175	271	91	10.7	8.6	139	20.4	138
4S6	29	364	0.1	96	104	78.4	6.3	42.8	157	279	98	10.8	4.2	149	21.1	139
5P5	3	38	0.8	10	10.7	0.3	0.4	0.4	5.5	15	272	0.2	3	<4	36.8	3
5S1	718	225	0.6	105	442	27	26.2	17.5	756	555	237	7.1	24.8	126	39.9	234
5S2	178	304	0.2	71	209	55.4	0.5	33.4	131	353	129	8.1	4	134	17.5	176
5S3	68	345	0.2	98	202	74.9	2.4	43.7	79.2	395	90	8.5	2.9	147	18.8	223
5S4	57	378	0.2	109	308	85.9	3.4	47.4	76.1	445	84	9.5	3.1	170	19.7	257
5S5	61	382	0.1	100	229	81.8	0.8	45	93.1	486	84	10.6	3	158	18.2	255
5S11	12	311	< 0.1	109	17.5	59.3	1.2	33.3	20.3	281	113	7.6	2.1	104	14.2	74
6P4	<1	37	1.3	11	1.3	<0.1	0.1	<0.1	0.6	4	278	0.5	5.7	<4	54.7	2
6P5	<1	63	1.6	12	9.2	0.2	0.1	0.5	2.2	9	348	1.1	10.7	<4	77.8	11
6S1	33	165	0.2	51	149	42.6	4	25.2	79.5	313	176	8.4	4.2	86	26.1	95
6S2	35	131	0.5	65	126	41.9	4.3	26.4	79.8	305	239	8.2	7.8	85	43.4	95
6S3	50	288	0.2	73	316	59.7	3.1	37.2	80	286	121	10.1	8.1	111	29.5	172
6S4	41	261	<0.1	60	214	45.4	3.6	26.9	89.9	317	254	8.5	3.3	89	20.7	109
6S5	53	119	0.2	86	434	52.1	3.6	30.7	96.2	309	162	8.7	4	101	25.6	163
6S6	66	115	0.3	74	641	57.6	4.4	32.8	110	319	143	9.1	3.8	108	26.9	204
6S7	74	172	0.2	91	749	61.9	5.5	35.6	120	331	146	9.7	3.8	113	25.2	226
6S10	12	302	<0.1	82	17.8	45.7	1	27.3	19.8	297	150	8.7	2.4	88	15.4	73
6S12	16	223	<0.1	86	33.3	47.8	1.7	29.1	27.5	343	152	8.2	2.7	93	16.5	73
6S14	16	233	<0.1	61	28.2	56.2	1.4	34	24.4	365	157	9.4	2.9	107	19.3	86
7P4	20	111	3.9	27	20	0.3	0.6	4.8	10.7	13	1320	2.1	17.7	18	45.3	36
7P6	24	68	4.4	36	32.4	0.3	1	6.1	15	20	762	2.1	27.6	28	57.9	36
7S1	794	170	2.2	82	774	30.2	10	44.7	205	483	167	5.7	8.3	85	15.3	925
7S3	168	339	0.6	99	383	67.7	7.4	37.5	115	612	104	9.4	5.4	143	17.8	423
7S4	77	343	1.7	122	323	73.1	3.9	39.1	91.2	326	115	10.4	4.5	144	22.1	255
7S5	47	370	2	93	320	80	2.3	48.2	98.9	361	92	10.9	5.1	141	22.3	522
7S14	7	287	< 0.1	85	25	44.8	0.4	33.1	27	362	163	9.6	2.3	81	17.2	93

Table S3.5
Location, depth, and number of samples taken from the cores.

Core	Zone	UTM (WGS89)	Total depth (m)	PG samples	Sediment samples
1	2	29 S 685500, 4124308	15	1	6
2	2	29 S 684532, 4123293	15	2	7
3	2	29 S 684456, 4124971	16	1	7
4	3	29 S 686257, 4126285	15.8	2	5
5	3	29 S 685947, 4125146	18	1	6
6	3	29 S 686101, 4124858	14	2	10
7	3	29 S 685089, 4125768	13.2	2	5

Table S3.6
Statistical summary of the pH and EC values in the PG and sediments samples. The uncertainty is given as the standard deviation of the mean.

	pH				EC (mS cm^{-1})			
Material	N	Mean	Range	SD	N	Mean	Range	SD
PG	11	2.9±0.2	2.1-4.1	0.61	11	12.2±0.8	8.6-15.9	2.7
Sediments 0 – 50 cm	27	5.9±0.2	4.0-8.3	1.1	27	22.6±1.4	12.6-38.4	1.4
Sediments > 50 cm	19	7.0±0.3	4.8-8.3	1.1	19	19.5±1.8	6.5-47.2	8.0

Table S3.7
Samples and physicochemical parameters.

Code	From (m)	To (m)	Contact	pH	EC (mS cm^{-1})
1P4	5.45	5.50		3.1	9.8
1S1	5.65	5.70		5.9	23.2
1S2	5.7	5.75		5.9	21.9
1S3	5.75	5.80	5.60	5.9	21.3
1S4	5.95	6.00		6.1	16.0
1S5	6.25	6.30		7.0	14.5
1S6	9.20	9.25		7.4	17.7
2P1	4.65	4.70		2.9	13.7
2P2	4.95	5.00		2.8	3.2
2S1	5.15	5.20		5.1	19.9
2S3	5.25	5.30		5.0	18.8
2S4	5.35	5.40	5.10	5.0	22.2
2S5	5.50	5.55		5.8	17.0
2S7	5.70	5.75		4.8	20.7
2S8	6.25	6.30		6.6	16.6
2S10	9.70	9.75		6.6	19.9
3P2	4.95	5.00		4.1	15.3
3S1	5.2	5.25		4.0	31.4
3S2	5.25	5.30		4.3	31.1
3S3	5.4	5.45	5.10	4.8	31.9
3S4	5.45	5.50		5.0	30.6
3S5	5.6	5.65		5.6	27.5
3S6	5.95	6.00		6.3	18.2
3S8	10.35	10.4		7.8	20.0
4P2	3.10	3.15		3.1	9.1
4P3	3.20	3.25		3.8	15.3
4S1	3.50	3.55		6.1	33.2
4S3	3.60	3.65	3.50	6.4	27.8
4S4	3.75	3.80		6.4	38.4
4S5	3.85	3.90		7.6	34.8
4S6	4.00	4.05		6.4	47.2
5P5	8.10	8.15		2.6	15.9
5S1	8.25	8.30		5.0	23.5
5S2	8.30	8.35		5.2	18.6
5S3	8.35	8.40	8.20	5.2	17.3
5S4	8.45	8.50		5.4	14.9
5S5	8.70	8.75		5.2	19.6
5S11	16.10	16.15		7.8	17.6
6P4	6.10	6.15		2.5	9.1
6P5	6.30	6.35		2.1	8.6
6S1	6.55	6.60	6.50	8.2	13.5
6S2	6.60	6.65		7.9	12.6
6S3	6.75	6.80		7.1	17.6

Code	From (m)	To (m)	Contact	pH	EC (mS cm^{-1})
6S4	6.95	7.00		8.3	16.6
6S5	7.00	7.05		7.9	15.3
6S6	7.05	7.10		7.4	24.1
6S7	7.10	7.15		7.9	16.4
6S10	11.37	11.42		8.1	12.4
6S12	11.75	11.80		8.1	21.8
6S14	13.25	13.30		8.2	16.5
7P4	2.20	2.25		2.3	12.6
7P6	2.35	2.40		2.3	11.3
7S1	2.50	2.55		5.5	18.7
7S3	2.60	2.65	2.40	5.6	18.2
7S4	2.65	2.70		6.0	18.5
7S5	2.90	2.95		5.2	17.3
7S14	14.52	14.57		8.3	6.5

Table S3.8
Activity concentration of the analysed radionuclides.

	^{238}U	^{234}U	^{228}Th	^{230}Th	^{232}Th	^{226}Ra	^{228}Ra	^{210}Pb	^{40}K
Code	Bq kg^{-1}								
1P4	181 ± 6	185 ± 6	5.2 ± 0.5	574 ± 13	6.6 ± 0.7	591 ± 34	<5.7	609 ± 24	< 20
1S1	467 ± 16	515 ± 18	27 ± 2	213 ± 7	28 ± 2	271 ± 16	29 ± 2	424 ± 15	437 ± 27
1S2	94 ± 5	95 ± 4	27 ± 2	54 ± 5	36 ± 2	34 ± 2	37 ± 3	35 ± 2	620 ± 38
1S3	52 ± 2	48 ± 2	34 ± 2	54 ± 3	45 ± 2	33 ± 2	42 ± 3	44 ± 2	763 ± 46
1S4	53 ± 3	54 ± 2	48 ± 2	41 ± 6	87 ± 4	34 ± 1	46 ± 2	36 ± 2	842 ± 27
1S5	45 ± 2	44 ± 2	41 ± 3	47 ± 2	34 ± 2	23 ± 1	46 ± 3	26 ± 2	921 ± 55
1S6	39 ± 2	41 ± 2	37 ± 2	33 ± 4	38 ± 2	26 ± 2	42 ± 3	28 ± 2	794 ± 47
2P1	88 ± 3	89 ± 4	< 2.8	142 ± 5	2.0 ± 0.4	278 ± 16	6.6 ± 0.7	355 ± 13	< 14
2P2	110 ± 5	116 ± 5	3 ± 1	249 ± 6	1.2 ± 0.1	260 ± 8	< 8.0	347 ± 17	6 ± 4
2S1	90 ± 3	101 ± 3	35 ± 2	97 ± 5	46 ± 3	209 ± 12	48 ± 3	574 ± 14	780 ± 47
2S3	43 ± 2	46 ± 3	39 ± 3	48 ± 2	46 ± 2	42 ± 3	43 ± 3	50 ± 3	852 ± 51
2S4	53 ± 3	56 ± 2	52 ± 3	40 ± 5	46 ± 3	37 ± 1	50 ± 2	32 ± 2	813 ± 28
2S5	42 ± 3	46 ± 2	54 ± 2	36 ± 6	46 ± 3	31 ± 1	49 ± 2	34 ± 2	835 ± 28
2S7	43 ± 3	44 ± 2	51 ± 3	35 ± 4	45 ± 3	38 ± 1	50 ± 3	32 ± 2	853 ± 29
2S8	39 ± 2	42 ± 2	35 ± 2	36 ± 2	40 ± 2	32 ± 2	37 ± 3	38 ± 2	738 ± 45
2S10	27 ± 1	27 ± 1	22 ± 2	24 ± 1	27 ± 1	25 ± 2	28 ± 2	31 ± 2	516 ± 32
3P2	354 ± 10	358 ± 10	4.8 ± 0.5	535 ± 17	6.3 ± 1.0	662 ± 39	< 5.9	660 ± 3	26 ± 5
3S1	192 ± 6	216 ± 7	14 ± 1	83 ± 4	17 ± 2	89 ± 5	19 ± 2	189 ± 7	342 ± 23
3S2	465 ± 13	508 ± 14	27 ± 2	121 ± 6	22 ± 2	573 ± 34	37 ± 3	559 ± 19	411 ± 28
3S3	44 ± 2	47 ± 2	24 ± 2	61 ± 6	45 ± 3	352 ± 30	32 ± 3	52 ± 3	402 ± 26
3S4	179 ± 9	187 ± 7	18 ± 1	68 ± 10	21 ± 1	37 ± 2	24 ± 2	73 ± 4	392 ± 26
3S5	98 ± 4	96 ± 4	51 ± 2	38 ± 1	31 ± 2	35 ± 1	48 ± 2	42 ± 2	653 ± 22
3S6	41 ± 2	42 ± 2	41 ± 3	40 ± 2	44 ± 2	25 ± 2	39 ± 3	31 ± 4	866 ± 53
3S8	35 ± 2	40 ± 2	35 ± 2	36 ± 2	43 ± 2	30 ± 2	40 ± 3	35 ± 2	809 ± 49
4P2	228 ± 7	245 ± 7	6.0 ± 0.7	814 ± 23	9.4 ± 1.0	844 ± 49	13 ± 1	692 ± 22	< 29
4P3	211 ± 8	219 ± 9	< 22	558 ± 8	3.2 ± 0.2	463 ± 14	6 ± 2	465 ± 23	9 ± 5
4S1	42 ± 3	36 ± 2	36 ± 2	45 ± 3	46 ± 3	24 ± 2	38 ± 3	44 ± 2	883 ± 53
4S3	41 ± 3	42 ± 3	37 ± 2	46 ± 3	52 ± 3	23 ± 1	41 ± 3	29 ± 2	903 ± 5
4S4	59 ± 3	63 ± 3	46 ± 2	39 ± 6	41 ± 3	28 ± 1	47 ± 2	23 ± 1	888 ± 29
4S5	58 ± 3	59 ± 2	47 ± 2	52 ± 6	43 ± 3	27 ± 1	48 ± 2	26 ± 1	901 ± 30
4S6	51 ± 3	49 ± 2	48 ± 2	50 ± 8	44 ± 3	35 ± 1	48 ± 2	32 ± 2	858 ± 28
5P5	45 ± 2	59 ± 2	< 3	297 ± 20	3.0 ± 1.2	446 ± 26	< 5.7	394 ± 12	< 19
5S1	280 ± 9	282 ± 10	30 ± 2	197 ± 7	31 ± 2	338 ± 20	30 ± 2	1143 ± 34	524 ± 33
5S2	49 ± 2	50 ± 2	40 ± 3	43 ± 4	33 ± 2	22 ± 1	45 ± 3	64 ± 2	835 ± 50
5S3	40 ± 1	40 ± 1	41 ± 3	53 ± 2	55 ± 2	25 ± 2	45 ± 3	39 ± 2	836 ± 50
5S4	38 ± 2	39 ± 2	50 ± 2	58 ± 10	38 ± 3	25 ± 1	47 ± 2	33 ± 2	824 ± 27
5S5	42 ± 3	44 ± 2	54 ± 2	42 ± 5	43 ± 3	32 ± 1	48 ± 2	27 ± 1	853 ± 28
5S11	26 ± 1	27 ± 1	37 ± 2	52 ± 6	31 ± 2	31 ± 2	43 ± 3	33 ± 2	765 ± 46
6P4	70 ± 3	73 ± 3	< 5.0	313 ± 22	4.8 ± 1.6	570 ± 33	7.8 ± 0.9	331 ± 8	16 ± 4

	^{238}U	^{234}U	^{228}Th	^{230}Th	^{232}Th	^{226}Ra	^{228}Ra	^{210}Pb	^{40}K
Code	Bq kg^{-1}								
6P5	129 ± 6	129 ± 5	9.4 ± 1.4	737 ± 14	4.5 ± 0.3	780 ± 24	6.1 ± 1.4	790 ± 40	< 22
6S1	51 ± 3	52 ± 2	39 ± 2	141 ± 5	34 ± 2	263 ± 8	35 ± 2	223 ± 11	548 ± 18
6S2	83 ± 5	84 ± 3	35 ± 2	405 ± 16	33 ± 2	762 ± 23	34 ± 2	634 ± 32	565 ± 2
6S3	72 ± 4	72 ± 3	48 ± 2	159 ± 9	41 ± 3	304 ± 9	42 ± 2	343 ± 17	686 ± 24
6S4	42 ± 3	43 ± 2	35 ± 2	67 ± 6	34 ± 2	107 ± 3	37 ± 2	94 ± 5	587 ± 21
6S5	50 ± 2	49 ± 2	32 ± 2	106 ± 3	36 ± 2	144 ± 8	35 ± 2	165 ± 7	606 ± 37
6S6	47 ± 2	48 ± 2	33 ± 2	97 ± 7	37 ± 3	142 ± 8	39 ± 2	146 ± 4	670 ± 40
6S7	44 ± 2	45 ± 2	32 ± 2	98 ± 6	47 ± 4	103 ± 6	34 ± 2	134 ± 6	612 ± 37
6S10	33 ± 2	31 ± 2	33 ± 2	53 ± 3	33 ± 2	28 ± 1	34 ± 2	37 ± 2	654 ± 32
6S12	41 ± 2	41 ± 2	36 ± 2	41 ± 4	33 ± 2	47 ± 1	37 ± 2	38 ± 2	685 ± 33
6S14	36 ± 2	37 ± 1	31 ± 1	44 ± 3	38 ± 3	56 ± 3	40 ± 3	45 ± 1	719 ± 43
7P4	218 ± 11	224 ± 9	8.3 ± 0.8	620 ± 10	8.8 ± 0.6	923 ± 21	7.3 ± 0.8	879 ± 32	14 ± 3
7P6	167 ± 5	171 ± 5	11.6 ± 0.9	872 ± 12	8.5 ± 0.6	984 ± 57	14 ± 1	706 ± 13	37 ± 5
7S1	268 ± 6	277 ± 6	15 ± 1.3	97 ± 3	15 ± 1	68 ± 4	14 ± 1	170 ± 9	305 ± 20
7S3	71 ± 2	71 ± 2	30 ± 2	52 ± 2	39 ± 2	33 ± 2	34 ± 2	70 ± 5	687 ± 42
7S4	58 ± 3	59 ± 2	53 ± 2	68 ± 5	42 ± 3	58 ± 2	46 ± 2	49 ± 2	810 ± 27
7S5	60 ± 3	60 ± 2	55 ± 3	43 ± 7	44 ± 3	35 ± 1	51 ± 2	34 ± 2	876 ± 29
7S14	28 ± 1	29 ± 1	34 ± 2	28 ± 3	39 ± 3	23 ± 1	37 ± 3	13 ± 1	729 ± 44

Table S3.9

Values of the most representative activity ratios.

Code	^{238}U/^{232}Th	^{226}Ra/^{228}Ra	^{230}Th/^{232}Th	^{230}Th/^{238}U	^{226}Ra/^{234}U	^{210}Pb/^{226}Ra	^{226}Ra/^{230}Th
1P4	27 ± 3	103 ± 6	86 ± 9	3.18 ± 0.13	3.19 ± 0.21	1.03 ± 0.07	1.03 ± 0.06
1S1	16.8 ± 1.3	9.2 ± 0.9	7.6 ± 0.6	0.45 ± 0.02	0.53 ± 0.04	1.56 ± 0.11	1.27 ± 0.09
1S2	2.6 ± 0.2	0.93 ± 0.09	1.51 ± 0.16	0.58 ± 0.06	0.36 ± 0.03	1.02 ± 0.08	0.63 ± 0.07
1S3	1.16 ± 0.07	0.77 ± 0.07	1.20 ± 0.09	1.03 ± 0.07	0.68 ± 0.05	1.35 ± 0.10	0.61 ± 0.05
1S4	0.61 ± 0.04	0.75 ± 0.04	0.47 ± 0.07	0.78 ± 0.12	0.63 ± 0.03	1.03 ± 0.06	0.84 ± 0.13
1S5	1.33 ± 0.10	0.50 ± 0.05	1.39 ± 0.10	1.05 ± 0.06	0.52 ± 0.04	1.14 ± 0.11	0.48 ± 0.04
1S6	1.04 ± 0.07	0.61 ± 0.05	0.86 ± 0.12	0.83 ± 0.11	0.63 ± 0.05	1.08 ± 0.10	0.79 ± 0.11
2P1	44 ± 9	42 ± 5	71 ± 14	1.62 ± 0.08	3.12 ± 0.23	1.28 ± 0.09	1.96 ± 0.13
2P2	91 ± 7	32.6 ± 1.0	205 ± 15	2.26 ± 0.11	2.24 ± 0.11	1.33 ± 0.08	1.05 ± 0.04
2S1	1.98 ± 0.15	4.4 ± 0.4	2.13 ± 0.18	1.08 ± 0.07	2.06 ± 0.14	2.75 ± 0.18	2.15 ± 0.17
2S3	0.93 ± 0.06	0.99 ± 0.09	1.04 ± 0.06	1.12 ± 0.07	0.92 ± 0.08	1.18 ± 0.10	0.88 ± 0.07
2S4	1.15 ± 0.11	0.73 ± 0.04	0.88 ± 0.13	0.76 ± 0.11	0.65 ± 0.04	0.88 ± 0.06	0.90 ± 0.12
2S5	0.92 ± 0.09	0.64 ± 0.04	0.78 ± 0.14	0.84 ± 0.15	0.69 ± 0.04	1.09 ± 0.07	0.88 ± 0.15
2S7	0.96 ± 0.10	0.77 ± 0.05	0.79 ± 0.11	0.83 ± 0.11	0.87 ± 0.05	0.83 ± 0.05	1.09 ± 0.13
2S8	0.96 ± 0.07	0.87 ± 0.08	0.89 ± 0.07	0.93 ± 0.07	0.76 ± 0.06	1.20 ± 0.10	0.88 ± 0.07
2S10	1.01 ± 0.05	0.92 ± 0.09	0.88 ± 0.05	0.87 ± 0.05	0.94 ± 0.07	1.21 ± 0.11	1.08 ± 0.08
3P2	56 ± 9	112 ± 7	85 ± 14	1.51 ± 0.06	1.85 ± 0.12	1.00 ± 0.06	1.24 ± 0.08
3S1	11.6 ± 1.4	4.7 ± 0.5	5.0 ± 0.7	0.43 ± 0.02	0.41 ± 0.03	2.12 ± 0.15	1.07 ± 0.08
3S2	21 ± 2	15.5 ± 1.5	5.5 ± 0.6	0.260 ± 0.015	1.13 ± 0.07	0.98 ± 0.07	4.74 ± 0.37
3S3	0.99 ± 0.08	10.9 ± 1.2	1.36 ± 0.17	1.38 ± 0.16	7.44 ± 0.69	0.147 ± 0.015	5.75 ± 0.75
3S4	8.7 ± 0.7	1.52 ± 0.17	3.3 ± 0.5	0.38 ± 0.06	0.198 ± 0.015	1.98 ± 0.17	0.54 ± 0.09
3S5	3.13 ± 0.25	0.73 ± 0.04	1.220.09	0.390 ± 0.019	0.365 ± 0.020	1.21 ± 0.08	0.92 ± 0.04
3S6	0.94 ± 0.06	0.65 ± 0.06	0.92 ± 0.06	0.97 ± 0.07	0.60 ± 0.05	1.23 ± 0.18	0.63 ± 0.05
3S8	0.82 ± 0.06	0.73 ± 0.07	0.84 ± 0.06	1.03 ± 0.08	0.73 ± 0.06	1.18 ± 0.10	0.82 ± 0.07
4P2	24 ± 3	65 ± 7	86 ± 9	3.56 ± 0.15	3.45 ± 0.22	0.82 ± 0.05	1.04 ± 0.07
4P3	65 ± 5	82 ± 23	172 ± 12	2.65 ± 0.11	2.12 ± 0.11	1.01 ± 0.06	0.83 ± 0.03
4S1	0.89 ± 0.09	0.64 ± 0.06	0.97 ± 0.09	1.08 ± 0.11	0.69 ± 0.06	1.81 ± 0.14	0.54 ± 0.05
4S3	0.78 ± 0.07	0.55 ± 0.05	0.89 ± 0.08	1.14 ± 0.11	0.55 ± 0.05	1.27 ± 0.12	0.49 ± 0.04
4S4	1.46 ± 0.13	0.59 ± 0.04	0.97 ± 0.16	0.66 ± 0.10	0.439 ± 0.025	0.83 ± 0.05	0.71 ± 0.11
4S5	1.35 ± 0.12	0.57 ± 0.04	1.21 ± 0.17	0.90 ± 0.12	0.46 ± 0.03	0.96 ± 0.06	0.52 ± 0.07
4S6	1.16 ± 0.10	0.74 ± 0.04	1.13 ± 0.20	0.97 ± 0.17	0.71 ± 0.04	0.91 ± 0.06	0.71 ± 0.12
5P5	15 ± 6	78 ± 5	101 ± 41	6.6 ± 0.5	7.56 ± 0.51	0.88 ± 0.06	1.50 ± 0.13
5S1	9.1 ± 0.7	11.1 ± 1.1	6.4 ± 0.5	0.70 ± 0.03	1.20 ± 0.08	3.38 ± 0.22	1.71 ± 0.12
5S2	1.50 ± 0.13	0.49 ± 0.05	1.30 ± 0.15	0.86 ± 0.09	0.44 ± 0.03	2.92 ± 0.22	0.52 ± 0.06
5S3	0.73 ± 0.03	0.55 ± 0.05	0.96 ± 0.05	1.32 ± 0.06	0.62 ± 0.04	1.58 ± 0.13	0.47 ± 0.03
5S4	1.00 ± 0.09	0.53 ± 0.03	1.5 ± 0.3	1.52 ± 0.28	0.63 ± 0.04	1.33 ± 0.08	0.43 ± 0.08

5S5	0.990.09	0.68 ± 0.04	0.97 ± 0.14	0.98 ± 0.13	0.73 ± 0.04	0.84 ± 0.05	0.78 ± 0.10
5S11	0.84 ± 0.07	0.73 ± 0.07	1.68 ± 0.24	1.99 ± 0.26	1.17 ± 0.09	1.04 ± 0.08	0.60 ± 0.08
6P4	15 ± 5	73 ± 9	65 ± 22	4.47 ± 0.37	7.8 ± 0.5	0.58 ± 0.04	1.82 ± 0.17
6P5	29 ± 3	127 ± 30	166 ± 12	5.7 ± 0.3	6.0 ± 0.3	1.01 ± 0.06	1.06 ± 0.04
6S1	1.51 ± 0.14	7.4 ± 0.4	4.1 ± 0.3	2.74 ± 0.19	5.09 ± 0.26	0.85 ± 0.05	1.87 ± 0.09
6S2	2.50 ± 0.23	22.7 ± 1.7	12 ± 1.0	4.87 ± 0.35	9.1 ± 0.4	0.83 ± 0.05	1.88 ± 0.09
6S3	1.76 ± 0.16	7.2 ± 0.5	3.9 ± 0.3	2.21 ± 0.18	4.20 ± 0.21	1.13 ± 0.07	1.91 ± 0.12
6S4	1.22 ± 0.12	2.9 ± 0.19	1.95 ± 0.21	1.60 ± 0.17	2.52 ± 0.13	0.88 ± 0.05	1.60 ± 0.14
6S5	1.41 ± 0.10	4.1 ± 0.4	2.98 ± 0.19	2.11 ± 0.10	2.91 ± 0.21	1.15 ± 0.08	1.35 ± 0.09
6S6	1.27 ± 0.11	3.7 ± 0.3	2.6 ± 0.3	2.08 ± 0.17	2.96 ± 0.21	1.03 ± 0.07	1.46 ± 0.13
6S7	0.93 ± 0.09	3.0 ± 0.3	2.06 ± 0.22	2.22 ± 0.17	2.31 ± 0.17	1.30 ± 0.10	1.06 ± 0.09
6S10	1.00 ± 0.09	0.83 ± 0.06	1.60 ± 0.13	1.61 ± 0.13	0.90 ± 0.07	1.32 ± 0.09	0.53 ± 0.04
6S12	1.23 ± 0.11	1.27 ± 0.09	1.22 ± 0.14	0.99 ± 0.10	1.15 ± 0.07	0.81 ± 0.05	1.15 ± 0.11
6S14	0.94 ± 0.08	1.41 ± 0.13	1.16 ± 0.12	1.23 ± 0.11	1.52 ± 0.11	0.81 ± 0.05	1.26 ± 0.12
7P4	25 ± 2	126 ± 14	71 ± 5	2.84 ± 0.15	4.12 ± 0.19	0.95 ± 0.04	1.49 ± 0.04
7P6	19.6 ± 1.5	73 ± 7	102 ± 7	5.22 ± 0.17	5.8 ± 0.4	0.72 ± 0.04	1.13 ± 0.07
7S1	17.8 ± 1.2	4.7 ± 0.5	6.4 ± 0.5	0.362 ± 0.013	0.24 ± 0.02	2.51 ± 0.20	0.70 ± 0.05
7S3	1.80 ± 0.11	0.98 ± 0.09	1.32 ± 0.08	0.73 ± 0.04	0.47 ± 0.03	2.09 ± 0.20	0.65 ± 0.05
7S4	1.38 ± 0.13	1.27 ± 0.08	1.62 ± 0.16	1.17 ± 0.11	0.99 ± 0.05	0.84 ± 0.05	0.86 ± 0.07
7S5	1.35 ± 0.12	0.68 ± 0.04	0.97 ± 0.16	0.71 ± 0.12	0.58 ± 0.03	0.99 ± 0.06	0.81 ± 0.13
7S14	0.73 ± 0.06	0.64 ± 0.05	0.71 ± 0.08	0.97 ± 0.11	0.80 ± 0.05	0.56 ± 0.06	0.85 ± 0.09

Table S3.10.
Physicochemical parameters in the sampling points. EC: electrical conductivity. PM: particulate matter.

	OR				TR				OE				TE			
Month	pH	EC (mS cm^{-1})	Eh (mV)	PM (mg L^{-1})	pH	EC (mS cm^{-1})	Eh (mV)	PM (mg L^{-1})	pH	EC (mS cm^{-1})	Eh (mV)	PM (mg L^{-1})	pH	EC (mS cm^{-1})	Eh (mV)	PM (mg L^{-1})
Oct	2.9	3.0	747	14	2.9	2	717	15	7.4	47	455	14	7.2	45	439	27
Nov	3.2	2.4	724	3.1	2.5	5.7	783	12	7.6	49	404	9.5	7.4	47	397	10
Dec	3.3	2.1	693	47	2.5	5.3	743	219	7.5	39	421	20	7.1	36	428	42
Jan	4.1	0.4	440	10	3.2	0.5	633	48	6	23	420	13	4.9	18	382	42
Feb	4.7	0.2	410	107	5	0.2	392	106	4.7	0.3	466	6	6.2	0.7	450	16
Mar	3	1.1	407	12	2.7	1.4	727	15	5.8	37	478	17	6.2	40	476	13
Apr	3.5	0.7	617	14	3.6	0.5	606	6.3	6.6	36	439	18	6.6	34	432	22
May	2.9	1.4	697	9.8	2.5	2.2	722	3.4	6.5	40	443	22	6.5	40	454	19
Jun	2.7	1.2	669	2.0	1.7	3	738	5.8	6.4	42	446	13	6.9	43	377	20
Jul	3.2	1.4	606	4.1	2.5	2.5	752	2.9	7.5	58	389	15	7.2	52	434	27
Aug	2.3	2.5	689	3.2	1.9	2.7	719	5.5	7.3	52	323	17	6.9	49	324	16
Sep	2.2	1.9	661	2.4	1.6	2.8	739	4.0	7.7	54	365	19	7.3	55	362	18

Table S3.11
Concentration of major and trace elements in the dissolved phase of the Odiel River (OR) sampling point (in mg L^{-1}). DL: Detection limit.

Month	Al	Ca	SO_4^{2-}	Cu	Fe	K	Mn	Na	Zn	Cd	Co	Cr	Li	Mg	Ni	P	Pb	Sn	Sr
Oct	62	156	1509	3.3	19	7.3	19	91	21	0.064	0.49	0.010	0.14	0.158	0.24	0.082	0.147	<DL	0.33
Nov	55	150	1461	2.7	27	6	18	61	19	0.057	0.47	0.008	0.125	0.15	0.23	<DL	0.032	<DL	0.30
Dec	154	120	2049	13	17	4.5	28	36	34	0.132	0.74	0.021	0.247	0.19	0.37	<DL	0.097	<DL	0.25
Jan	12	22	234	1.6	0.26	<DL	2.1	14	3.5	0.012	0.07	<DL	<DL	0.024	0.030	<DL	<DL	<DL	0.05
Feb	2.7	13	99	0.6	0.48	<DL	0.77	9.3	1.3	0.0034	0.03	<DL	<DL	0.011	0.015	<DL	<DL	<DL	0.03
Mar	39	34	585	4.6	2.7	<DL	5.5	16	9.5	0.035	0.19	<DL	0.063	0.055	0.091	<DL	0.037	0.021	0.07
Apr	19	23	309	2.7	0.38	<DL	2.8	12	5.3	0.018	0.10	0.007	0.035	0.031	0.045	<DL	<DL	<DL	0.05
May	53	46	765	6.1	3.7	0.96	8	17	12	0.047	0.29	<DL	0.095	0.079	0.13	<DL	0.047	<DL	0.09
Jun	40	43	693	5	4.2	<DL	7.4	17	12	0.039	0.25	<DL	0.083	0.07	0.13	<DL	0.058	<DL	0.09
Jul	58	59	930	5.9	3.3	<DL	11	21	15	0.055	0.32	<DL	0.123	0.096	0.16	<DL	0.082	<DL	0.12
Aug	119	95	1704	11	6.2	1.9	22	28	30	0.104	0.59	<DL	0.222	0.17	0.30	<DL	0.117	0.015	0.18
Sep	83	91	1305	6.6	5.9	2.7	18	31	21	0.073	0.47	0.008	0.161	0.14	0.23	<DL	0.107	0.029	0.18

Table S3.12
Concentration of major and trace elements in the dissolved phase of the Tinto River (TR) sampling point (in mg L^{-1}). DL: Detection limit.

Month	Al	Ca	SO_4^{2-}	Cu	Fe	K	Mn	Na	Zn	Cd	Co	Cr	Li	Mg	Ni	P	Pb	Sn	Sr
Oct	52	89	1077	9.6	44	13	6.2	89	12	0.050	0.34	<DL	0.21	0.063	0.11	<DL	0.052	<DL	0.45
Nov	323	164	4941	60	592	4.8	32	77	74	0.310	1.93	0.091	0.51	0.280	0.53	0.31	0.08	<DL	0.42
Dec	191	187	3939	41	558	4.7	19	42	48	0.186	1.16	0.068	0.30	0.167	0.35	0.62	0.094	0.018	0.32
Jan	13	21	243	3	6.2	<DL	1.1	16	3	0.012	0.07	<DL	<DL	0.017	0.02	<DL	0.057	<DL	0.07
Feb	0.75	32	135	1.1	5.3	<DL	0.6	9.1	1.6	0.006	0.04	<DL	0.00	0.011	0.01	<DL	0.073	<DL	0.06
Mar	36	28	603	10	41	<DL	3.1	17	9.6	0.046	0.24	0.011	0.06	0.037	0.07	<DL	0.083	<DL	0.10
Apr	7.9	19	174	2.2	0.3	<DL	0.9	15	2.2	0.009	0.06	0.0043	<DL	0.015	0.02	<DL	0.104	<DL	0.08
May	75	50	1122	19	85	<DL	5.9	30	17	0.081	0.44	0.013	0.11	0.069	0.11	0.04	0.145	<DL	0.17
Jun	<DL	65	1905	30	172	2.6	10	40	28	0.119	0.72	0.023	0.16	0.108	0.16	0.15	0.104	<DL	0.21
Jul	79	102	1437	17	81	4.4	7.3	50	18	0.081	0.49	0.018	0.15	0.079	0.12	<DL	0.188	0.0053	0.32
Aug	73	105	1338	15	59	11	7.3	71	15	0.069	0.44	0.014	0.16	0.077	0.11	<DL	0.098	<DL	0.40
Sep	95	118	1692	19	82	8.3	9.6	101	20	0.096	0.59	0.019	0.22	0.102	0.14	6.07	0.086	0	0.49

Table S3.13
Concentration of major and trace elements in the Odiel estuary (OE) sampling point (in mg L^{-1}). DL: Detection limit.

Month	Al	Ca	SO_4^{2-}	Cu	Fe	K	Mn	Na	Zn	Cd	Co	Cr	Li	Mg	Ni	P	Pb	Sn	Sr
Oct	<DL	361	2739	0.020	0.03	426	0.06	9722	0.12	0.0016	<DL	0.0039	0.25	1.30	0.0056	0.082	<DL	<DL	6.96
Nov	<DL	360	2703	0.010	<DL	411	0.02	9767	0.06	<DL	<DL	0.0034	0.28	1.26	0.0044	<DL	<DL	<DL	6.56
Dec	<DL	343	2559	0.010	<DL	394	<DL	9005	0.3	<DL	0.0023	<DL	<DL	1.16	<DL	0.166	<DL	<DL	6.44
Jan	<DL	212	1413	0.310	<DL	234	0.73	5155	1.2	0.0044	0.026	<DL	0.15	0.68	0.012	<DL	<DL	<DL	3.58
Feb	3.5	17	144	0.640	0.16	11	0.98	125	1.6	0.0048	0.035	<DL	0.02	0.02	0.016	<DL	0.017	<DL	0.10
Mar	<DL	297	2049	0.100	<DL	313	0.49	7495	0.65	0.0035	0.017	0.0032	0.23	0.97	0.0085	<DL	<DL	<DL	5.10
Apr	<DL	248	1671	0.040	<DL	251	0.45	6273	0.58	0.0032	0.013	0.0057	0.17	0.81	0.0075	<DL	<DL	<DL	4.22
May	<DL	297	2217	0.130	<DL	311	0.74	7487	0.98	0.0053	0.021	<DL	0.23	0.96	0.012	<DL	<DL	<DL	4.86
Jun	<DL	334	2478	0.090	<DL	360	0.67	8762	0.83	0.0044	0.017	<DL	0.25	1.11	0.012	<DL	0.013	<DL	6.20
Jul	<DL	374	2781	0.020	<DL	411	0.16	9900	0.12	0.0025	0.0031	<DL	0.26	1.27	0.0043	<DL	<DL	0.017	7.06
Aug	0.22	388	2781	0.040	<DL	425	0.32	9833	0.31	<DL	0.0078	<DL	0.26	1.28	0.0058	0.045	<DL	0.0034	7.13
Sep	<DL	374	2895	0.010	<DL	455	0.04	9846	0.07	<DL	<DL	<DL	0.27	1.27	<DL	<DL	<DL	<DL	7.06

Table S3.14
Concentration of major and trace elements in the dissolved phase of the Tinto estuary (TE) sampling point (in mg L^{-1}). DL: Detection limit.

Month	Al	Ca	SO_4^{2-}	Cu	Fe	K	Mn	Na	Zn	Cd	Co	Cr	Li	Mg	Ni	P	Pb	Sn	Sr
Oct	<DL	372	2433	0.050	<DL	394	0.05	8973	0.10	0.0027	<DL	<DL	0.26	1.15	0.0054	0.52	<DL	<DL	5.95
Nov	<DL	367	2730	0.020	<DL	427	0.05	9101	0.09	<DL	0.0043	0.0021	0.28	1.23	0.0044	0.47	<DL	0.012	6.39
Dec	<DL	338	2385	0.020	<DL	402	0.06	8939	0.29	0.0017	<DL	0.0035	0.25	1.16	<DL	0.63	<DL	<DL	6.45
Jan	3.1	187	1248	1.800	0.16	170	0.8	3840	2.00	0.015	0.050	0.0044	0.12	0.47	0.019	<DL	<DL	<DL	<DL
Feb	<DL	38	141	0.020	<DL	8.5	0.55	120	0.55	0.0032	0.026	<DL	0.00	0.02	0.0098	0.23	<DL	<DL	0.16
Mar	<DL	269	1917	0.410	0.06	301	0.57	6924	1.00	0.0075	0.029	<DL	0.21	0.89	0.01	0.04	<DL	<DL	4.62
Apr	<DL	232	1527	0.100	<DL	219	0.51	5583	0.88	0.007	0.024	0.0036	0.15	0.71	<DL	0.07	<DL	<DL	3.78
May	<DL	324	2214	0.370	<DL	319	0.74	7620	1.20	0.009	0.036	<DL	<DL	0.97	0.013	0.13	0.014	<DL	5.15
Jun	0.12	365	2565	0.060	0.1	385	0.31	8828	0.29	0.0046	0.012	0.0042	0.27	1.14	0.0083	0.48	<DL	<DL	6.54
Jul	<DL	392	2886	0.040	<DL	421	0.3	9092	0.25	0.0052	0.0074	<DL	0.24	1.17	<DL	0.10	<DL	<DL	6.65
Aug	<DL	400	2853	0.050	0.04	437	0.23	9497	0.16	<DL	0.0064	0.0028	0.23	1.21	0.0059	0.13	<DL	<DL	6.72
Sep	0.1	397	2793	0.040	0.08	437	0.1	9800	0.12	0.0024	0.0033	<DL	0.24	1.23	0.005	0.61	<DL	<DL	6.76

Table S3.15
^{238}U activity concentration in the dissolved and particulate phase of the sampling points. NM: not measured. DL: Detection limit.

	OR		TR		OE		TE	
Month	$^{238}U_D$ (mBq L^{-1})	$^{238}U_P$ (mBq g^{-1})	$^{238}U_D$ (mBq L^{-1})	$^{238}U_P$ (mBq g^{-1})	$^{238}U_D$ (mBq L^{-1})	$^{238}U_P$ (mBq g^{-1})	$^{238}U_D$ (mBq L^{-1})	$^{238}U_P$ (mBq g^{-1})
Oct	48 ± 1	36 ± 6	44 ± 2	<DL	56 ± 4	13 ± 1	56 ± 3	72 ± 7
Nov	38 ± 1	<DL	182 ± 13	9 ± 2	55 ± 4	27 ± 3	88 ± 7	89 ± 7
Dec	26.4 ± 0.8	29 ± 2	22 ± 3	11 ± 1	51 ± 3	65 ± 5	54 ± 4	239 ± 10
Jan	14.0 ± 0.5	26 ± 3	13 ± 0.5	12 ± 1	8 ± 1	588 ± 31	1.7 ± 0.2	1378 ± 49
Feb	4.1 ± 0.2	47 ± 2	3.2 ± 0.3	NM	5.2 ± 0.3	53 ± 8	1.7 ± 0.2	406 ± 18
Mar	54 ± 1	6.7 ± 1.6	36 ± 1	8.2 ± 1.7	26 ± 1	634 ± 26	18 ± 1	353 ± 20
Apr	26 ± 1	30 ± 3	8.7 ± 0.4	14 ± 4	18 ± 1	115 ± 7	12 ± 1	142 ± 10
May	67 ± 2	42 ± 5	NM	17 ± 6	15 ± 1	50 ± 5	10 ± 1	498 ± 22
Jun	54 ± 2	103 ± 28	86 ± 3	<DL	27 ± 1	101 ± 9	45 ± 2	258 ± 12
Jul	63 ± 3	56 ± 9	49 ± 1	128 ± 23	43 ± 3	11 ± 2	33 ± 2	45 ± 3
Aug	140 ± 4	43 ± 9	58 ± 2	18 ± 4	40 ± 2	31 ± 3	50 ± 2	37 ± 3
Sep	51 ± 2	<DL	120 ± 3	<DL	54 ± 2	29 ± 2	63 ± 3	75 ± 5

Table S3.16
Percentage (%) of ^{238}U activity concentration in the particulate matter of the sampling points.

	Point	Oct	Nov	Dec	Jan	Feb	Mar	Apr	May	Jun	Jul	Aug	Sep
^{238}U	OR	1.1	<1	5.0	1.8	55	0.2	1.6	0.6	0.4	0.4	<1	<1
	TR	<1	<1	9.9	4.3	-	0.3	1.0	-	<1	0.8	0.2	<1
	OE	0.3	0.5	2.5	49	5.3	29	10	6.7	4.8	0.4	1.3	1.0
	TE	3.4	1.0	16	97	80	20	21	48	10	3.6	1.2	2.1

Table S3.17
$^{234}U/^{238}$Activity ratio in the dissolved and particulate phase of the sampling points.

	OR		TR		OE		TE	
Month	$^{234}U/^{238}U_D$	$^{234}U/^{238}U_P$	$^{234}U/^{238}U_D$	$^{234}U/^{238}U_P$	$^{234}U/^{238}U_D$	$^{234}U/^{238}U_P$	$^{234}U/^{238}U_D$	$^{234}U/^{238}U_P$
Oct	1.69 ± 0.05	1.3 ± 0.3	2.07 ± 0.12	-	1.14 ± 0.11	1.23 ± 0.18	1.05 ± 0.08	1.06 ± 0.15
Nov	1.71 ± 0.07	-	2.3 ± 0.2	1.4 ± 0.4	1.13 ± 0.11	1.30 ± 0.18	0.99 ± 0.11	1.12 ± 0.12
Dec	1.45 ± 0.06	1.00 ± 0.10	1.6 ± 0.3	1.00 ± 0.13	1.16 ± 0.10	1.23 ± 0.12	1.17 ± 0.11	1.01 ± 0.06
Jan	1.69 ± 0.08	1.5 ± 0.2	1.92 ± 0.11	1.08 ± 0.12	1.38 ± 0.21	1.24 ± 0.09	1.13 ± 0.19	1.09 ± 0.06
Feb	1.50 ± 0.11	1.17 ± 0.07	1.6 ± 0.2	-	1.46 ± 0.10	1.3 ± 0.3	0.96 ± 0.15	1.07 ± 0.07
Mar	1.56 ± 0.05	1.3 ± 0.4	2.19 ± 0.08	1.4 ± 0.4	1.19 ± 0.06	1.22 ± 0.07	1.11 ± 0.08	1.11 ± 0.09
Apr	1.62 ± 0.10	1.6 ± 0.2	1.95 ± 0.15	1.4 ± 0.5	1.28 ± 0.13	1.12 ± 0.09	1.25 ± 0.13	1.19 ± 0.11
May	1.58 ± 0.07	1.2 ± 0.2	-	1.4 ± 0.6	1.20 ± 0.10	1.16 ± 0.17	1.20 ± 0.16	1.08 ± 0.07
Jun	1.57 ± 0.08	1.5 ± 0.5	2.10 ± 0.10	-	1.15 ± 0.06	1.06 ± 0.13	1.13 ± 0.07	1.08 ± 0.07
Jul	1.68 ± 0.11	1.0 ± 0.2	2.06 ± 0.07	1.3 ± 0.3	1.16 ± 0.11	1.1 ± 0.3	1.09 ± 0.09	1.04 ± 0.11
Aug	1.63 ± 0.07	1.0 ± 0.3	1.97 ± 0.09	1.5 ± 0.4	1.15 ± 0.09	1.00 ± 0.14	1.08 ± 0.06	1.16 ± 0.14
Sep	1.63 ± 0.07	-	1.41 ± 0.05	-	1.11 ± 0.07	1.21 ± 0.13	1.13 ± 0.07	1.08 ± 0.11

Table S3.18
^{210}Po activity concentration in the dissolved and particulate phase of the sampling points. NM: not measured. DL: Detection limit.

	OR		TR		OE		TE	
Month	$^{210}Po_D$ (mBq L^{-1})	$^{210}Po_P$ (mBq g^{-1})	$^{210}Po_D$ (mBq L^{-1})	$^{210}Po_P$ (mBq g^{-1})	$^{210}Po_D$ (mBq L^{-1})	$^{210}Po_P$ (mBq g^{-1})	$^{210}Po_D$ (mBq L^{-1})	$^{210}Po_P$ (mBq g^{-1})
Oct	2.3 ± 0.1	20 ± 4	1.57 ± 0.12	16 ±2	0.38 ± 0.06	53 ± 4	<DL	68 ± 7
Nov	2.44 ± 0.14	128 ±13	2.2 ± 0.4	<DL	0.97 ± 0.08	72 ± 7	0.68 ± 0.07	110 ± 8
Dec	28.8 ± 1.3	50 ± 3	22 ± 1	23 ± 1	0.60 ± 0.04	131 ± 10	0.45 ± 0.05	156 ± 8
Jan	0.3 ± 0.04	47 ± 5	0.57 ± 0.04	23 ± 2	0.47 ± 0.05	40 ± 7	0.73 ± 0.08	200 ± 13
Feb	0.65 ± 0.07	73 ± 3	0.76 ± 0.07	NM	0.55 ± 0.06	69 ± 9	0.54 ± 0.06	119 ± 9
Mar	1.15 ± 0.08	22 ± 4	0.95 ± 0.08	20 ± 3	0.53 ± 0.05	NM	0.4 ± 0.04	126 ± 12
Apr	3.35 ± 0.16	41 ± 5	0.57 ± 0.06	37 ± 7	0.75 ± 0.05	46 ± 6	0.76 ± 0.08	74 ± 9
May	0.95 ± 0.12	79 ± 8	3.1 ± 0.2	<DL	0.59 ± 0.05	25 ± 3	0.64 ± 0.09	126 ± 13
Jun	5.6 ± 0.3	168 ± 22	NM	25 ±6	0.57 ± 0.10	139 ± 10	0.49 ± 0.05	154 ± 12
Jul	NM	223 ± 16	6.3 ± 0.3	122 ± 14	0.28 ± 0.04	31 ± 3	0.58 ± 0.09	76 ± 5
Aug	3.49 ± 0.19	151 ± 14	3.5 ± 0.2	108 ± 8	0.81 ± 0.07	42 ± 3	0.45 ± 0.04	44 ± 4
Sep	4.7 ± 0.2	140 ± 22	8.2 ± 0.2	161 ±12	0.3 ± 0.04	60 ± 4	0.6 ± 0.05	62 ± 4

Table S3.19
Percentage (%) of ^{210}Po activity concentration in the particulate matter of the sampling points

	Point	Oct	Nov	Dec	Jan	Feb	Mar	Apr	May	Jun	Jul	Aug	Sep
^{210}Po	OR	1.0	14	1.0	61	92	19	15	45	6	-	12	7
	TR	13	-	19	66	-	24	29	-	-	5	14	1.0
	OE	66	41	81	52	41	-	52	48	77	63	48	79
	TE	-	62	94	92	78	80	68	79	86	78	61	65

Table S3.20
^{230}Th activity concentration in the dissolved and particulate phase of the sampling points. NM: not measured. DL: Detection limit.

	OR		TR		OE		TE	
Month	$^{230}Th_D$ (mBq L^{-1})	$^{230}Th_P$ (mBq g^{-1})	$^{230}Th_D$ (mBq L^{-1})	$^{230}Th_P$ (mBq g^{-1})	$^{230}Th_D$ (mBq L^{-1})	$^{230}Th_P$ (mBq g^{-1})	$^{230}Th_D$ (mBq L^{-1})	$^{230}Th_P$ (mBq g^{-1})
Oct	14 ± 1	<DL	13 ± 2	<DL	<DL	13 ± 2	<DL	<DL
Nov	<DL	<DL	93 ± 7	<DL	<DL	<DL	<DL	<DL
Dec	115 ± 4	56 ± 3	98 ± 6	18 ± 1	<DL	67 ± 4	<DL	83 ± 6
Jan	<DL	58 ± 7	4.4 ± 0.25	43 ± 2	0.30 ± 0.06	<DL	<DL	20 ± 2
Feb	<DL	NM	<DL	NM	<DL	<DL	<DL	45 ± 4
Mar	<DL	84 ± 5	<DL	33 ± 4	<DL	29 ± 3	<DL	30 ± 7
Apr	<DL	73 ± 6	<DL	135 ± 11	<DL	22 ± 3	<DL	46 ± 5
May	7.64 ± 0.33	49 ± 6	27 ±1	33 ± 7	<DL	26 ± 3	<DL	55 ± 5
Jun	4.98 ± 0.2	143 ± 25	48 ± 2	34 ±6	<DL	166 ± 13	0.54 ± 0.05	25 ± 4
Jul	21 ± 2	59 ± 13	137 ± 9	46 ± 14	<DL	16 ± 4	<DL	15 ± 3
Aug	17.0 ± 0.7	50 ± 8	27 ± 1.5	24 ± 5	<DL	13 ± 2	<DL	15 ± 2
Sep	5.98 ± 0.31	<DL	33 ± 1	<DL	0.39 ± 0.06	35 ± 3	0.27 ± 0.05	12 ± 2

Table S3.21
^{232}Th activity concentration in the dissolved and particulate phase of the sampling points. NM: not measured. DL: Detection limit.

	OR		TR		OE		TE	
Month	$^{232}Th_D$ (mBq L^{-1})	$^{232}Th_P$ (mBq g^{-1})	$^{232}Th_D$ (mBq L^{-1})	$^{232}Th_P$ (mBq g^{-1})	$^{232}Th_D$ (mBq L^{-1})	$^{232}Th_P$ (mBq g^{-1})	$^{232}Th_D$ (mBq L^{-1})	$^{232}Th_P$ (mBq g^{-1})
Oct	9 ± 0.9	<DL	5 ± 0.9	<DL	<DL	<DL	<DL	<DL
Nov	<DL	<DL	54 ± 4	<DL	<DL	<DL	<DL	<DL
Dec	75 ± 12	46 ± 2	62 ± 4	17 ± 1	<DL	20 ± 2	<DL	28 ± 3
Jan	<DL	53 ± 7	2.2 ± 0.17	34 ± 2	<DL	<DL	<DL	8 ± 1
Feb	<DL	NM	<DL	NM	<DL	<DL	<DL	39 ± 4
Mar	<DL	56 ± 4	<DL	<DL	<DL	16 ± 2	<DL	<DL
Apr	<DL	65 ± 5	<DL	79 ± 8	<DL	19 ± 2	<DL	23 ± 3
May	4.2 ± 0.2	48 ± 6	13.8 ± 0.6	<DL	<DL	9 ± 2	<DL	<DL
Jun	2.24 ± 0.12	76 ± 18	27 ± 1	<DL	<DL	28 ± 4	<DL	<DL
Jul	6.3 ± 0.9	97 ± 17	60 ± 14	<DL	<DL	11 ± 3	<DL	9.5 ± 2.1
Aug	11.1 ± 0.5	36 ± 7	13 ± 0.8	<DL	<DL	<DL	<DL	8.5 ± 1.8
Sep	3.7 ± 0.2	<DL	19 ± 1	<DL	2.08 ± 0.15	17 ± 2	0.12 ± 0.03	8.2 ± 1.7

Table S3.22
Results of the experiments A and B. PGL: phosphogypsum leachate. SW: seawater. EC: electrical conductivity. M: mass of the obtained precipitates.

Experiment	PGL (mL)	SW (L)	pH	EC (mS cm^{-1})	Eh (mV)	T (ºC)	M (g)
A	20.01	1.46	3.01	64.3	578	19.4	0.014
	20.02	2.09	3.87	64.4	484	19.5	0.020
	20.00	2.57	4.83	64.2	386	19.4	0.022
	19.99	6.1	5.88	64.5	384	19.9	0.035
	20.01	15.1	6.93	64.4	394	20.0	0.059
B	20.01	1.6	3.03	63.2	570	19.9	0.022
	20.01	2.1	3.90	63.7	476	20.2	0.026
	20.02	2.7	4.83	64.1	379	20.2	0.026
	20.01	6.2	5.90	64.3	375	20.2	0.041
	20.02	15.1	6.89	63.8	387	20.7	0.070

Table S3.23
Concentration of the most significant elements in the samples B1 and B2.

Element	B1	B2	Element	B1	B2
Al	4.3	31.5	Zn	57	<2
Ca	1011.6	1353.2	Cr	2.8	9.0
Fe	45.1	116.1	Si	195	227
K	157.1	371.5	Cu	2.0	10.5
Mg	392.4	897.1	As	7.79	14.9
Mn	4.8	14.8	Sr	11.7	23.6
Co	0.519	0.542	Cd	1.7	8.1
Ni	1.16	5.71	Ba	0.031	0.038
Na	3909	4912	Sb	0.153	0.217
P	1376	8501	Pb	0.23	0.55
S	1129	1665	U	3.7	14.5

Table S3.24
Concentrations (mg L^{-1}) of the most significant elements in the obtained solutions after the neutralisation in the experiment B.

Element	pH ≈ 3	pH ≈ 4	pH ≈ 5	pH ≈ 6	pH ≈ 7
Al	0.21	0.15	0.16	0.12	0.09
Ca	442	440	438	426	438
Fe	0.98	0.389	0.256	0.135	0.032
K	418	423	425	421	434
Mg	1428	1434	1452	1409	1424
Mn	0.194	0.142	0.116	0.047	0.017
Co	0.012	0.009	0.007	<0.002	<0.002
Ni	0.079	0.062	0.049	0.017	0.009
Na	11513	11737	11769	11509	11633
P	133	105	84	25	16
S	1049	1033	1043	1015	1023
Zn	0.789	0.573	0.432	0.185	0.123
Cr	0.142	0.036	0.003	<0.002	<0.002
Si	6.1	5.0	3.8	<2	<2
Cu	0.121	0.091	0.069	0.012	0.009
As	0.367	0.280	0.225	0.078	0.043
Sr	8.5	8.4	8.2	8.3	8.3
Cd	0.104	0.078	0.064	0.021	0.011
Ba	0.008	0.008	0.008	0.007	0.008
Sb	0.028	0.021	0.017	0.014	0.012
Pb	0.01	0.005	0.004	0.003	0.002
U	0.26	0.093	0.008	0.013	0.024

Annex II
Report on the impact factor of the publications

Report on the impact factor (IF) of the publications

- Doctoral Thesis presented by D. José Luis Guerrero Márquez, in the mode of "compendium of publication"
- Number of published articles: 4
- Number of articles accepted for publication: 4

Impact factor (IF) of the publications according to the Journal Citation Reports of the year 2019

Journal	Number of publications	IF	Category	Quartile	Position in the category	Journals in the category
Environmental pollution	2	6.793	Environmental sciences	Q1	21	265
Chemosphere	1	5.778	Environmental sciences	Q1	29	265
Catena	1	4.333	Geosciences	Q1	21	200
			Water resources	Q1	8	94
			Soil sciences	Q1	5	38

Annex III
Publications

Chemosphere 230 (2019) 219–229

Contents lists available at ScienceDirect

Chemosphere

journal homepage: www.elsevier.com/locate/chemosphere

Pollution evaluation on the salt-marshes under the phosphogypsum stacks of Huelva due to deep leachates

José Luis Guerrero [a, *], Isidoro Gutiérrez-Álvarez [a], Fernando Mosqueda [a], Manuel Olías [b], Rafael García-Tenorio [c], Juan Pedro Bolívar [a]

[a] Department of Integrated Sciences, Center for Natural Resources, Health and Environment (RENSMA), University of Huelva, 21071, Huelva, Spain
[b] Department of Geodynamics and Palaeontology, Center for Natural Resources, Health and Environment (RENSMA), University of Huelva, 21071, Huelva, Spain
[c] Department of Applied Physics II, University of Seville, 41012, Seville, Spain

HIGHLIGHTS

- Salt-marsh sediments act as a "barrier" for leachates from the phosphogypsum stacks.
- Pollutants reach only the first 0.5 m of salt-marsh sediments under the stacks.
- P is a good tracer of the pollution coming from PG piles.
- Very useful results for the design of the restauration project of the PG stacks.

GRAPHICAL ABSTRACT

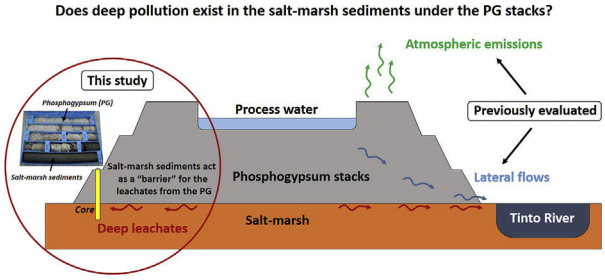

ARTICLE INFO

Article history:
Received 30 November 2018
Received in revised form
25 April 2019
Accepted 29 April 2019
Available online 9 May 2019

Handling Editor: X. Cao

Keywords:
Phosphogypsum
Pollution
Salt-marsh
Tinto River estuary

ABSTRACT

In the salth-marshes of the Tinto River (Huelva estuary, SW Spain), are stored in stacks around 100 Mt of PG, covering a surface of 1000 ha without any type of isolation, which produce an important impact in the surrounding environment. On the other hand, this ecosystem it is affected by acid mine drainage (AMD) from sulphide mines located upstream the Tinto River.

The aim of this study is to evaluate the deep pollution of the underlain salt-marsh sediments due to leachates from the PG stacks. For that purpose, 7 cores were collected from zones 2 and 3 of the stacks, and PG and salt-marsh sediments samples from different depths were analyzed. The physicochemical parameters, mineralogy, granulometry and the concentration of the main elements of interest were determined in the samples.

Most analysed salt-marsh sediments are not affected by PG stacks pollution, because sediments act as a "barrier" for the leachates from the PG, concentrating the contaminants in the first decimetres (0.5 m) under PG-sediments contact, and the deep infiltration is very limited. The obtained results suggest that the perimeter channel which is projected to build in the restauration project, should has a depth of 1 m below the level of the PG stacks for assuring the complete collection of leachates from the stacks, and avoid their liberation into the Tinto River estuary.

* Corresponding author.
E-mail addresses: joseluis.guerrero@dfa.uhu.es (J.L. Guerrero), isidoro.gutierrez@dfa.uhu.es (I. Gutiérrez-Álvarez), fernando.mosqueda@dfa.uhu.es (F. Mosqueda), manuel.olias@dgyp.uhu.es (M. Olías), gtenorio@us.es (R. García-Tenorio), bolivar@uhu.es (J.P. Bolívar).

https://doi.org/10.1016/j.chemosphere.2019.04.212
0045-6535/

Environmental Pollution 258 (2020) 113729

Contents lists available at ScienceDirect

Environmental Pollution

journal homepage: www.elsevier.com/locate/envpol

Evaluation of the radioactive pollution in the salt-marshes under a phosphogypsum stack system☆

José Luis Guerrero [a, *], Isidoro Gutiérrez-Álvarez [a], Fernando Mosqueda [a], Manuel Jesús Gázquez [b], Rafael García-Tenorio [c], Manuel Olías [d], Juan Pedro Bolívar [a]

[a] Department of Integrated Sciences, Center for Natural Resources, Health and Environment (RENSMA), University of Huelva, 21071, Huelva, Spain
[b] Department of Applied Physics, University of Cádiz, Instituto Universitario de Investigación Marina (INMAR), 11510, Cádiz, Spain
[c] Department of Applied Physics II, University of Seville, 41012, Seville, Spain
[d] Department of Earth Sciences, Center for Natural Resources, Health and Environment (RENSMA), University of Huelva, 21071, Huelva, Spain

ARTICLE INFO

Article history:
Received 12 July 2019
Received in revised form
26 November 2019
Accepted 3 December 2019
Available online 6 December 2019

Keywords:
Phosphogypsum
Natural radionuclides
Radioactive pollution
Radionuclide mobility
Salt-marsh

ABSTRACT

Next to the city of Huelva (SW of Spain), around 100 Mt of phosphogypsum (PG) are stored in stacks on the salt-marshes of the Tinto River estuary covering a surface of about 1000 ha. Due to the high content of ^{238}U series natural radionuclides of the PG, its acidic nature (pH about 3), and the fact that PG stacks were disposed without any kind of isolation from the substrate, they could produce a potential radioactive impact into the underlying sediments.

The aim of this work is to assess the pollution of the underlying sediments by natural radionuclides coming from the PG stacks. To this end, seven cores were taken, and PG and sediments samples collected at different depths were analysed. The activity concentrations of the main long half-live natural radionuclides of interest were determined by applying both gamma-ray and alpha-particle spectrometry radiometric techniques.

The results of this study showed that the first decimeters of salt-marsh sediment act as a "barrier" for the radionuclides coming from the PG stacks decreasing rapidly its activity concentration in depth, affecting mainly sediments located in the first 20 cm below the contact due to mixing processes. While ^{230}Th, ^{226}Ra and ^{210}Pb pollution is mainly restricted to the first 20 cm of sediments, U-isotopes can reach higher depths (up to around 50 cm) by leaching processes due to their lower reactivity and higher concentration in the polluted leachates. The obtained results have high relevance for the design of the perimeter channel which is projected to build in the restoration project, suggesting that should has around 1 m deep under the base of the PG stacks, to ensure the full collection of polluting leachates, and to prevent their release into the estuary of the Tinto River.

1. Introduction

On the salt-marshes of the Tinto River (SW Spain), close the Huelva city, large phosphogypsum (PG) stacks are located (Fig. 1). The confluence of the Tinto and Odiel Rivers form the Huelva estuary, which is an ecosystem of great interest and special characteristics, due to the acid mine drainage (AMD) provoked mainly by old abandoned sulphide mines located upriver, and the chemical industrial complex located at their mouths.

About 300 Mt of PG are produced worldwide every year (Yang et al., 2016). Only 15% of world PG production is recycled, and hence it is mainly disposed by dumping in large stacks, usually placed in coastal zones close to the factories, where PG is frequently exposed to weathering agents and may provoke severe environmental damages (Tayibi et al., 2009). The manufacturing of phosphoric acid (H_3PO_4) from the wet chemical attack of the phosphate rock with sulfuric acid (H_2SO_4) generate PG as a waste, which is more than 95% constituted by gypsum ($CaSO_4 \cdot 2H_2O$).

Since 1965 the five acid phosphoric factories included in the industrial complex of Huelva (Spain), have produced annually

☆ This paper has been recommended for acceptance by Jörg Rinklebe.

* Corresponding author.
E-mail addresses: joseluis.guerrero@dfa.uhu.es (J.L. Guerrero), isidoro.gutierrez@dfa.uhu.es (I. Gutiérrez-Álvarez), fernando.mosqueda@dfa.uhu.es (F. Mosqueda), manueljesus.gazquez@uca.es (M.J. Gázquez), gtenorio@us.es (R. García-Tenorio), manuel.olias@dgyp.uhu.es (M. Olías), bolivar@uhu.es (J.P. Bolívar).

https://doi.org/10.1016/j.envpol.2019.113729
0269-7491/

Catena 197 (2021) 104978

Contents lists available at ScienceDirect

Catena

journal homepage: www.elsevier.com/locate/catena

Seasonal evolution of natural radionuclides in two rivers affected by acid mine drainage and phosphogypsum pollution

J.L. Guerrero[a,*], I. Gutiérrez-Álvarez[a], A. Hierro[a], S.M. Pérez-Moreno[a], M. Olías[b], J.P. Bolívar[a]

[a] Department of Integrated Sciences, Center for Natural Resources, Health and Environment (RENSMA), University of Huelva, 21071 Huelva, Spain
[b] Department of Geodynamics and Palaeontology, Center for Natural Resources, Health and Environment (RENSMA), University of Huelva, 21071 Huelva, Spain

ARTICLE INFO

Keywords:
Natural radionuclides
Acid mine drainage
Phosphogypsum
Non-conservative
Water mixing

ABSTRACT

The Odiel and Tinto rivers show singular characteristics due to the significant acid mine drainage (AMD) generated in the first section of their basins and the phosphogypsum (PG) stacks located on their common estuary. AMD leads to low pH and high redox potential, which keep high amounts of toxic elements and radionuclides in dissolution. The objective of this work was to analyse the seasonal evolution of U-Th isotopes and ^{210}Po in these rivers and the estuarine mixing zone. Four sampling points were selected (a fluvial point and an estuarine one for each river) and water samples were collected monthly throughout a year. The concentrations of natural radionuclides in the dissolved and particulate phases were determined by alpha spectrometry. The Odiel and Tinto rivers show concentrations of U-Th isotopes and ^{210}Po from one to three orders of magnitude higher than background continental waters due to the strong effect of AMD, and ^{234}U/^{238}U activity ratios up to 2.

The studied radionuclides show a clear seasonal behaviour in these rivers, with three different stages during the year: (1) concentration peaks observed during November and December due to the "washing effect" produced by the first rainfalls of the hydrological year, (2) a "dilution effect" by runoff in the rainy winter, and (3) a progressive "concentration effect" during the spring and summer. A non-conservative behaviour of the analysed radionuclides in the estuaries was demonstrated due to precipitation processes produced by the increase of pH. The polluted outflows from the PG stacks located in the Tinto estuary produce a significant radioactive impact, mainly during the rainiest months, increasing the concentration of U-isotopes and ^{210}Po in the particulate phase.

1. Introduction

The Tinto and Odiel rivers are located in southwest Spain in the province of Huelva. They present marine influence in their final reach, converging in the common Huelva estuary (Fig. 1). The Tinto River is 101 km long while the Odiel River is 140 km long, and their catchments cover 1600 and 2300 km^2, respectively. These rivers and their estuary have a great hydrochemical and environmental interest due to two factors. The first is the extensive acid mine drainage (AMD) affecting both rivers because of the existence of several old abandoned sulfide mines in their basins and second is the large chemical industrial complex and phosphogypsum (PG) stacks located by the Huelva estuary.

Regarding the AMD, these rivers drain one of the biggest metallogenic regions of massive sulfides in the world: the Iberian Pyritic Belt (IPB). Mining works date from the year 2500BCE in this region, although the large-scale exploitation of these deposits took place during the nineteenth and twentieth centuries (Leblanc et al., 2000). The sulfide deposits are predominately composed of pyrite (FeS_2, > 90% of volume), with variable amounts of sphalerite (ZnS), chalcopyrite ($CuFeS_2$) and galena (PbS) (Sáez et al., 1999; Venkateswarlu et al., 2016). The exposure of these sulfides to oxygen and water liberates sulfate ions and metals and leads to acidity (pH = 2.5–3.0), polluting the waters (Cánovas et al, 2007). There are few works worldwide about concentrations and behaviour of natural radionuclides in locations affected by AMD, but high activity concentrations in these polluted environments have been found mainly for U-isotopes (Fernandes et al., 1998; Yamamoto et al., 2010; Durand, 2012; Madzivire, et al., 2014). In the study area some previous works also shown large concentrations of natural radionuclides with enhanced contents of U-Th isotopes and ^{210}Po in both waters and sediments (Blasco et al., 2016; Hierro et al., 2012, 2013; Manjón et al., 2019).

The AMD confers extreme physicochemical conditions on these rivers, which maintain high concentrations of toxic elements in solution (Cánovas et al., 2007; Nieto et al., 2007; Hierro et al., 2014) and

* Corresponding author.
E-mail addresses: joseluis.guerrero@dfa.uhu.es (J.L. Guerrero), isidoro.gutierrez@dfa.uhu.es (I. Gutiérrez-Álvarez), almudena.hierro@dfa.uhu.es (A. Hierro), silvia.perez@dci.uhu.es (S.M. Pérez-Moreno), manuel.olias@dgyp.uhu.es (M. Olías), bolivar@uhu.es (J.P. Bolívar).

https://doi.org/10.1016/j.catena.2020.104978
Received 4 March 2020; Received in revised form 1 October 2020; Accepted 12 October 2020

Environmental Pollution 268 (2021) 115843

Contents lists available at ScienceDirect

Environmental Pollution

journal homepage: www.elsevier.com/locate/envpol

Behaviour of heavy metals and natural radionuclides in the mixing of phosphogypsum leachates with seawater☆

J.L. Guerrero [a, *], S.M. Pérez-Moreno [a], I. Gutiérrez-Álvarez [a], M.J. Gázquez [b], J.P. Bolívar [a]

[a] Department of Integrated Sciences, Center for Natural Resources, Health and Environment (RENSMA), University of Huelva, 21071, Huelva, Spain
[b] Department of Applied Physics, University of Cadiz, University Marine Research Institute (INMAR), 11510, Cádiz, Spain

ARTICLE INFO

Article history:
Received 18 August 2020
Received in revised form
30 September 2020
Accepted 11 October 2020
Available online 27 October 2020

Keywords:
Heavy metals
Natural radionuclides
Phosphogypsum
Water mixing
Precipitation
Acidity

ABSTRACT

Phosphogypsum (PG) is disposed worldwide in large stacks usually placed in coastal zones, as in the case of Huelva (SW of Spain), where around 100 Mt of PG are stored on the salt marshes of the Tinto River estuary covering a surface of about 1000 ha. This management generates the weathering of PG, and due to its high acidity (pH ≈ 2) and pollutant load can provoke significant emissions into their surroundings. In this work were evaluated by laboratory experiments the effects of pH increase in the behaviour of heavy metals and natural radionuclides during the mixing of phosphogypsum leachates with seawater.

The acidic phosphogypsum leachates showed concentrations of heavy metals from two to three orders of magnitude higher than natural continental waters, and natural radionuclides (U-isotopes and ^{210}Po) from four to five orders of magnitude higher than unperturbed aquatic systems. Major elements and some heavy metals as Mn, Ni, Cd, As, Sb and Co showed a conservative behaviour during the neutralisation of the leachates with seawater, remaining in the liquid phase, while other ones as Al, Fe, Cr, Zn, Cu, Pb precipitated and/or were adsorbed onto the solid phase. The U-isotopes and ^{210}Po showed a clear non-conservative behaviour probably due to coprecipitation/adsorption processes onto the formed precipitates, but while ^{210}Po reached a total removal at pH ≈ 7, U- isotopes after a total removal at pH ≈ 5 returned into the liquid phase due to redissolution/desorption processes at near neutral pH.

The formed precipitates, mainly composed by iron phosphates particles, showed heavy metal and natural radionuclide concentrations from one to three orders of magnitude higher than unperturbed soils. All these facts demonstrate the serious environmental impact produced by the PG stacks into their surroundings and the urgency of effective restoration measures.

1. Introduction

Phosphogypsum (PG) is a by-product from the manufacturing fertilizer industry generated during the production of phosphoric acid (H_3PO_4), mainly composed by gypsum ($CaSO_4 \cdot 2H_2O$), but also contains high levels of pollutants such as heavy metals, acids, natural radionuclides, and some others trace elements (Rentería-Villalobos et al., 2010; Madruga et al., 2019) which may be leached. Globally, about 300 Mt of PG are produced every year (Yang et al., 2016) but only 15% of this amount is recycled, being mainly disposed by dumping in large stacks, usually placed in coastal zones close to the factories (Sanders et al., 2013; El Samad et al., 2014). This management of PG frequently generates its weathering which can provoke significant emissions into their surroundings (Tayibi et al., 2009).

Close to the Huelva city (SW of Spain), around 100 Mt of PG are stored in piles on the salt marshes of the Tinto River estuary covering a surface of about 1000 ha. This PG was generated in five acid phosphoric plants located in the industrial complex of Huelva at a rate of around $2.5 \cdot 10^6$ t/year (Bolívar et al., 2002) since 1968 until the end of 2010, when the production of phosphoric acid stopped. The industrial process is based on the wet chemical attack of phosphate rock ore, in the case of Huelva fluorapatite ($Ca_5(PO_4)_3F$) was used, with sulphuric acid (H_2SO_4). The process can be summarized in the following general reaction (Eq. (1)):

$$Ca_5(PO_4)_3F + 5H_2SO_4 + 10H_2O \rightarrow 3H_3PO_4 + 5CaSO_4 \cdot 2H_2O + HF \quad (1)$$

☆ This paper has been recommended for acceptance by Dr. Jörg Rinklebe.

* Corresponding author.
E-mail addresses: joseluis.guerrero@dfa.uhu.es (J.L. Guerrero), silvia.perez@dci.uhu.es (S.M. Pérez-Moreno), isidoro.gutierrez@dfa.uhu.es (I. Gutiérrez-Álvarez), manueljesus.gazquez@uca.es (M.J. Gázquez), bolivar@uhu.es (J.P. Bolívar).

https://doi.org/10.1016/j.envpol.2020.115843
0269-7491/